

CHLOROPHYLL FLUORESCENCE IMAGING ANALYSIS IN BIOTIC AND ABIOTIC STRESS

EDITED BY: Michael Moustakas, Angeles Calatayud and Lucia Guidi
PUBLISHED IN: Frontiers in Plant Science





frontiers

Frontiers eBook Copyright Statement

The copyright in the text of individual articles in this eBook is the property of their respective authors or their respective institutions or funders. The copyright in graphics and images within each article may be subject to copyright of other parties. In both cases this is subject to a license granted to Frontiers.

The compilation of articles constituting this eBook is the property of Frontiers.

Each article within this eBook, and the eBook itself, are published under the most recent version of the Creative Commons CC-BY licence.

The version current at the date of publication of this eBook is CC-BY 4.0. If the CC-BY licence is updated, the licence granted by Frontiers is automatically updated to the new version.

When exercising any right under the CC-BY licence, Frontiers must be attributed as the original publisher of the article or eBook, as applicable.

Authors have the responsibility of ensuring that any graphics or other materials which are the property of others may be included in the CC-BY licence, but this should be checked before relying on the CC-BY licence to reproduce those materials. Any copyright notices relating to those materials must be complied with.

Copyright and source acknowledgement notices may not be removed and must be displayed in any copy, derivative work or partial copy which includes the elements in question.

All copyright, and all rights therein, are protected by national and international copyright laws. The above represents a summary only. For further information please read Frontiers' Conditions for Website Use and Copyright Statement, and the applicable CC-BY licence.

ISSN 1664-8714

ISBN 978-2-88966-867-0

DOI 10.3389/978-2-88966-867-0

About Frontiers

Frontiers is more than just an open-access publisher of scholarly articles: it is a pioneering approach to the world of academia, radically improving the way scholarly research is managed. The grand vision of Frontiers is a world where all people have an equal opportunity to seek, share and generate knowledge. Frontiers provides immediate and permanent online open access to all its publications, but this alone is not enough to realize our grand goals.

Frontiers Journal Series

The Frontiers Journal Series is a multi-tier and interdisciplinary set of open-access, online journals, promising a paradigm shift from the current review, selection and dissemination processes in academic publishing. All Frontiers journals are driven by researchers for researchers; therefore, they constitute a service to the scholarly community. At the same time, the Frontiers Journal Series operates on a revolutionary invention, the tiered publishing system, initially addressing specific communities of scholars, and gradually climbing up to broader public understanding, thus serving the interests of the lay society, too.

Dedication to Quality

Each Frontiers article is a landmark of the highest quality, thanks to genuinely collaborative interactions between authors and review editors, who include some of the world's best academicians. Research must be certified by peers before entering a stream of knowledge that may eventually reach the public - and shape society; therefore, Frontiers only applies the most rigorous and unbiased reviews.

Frontiers revolutionizes research publishing by freely delivering the most outstanding research, evaluated with no bias from both the academic and social point of view. By applying the most advanced information technologies, Frontiers is catapulting scholarly publishing into a new generation.

What are Frontiers Research Topics?

Frontiers Research Topics are very popular trademarks of the Frontiers Journals Series: they are collections of at least ten articles, all centered on a particular subject. With their unique mix of varied contributions from Original Research to Review Articles, Frontiers Research Topics unify the most influential researchers, the latest key findings and historical advances in a hot research area! Find out more on how to host your own Frontiers Research Topic or contribute to one as an author by contacting the Frontiers Editorial Office: frontiersin.org/about/contact

CHLOROPHYLL FLUORESCENCE IMAGING ANALYSIS IN BIOTIC AND ABIOTIC STRESS

Topic Editors:

Michael Moustakas, Aristotle University of Thessaloniki, Greece

Angeles Calatayud, Instituto Valenciano de Investigaciones Agrarias, Spain

Lucia Guidi, University of Pisa, Italy

Citation: Moustakas, M., Calatayud, A., Guidi, L., eds. (2021). Chlorophyll Fluorescence Imaging Analysis in Biotic and Abiotic Stress. Lausanne: Frontiers Media SA. doi: 10.3389/978-2-88966-867-0

Table of Contents

- 04 Editorial: Chlorophyll Fluorescence Imaging Analysis in Biotic and Abiotic Stress**
Michael Moustakas, Ángeles Calatayud and Lucia Guidi
- 07 Exogenous Melatonin Alleviates Oxidative Damages and Protects Photosystem II in Maize Seedlings Under Drought Stress**
Bo Huang, Yang-Er Chen, Yu-Qing Zhao, Chun-Bang Ding, Jin-Qiu Liao, Chao Hu, Li-Jun Zhou, Zhong-Wei Zhang, Shu Yuan and Ming Yuan
- 23 Phenotyping Plant Responses to Biotic Stress by Chlorophyll Fluorescence Imaging**
María Luisa Pérez-Bueno, Mónica Pineda and Matilde Barón
- 38 Whole Irradiated Plant Leaves Showed Faster Photosynthetic Induction Than Individually Irradiated Leaves via Improved Stomatal Opening**
Shunji Shimadzu, Mitsunori Seo, Ichiro Terashima and Wataru Yamori
- 48 Novel Action Targets of Natural Product Gliotoxin in Photosynthetic Apparatus**
Yanjing Guo, Jing Cheng, Yuping Lu, He Wang, Yazhi Gao, Jiale Shi, Cancan Yin, Xiaoxiong Wang, Shiguo Chen, Reto Jörg Strasser and Sheng Qiang
- 65 Hydrogen Peroxide Production by the Spot-Like Mode Action of Bisphenol A**
Ioannis-Dimosthenis S. Adamakis, Ilektra Sperdouli, Eleftherios P. Eleftheriou and Michael Moustakas
- 77 Phenotypic Variation of Botrytis cinerea Isolates is Influenced by Spectral Light Quality**
Lijuan Meng, Hanna Mestdagh, Maarten Ameye, Kris Audenaert, Monica Höfte and Marie-Christine Van Labeke
- 92 Combined Proteome and Transcriptome Analysis of Heat-Primed Azalea Reveals New Insights Into Plant Heat Acclimation Memory**
Xiuyun Wang, Zheng Li, Bing Liu, Hong Zhou, Mohamed S. Elmongy and Yiping Xia
- 109 Imaging of Chlorophyll a Fluorescence in Natural Compound-Induced Stress Detection**
Adela M. Sánchez-Moreiras, Elisa Graña, Manuel J. Reigosa and Fabrizio Araniti



Editorial: Chlorophyll Fluorescence Imaging Analysis in Biotic and Abiotic Stress

Michael Moustakas^{1*}, Ángeles Calatayud² and Lucia Guidi³

¹ Department of Botany, School of Biology, Aristotle University of Thessaloniki, Thessaloniki, Greece, ² Departamento de Horticultura, Centro de Citricultura y Producción Vegetal, Instituto Valenciano de Investigaciones Agrarias, Valencia, Spain, ³ Department of Agriculture, Food and Environment, University of Pisa, Pisa, Italy

Keywords: photochemical efficiency, photosynthetic heterogeneity, reactive oxygen species, environmental stress, energy partitioning, oxidative stress, photosystem II, non-photochemical quenching

The Editorial on the Research Topic

Chlorophyll Fluorescence Imaging Analysis in Biotic and Abiotic Stress

Chlorophyll *a* fluorescence that results from the absorbed light energy can be interpreted in terms of photosynthetic activity to obtain information about the state of photosynthetic apparatus and especially of photosystem II (PSII) (Krause and Weis, 1991; Murchie and Lawson, 2013). Measurements of chlorophyll *a* fluorescence have been extensively used to probe the function of the photosynthetic machinery and for screening different crops for plant tolerance to numerous stresses, and nutritional requirements (Guidi and Calatayud, 2014; Sperdoui and Moustakas, 2014; Kalaji et al., 2016; Bayçu et al., 2018). However, photosynthetic performance is not homogeneous at the leaf surface, which makes conventional chlorophyll fluorescence analysis non-representative of the physiological status of the whole leaf (Barbagallo et al., 2003; Moustakas et al., 2019a,b).

The development of chlorophyll fluorescence imaging instruments that are capable of identifying spatiotemporal heterogeneity of leaf photosynthetic performance offer new possibilities to understand the operation and regulation of photosynthesis at the whole leaf surface that cannot be identified through conventional chlorophyll fluorescence analysis (Calatayud et al., 2006; Chaerle et al., 2007; Sperdoui et al., 2019).

In the present work, we summarize the articles in this Research Topic that update the readers on the subject, and discuss current applications of chlorophyll fluorescence imaging analysis. Shimadzu et al., by combining gas-exchange and chlorophyll fluorescence measurements, demonstrated that whole irradiated plant promoted its photosynthetic induction, via improved stomatal opening, compared with individually irradiated leaf. By analyzing chlorophyll fluorescence data, Guo et al., revealed that gliotoxin (GT), a fungal secondary metabolite, affects both PSII electron transport at the acceptor side, and the reduction rate of PSI end electron acceptors' pool. They concluded that GT inserts in the plastoquinone Q_B-site by replacing native plastoquinone, interrupting electron flow beyond plastoquinone Q_A, and thus it may have the potential for being utilized as bioherbicide.

Bisphenol A (BPA), an intermediate chemical used for synthesizing plastic materials, has a spot-like mode of action on *Arabidopsis thaliana* leaves that was revealed by Adamakis et al., using chlorophyll fluorescence imaging analysis. They concluded that the necrotic death-like spots under BPA exposure could be due to reactive oxygen species (ROS) accumulation, while on the other hand the increased hydrogen peroxide (H₂O₂) generation played a role in the leaf response against BPA. ROS can activate the plant's defense mechanisms to cope with the oxidative stress and are essential for redox sensing, signaling, and regulation (Foyer, 2018; Moustaka et al., 2020; Adamakis et al., 2021a,b).

OPEN ACCESS

Edited by:

Vladimir Orbovic,
University of Florida, United States

Reviewed by:

Omar Vergara-Díaz,
University of Barcelona, Spain
James Syvertsen,
University of Florida, United States

*Correspondence:

Michael Moustakas
moustak@bio.auth.gr

Specialty section:

This article was submitted to
Technical Advances in Plant Science,
a section of the journal
Frontiers in Plant Science

Received: 25 January 2021

Accepted: 22 March 2021

Published: 14 April 2021

Citation:

Moustakas M, Calatayud Á and
Guidi L (2021) Editorial: Chlorophyll
Fluorescence Imaging Analysis in
Biotic and Abiotic Stress.
Front. Plant Sci. 12:658500.
doi: 10.3389/fpls.2021.658500

The ability to retain “a memory” or “stress imprint” of prior exposure to certain priming conditions, for a certain length of time, can make a plant more tolerant to future stress (Martinez-Medina et al., 2016). In this way, Wang et al. reported a study aimed to characterize the mechanism of heat acclimation memory in *Rhododendron hainanense*, a typical thermotolerant wild species. By transcriptomic and proteomic analysis it was evidenced that a lot of heat-responsive genes still maintained high protein abundance rather than transcript level after a recovery period of 2 days in heat-acclimated (37°C for 1 h) plants. From the transcriptome and proteome analyses, together with photochemical efficiency measurements, they were able to figure out the response patterns of chaperonins at transcript and protein levels in *R. hainanense*.

As mentioned above, chlorophyll *a* fluorescence imaging has been used to evaluate the effect of abiotic stress on photosynthesis. In this way, drought stress is one of the most important abiotic stresses in the world with a major effect the rapid accumulation of ROS that cause photoinhibition in PSII reaction centers (Sperdoui and Moustakas, 2012). Many researchers have studied the addition of external substances to cope with water stress in plants (Moustakas et al., 2011). In this sense, Huang et al. reported that leaf application of melatonin improved photosynthetic activity in maize seedlings through a higher photochemical activity mediated by the activation of antioxidative defense. The alleviation of water stress effects by melatonin application on leaves were higher when melatonin was applied in the roots compared with foliar spray indicating a melatonin signal from roots to leaves.

Chlorophyll fluorescence imaging has been utilized by Meng et al. to detect the virulence of 15 isolates of *Botrytis cinerea* on strawberry leaves grown under white, blue and red-light emitting diodes (LEDs). The maximum photochemical efficiency (F_v/F_m) ratio was strongly correlated with disease severity and it can represent a good indicator of the “gray mold” on strawberry leaves as has been previously shown (Guidi et al., 2007). In addition, Pérez-Bueno et al. recapitulate, in a

review, photosynthetic responses to biotic stress, considering virus, bacteria, fungi, and pest, and evaluating their impact by chlorophyll fluorescence imaging analysis. In general terms, biotic stress impact on the leaf could be discriminated by spatial distribution of fluorescence quenching. On this matter, decrease in quenching fluorescence parameters and increase in non-photochemical quenching (NPQ) was observed in inoculated area, while in areas surrounding the infection, opposite behavior was detected. It was concluded that changes in chlorophyll fluorescence parameters can be observed prior to the development of visible symptoms, but there were not clear differences between healthy and infected leaf areas at late stages of the disease.

Finally, the Research Topic also illustrates the use of chlorophyll *a* fluorescence imaging not only to check plant performance under biotic and abiotic stresses, but also to the use of this technique to monitor the phytotoxic effect provoked by plant natural compounds (secondary plant metabolites). Sánchez-Moreiras et al. revealed that natural compounds can be highly phytotoxic at high doses or play a stimulant role at low doses. At phytotoxic level, the natural compounds reduced F_v/F_m , while the impact on non-photochemical quenching parameters was more variable, probably associated with the chemical structure of the compound or the dose applied.

Overall, from the significant articles presented it was concluded that photosynthetic performance is extremely heterogeneous at the leaf surface, especially under stress conditions, and that chlorophyll *a* fluorescence imaging constitutes a promising basis for investigating biotic and abiotic stress effects on plants. Contributions included in this e-book can be useful for scientists working on this topic, since recent advances in the subject were attractively presented and explained.

AUTHOR CONTRIBUTIONS

All authors listed have made a substantial, direct and intellectual contribution to the work, and approved it for publication.

REFERENCES

- Adamakis, I. D. S., Malea, P., Sperdoui, I., Panteris, E., Kokkinidi, D., and Moustakas, M. (2021b). Evaluation of the spatiotemporal effects of bisphenol A on the leaves of the seagrass *Cymodocea nodosa*. *J. Hazard. Mater.* 404:124001. doi: 10.1016/j.jhazmat.2020.124001
- Adamakis, I. D. S., Sperdoui, I., Hanč, A., Dobrikova, A., Apostolova, E., and Moustakas, M. (2021a). Rapid hormetic responses of photosystem II photochemistry of clary sage to cadmium exposure. *Int. J. Mol. Sci.* 22:41. doi: 10.3390/ijms22010041
- Barbagallo, R. P., Oxborough, K., Pallett, K. E., and Baker, N. R. (2003). Rapid, noninvasive screening for perturbations of metabolism and plant growth using chlorophyll fluorescence imaging. *Plant Physiol.* 132, 485–493. doi: 10.1104/pp.102.018093
- Bayçu, G., Moustaka, J., Grevrek-Kürüm, N., and Moustakas, M. (2018). Chlorophyll fluorescence imaging analysis for elucidating the mechanism of photosystem II acclimation to cadmium exposure in the hyperaccumulating plant *Noccaea caerulea*. *Materials* 11:2580. doi: 10.3390/ma11122580
- Calatayud, A., Roca, D., and Martínez, P. F. (2006). Spatial-temporal variations in rose leaves under water stress conditions studied by chlorophyll fluorescence imaging. *Plant Physiol. Biochem.* 44, 564–573. doi: 10.1016/j.plaphy.2006.09.015
- Chaerle, L., Lenk, S., Hagenbeek, D., Buschmann, C., and Van Der Straeten, D. (2007). Multi-color fluorescence imaging for early detection of the hypersensitive reaction to tobacco mosaic virus. *J. Plant Physiol.* 164, 253–262. doi: 10.1016/j.jplph.2006.01.011
- Foyer, C. H. (2018). Reactive oxygen species, oxidative signaling and the regulation of photosynthesis. *Environ. Exp. Bot.* 154, 134–142. doi: 10.1016/j.envexpbot.2018.05.003
- Guidi, L., and Calatayud, A. (2014). Non-invasive tools to estimate stress-induced changes in photosynthetic performance in plants inhabiting Mediterranean areas. *Environ. Exp. Bot.* 103, 42–52. doi: 10.1016/j.envexpbot.2013.12.007
- Guidi, L., Mori, S., Degl'Innocenti, E., and Pecchia, S. (2007). Effects of ozone exposure or fungal pathogen on white lupin leaves as determined by imaging of chlorophyll *a* fluorescence. *Plant Physiol. Biochem.* 45, 851–857. doi: 10.1016/j.plaphy.2007.07.001
- Kalaji, H. M., Jajoo, A., Oukarroum, A., Brestic, M., Zivcak, M., Samborska, I. A., et al. (2016). Chlorophyll *a* fluorescence as a tool to monitor physiological status of plants under abiotic stress conditions. *Acta Physiol. Plant.* 38:102. doi: 10.1007/s11738-016-2113-y

- Krause, G. H., and Weis, E. (1991). Chlorophyll fluorescence and photosynthesis: the basics. *Annu. Rev. Plant Physiol. Plant Mol. Biol.* 42, 313–349. doi: 10.1146/annurev.pp.42.060191.001525
- Martinez-Medina, A., Flors, V., Heil, M., Mauch-Mani, B., Pieterse, C. M., Pozo, M. J., et al. (2016). Recognizing plant defense priming. *Trends Plant Sci.* 21, 818–822. doi: 10.1016/j.tplants.2016.07.009
- Moustaka, J., Tanou, G., Giannakoula, A., Adamakis, I. D. S., Panteris, E., Eleftheriou, E. P., and Moustakas, M. (2020). Anthocyanin accumulation in poinsettia leaves and its functional role in photo-oxidative stress. *Environ. Exp. Bot.* 175:104065. doi: 10.1016/j.envexpbot.2020.104065
- Moustakas, M., Bayçu, G., Gevrek-Kürüm, N., Moustaka, J., Csátri, I., and Rognes, S. E. (2019a). Spatiotemporal heterogeneity of photosystem II function during acclimation to zinc exposure and mineral nutrition changes in the hyperaccumulator *Noccaea caerulea*. *Environ. Sci. Pollut. Res.* 26, 6613–6624. doi: 10.1007/s11356-019-04126-0
- Moustakas, M., Hanć, A., Dobrikova, A., Sperdouli, I., Adamakis, I. D. S., and Apostolova, E. (2019b). Spatial heterogeneity of cadmium effects on *Salvia sclarea* leaves revealed by chlorophyll fluorescence imaging analysis and laser ablation inductively coupled plasma mass spectrometry. *Materials* 12:2953. doi: 10.3390/ma12182953
- Moustakas, M., Sperdouli, I., Kouna, T., Antonopoulou, C. I., and Therios, I. (2011). Exogenous proline induces soluble sugar accumulation and alleviates drought stress effects on photosystem II functioning of *Arabidopsis thaliana* leaves. *Plant Growth Regul.* 65, 315–325. doi: 10.1007/s10725-011-9604-z
- Murchie, E. H., and Lawson, T. (2013). Chlorophyll fluorescence analysis: a guide to good practice and understanding some new applications. *J. Exp. Bot.* 64, 3983–3998. doi: 10.1093/jxb/ert208
- Sperdouli, I., Moustaka, J., Antonoglou, O., Adamakis, I. D. S., Dendrinos-Samara, C., and Moustakas, M. (2019). Leaf age-dependent effects of foliar sprayed CuZn nanoparticles on photosynthetic efficiency and ROS generation in *Arabidopsis thaliana*. *Materials* 12:2498. doi: 10.3390/ma12152498
- Sperdouli, I., and Moustakas, M. (2012). Spatio-temporal heterogeneity in *Arabidopsis thaliana* leaves under drought stress. *Plant Biol.* 14, 118–128. doi: 10.1111/j.1438-8677.2011.00473.x
- Sperdouli, I., and Moustakas, M. (2014). A better energy allocation of absorbed light in photosystem II and less photooxidative damage contribute to acclimation of *Arabidopsis thaliana* young leaves to water deficit. *J. Plant Physiol.* 171, 587–593. doi: 10.1016/j.jplph.2013.11.014

Conflict of Interest: The authors declare that the research was conducted in the absence of any commercial or financial relationships that could be construed as a potential conflict of interest.

Copyright © 2021 Moustakas, Calatayud and Guidi. This is an open-access article distributed under the terms of the Creative Commons Attribution License (CC BY). The use, distribution or reproduction in other forums is permitted, provided the original author(s) and the copyright owner(s) are credited and that the original publication in this journal is cited, in accordance with accepted academic practice. No use, distribution or reproduction is permitted which does not comply with these terms.



Exogenous Melatonin Alleviates Oxidative Damages and Protects Photosystem II in Maize Seedlings Under Drought Stress

Bo Huang^{1†}, Yang-Er Chen^{1†}, Yu-Qing Zhao^{1†}, Chun-Bang Ding¹, Jin-Qiu Liao¹, Chao Hu¹, Li-Jun Zhou¹, Zhong-Wei Zhang², Shu Yuan² and Ming Yuan^{1*}

¹ College of Life Sciences, Sichuan Agricultural University, Ya'an, China, ² College of Resources Science and Technology, Sichuan Agricultural University, Chengdu, China

OPEN ACCESS

Edited by:

Angeles Calatayud,
Instituto Valenciano
de Investigaciones Agrarias, Spain

Reviewed by:

Nobuhiro Suzuki,
Sophia University, Japan
Parvathi Madathil Sreekumar,
Kerala Agricultural University, India

*Correspondence:

Ming Yuan
yuanming@sicau.edu.cn

[†] These authors have contributed
equally to this work

Specialty section:

This article was submitted to
Plant Abiotic Stress,
a section of the journal
Frontiers in Plant Science

Received: 19 February 2019

Accepted: 06 May 2019

Published: 24 May 2019

Citation:

Huang B, Chen Y-E, Zhao Y-Q,
Ding C-B, Liao J-Q, Hu C, Zhou L-J,
Zhang Z-W, Yuan S and Yuan M
(2019) Exogenous Melatonin
Alleviates Oxidative Damages
and Protects Photosystem II in Maize
Seedlings Under Drought Stress.
Front. Plant Sci. 10:677.
doi: 10.3389/fpls.2019.00677

The protective role of melatonin in plants against various abiotic stresses have been widely demonstrated, but poorly explored in organ-specific responses and the transmission of melatonin signals across organs. In this study, the effects of melatonin with the root-irrigation method and the leaf-spraying method on the antioxidant system and photosynthetic machinery in maize seedlings under drought stress were investigated. The results showed that drought stress led to the rise in reactive oxygen species (ROS), severe cell death, and degradation of D1 protein, which were mitigated by the melatonin application. The application of melatonin improved the photosynthetic activities and alleviated the oxidative damages of maize seedlings under the drought stress. Compared with the leaf-spraying method, the root-irrigation method was more effective on enhancing drought tolerance. Moreover, maize seedlings made organ-specific physiological responses to the drought stress, and the physiological effects of melatonin varied with the dosage, application methods and plant organs. The signals of exogenous melatonin received by roots could affect the stress responses of leaves, and the melatonin signals perceived by leaves also led to changes in physiological metabolisms in roots under the stress. Consequently, the whole seedlings coordinated the different parts and made a systemic acclimation against the drought stress. Melatonin as a protective agent against abiotic stresses has a potential application prospect in the agricultural industry.

Keywords: melatonin, maize, drought, antioxidant system, photosynthesis

INTRODUCTION

Water is thought to be one of the main environmental elements which restrict crop growth, development and yield. Water deficit in the soil, described as drought stress, usually results in various physiological and metabolic disorders of plants. Drought stress is the key restrictive factor for crop production, and has led to a rough 40% reduction of maize over the past 25 years in the world (Daryanto et al., 2016). Responses of plants to drought are usually interconnected

and multiple. A lot of researches have shown that drought leads to limitation in total nutrient uptake, decreases in water and photosynthetic pigment contents, depression of the photochemical efficiency, and reduction in growth (Wahid and Rasul, 2005; Farooq et al., 2009; Chen et al., 2016a). Most of these drought damages are involved in the photosynthetic process in plants. Some researchers have demonstrated that the reduction of the photosynthetic activity might be due to non-stomatal and stomatal limitations under drought stress (Zlatev and Yordanov, 2004). In addition, several reports have indicated that drought stress led to damages to the oxygen evolving complex and the reaction center of photosystem II (PSII; Lu and Zhang, 1999).

Furthermore, a major effect of drought in plant leaves and roots is the rapid accumulation of reactive oxygen species (ROS), which can cause photoinhibition, the peroxidation of membrane lipids, degradation of biomacromolecules, and oxidative damages (Farooq et al., 2009; Chen et al., 2016b). Under drought stress, excessive ROS can impair the chloroplasts, decrease the photochemical reactions, and finally suppress the photosynthesis and yield of the crop (Li T. et al., 2014). Plants have developed several enzymatic and non-enzymatic antioxidant protection mechanisms to counteract the damaging effects of ROS under environmental stresses (Wang et al., 2010). At the same time, plants can deal with environmental stresses through increasing dissipation of excess excitation energy or synthesizing and accumulating some stress-resistant substances (Chen et al., 2017). During the last 50 years, global climate change has significantly adverse effects on crop yields because of the increases in drought and heat stresses (Hillel and Rosenzweig, 2002). Therefore, the improvement of crop yields under various abiotic stresses is an urgent task to meet the booming food demands of the ever increasing population. The application of exogenous plant growth substances has been demonstrated to be an effective approach to enhance crops resistance to drought (Peleg and Blumwald, 2011).

Melatonin (N-acetyl-5-methoxytryptamine) was initially identified in the bovine pineal gland (Lerner et al., 1958). It acts as a biological regulator of circadian rhythms, sleep, immunological systems, sexual behavior, reproduction, and antioxidative activities in animals (Hattori et al., 1995; Jan et al., 2009; Reiter et al., 2010; Hardeland et al., 2012; Carrillo-Vico et al., 2013). In addition, melatonin as a naturally antioxidant may play important regulatory roles in the growth and development, and various stress responses in plants (Dubbels et al., 1995; García et al., 2014). Many evidences have demonstrated that melatonin can enhance the resistance against multiple adverse environmental factors, such as cold, drought, salinity, high temperature, ultraviolet radiations, heavy metals, and pathogen infections (Afreen et al., 2006; Posmyk et al., 2008; Yin et al., 2013; Han et al., 2017). Although the antioxidative effects of melatonin on alleviating different environmental stresses have been widely investigated in plants (Wang et al., 2013b; Zhang et al., 2013; Li C. et al., 2014; Ye et al., 2016), there is little study on organ-specific physiological responses to melatonin applications under drought stress.

As one of the three primary crops across the world, maize (*Zea mays* L.) is drought-sensitive. In recent decades, drought

has found to be the largest limitation for the production of maize in many regions of the world. Therefore, it is of important significance to increase the drought resistance of maize and make it maintain productivity under drought. Although many reports have shown that the application of exogenous melatonin can enhance drought tolerance in different plant species, there is no study on the comparison of photosynthesis and oxidative damages under drought stress through the two different methods of melatonin applications. Furthermore, few researches have looked into the role of melatonin in protecting the photosynthetic apparatus, and the organ-specific physiological responses to drought stress have not been reported previously. In this research, we investigated the protective role of melatonin in maize roots and leaves under drought stress with two different application methods through comparing ROS accumulation, the abilities of antioxidant enzymes, and photochemical capacities. Here we expect to provide the better understanding in the regulatory role and effective application methods of melatonin in improving of the drought tolerance of plants.

MATERIALS AND METHODS

Plant Materials and Treatments

Maize (*Z. mays* L.) seeds were sterilized with 0.1% HgCl₂ (w/v) for 10 min and washed with distilled water for 5 times. These seeds germinated on the wetted filter paper at 25°C for 1 day in dark. The seedlings with uniform size were transplanted in black plastic pots with equal quantity nutritive soil and placed in intelligent greenhouse, which was set to a photoperiodic cycle (14 h light, 10 h dark at 25 and 20°C, respectively), roughly 70% relative humidity, and 180 $\mu\text{mol m}^{-2} \text{s}^{-1}$ light intensity. Each pot (14 cm diameter at bottom and 16 cm high) contained six seedlings, and irrigated with 1/2 Hoagland's solution every 2 days.

One-week-old maize plants with the same size were selected and treated with two different application methods for 2 days. One method was that the maize seedlings were irrigated with different concentrations of melatonin solutions (I). The other method was that melatonin solution was sprayed on the leaves 5 times every day at 2 h intervals with the same concentrations containing 0.05% (V/V) Tween-20 as a non-ionic surfactant (II). Then, all the plants were divided into nine groups as follows: (1) non-melatonin plus well watered (Control, CK); (2) 20 $\mu\text{mol/L}$ melatonin plus well watered (M₂₀); (3) 100 $\mu\text{mol/L}$ melatonin plus well watered (M₁₀₀); (4) 0 $\mu\text{mol/L}$ melatonin plus progressive drought stress (Dr); (5) 20 $\mu\text{mol/L}$ melatonin pretreatment plus progressive drought stress; (6) 100 $\mu\text{mol/L}$ melatonin pretreatment plus progressive drought stress. (7) 0.05% Tween-20 solution was sprayed on the leaves and progressive drought stress; (8) 0.05% Tween-20 solution plus 20 $\mu\text{mol/L}$ melatonin pretreatment and progressive drought stress; (9) 0.05% Tween-20 solution plus 100 $\mu\text{mol/L}$ melatonin pretreatment and progressive drought stress. Then stopped watering to apply progressive drought stress. After drought

for 7 days, rehydration was applied to all drought treatment groups. Root and the second leaves from the top were gathered at the final day of drought treatment for the following measurements.

Determination of Chlorophyll Content, Leaf Relative Water Content (RWC), Plant Dry Weight and Soil Water Content

Fresh leaves of 1 cm² were thoroughly cut and submerged into 2 mL 80% acetone in the dark for 24 h (4°C). The absorbance of the solution was measured at 646.6 nm and 663.6 nm with a spectrophotometer A560 (AOE Instruments, Shanghai, China). Chlorophyll content was calculated according to Porra et al. (1989). The leaf relative water content (RWC) and the plant dry weight were determined according to Li T. et al. (2014). Soil water content was measured by oven drying soil at 110°C for 24 h (Sainju et al., 2017).

Melatonin Extraction and Quantification

The measurement of melatonin was done with the method of Sturtz et al. (2011). 1 g of fresh tissue samples were grounded and 2 mL of acetone was added, then transferred into 10 mL tube. After mixing well and shaking with ultrasonic bath for 0.5 h at 25°C, the mixture was centrifuged with 3000 g at 4°C, the supernatant was evaporated under vacuum and resolved with 2 mL water. After purification with C18-SPE cartridges (Bonna-Agela Technologies Instruments, Tianjin, China), the quantitative analysis of melatonin was carried out through a high performance liquid chromatography (HPLC) system (1290 LC, Agilent, Santa Clara, CA, United States) with a tandem mass spectrum (MS) system (6470 LC-MS/MS, Agilent, Santa Clara, CA, United States). LC-MS/MS parameters were set as Han et al. (2017).

Determination of Photosynthetic Parameters and Chlorophyll Fluorescence

A portable gas exchange system GFS-3000 (Heinz Walz Instruments, Effeltrich, Germany) was used to measure photosynthetic parameters according to Kaling et al. (2015). The measurement was performed at ten o'clock in the morning on the 2nd leaf from the top. A 4 cm² area of the leaf was clamped and exposed to the general parameter (flow of 750 $\mu\text{mol s}^{-1}$, leaf temperature of 25°C, incident light intensity of 180 $\mu\text{mol m}^{-2} \text{s}^{-1}$ and a relative humidity of 70%). Photosynthesis and gas exchange rates were recorded after reached a steady state. Water-use efficiency (WUE) was calculated as the ratio of net photosynthetic rate to transpiration rate.

Chlorophyll fluorescence was imaged with a modulated imaging fluorometer (the Imaging PAM M-Series Chlorophyll Fluorescence System, Heinz Walz Instruments, Effeltrich, Germany). The maximum efficiency of PSII photochemistry (F_v/F_m), the quantum yield of PSII photochemistry [$Y(II)$],

photochemical quenching (qP) and non-photochemical quenching (NPQ) were imaged and calculated after adaption in the dark for 30 min (Naranjo et al., 2016).

Quantification of Lipid Peroxidation and Relative Electrolyte Leakage

Taking malondialdehyde (MDA) content as assessment index of lipid peroxidation, and MDA content was determined with thiobarbituric acid (TBA) method via recording the absorbance at 600, 532, 450 nm as described by Zhang et al. (2013). The electrolyte leakage (EL) of the root and leaves was determined based on Fan et al. (2015). 0.5 g of detached material was washed with ultrapure water, and cut into 0.5 cm fragments. Then, the samples were submerged into 30 mL deionized water for 24 h, and the conductivity (EL1) was recorded with a conductance meter DDS-309+ (ARK Instruments, Chengdu, China). Then the sample in the tube were completely damaged by boiling water bath for 30 min, and the conductivity (EL2) was read again after cooling to room temperature. Relative electrolyte leakage (REL) was calculated as the ratio of EL1 to EL2.

Quantification of Soluble Sugar Contents and Proline

The soluble sugar content was performed with the anthrone method as described by Shi et al. (2015b). Briefly, 0.1 g sample was added to 2 mL of 80% (V/V) ethanol at 80°C for 30 min. 100 μL of extracts was mixed with 2 mL anthrone, and then boiled for 10 min. The absorption was recorded at 630 nm, and the content was calculated according to the calibration curve of sucrose standard. Proline was determined based on Ye et al. (2015). Briefly, 0.5 g frozen powder sample was blended with 5 mL of 3% (W/V) sulfosalicylic acid. Then, mixed with 2 mL of ninhydrin reagent and 2 mL of glacial acetic acid, and heated in boiling water for 30 min. After cooling to 25°C, the reaction solution was centrifugation at 10000 g for 10 min, and the absorbance at 520 nm was recorded and the proline level was calculated according to the standard curve.

Assays for Cell Death

Dead cells were stained by trypan blue (Lin et al., 2012). The leaves were detached and infiltrated with the lactophenol-trypan blue solution for 1 h at 70°C, then placed in the boiling water for 5 min and stained for 12 h. The background staining was removed by 2.5 g/mL chloral hydrate solution for 3 days, tissues were equilibrated with 70% glycerol for photographing.

Measurements of Reactive Oxygen Species (ROS)

Histochemical detection of ROS was conducted as described by Chen et al. (2017). Briefly, hydrogen peroxide (H_2O_2) and superoxide anion radicals (O_2^-) were visually detected with 0.5 mg/mL 3, 3'-diaminobenzidine (DAB) and 1 mg/mL nitro blue tetrazolium (NBT), respectively. Then, the tissues were

decolorized for 2 h in boiling ethanol (85%). The quantification of H_2O_2 and superoxide anion radicals was determined as described by Chen et al. (2016a).

Determination of Antioxidant Enzyme Activities

Fresh tissue of 0.2 g was grounded in 4 mL of 150 mM, pH 7.8 ice-cold sodium phosphate buffer on ice, and then centrifuged at 12000 g at 4°C for 20 min. The supernatant was used for the next enzyme activity assays.

Superoxide dismutase (SOD) activity was evaluated according to the ability to inhibit the photochemical reduction of NBT (Abedi and Pakniyat, 2010). Guaiacol peroxidase (POD) activity was evaluated with the ability to convert guaiacol to tetraguaiacol (Abedi and Pakniyat, 2010). Catalase (CAT) activity was assayed by monitoring the absorbance of H_2O_2 at 240 nm (Wang, 1995). Ascorbate peroxidase (APX) activity was measured based on the decrease in ascorbate (Nakano and Asada, 1981). Glutathione peroxidase (GPX) activity was estimated as described by Sayfzadeh and Rashidi (2010). Glutathione reductase (GR) activity was measured based on Balabusta et al. (2016) and depends on the rate of the oxidation of NADPH. Activity of dehydroascorbate reductase (DHAR) was determined by the increase in reduced ascorbate (de Pinto et al., 2000).

Determination of Antioxidant Metabolites

The antioxidant metabolites include reduced ascorbic acid (AsA), dehydroascorbate (DHA), reduced glutathione (GSH) and oxidized glutathione (GSSG). They were determined with the enzymatic cycling assay method (Wang et al., 2013b).

Isolation of Thylakoid Membranes and Western Blotting

The thylakoid membrane protein was prepared as described by Fristedt et al. (2010). Thylakoid membrane protein was quantified based on total chlorophyll (Porra et al., 1989). For analysis of thylakoid proteins, an equivalent chlorophyll basis were loaded in gels and were separated by 15% sodium dodecyl sulfate polyacrylamide gel electrophoresis. Then, the protein was transferred to a PVDF membrane (Bio-Rad, Hercules, CA, United States). The primary antibodies including anti-D1, anti-D2, anti-LHCB1, anti-LHCB2, and anti-LHCB3 were purchased from Agrisera (Umea, Sweden). A chemiluminescent detection system (ECL, GE Healthcare, Buckinghamshire, United Kingdom) was used to perform the immunoblots. The quantification of immunoblots was done with the Quantity One software (Bio-Rad, Hercules, CA, United States).

Statistical Analysis

We repeated all experiments at least three times of independent experiments. Results were analyzed via one-way ANOVA and then Duncan's multiple range test was carried out to indicate a significant difference at $P < 0.05$. All data were expressed as means \pm standard deviation (SD).

RESULTS

The Effects of Exogenous Melatonin on Plant Growth

There was no significant difference between melatonin-treated and non-treated seedlings under the well-irrigated condition, and their growth was generally equivalent (Figure 1A). When we stopped watering and a progressive drought stress was applied, water content of soil in the pot decreased gradually (Figure 1C) and the growth of all seedlings was significantly inhibited, but the plants treated with melatonin had greener leaf tissues and higher chlorophyll contents than the non-treated plants (Figures 1A,F). Drought stress decreased both the length and the dry weight of shoots. Stopping watering increased the length of the longest root, but decreased the dry weight of all roots. And the application of exogenous melatonin could reverse these trends to some extents (Figures 1G,H). Consistently, the RWC (Figure 1D) and plant biomass of melatonin treated plants (Figure 1H) were significantly higher than those of the non-treated plants. And 100 μM melatonin could provide a better protection than 20 μM melatonin. Moreover, the root-irrigation method was more effective than the leaf spraying method, and the seedlings of root irrigation with 100 μM melatonin exhibited healthy growth with significantly higher chlorophyll contents and plant biomass. After rehydration, the turgidity of the leaf cells was regained and the slight withering leaves stood up again (Figure 1B). These results indicated that exogenous melatonin can help maize seedlings to resist the drought stress.

The Effects of Exogenous Melatonin on Endogenous Melatonin Level

To evaluate the effect of drought stress on the melatonin biosynthesis, endogenous melatonin levels of the leaf tissues were quantified after the progressive drought stress for 7 days. The melatonin of the leaves was about 22 pg g^{-1} dry weight (DW) and the application of exogenous melatonin showed no remarkable induces of endogenous melatonin content under the well-irrigated condition (Figure 1E). When subjected to the drought stress, melatonin levels were markedly induced. Irrigation with 100 μM melatonin improved the level of endogenous melatonin under drought stress. These results suggested the melatonin is involved in the responses of maize seedlings to drought stress and the application of exogenous melatonin could change the accumulation of endogenous melatonin under stress.

Exogenous Melatonin Treatment Decreased the Accumulation of ROS Under Drought Stress

It has been reported that melatonin and its metabolites are highly effective ROS scavengers (Tan et al., 2007). The levels of two major ROS species, O_2^- and H_2O_2 , in leaves and roots were analyzed by histochemical staining and spectrophotometry. The application of exogenous melatonin led to no significant

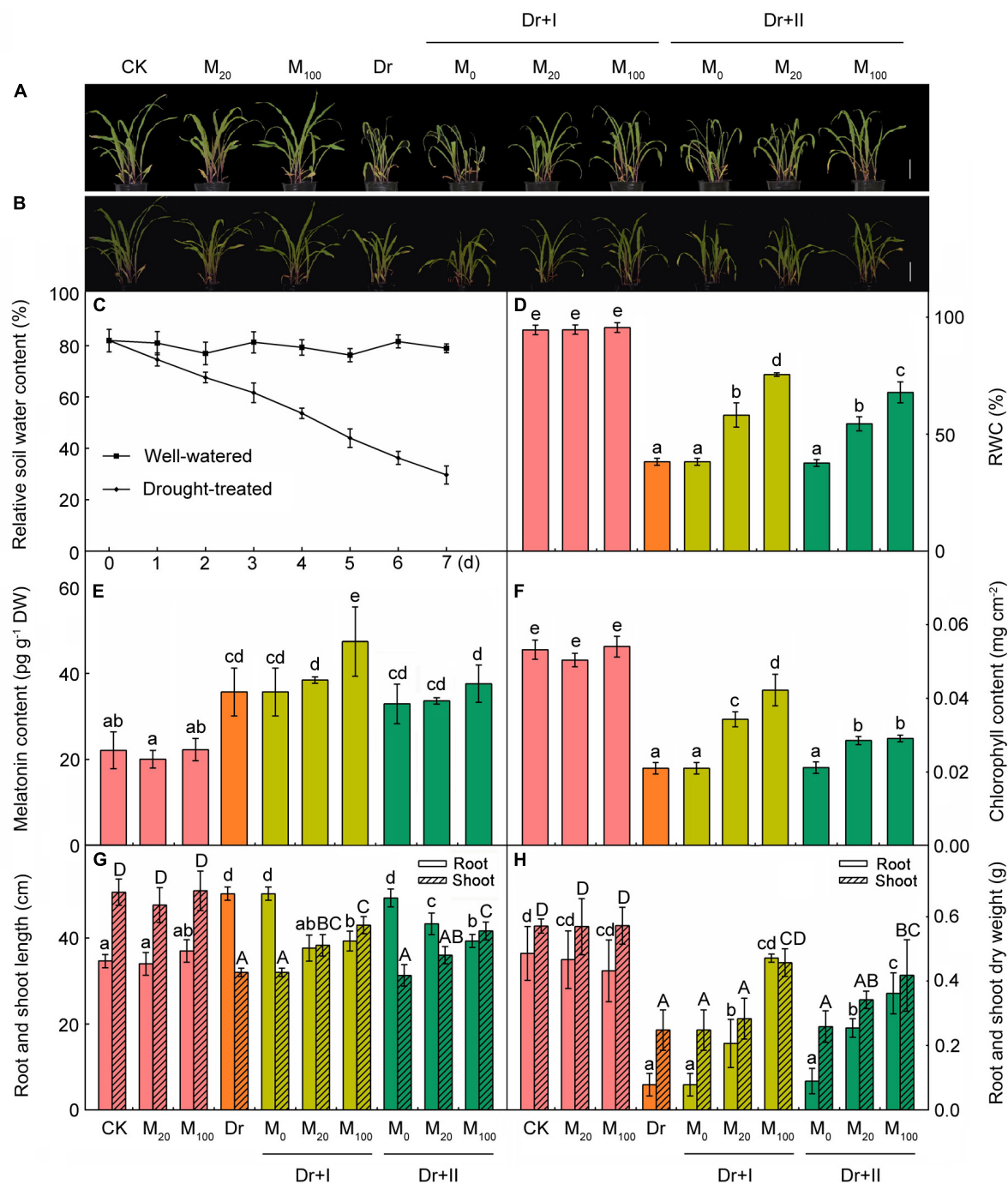
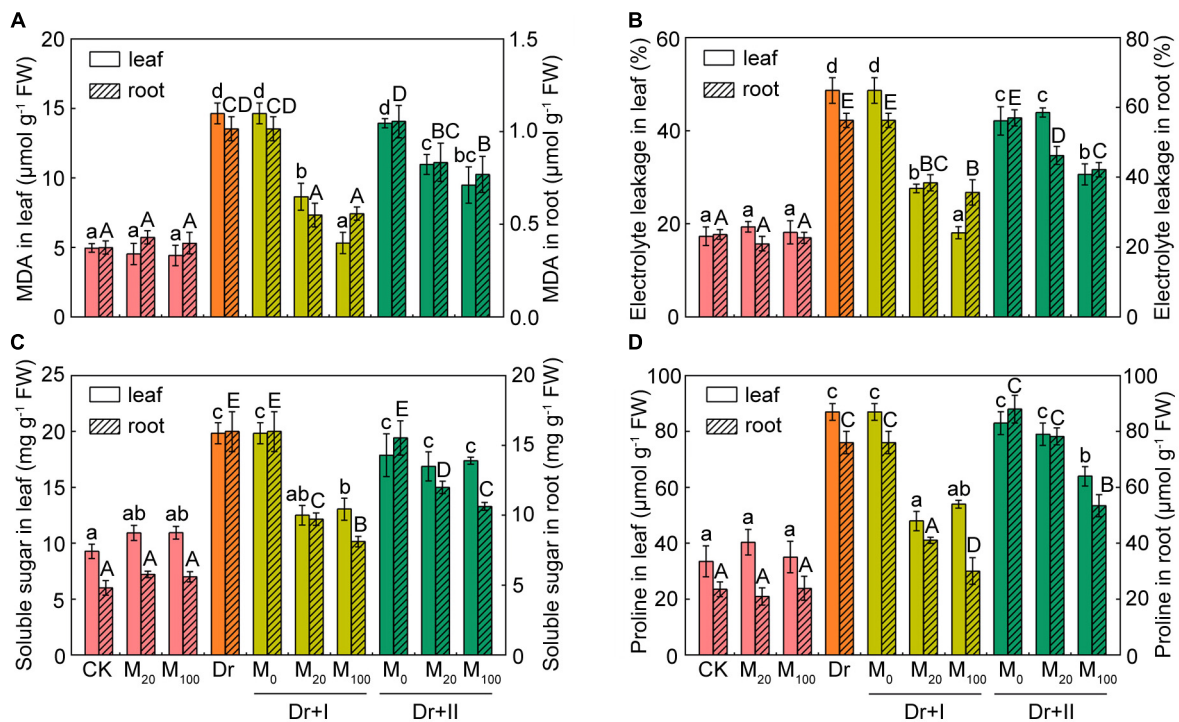
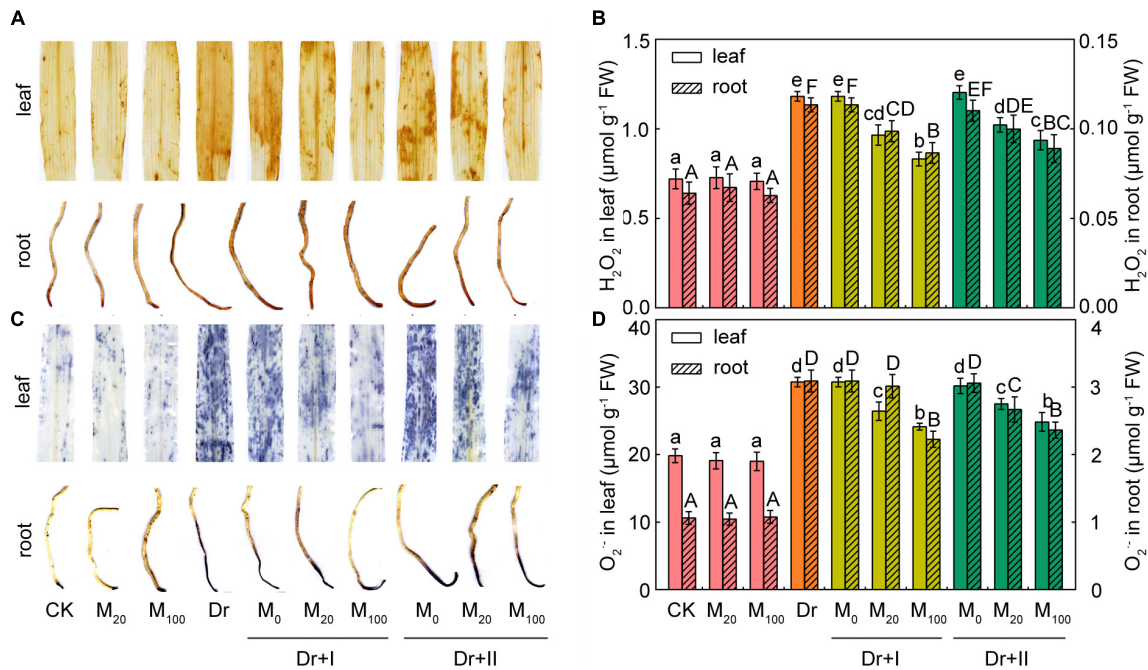


FIGURE 1 | Exogenous melatonin improved drought stress resistance in maize seedlings. **(A)** The phenotype of melatonin pre-treated or non-treated seedlings after 7-day drought stress; **(B)** the phenotype of plants after 24 h rehydration; **(C)** the soil water content during drought stress; **(D)** leaf relative water content after 7-day drought; **(E)** the content of melatonin in leaves after 7-day drought; **(F)** the chlorophyll content in leaves after 7-days drought stress; **(G)** the length of root and shoot after 7-day drought; and **(H)** the dry weight of root and shoot after 7-day drought. Values are the averages of 3 replicates \pm SD. Different letters indicate significant differences according to Duncan's multiple range tests ($P < 0.05$).

change under the well-irrigated condition. While significant H_2O_2 and O_2^- bursts occurred in the leaves and roots under the drought condition, but exogenous melatonin application markedly reduced the accumulation of ROS (Figure 2). The

melatonin treatment of 100 μM worked more effectively to scavenge ROS than 20 μM , and root-irrigation method was more efficient to slow the accumulation of ROS than the leaf spraying.



Exogenous Melatonin Protected Cell Membranes and Alleviated Cell Death Under the Drought Stress

To evaluate the protective effect of exogenous melatonin on the integrity of membrane system under the drought condition, malonaldehyde (MDA) level and relative electrolyte leakage (EL) were investigated. MDA content and EL in the leaves and roots were not altered by exogenous melatonin under the normal growth condition (**Figures 3A,B**). MDA content and EL increased obviously in drought-stress seedlings, which suggested that drought damaged the integrity and fluidity of the cell membrane system. But exogenous melatonin markedly decreased the level of MDA and the rise of EL under the drought condition. At the same time, the root-irrigation method was more effective in protection of cell membrane than the leaf-spraying method. And the root irrigation with 100 μM melatonin was more effective in maintaining the stability of cell membrane and protecting from lipid peroxidation.

The leaf water potential often decreased during drought stress, and compatible solutes (such as proline and soluble sugar) could improve the cytoplasmic osmotic pressure, balance the water potential, protect the membrane system and the other biological macromolecules and thereby reduce water loss from cells. Under the well-irrigated condition, soluble sugar content of leaves increased slightly after the melatonin treatment, but there were no significant differences in both leaves and roots between the melatonin-treated and non-treated seedlings. Proline and soluble sugars increased under the drought stress in both leaves and roots. Root irrigation with melatonin could down-regulate levels of these osmotic substances under the drought stress. 20 and 100 μM melatonin treatments showed no statistical difference in proline and soluble sugar levels in leaves, but the roots of 100 μM melatonin treatment had lower levels of osmotic substances than those of 20 μM melatonin treatment after 7 days-drought stress. As for leaf spraying treatment, soluble sugar content of the leaves did not changed significantly, but markedly decreased in the roots (**Figures 3C,D**). Leaf spraying with 20 μM melatonin had no significant influence on proline level both in both leaves and roots, and 100 μM melatonin lowered their levels under the drought condition. These results suggested soluble sugar and proline in shoots and roots of the maize adopted different strategies to adapt to the progressive drought stress, and exogenous melatonin could partly reverse these changes. In general, the irrigation method exhibited a better protective effect than spraying.

Cell death is usually induced by abiotic stresses. The tissues of leaves and roots showed obvious cell death under the drought condition, particularly in leaf tips and root tips (**Figure 4**). However, melatonin treatment alleviated the cell death, especially by the irrigation method of 100 μM melatonin.

Exogenous Melatonin Protected Photosynthesis Under Drought Condition

Drought stress can inhibit photosynthesis. Under drought stress, melatonin treatment significantly inhibited the decrease in chlorophyll contents (**Figure 1F**). Gas exchange parameters were measured in order to explore the impacts of melatonin on

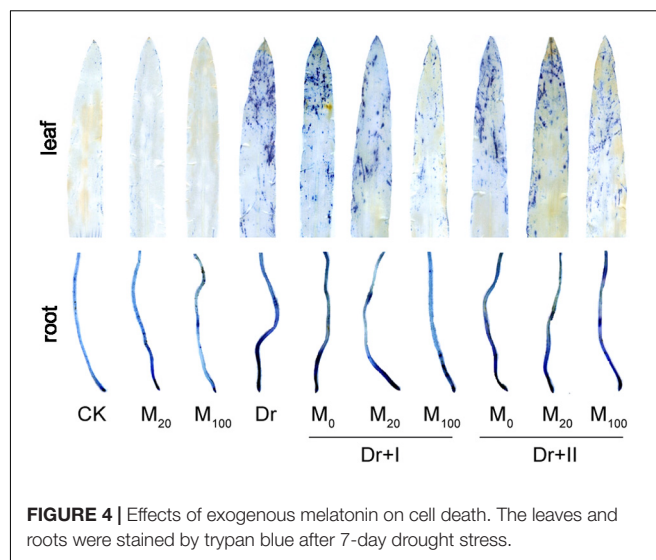


FIGURE 4 | Effects of exogenous melatonin on cell death. The leaves and roots were stained by trypan blue after 7-day drought stress.

photosynthesis. The application of exogenous melatonin did not significantly affect the gas exchange parameters under the well-irrigated condition. Net photosynthetic rate (P_n) (**Figure 5A**), transpiration rate (T_r) (**Figure 5B**), and stomatal conductance (G_s) (**Figure 5C**) all decreased under the water deficit condition, and the application of exogenous melatonin relieved these downtrends. Irrigation with 100 μM melatonin had a better protective effect. Intercellular CO_2 concentration (C_i) dropped under drought, whereas this decline was not reversed by the melatonin application (**Figure 5D**). These data showed that the CO_2 assimilation significantly decreased under drought condition, and exogenous melatonin could provide a significantly protective role. Similar results have been demonstrated in cucumber (Zhang et al., 2013). Water-use efficiency (WUE; calculated as the ratio of net photosynthetic rate to transpiration rate) increased under the drought stress, however, kept stable after the exogenous melatonin treatments (**Figure 5E**).

Chlorophyll fluorescence is an effective tool to explore the work status of photosystem II (Wang et al., 2013a). The fluorescence images showed that under the well-irrigated condition, the application of melatonin did not change F_v/F_m , $Y(\text{II})$, NPQ and qP (**Figure 6**). F_v/F_m , $Y(\text{II})$ and qP decreased significantly under the drought condition. In contrast, the NPQ value rose, indicating that the thermal energy dissipation in PSII was enhanced. However, F_v/F_m , $Y(\text{II})$ and qP was increased and NPQ was decreased by exogenous melatonin treatments in maize seedlings under the drought stress. Meanwhile, the root-irrigation method worked more effectively than the leaf spraying method.

The Effects of Exogenous Melatonin on Antioxidant System

Plants evolve antioxidant defense system to avoid the damages of ROS accumulation and lipid peroxidation. Thus, the changes of non-enzymatic antioxidants (AsA-DHA and GSH-GSSG) and enzymatic antioxidants (POD, CAT, SOD, APX, GPX, GR, and

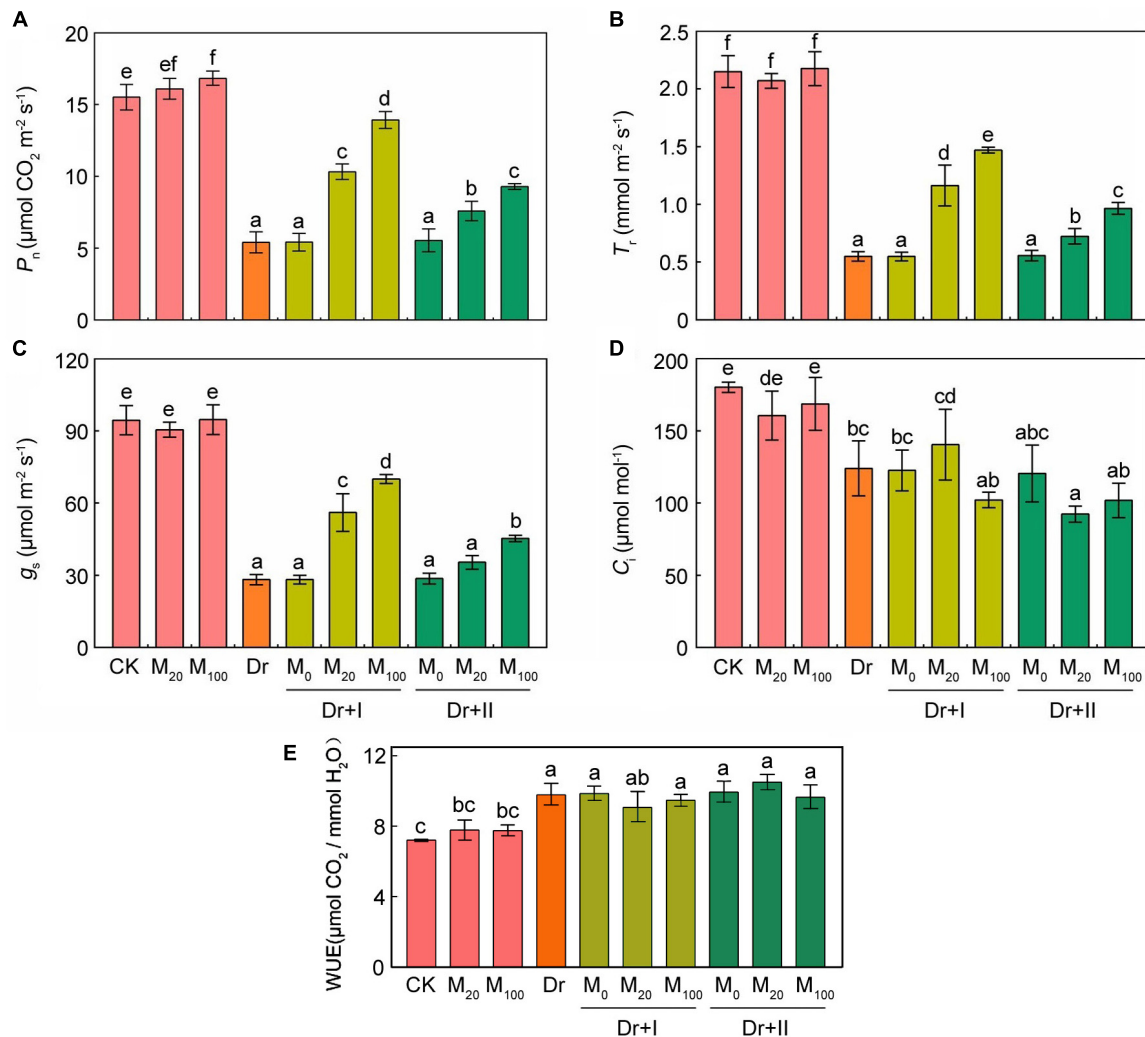


FIGURE 5 | Effects of exogenous melatonin on photosynthetic parameters. **(A)** Net photosynthetic rate (P_n), **(B)** transpiration rate (T_r), **(C)** stomatal conductance (G_s), **(D)** intercellular CO_2 concentration (C_i), and **(E)** Water-use efficiency (WUE) after 7-days drought stress. Values are the averages of 3 replicates \pm SD. Different letters indicate significant differences according to Duncan's multiple range tests ($P < 0.05$).

DHAR) of maize leaves and roots in the absence and presence of melatonin were determined.

As shown in **Figure 7**, reduced AsA contents (**Figure 7A**) and DHA contents (**Figure 7B**) in leaves and roots tended to vary analogically. Under the drought condition, the contents of AsA and DHA significantly increased in both leaves and roots, and root irrigation with 20 μM melatonin further boosted AsA and DHA levels. 100 μM melatonin could further increase their levels in leaves, but there was no significant change for AsA and DHA in roots. Leaf-spraying with melatonin did not significantly change AsA and DHA contents in both leaves and roots, except that 100 μM melatonin decreased their levels in roots. Under the drought condition, the GSH level decreased in leaves but increased in roots, while the content of GSSG increased in leaves and almost remained unchanged in roots. Root irrigation with melatonin could improve the level of GSH and lower the GSSG content, but leaf spraying had no

influence on GSH and GSSG in leaves (**Figure 7C**). However, both root irrigation and leaf spraying lowered the level of GSH and the GSSG remained unchanged in roots (**Figure 7D**). Overall, the melatonin application further increased AsA and GSH contents when exposed to the drought condition, and the root-irrigation method showed a better inductive effect than the leaf spraying method.

The activities of the six antioxidant enzymes were hardly affected by exogenous melatonin under the well-irrigated condition. While the drought stress improved the antioxidant enzymic activities in both leaves and roots except the activities of GPX and GR. The activity of GPX reduced in roots and increased in leaves, but the activity of GR decreased in leaves but up-regulated in roots (**Figure 8**). The POD and DHAR activities increased in both leaves and roots no matter with root irrigation or leaf spraying (**Figures 8A,G,H**). Melatonin enhanced CAT activity in both leaves and roots, but leaf

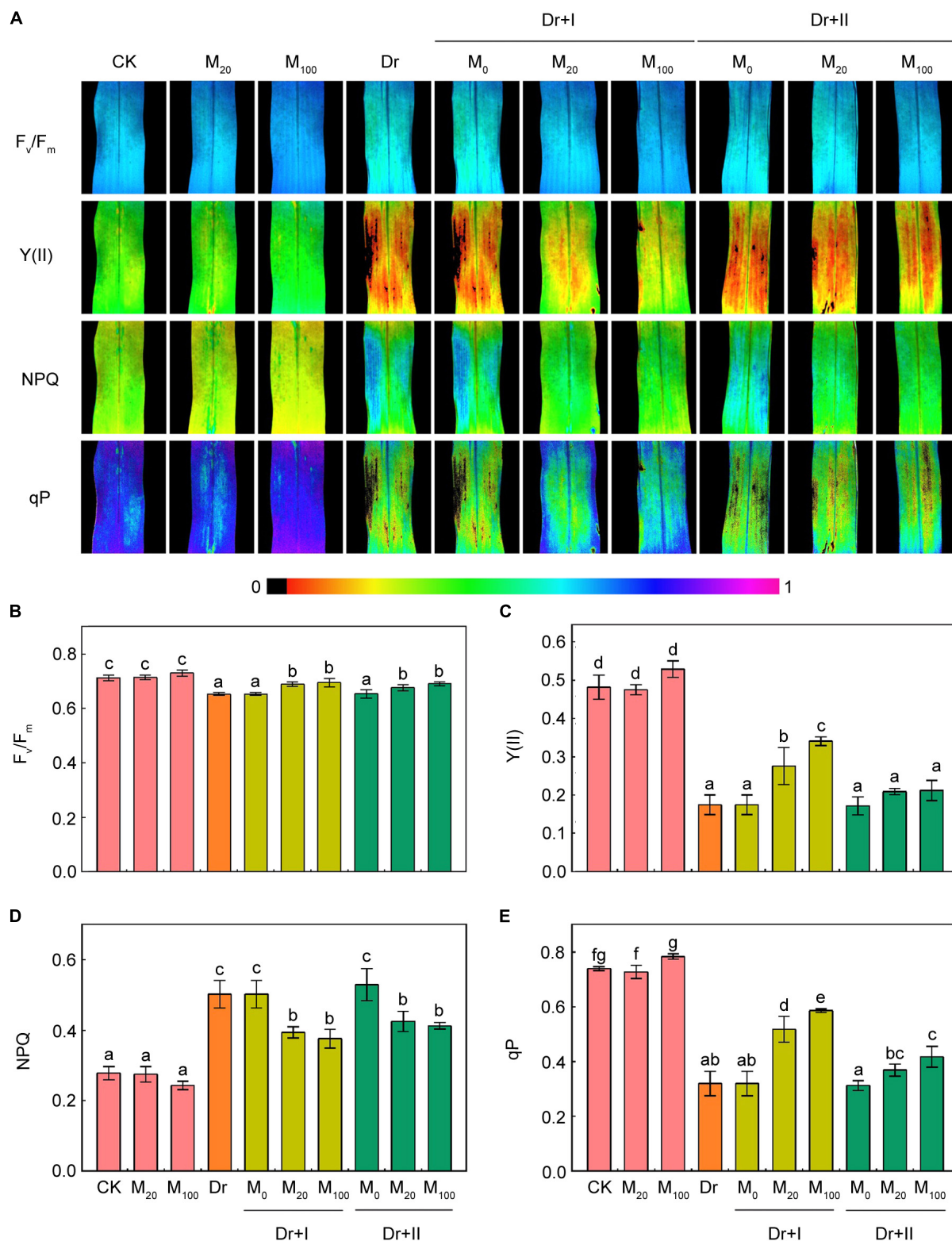


FIGURE 6 | Effects of exogenous melatonin on chlorophyll fluorescence parameters. Quantitative values of maximum PSII yield (F_v/F_m) (**B**), effective quantum yield of PSII [$Y(II)$] (**C**), non-photochemical quenching (NPQ) (**D**), and photochemical quenching (qP) (**E**) were matched with the fluorescence images (**A**). Values are the averages of 3 replicates \pm SD. Different letters indicate significant differences according to Duncan's multiple range tests ($P < 0.05$).

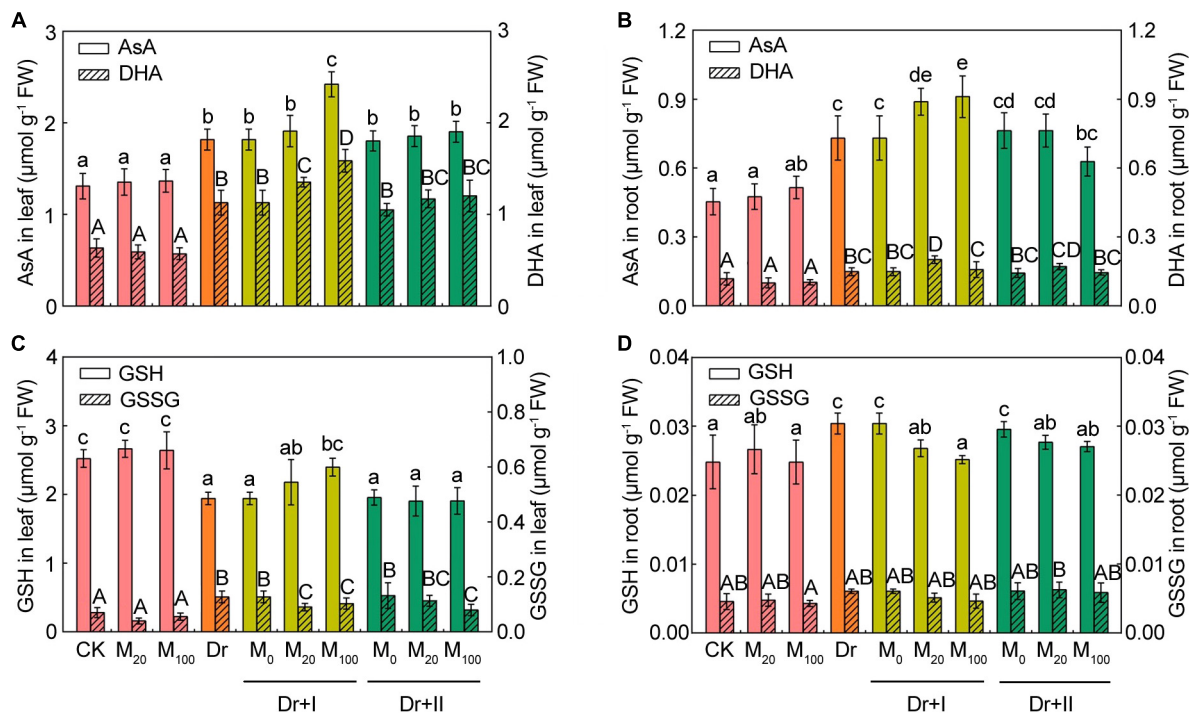


FIGURE 7 | Effects of exogenous melatonin on the non-enzymatic antioxidants. The contents of reduced ascorbic acid (AsA) and dehydroascorbate (DHA) in leaves (A) and roots (B), reduced glutathione (GSH) and oxidized glutathione (GSSG) in leaves (C) and roots (D) after 7-days drought stress. Values are the averages of 3 replicates \pm SD. Different letters indicate significant differences according to Duncan's multiple range tests ($P < 0.05$).

spraying method showed a weaker effect than the root-irrigation method (Figure 8B). Root irrigation with melatonin lowered SOD activity, but leaf-spraying with melatonin increased the activity in both roots and leaves (Figure 8C). The activity of APX was enhanced by the root-irrigation method in both leaves and roots, and the leaf-spraying method elevated its activity in leaves but reduced its activity in roots (Figure 8D). The activity of GPX reduced in leaves and increased in roots no matter with root irrigation or leaf spraying under the drought condition (Figure 8E). The activity of GR increased in leaves and decreased in roots no matter with root irrigation or leaf spraying under the drought condition (Figure 8F). These data indicated that antioxidant enzymatic activities made organ-specific responses to the drought stress. Yang et al. (2015) also found antioxidant enzymatic activities had tissue-specific responses to water logging. Furthermore, the effects of exogenous melatonin on the antioxidant enzymatic activities varied with the dosage, application methods and plant organs. Drought stress could induce distinct changes of antioxidant enzymatic activities in roots and leaves, and exogenous melatonin could weaken or strengthen these fluctuation trends.

Melatonin Protected PSII by Increasing D1 Protein Level Under Drought Stress

To gain insights into the photosystem II proteins changes by exogenous melatonin treatment under the drought stress, thylakoid membrane protein was analyzed by the

immunoblotting (Supplementary Figures S1–S6). Melatonin treatment did not change the level of PSII protein under the well-irrigated condition. When exposed to the drought stress, D1 protein reduced significantly while the other proteins of PSII showed no significant changes (Figure 9). The melatonin treatment alleviated the decrease in D1 protein under the drought condition. The root-irrigation method showed a better protective effect on D1 protein than the leaf spraying method, and 100 μM melatonin could better protect D1 from damages than 20 μM concentration. These results indicated that melatonin application could alleviate the damages of PSII protein to maintain a higher PSII activity and normal photosynthesis under the drought stress.

DISCUSSION

It is well known that the growth, development and production of crops are inhibited by abiotic stresses (Rahdari and Hoseini, 2012). However, higher plants have evolved diverse physiological, biochemical and morphological strategies to response to drought (Farooq et al., 2009). Melatonin is a new plant growth regulator, and it has been reported to alleviate the oxidative damages caused by drought stress (Wang et al., 2013b; Zhang et al., 2013; Shi et al., 2015a; Wei et al., 2015; Ye et al., 2016). In the present experiment, the protective effects of two different melatonin-application methods in maize roots and leaves exposed to drought were investigated.

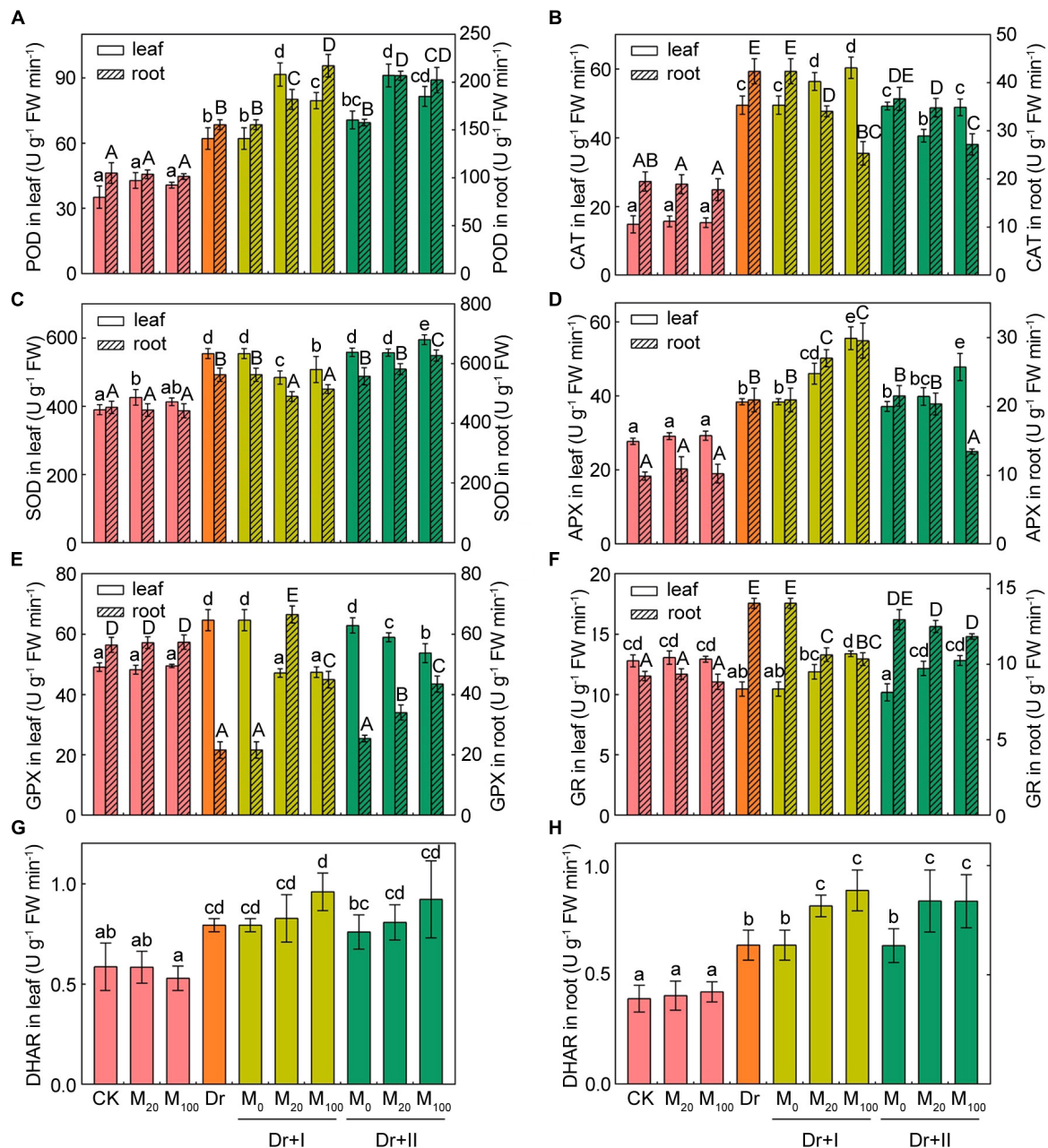


FIGURE 8 | Effects of exogenous melatonin on antioxidant enzymes activities. The peroxidase (POD) (A), catalase (CAT) (B), superoxide dismutase (SOD) (C), ascorbate peroxidase (APX) (D), glutathione peroxidase (GPX) (E), glutathione reductase (GR) (F), and dehydroascorbate reductase (DHAR) (G,H) activities in leaves and roots after 7-days drought stress. Values are the averages of 3 replicates \pm SD. Different letters indicate significant differences according to Duncan's multiple range tests (*P* < 0.05).

It has been reported that melatonin might play a key role in the regulation of plant growth and development (Tan et al., 2012; Wei et al., 2015). In this study, our results indicated that melatonin pre-treated plants presented higher chlorophyll levels, shoot height, and plant weight compared with the non-treated plants under the drought condition. These results were in agreement with the previous reports (Liu et al., 2015; Ye et al., 2016). Moreover, the melatonin pre-treated seedlings

showed a higher level of endogenous melatonin under the drought stress, suggesting that the endogenous melatonin might be closely related to the drought resistance. In addition, we found that the root-irrigation method was more effective in improving drought resistance than the leaf spraying method.

It has been shown that the drought-induced stomatal closure could lead to the decline in photosynthetic capacity (Farooq et al., 2009). Here, we showed that drought stress

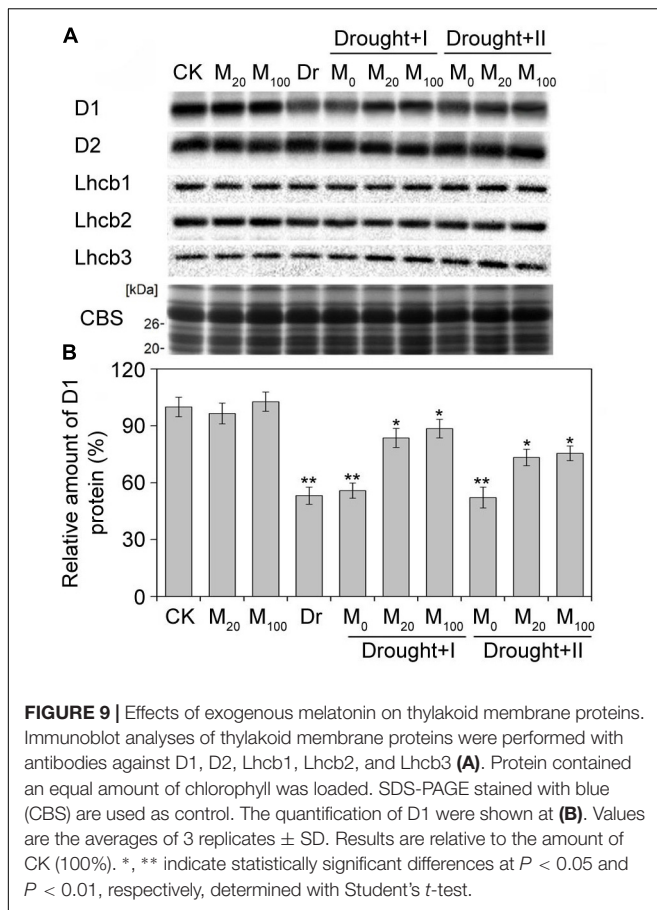


FIGURE 9 | Effects of exogenous melatonin on thylakoid membrane proteins. Immunoblot analyses of thylakoid membrane proteins were performed with antibodies against D1, D2, Lhcb1, Lhcb2, and Lhcb3 (A). Protein contained an equal amount of chlorophyll was loaded. SDS-PAGE stained with blue (CBS) are used as control. The quantification of D1 were shown at (B). Values are the averages of 3 replicates \pm SD. Results are relative to the amount of CK (100%). *, ** indicate statistically significant differences at $P < 0.05$ and $P < 0.01$, respectively, determined with Student's *t*-test.

declined the *Pn*, *Tr*, *Gs*, and *Ci*, while these decreases were partly recovered by exogenous melatonin application, except *Ci* (Figure 5). These results suggested that the application of exogenous melatonin might affect the stomata open status under drought stress. Similar research results were observed in tomato and apple (Wang et al., 2013b; Liu et al., 2015). In addition, our results further showed that root irrigation with melatonin provided better protective effects on the gas exchange than the leaf-spraying. Indeed, stomatal opening under drought can be also risky for plants because of the water loss through transpiration. However, carbon assimilation (photosynthesis) and transpiration rate increased simultaneously and thus the water-use efficiency (WUE) kept stable after the melatonin treatments (Figure 5E). Excessive stomatal opening under the drought stress may not occur after the melatonin treatments.

Chloroplast is the major source of free radical generation in plants, which require strong protection from free radicals and associated oxidative stress. It has been found that the biosynthesis of melatonin in plants might take place in chloroplast (Zheng et al., 2017). Previous studies showed that application of exogenous melatonin could induce endogenous melatonin biosynthesis in chloroplast (Zheng et al., 2017). In this study, we found that exogenous melatonin could change the accumulation of endogenous melatonin under drought stress and

the increased endogenous melatonin might maintain chloroplast integrity and enhance net photosynthesis rate.

Chlorophyll fluorescence has become a powerful approach for the study of plant photosynthetic characteristics under various environmental stresses (Govindjee., 2004). Some studies showed that severe or long-time drought leads to photoinhibition in the PSII reaction center (Sperdouli and Moustakas, 2012; Chen et al., 2016b). In consistent with these findings, we found that Fv/Fm, Φ PSII, and qP significantly decreased under the drought stress (Figure 6). The reduction in Fv/Fm, qP and Φ PSII, and the increase in the level of NPQ suggested that drought stress induced a severe damage to photosynthetic apparatus in maize seedlings. In addition, it is well known that melatonin could improve the photosynthetic efficiency in higher plants under stressful conditions (Yin et al., 2013; Zhao et al., 2015; Jiang et al., 2016). In the present experiments, melatonin application significantly improved the photosynthetic capacity of PSII under the drought condition. These results were in accordance with previous studies in apple and cucumber (Wang et al., 2013a; Zhang et al., 2013). In addition, higher photochemical capacity was observed for the root-irrigation method, suggesting that the applications to the roots were more efficient compared with leaves as far as the protective roles of exogenous melatonin to the photosynthetic efficiency under environmental stresses were concerned.

Photosystem II has been known as a primary target of photodamages under environmental stresses (Kato et al., 2012). When the PSII photodamage rate exceeds the repair ability, photoinhibition becomes apparent (Nishiyama et al., 2006). However, *de novo* synthesis of D1 protein is necessary for the repair cycle of PSII. It has been reported that drought stress inhibits the protein synthesis of D1 (Chen et al., 2016b). In accordance with the previous report, our work also showed that D1 protein decreased obviously under the drought stress. However, melatonin has been reported to protect PSII proteins from oxidative injuries and regulate the levels of senescence-associated proteins (Byeon et al., 2012; Zhang et al., 2015). A recent research indicated that melatonin is effective in the process of the PSII repair by maintaining the protein availability of D1 in tomato under salt (Zhou et al., 2016). Our work further confirmed the protective role of melatonin on PSII proteins in maize under drought stress. Melatonin with two different applications partly counteracted the decline in D1 protein under the stress. Therefore, these results suggested that melatonin played a vital role in maintaining photosynthetic efficiency by regulating the repair cycle of PSII under environmental stresses.

Under stress conditions, plants usually generate much ROS, which subsequently induce the peroxidation of membrane lipids and oxidative damages (Munné-Bosch and Peñuelas, 2003; Kar, 2011). However, previous studies had shown that melatonin played an important role in the detoxification of reactive oxygen and free radicals and functions as an antioxidant in living organisms (Reiter, 1998; Tan et al., 2000a; Reiter et al., 2007). As a broad-spectrum antioxidant, melatonin can directly eliminated ROS and the subsequent products, its derivatives, AFMK (N1-acetyl-N2-formyl-5-methoxykynuramine) and AMK (N1-acetyl-5-methoxykynuramine), can also scavenge ROS, and further terminate the cascade reaction of lipid peroxidation

(Ressmeyer et al., 2003; López-Burillo et al., 2010). Thus, one molecule of melatonin may eventually scavenge ten molecules of radicals at least (Tan et al., 2007). Melatonin treatment can markedly decreased the content of ROS and thus alleviate oxidative damages induced by the excessive ROS accumulation (Wang et al., 2013b; Meng et al., 2014; Shi et al., 2015a,c). Our results showed that drought induced the significant accumulation of ROS in the maize leaves as well as higher levels of EL and MDA, which are important oxidative-damage indicators of the integrity of cell membranes (Liu et al., 2015). However, exogenous melatonin treatment obviously alleviated oxidative damages of leaves, especially with the root-irrigation method, suggesting that melatonin application might effectively protect cell membranes against oxidative damages under drought stress. Melatonin is a lipophilic and hydrophilic molecule and can distribute in cytoplasm and lipid membranes (Angel, 2007). Melatonin, located in hydrophilic side of the lipid bilayer, prevents biological membrane from the lipid peroxidation by directly neutralizing the toxic reactants (Ceraulo et al., 1999; de Lima et al., 2010). Interestingly, the organization of melatonin in lipid membranes depends on its concentration. At low concentrations, the melatonin molecules arrange parallel to the lipid tails; in contrast, they arrange parallel to the bilayers at high concentrations (Dies et al., 2015). The location of melatonin in the lipid bilayer is speculated to monitor disordering in the hydrophobic tail of lipid bilayer.

Drought stress often leads to the instability of cell membranes in plants (Wang and Huang, 2004). Osmotic regulation is thought to be the most important basic response to drought stress (Ali et al., 2013). Soluble sugars and proline, as two key osmotic regulators, often increase in plants under drought stress (Xiong and Zhu, 2002), which were also confirmed in the present work. However, melatonin application significantly decreased proline and soluble sugar levels, especially with the root-irrigation method. Therefore, our results indicate that melatonin may maintain a positive turgor pressure to meet the water balance.

In addition, ROS could increase the permeability of cell membranes and subsequently result in cell death (Alvarez et al., 1998). Our result of trypan-blue staining indicated that exogenous melatonin application can effectively reduce cell death by scavenging ROS.

In order to reduce stress-triggered ROS accumulation, plants have developed a complex array of enzymatic and non-enzymatic defense systems against oxidative damages (de Souza et al., 2014). Many studies have found that antioxidant enzymatic activities could respond to osmotic stress (Chen et al., 2017), and exogenous melatonin application could regulate some antioxidant enzymatic activities to alleviate the stress-induced ROS burst in plants (Tan et al., 2000b; Shi et al., 2015a). Our results indicated that melatonin application promoted some antioxidant enzymatic activities of maize roots and leaves under the drought condition, especially with the root-irrigation method. Previous studies showed that application of exogenous melatonin could induce endogenous nitric oxide generation (Zhao et al., 2018), which has emerged as an important signaling molecule in plants, activating ROS scavenging enzymes under drought conditions (Kolbert et al., 2005). Meanwhile,

melatonin could decrease *miR398s* expression that could activate ROS scavenging enzyme gene expression, such as *Cu/Zn SOD* and *Mn SOD* (Gu et al., 2017). Thus, nitric oxide is required for melatonin-enhanced tolerance against abiotic stresses, which might down-regulate *miR398* expression to activate ROS scavenging enzymatic activities and promote the expression of related genes and finally scavenging intracellular ROS. Furthermore, the AsA-GSH cycle played an important role against oxidative damages in plants (Zhang et al., 2015). Melatonin could act as a bridge to contact water-soluble antioxidants (e.g., AsA, GSH, and NADPH) with lipid-soluble antioxidants (e.g., Ve) to forms an antioxidant network (Mahal et al., 1999; Tan et al., 2005). Previous studies showed that melatonin application could maintain higher levels of GSH and AsA (Wang et al., 2013a; Shi et al., 2015a). Consistent with these reports, our study suggested that AsA and GSH contents of leaves were markedly induced in melatonin-treated seedlings under the drought stress, although melatonin application decreased the GSH content of roots. These results suggested that melatonin can maintain tissular redox homeostasis through activating the antioxidative defense system and subsequently improve the drought resistance of maize seedlings. Yang et al. (2015) reported that the plants of the genus *Plantago* showed organ-specific responses to submergence stress at the level of ROS, non-enzymatic antioxidants and the activities of antioxidative enzymes. We found the leaves and roots of maize seedlings showed different responses to the drought stress.

The multicellular plant is an organic whole, and all the organs in plant are interrelated. Plants usually face with numerous environmental stresses during their growth, and the adaption to the varying circumstances in different organs or tissues of plant is not independent. The tissues of plants can respond to environmental stresses far away from the primary attacking organs, and these strategies are called “systemic acquired acclimation” (SAA) (Rossel et al., 2007; Burns et al., 2018). Our results indicated that the signal of exogenous melatonin could be transmitted across organs in plants. under drought stress, the exogenous melatonin applied to the roots could not only reduce the accumulation of ROS, affect antioxidative enzyme activities in roots, but also promote growth of the seedlings and improve photosynthesis in leaves. At the same time, the exogenous melatonin applied to the leaves not only reduced cell death and improved photosynthesis efficiency in leaves, but also affected the growth and metabolic activities in roots under drought stress.

In summary, the protective roles of melatonin with two different application methods to drought stress in both maize roots and leaves were investigated by comparing the antioxidative defense system, ROS accumulation levels and photosynthetic characteristics. Our results further demonstrated that the application of exogenous melatonin can alleviate the drought-induced damages and improve drought tolerance in plants through the activation of antioxidative defense systems and the elimination of ROS. Moreover, the melatonin application with the root irrigation showed more effective protective roles than the leaf-spraying method, and the signal of exogenous melatonin could be transmitted across organs in the plant.

DATA AVAILABILITY

All datasets for this study are included in the manuscript and the **Supplementary Files**.

AUTHOR CONTRIBUTIONS

SY, MY, and Y-EC conceived the study. BH, Y-QZ, C-BD, J-QL, CH, L-JZ, and Z-WZ performed the experiments and carried out the analysis. BH, MY, and Y-EC wrote the manuscript.

FUNDING

This work was supported by Sichuan Agricultural University.

REFERENCES

- Abedi, T., and Pakniyat, H. (2010). Antioxidant enzyme changes in response to drought stress in ten cultivars of oilseed rape (*Brassica napus* L.). *Czech J. Genet. Plant Breed.* 46, 27–34. doi: 10.17221/67/2009-CJGPB
- Afreen, F., Zobayed, S. M. A., and Kozai, T. (2006). Melatonin in *Glycyrrhiza uralensis*: response of plant roots to spectral quality of light and UV-B radiation. *J. Pineal Res.* 41, 108–115. doi: 10.1111/j.1600-079X.2006.00337.x
- Ali, B., Tao, Q., Zhou, Y., Gill, R. A., Ali, S., Rafiq, M. T., et al. (2013). 5-Aminolevulinic acid mitigates the cadmium-induced changes in *Brassica napus* as revealed by the biochemical and ultra-structural evaluation of roots. *Ecotoxicol. Environ. Saf.* 92, 271–280. doi: 10.1016/j.ecoenv.2013.02.006
- Alvarez, M. E., Pennell, R. I., Meijer, P. J., Ishikawa, A., Dixon, R. A., and Lamb, C. (1998). Reactive oxygen intermediates mediate a systemic signal network in the establishment of plant immunity. *Cell* 92, 773–784. doi: 10.1016/S0092-8674(00)81405-1
- Angel, C. (2007). The ability of melatonin to counteract lipid peroxidation in biological membranes. *Curr. Mol. Med.* 7, 638–649. doi: 10.2174/156652407782564444
- Balabusta, M., Szafranska, K., and Posmyk, M. M. (2016). Exogenous melatonin improves antioxidant defense in cucumber seeds (*Cucumis sativus* L.) germinated under chilling stress. *Front. Plant Sci.* 7:575. doi: 10.3389/fpls.2016.00575
- Burns, E. E., Barbara, K. K., Mohammed, Y. R., Bothner, B., and Dyer, W. E. (2018). Constitutive redox and phosphoproteome changes in multiple herbicide resistant *Avena fatua* L. are similar to those of systemic acquired resistance and systemic acquired acclimation. *J. Plant Physiol.* 220, 105–114. doi: 10.1016/j.jplph.2017.11.004
- Byeon, Y., Park, S., Kim, Y. S., Park, D. H., Lee, S., and Back, K. (2012). Light-regulated melatonin biosynthesis in rice during the senescence process in detached leaves. *J. Pineal Res.* 53, 107–111. doi: 10.1111/j.1600-079X.2012.00976.x
- Carrillo-Vico, A., Lardone, P. J., Álvarez-Sánchez, N., Rodríguez-Rodríguez, A., and Guerrero, J. M. (2013). Melatonin: buffering the immune system. *Int. J. Mol. Sci.* 14, 8638–8683. doi: 10.3390/ijms14048638
- Ceraulo, L., Ferrugia, M., Tesoriere, L., Segreto, S., Livrea, M. A., and Turco Liveri, V. (1999). Interactions of melatonin with membrane models: portioning of melatonin in AOT and lecithin reversed micelles. *J. Pineal Res.* 26, 108–120. doi: 10.1111/j.1600-079X.1999.tb00570.x
- Chen, Y. E., Cui, J. M., Li, G. X., Yuan, M., Zhang, Z. W., Yuan, S., et al. (2016a). Effect of salicylic acid on the antioxidant system and photosystem II in wheat seedlings. *Biol. Plant* 60, 139–147. doi: 10.1007/s10535-015-0564-4
- Chen, Y. E., Liu, W. J., Su, Y. Q., Cui, J. M., Zhang, Z. W., Yuan, M., et al. (2016b). Different response of photosystem II to short and long-term drought stress in *Arabidopsis thaliana*. *Physiol. Plant* 158, 225–235. doi: 10.1111/pp.12438

SUPPLEMENTARY MATERIAL

The Supplementary Material for this article can be found online at: <https://www.frontiersin.org/articles/10.3389/fpls.2019.00677/full#supplementary-material>

FIGURE S1 | Effect of exogenous melatonin on D1 under drought stress.

FIGURE S2 | Effect of exogenous melatonin on D2 under drought stress.

FIGURE S3 | Effect of exogenous melatonin on Lhcb1 under drought stress.

FIGURE S4 | Effect of exogenous melatonin on Lhcb2 under drought stress.

FIGURE S5 | Effect of exogenous melatonin on Lhcb3 under drought stress.

FIGURE S6 | Isolation of thylakoid membranes proteins by SDS-PAGE. Protein contained an equal amount of chlorophyll was loaded. SDS-PAGE stained with blue (CBS) are used as control.

- Chen, Y. E., Cui, J. M., Su, Y. Q., Zhang, C. M., Ma, J., Zhang, Z. W., et al. (2017). Comparison of phosphorylation and assembly of photosystem complexes and redox homeostasis in two wheat cultivars with different drought. *Sci. Rep.* 7:12718. doi: 10.1038/s41598-017-13145-1
- Daryanto, S., Wang, L., and Jacinthe, P. A. (2016). Global synthesis of drought effects on maize and wheat production. *PLoS One* 11:e0156362. doi: 10.1371/journal.pone.0156362
- de Lima, V. R., Caro, M. S., Munford, M. L., Desbat, B., Dufourc, E., Pasa, A. A., et al. (2010). Influence of melatonin on the order of phosphatidylcholine-based membranes. *J. Pineal Res.* 49, 169–175. doi: 10.1111/j.1600-079X.2010.00782.x
- de Pinto, M. C., Tommasi, F., and De Gara, L. (2000). Enzymes of the ascorbate biosynthesis and ascorbate-glutathione cycle in cultured cells of tobacco bright yellow 2. *Plant Physiol. Biochem.* 38, 541–550. doi: 10.1016/S0981-9428(00)00773-7
- de Souza, T. C., Magalhães, P. C., de Castro, E. M., Carneiro, N. P., Padilha, F. A., and Júnior, C. C. G. (2014). ABA application to maize hybrids contrasting for drought tolerance: changes in water parameters and in antioxidant enzyme activity. *Plant Growth Regul.* 73, 205–217. doi: 10.1007/s10725-013-9881-9
- Dies, H., Cheung, B., Tang, J., and Rheinstädter, M. C. (2015). The organization of melatonin in lipid membranes. *Biochim. Biophys. Acta* 1848, 1032–1040. doi: 10.1016/j.bbame.2015.01.006
- Dubbels, R., Reiter, R. J., Klenke, E., Goebel, A., Schnakenberg, E., Ehlers, C., et al. (1995). Melatonin in edible plants identified by radioimmunoassay and by high performance liquid chromatography-mass spectrometry. *J. Pineal Res.* 18, 28–31. doi: 10.1111/j.1600-079X.1995.tb00136.x
- Fan, J., Hu, Z., Xie, Y., Chan, Z., Chen, K., Amombo, E., et al. (2015). Alleviation of cold damage to photosystem II and metabolisms by melatonin in Bermudagrass. *Front. Plant Sci.* 6:925. doi: 10.3389/fpls.2015.00925
- Farooq, M., Wahid, A., Kobayashi, N., Fujita, D., and Basra, S. M. A. (2009). Plant drought stress: effects, mechanisms and management. *Agron. Sustain. Dev.* 29, 185–212. doi: 10.1051/agro:2008021
- Fristedt, R., Granath, P., and Vener, A. V. (2010). A protein phosphorylation threshold for functional stacking of plant photosynthetic membranes. *PLoS One* 5:e10963. doi: 10.1371/journal.pone.0010963
- García, J. J., López-Pingarrón, L., Almeida-Souza, P., Tres, A., Escudero, P., García-Gil, F. A., et al. (2014). Protective effects of melatonin in reducing oxidative stress and in preserving the fluidity of biological membranes: a review. *J. Pineal Res.* 56, 225–237. doi: 10.1111/jpi.12128
- Govindjee. (2004). “Chlorophyll a fluorescence: a bit of basics and history,” in *Chlorophyll Fluorescence: A Signature of Photosynthesis*, eds G. C. Papageorgiou and Govindjee (Dordrecht: Springer), 1–42.
- Gu, Q., Chen, Z. P., Yu, X. L., Cui, W. T., Pan, J. C., Zhao, G., et al. (2017). Melatonin confers plant tolerance against cadmium stress via the decrease of cadmium accumulation and reestablishment of microRNA-mediated redox homeostasis. *Plant Sci.* 261, 28–37. doi: 10.1016/j.plantsci.2017.05.001
- Han, Q. H., Huang, B., Ding, C. B., Zhang, Z. W., Chen, Y. E., Hu, C., et al. (2017). Effects of melatonin on anti-oxidative systems and photosystem ii in cold-stressed rice seedlings. *Front. Plant Sci.* 8:785. doi: 10.3389/fpls.2017.00785

- Hardeland, R., Madrid, J. A., Tan, D. X., and Reiter, R. J. (2012). Melatonin, the circadian multioscillator system and health: the need for detailed analyses of peripheral melatonin signaling. *J. Pineal Res.* 52, 139–166. doi: 10.1111/j.1600-079x.2011.00934.x
- Hattori, A., Migita, H., Iigo, M., Itoh, M., Yamamoto, K., Ohtani-Kaneko, R., et al. (1995). Identification of melatonin in plants and its effects on plasma melatonin levels and binding to melatonin receptors in vertebrates. *Biochem. Mol. Biol. Int.* 35, 627–634.
- Hillel, D., and Rosenzweig, C. (2002). Desertification in relation to climate variability and change. *Adv. Agron.* 77, 1–38. doi: 10.1016/s0065-2113(02)77012-0
- Jan, J. E., Reiter, R. J., Wasdell, M. B., and Bax, M. (2009). The role of the thalamus in sleep, pineal melatonin production, and circadian rhythm sleep disorders. *J. Pineal Res.* 46, 1–7. doi: 10.1111/j.1600-079x.2008.00628.x doi: 10.1111/j.1600-079x.2008.00628.x
- Jiang, C., Cui, Q., Feng, K., Xu, D., Li, C., and Zheng, Q. (2016). Melatonin improves antioxidant capacity and ion homeostasis and enhances salt tolerance in maize seedlings. *Acta Physiol. Plant* 38, 1–9. doi: 10.1007/s11738-016-2101-2
- Kaling, M., Kanawati, B., Ghirardo, A., Albert, A., Winkler, J. B., Heller, W., et al. (2015). UV-B mediated metabolic rearrangements in poplar revealed by non-targeted metabolomics. *Plant Cell Environ.* 38, 892–904. doi: 10.1111/pce.12348 doi: 10.1111/pce.12348
- Kar, R. K. (2011). Plant responses to water stress: role of reactive oxygen species. *Plant Signal. Behav.* 6, 1741–1745. doi: 10.4161/psb.6.11.17729
- Kato, Y., Sun, X., Zhang, L., and Sakamoto, W. (2012). Cooperative D1 degradation in the photosystem II repair mediated by chloroplastic proteases in *Arabidopsis*. *Plant Physiol.* 159, 1428–1439. doi: 10.1104/pp.112.199042
- Kolbert, Z., Bartha, B., and Erdei, L. (2005). Generation of nitric oxide in roots of *Pisum sativum*, *Triticum aestivum* and *Petroselinum crispum* plants under osmotic and drought stress. *Acta Biol. Szeged.* 49, 13–16.
- Lerner, A. B., Case, J. D., Takahashi, Y., Lee, T. H., and Mori, W. (1958). Isolation of melatonin, the pineal gland factor that lightens melanocytes. *J. Am. Chem. Soc.* 80, 2587–2587. doi: 10.1021/ja01543a060
- Li, T., Hu, Y., Du, X., Tang, H., Shen, C., and Wu, J. (2014). Salicylic acid alleviates the adverse effects of salt stress in *Torreya grandis* cv. Merrillii seedlings by activating photosynthesis and enhancing antioxidant systems. *PLoS One* 9:e109492. doi: 10.1371/journal.pone.0109492
- Li, C., Tan, D. X., Liang, D., Chang, C., Jia, D., and Ma, F. (2014). Melatonin mediates the regulation of ABA metabolism, free-radical scavenging, and stomatal behaviour in two *Malus* species under drought stress. *J. Exp. Bot.* 66, 669–680. doi: 10.1093/jxb/eru476
- Lin, A., Wang, Y., Tang, J., Xue, P., Li, C., Liu, L., et al. (2012). Nitric oxide and protein S-nitrosylation are integral to hydrogen peroxide-induced leaf cell death in rice. *Plant Physiol.* 158, 451–464. doi: 10.1104/pp.111.184531
- Liu, J., Wang, W., Wang, L., and Sun, Y. (2015). Exogenous melatonin improves seedling health index and drought tolerance in tomato. *Plant Growth Regul.* 77, 317–326. doi: 10.1007/s10725-015-0066-6
- López-Burillo, S., Tan, D. X., Rodríguez-Gallego, V., Manchester, L. C., Mayo, J. C., Sainz, R. M., et al. (2010). Melatonin and its derivatives cyclic 3-hydroxymelatonin, N1-acetyl-N2-formyl-5-methoxykynuramine and 6-methoxymelatonin reduce oxidative DNA damage induced by Fenton reagents. *J. Pineal Res.* 34, 178–184. doi: 10.1034/j.1600-079x.2003.00025.x
- Lu, C., and Zhang, J. (1999). Effects of water stress on photosystem II photochemistry and its thermostability in wheat plants. *J. Exp. Bot.* 50, 1199–1206. doi: 10.1093/jxb/50.336.1199
- Mahal, H. S., Sharma, H. S., and Mukherjee, T. (1999). Antioxidant properties of melatonin: a pulse radiolysis study. *Free Radic. Biol. Med.* 26, 557–565. doi: 10.1016/S0891-5849(98)00226-3
- Meng, J. F., Xu, T. F., Wang, Z. Z., Fang, Y. L., Xi, Z. M., and Zhang, Z. W. (2014). The ameliorative effects of exogenous melatonin on grape cuttings under water-deficient stress: antioxidant metabolites, leaf anatomy, and chloroplast morphology. *J. Pineal Res.* 57, 200–212. doi: 10.1111/jpi.12159
- Munné-Bosch, S., and Peñuelas, J. (2003). Photo- and antioxidative protection, and a role for salicylic acid during drought and recovery in field-grown *Phillyrea angustifolia* plants. *Planta* 217, 758–766. doi: 10.1007/s00425-003-1037-0
- Nakano, Y., and Asada, K. (1981). Hydrogen peroxide is scavenged by ascorbate-specific peroxidase in spinach chloroplasts. *Plant Cell Physiol.* 22, 867–880. doi: 10.1093/oxfordjournals.pcp.a076232
- Naranjo, B., Mignée, C., Krieger-Liszskay, A., Hornero-Méndez, D., Gallardo-Guerrero, L., Cejudo, F. J., et al. (2016). The chloroplast NADPH thioredoxin reductase C, NTRC, controls non-photochemical quenching of light energy and photosynthetic electron transport in *Arabidopsis*. *Plant Cell Environ.* 39, 804–822. doi: 10.1111/pce.12652
- Nishiyama, Y., Allakhverdiev, S. I., and Murata, N. (2006). A new paradigm for the action of reactive oxygen species in the photoinhibition of photosystem II. *Biochim. Biophys. Acta* 1757, 742–749. doi: 10.1016/j.bbabi.2006.05.013 doi: 10.1016/j.bbabi.2006.05.013
- Peleg, Z., and Blumwald, E. (2011). Hormone balance and abiotic stress tolerance in crop plants. *Curr. Opin. Plant Biol.* 14, 290–295. doi: 10.1016/j.pbi.2011.02.001
- Porra, R. J., Thompson, W. A., and Kriedemann, P. E. (1989). Determination of accurate extinction coefficients and simultaneous equations for assaying chlorophylls a and b extracted with four different solvents: verification of the concentration of chlorophyll standards by atomic absorption spectroscopy. *Biochim. Biophys. Acta* 975, 384–394. doi: 10.1016/S0005-2728(89)80347-0
- Posmyk, M. M., Kuran, H., Marciniak, K., and Janas, K. M. (2008). Presowing seed treatment with melatonin protects red cabbage seedlings against toxic copper ion concentrations. *J. Pineal Res.* 45, 24–31. doi: 10.1111/j.1600-079x.2007.00552.x
- Rahdari, P., and Hoseini, S. M. (2012). Effect of different levels of drought stress (PEG 6000 concentrations) on seed germination and inorganic elements content in purslane (*Portulaca oleraceae* L.) leaves. *J. Stress Physiol. Biochem.* 8, 51–61.
- Reiter, R. J. (1998). Oxidative damage in the central nervous system: protection by melatonin. *Prog. Neurobiol.* 56, 359–384. doi: 10.1016/S0301-0082(98)00052-5
- Reiter, R. J., Tan, D. X., and Fuentes-Broto, L. (2010). Melatonin: a multitasking molecule. *Prog. Brain Res.* 181, 127–151. doi: 10.1016/S0079-6123(08)10008-4
- Reiter, R. J., Tan, D. X., Terron, M. P., Flores, L. J., and Czarnecki, Z. (2007). Melatonin and its metabolites: new findings regarding their production and their radical scavenging actions. *Acta Biochim. Pol.* 54, 1–9.
- Ressmeyer, A. R., Mayo, J. C., Zelosko, V., Sáinz, R. M., Tan, D. X., Poeggeler, B., et al. (2003). Antioxidant properties of the melatonin metabolite N1-acetyl-5-methoxykynuramine (AMK): scavenging of free radicals and prevention of protein destruction. *Redox. Rep.* 8, 205–213. doi: 10.1179/135100003225002709
- Rossel, J. B., Wilson, P. B., Hussain, D., Woo, N. S., Gordon, M. J., Mewett, O. P., et al. (2007). Systemic and intracellular responses to photooxidative stress in *Arabidopsis*. *Plant Cell* 19, 4091–4110. doi: 10.1105/tpc.106.045898
- Sainju, U. M., Allen, B. L., Lenssen, A. W., and Ghimire, R. P. (2017). Root biomass, root/shoot ratio, and soil water content under perennial grasses with different nitrogen rates. *Field Crops Res.* 210, 183–191. doi: 10.1016/j.fcr.2017.05.029
- Sayfzadeh, S., and Rashidi, M. (2010). Effect of drought stress on antioxidant enzyme activities and root yield of sugar beet (*Beta vulgaris*). *Am. Euras. J. Agric. Environ. Sci.* 9, 223–230.
- Shi, H., Jiang, C., Ye, T., Tan, D. X., Reiter, R. J., Zhang, H., et al. (2015a). Comparative physiological, metabolomic, and transcriptomic analyses reveal mechanisms of improved abiotic stress resistance in bermudagrass [*Cynodon dactylon* (L.) Pers.] by exogenous melatonin. *J. Exp. Bot.* 66, 681–694. doi: 10.1093/jxb/eru373
- Shi, H., Qian, Y., Tan, D. X., Reiter, R. J., and He, C. (2015b). Melatonin induces the transcripts of CBF/DREB1s and their involvement in both abiotic and biotic stresses in *Arabidopsis*. *J. Pineal Res.* 59, 334–342. doi: 10.1111/jpi.12262
- Shi, H., Wang, X., Tan, D. X., Reiter, R. J., and Chan, Z. (2015c). Comparative physiological and proteomic analyses reveal the actions of melatonin in the reduction of oxidative stress in Bermuda grass (*Cynodon dactylon* (L.) Pers.). *J. Pineal Res.* 59, 120–131. doi: 10.1111/jpi.12246
- Sperdoui, I., and Moustakas, M. (2012). Differential response of photosystem II photochemistry in young and mature leaves of *Arabidopsis thaliana* to the onset of drought stress. *Acta Physiol. Plant* 34, 1267–1276. doi: 10.1007/s11738-011-0920-8
- Sturtz, M., Cerezo, A. B., Cantos-Villar, E., and Garcia-Parrilla, M. C. (2011). Determination of the melatonin content of different varieties of tomatoes (*Lycopersicon esculentum*) and strawberries (*Fragaria ananassa*). *Food Chem.* 127, 1329–1334. doi: 10.1016/j.foodchem.2011.01.093

- Tan, D.-X., Hardeland, R., Manchester, L. C., Korkmaz, A., Ma, S., Rosales-Corral, S. A., et al. (2012). Functional roles of melatonin in plants, and perspectives in nutritional and agricultural science. *J. Exp. Bot.* 63, 577–597. doi: 10.1093/jxb/err256
- Tan, D.-X., Manchester, L. C., Reiter, R. J., Plummer, B., Limson, J., Weintraub, S. T., et al. (2000a). Melatonin directly scavenges hydrogen peroxide: a potentially new metabolic pathway of melatonin biotransformation. *Free Radic. Biol. Med.* 29, 1177–1185. doi: 10.1016/S0891-5849(00)00435-4
- Tan, D.-X., Manchester, L. C., Reiter, R. J., Qi, W. B., Karbownik, M., and Calvo, J. R. (2000b). Significance of melatonin in antioxidative defense system: reactions and products. *Biol. Signal. Recept.* 9, 137–159. doi: 10.1159/000014635
- Tan, D.-X., Manchester, L. C., Sainz, R. M., Mayo, J. C., Leon, J., Hardeland, R., et al. (2005). Interactions between melatonin and nicotinamide nucleotide: NADH preservation in cells and in cell-free systems by melatonin. *J. Pineal Res.* 39, 185–194. doi: 10.1111/j.1600-079X.2005.00234.x
- Tan, D.-X., Manchester, L. C., Terron, M. P., Flores, L. J., and Reiter, R. J. (2007). One molecule, many derivatives: a never-ending interaction of melatonin with reactive oxygen and nitrogen species? *J. Pineal Res.* 42, 28–42. doi: 10.1111/j.1600-079X.2006.00407.x
- Wahid, A., and Rasul, E. (2005). “Photosynthesis in leaf, stem, flower, and fruit,” in *Handbook of Photosynthesis*, ed. M. Pessarakli (Florida: CRC Press), 479–497.
- Wang, C. Y. (1995). Effect of temperature preconditioning on catalase, peroxidase, and superoxide dismutase in chilled zucchini squash. *Postharvest. Biol. Tech.* 5, 67–76. doi: 10.1016/0925-5214(94)00020-S
- Wang, H. Z., Zhang, L. H., Ma, J., Li, X. Y., Li, Y., Zhang, R. P., et al. (2010). Effects of water stress on reactive oxygen species generation and protection system in rice during grain-filling stage. *Agr. Sci. China* 9, 633–641. doi: 10.1016/S1671-2927(09)60138-3
- Wang, P., Sun, X., Chang, C., Feng, F., Liang, D., Cheng, L., et al. (2013a). Delay in leaf senescence of *Malus hupehensis* by long-term melatonin application is associated with its regulation of metabolic status and protein degradation. *J. Pineal Res.* 55, 424–434. doi: 10.1111/jpi.12091
- Wang, P., Sun, X., Li, C., Wei, Z., Liang, D., and Ma, F. (2013b). Long-term exogenous application of melatonin delays drought-induced leaf senescence in apple. *J. Pineal Res.* 54, 292–302. doi: 10.1111/jpi.12017
- Wang, Z., and Huang, B. (2004). Physiological recovery of Kentucky bluegrass from simultaneous drought and heat stress. *Crop Sci.* 44, 1729–1736. doi: 10.2135/cropsci2004.1729
- Wei, W., Li, Q. T., Chu, Y. N., Reiter, R. J., Yu, X. M., Zhu, D. H., et al. (2015). Melatonin enhances plant growth and abiotic stress tolerance in soybean plants. *J. Exp. Bot.* 66, 695–707. doi: 10.1093/jxb/eru392
- Xiong, L., and Zhu, J. K. (2002). Molecular and genetic aspects of plant responses to osmotic stress. *Plant Cell Environ.* 25, 131–139. doi: 10.1046/j.1365-3040.2002.00782.x
- Yang, F., Han, C. Y., Li, Z., Guo, Y. N., and Chan, Z. L. (2015). Dissecting tissue- and species-specific responses of two *Plantago* species to waterlogging stress at physiological level. *Environ. Exp. Bot.* 109, 177–185. doi: 10.1016/j.envexpbot.2014.07.011
- Ye, J., Wang, S., Deng, X., Yin, L., Xiong, B., and Wang, X. (2016). Melatonin increased maize (*Zea mays* L.) seedling drought tolerance by alleviating drought-induced photosynthetic inhibition and oxidative damage. *Acta Physiol. Plant* 38, 1–13. doi: 10.1007/s11738-015-2045-y
- Ye, T., Shi, H., Wang, Y., and Chan, Z. (2015). Contrasting changes caused by drought and submergence stresses in bermudagrass (*Cynodon dactylon*). *Front. Plant Sci.* 6:951. doi: 10.3389/fpls.2015.00951
- Yin, L., Wang, P., Li, M., Ke, X., Li, C., Liang, D., et al. (2013). Exogenous melatonin improves *Malus* resistance to Marssonina apple blotch. *J. Pineal Res.* 54, 426–434. doi: 10.1111/jpi.12038
- Zhang, N., Sun, Q., Zhang, H., Cao, Y., Weeda, S., Ren, S., et al. (2015). Roles of melatonin in abiotic stress resistance in plants. *J. Exp. Bot.* 66, 647–656. doi: 10.1093/jxb/eru336
- Zhang, N., Zhao, B., Zhang, H. J., Weeda, S., Yang, C., Yang, Z. C., et al. (2013). Melatonin promotes water-stress tolerance, lateral root formation, and seed germination in cucumber (*Cucumis sativus* L.). *J. Pineal Res.* 54, 15–23. doi: 10.1111/j.1600-079X.2012.01015.x
- Zhao, G., Zhao, Y. Y., Yu, X. L., Kiprotich, F., Han, H., Guan, R. Z., et al. (2018). Nitric oxide is required for melatonin-enhanced tolerance against salinity stress in rapeseed (*Brassica napus* L.) Seedlings. *Int. J. Mol. Sci.* 19:e1912. doi: 10.3390/ijms19071912
- Zhao, H., Su, T., Huo, L., Wei, H., Jiang, Y., Xu, L., et al. (2015). Unveiling the mechanism of melatonin impacts on maize seedling growth: sugar metabolism as a case. *J. Pineal Res.* 59, 255–266. doi: 10.1111/jpi.12258
- Zheng, X. D., Tan, D.-X., Allan, A. C., Zuo, B., Zhao, Y., Reiter, R. J., et al. (2017). Chloroplastic biosynthesis of melatonin and its involvement in protection of plants from salt stress. *Sci. Rep.* 7:41236. doi: 10.1038/srep41236
- Zhou, X., Zhao, H., Cao, K., Hu, L., Du, T., Baluška, F., et al. (2016). Beneficial roles of melatonin on redox regulation of photosynthetic electron transport and synthesis of D1 protein in tomato seedlings under salt stress. *Front. Plant Sci.* 7:1823. doi: 10.3389/fpls.2016.01823
- Zlatev, Z. S., and Yordanov, I. T. (2004). Effects of soil drought on photosynthesis and chlorophyll fluorescence in bean plants. *Bulg. J. Plant Physiol.* 30, 3–18.

Conflict of Interest Statement: The authors declare that the research was conducted in the absence of any commercial or financial relationships that could be construed as a potential conflict of interest.

Copyright © 2019 Huang, Chen, Zhao, Ding, Liao, Hu, Zhou, Zhang, Yuan and Yuan. This is an open-access article distributed under the terms of the Creative Commons Attribution License (CC BY). The use, distribution or reproduction in other forums is permitted, provided the original author(s) and the copyright owner(s) are credited and that the original publication in this journal is cited, in accordance with accepted academic practice. No use, distribution or reproduction is permitted which does not comply with these terms.



Phenotyping Plant Responses to Biotic Stress by Chlorophyll Fluorescence Imaging

María Luisa Pérez-Bueno *, Mónica Pineda and Matilde Barón

Department of Biochemistry and Molecular and Cell Biology of Plants, Estación Experimental del Zaidín, Consejo Superior de Investigaciones Científicas, Granada, Spain

OPEN ACCESS

Edited by:

Angeles Calatayud,
Instituto Valenciano de
Investigaciones Agrarias, Spain

Reviewed by:

Pedro Carrasco,
University of Valencia, Spain
Andrés Gárriz,
CONICET Institute of
Biotechnological Research
(IIB-INTECH), Argentina

*Correspondence:

María Luisa Pérez-Bueno
marisa.perez@eez.csic.es

Specialty section:

This article was submitted to
Technical Advances in Plant Science,
a section of the journal
Frontiers in Plant Science

Received: 07 June 2019

Accepted: 16 August 2019

Published: 18 September 2019

Citation:

Pérez-Bueno ML, Pineda M and
Barón M (2019) Phenotyping Plant
Responses to Biotic Stress by
Chlorophyll Fluorescence Imaging.
Front. Plant Sci. 10:1135.
doi: 10.3389/fpls.2019.01135

Photosynthesis is a pivotal process in plant physiology, and its regulation plays an important role in plant defense against biotic stress. Interactions with pathogens and pests often cause alterations in the metabolism of sugars and sink/source relationships. These changes can be part of the plant defense mechanisms to limit nutrient availability to the pathogens. In other cases, these alterations can be the result of pests manipulating the plant metabolism for their own benefit. The effects of biotic stress on plant physiology are typically heterogeneous, both spatially and temporarily. Chlorophyll fluorescence imaging is a powerful tool to mine the activity of photosynthesis at cellular, leaf, and whole-plant scale, allowing the phenotyping of plants. This review will recapitulate the responses of the photosynthetic machinery to biotic stress factors, from pathogens (viruses, bacteria, and fungi) to pests (herbivory) analyzed by chlorophyll fluorescence imaging both at the lab and field scale. Moreover, chlorophyll fluorescence imagers and alternative techniques to indirectly evaluate photosynthetic traits used at field scale are also revised.

Keywords: photosynthesis, quenching, plant pathogen, laser-induced fluorescence, sun-induced fluorescence, hyperspectral reflectance, vegetation indices

INTRODUCTION

Changes in red chlorophyll *a* fluorescence (Chl-F) emission after illumination of dark-adapted plants with photosynthetically active radiance (PAR) were first reported by Kautsky and Hirsch (1931). This Chl-F showed a high correlation with photosynthetic rates. Ever since then, this technique has been heavily exploited to monitor photosynthetic performance and stress in plants. Indeed, no investigation regarding the activity of photosynthesis seems complete without some Chl-F data (Baker, 2008; Murchie and Lawson, 2013). Moreover, the sensitivity of Chl-F to even minor alterations in plant metabolism makes this technique suitable to provide insight into plant-stress factor interactions. Finally, the development of instruments capable of imaging Chl-F has provided a powerful tool to resolve spatial heterogeneity of plant and leaf photosynthetic performance under stress conditions. Chlorophyll fluorescence imaging (Chl-FI) makes available a wealth of information on the timing and location of pathogen development as well as to understand the regulation of photosynthesis from leaf to crop scale (Rolfe and Scholes, 2010). Moreover, Chl-FI is often included in phenomics together with metabolomics, genomics, transcriptomics, and proteomics. Indeed, Mir et al. (2019) have recently reviewed the high-throughput phenotyping platforms equipped with Chl-FI devices.

The study of Chl-F kinetics provides information on the efficiency of photosystem II (PSII) following the model proposed by Butler (1978). Basically, the model establishes that photochemistry (the so-called photochemical quenching) competes with the processes of energy dissipation as Chl-F and heat (the

so-called non-photochemical quenching) for excitation energy in the antenna pigments of PSII. Thus, to analyze the photosynthetic performance of a sample from Chl-FI measurements, it is necessary to differentiate between the photochemical and non-photochemical components of quenching. The usual approach is to transiently reduce to zero the photochemistry component using saturating light flashes, so that the Chl-FI yield in the presence of the non-photochemical quenching alone can be estimated (Maxwell and Johnson, 2000).

The most commonly used Chl-F parameters related with photosynthetic activity are summarized in **Table 1**. In general terms, plants respond to stress conditions activating acclimation mechanisms to adjust the machinery to the new environment with the aim of maintaining the photosynthetic activity. It might include the increase in the capacity for energy dissipation, detected by increases in non-photochemical quenching (measured as NPQ and qN) with no alterations in maximum quantum efficiency of PSII (F_v/F_m). When the stress overcomes the capacity of acclimation, permanent photoinhibition occurs and can be detected by decreases in F_v/F_m . When stress is strong or prolonged enough, the effective quantum yield of PSII (Φ_{PSII}) and the photochemical quenching (qP) decrease, meaning an inhibition of the electron transport chain. This inhibition of the light-dependent reactions can be accompanied by an increase in NPQ and qN. However, severe stress conditions might cause a severe loss of functionality of the PSII, and these three parameters would decrease (Horton et al., 2008; Murchie and Lawson, 2013). In the following sections, alterations in Chl-F parameters for individual host-pathogen systems will be described in more detail.

This review addresses: (i) the different responses of the photosynthetic machinery to biotic stress factors—pathogens (viruses, bacteria, and fungi) and pests (herbivory and parasites)—analyzed by Chl-FI at lab scale and (ii) the different techniques based on Chl-F and alternatives that have been developed to investigate the photosynthetic performance in the field, with application to the diagnosis of biotic stress. Finally, prospects of Chl-F-based technologies applied to remote sensing and crop protection are discussed.

Abbreviations: APAR, absorbed photosynthetically active radiance; BD, 2R,3R-butanediol; cfu, colony forming units; Chl, chlorophyll; Chl-F, chlorophyll fluorescence; Chl-FI, chlorophyll fluorescence imaging; CMV, *Cucumber mosaic virus*; dpi, days post-inoculation; ETR, electron transport rate; Φ_{PSII} , effective quantum yield of photosystem II; FLD, Fraunhofer line depth; FLD3, Fraunhofer line depth based on three spectral bands; F_0 , minimum fluorescence in the dark-adapted state; F'_0 , minimum fluorescence in the light-adapted state; F_m , maximum fluorescence in the dark-adapted state; F'_m , maximum fluorescence in the light-adapted state; FRSIF, far-red solar-induced fluorescence; F_s , chlorophyll fluorescence at the light-adapted steady state; F_t , current fluorescence in the light-adapted state; F_v/F_m , maximum quantum yield of photosystem; GPP, gross primary production; hpi, hours post-inoculation; HR, hypersensitive response; ISR, induced systemic response; LICE, laser-induced chlorophyll fluorescence; LiDAR, Laser imaging detection and ranging; LIF, laser-induced fluorescence; LIFS, laser-induced fluorescence spectroscopy; LIFT, laser-induced fluorescence transients; NDVI, normalized difference vegetation index; NPQ, non-photochemical quenching; PAM, pulse-amplitude modulation; PAR, photosynthetically active radiance; PRI, physiological reflectance index; PSII, photosystem II; qN, non-photochemical quenching; qP, photochemical quenching; ROS, reactive oxygen species; RSiF, red solar-induced fluorescence; SiF, solar-induced fluorescence; SR, single ratio; TCV, *Turnip crinkle virus*; TMV, *Tobacco mosaic virus*; UAV, unmanned aerial vehicle; UCP, uncoupling protein; VI, vegetation index.

TABLE 1 | Chl-F parameters of common use in biotic stress detection. For further details, see Roháček and Barták (1999), Maxwell and Johnson (2000), and Murchie and Lawson (2013).

Chl-F parameters	Known as	Formula
Maximum quantum yield of PSII	F_v/F_m	$(F_m - F_0)/F_m$
Effective quantum yield of PSII	Φ_{PSII}	$(F'_m - F_0)/F'_m$
Photochemical quenching	qP	$(F'_m - F_0)/(F'_m - F'_0)$
Non-photochemical quenching	NPQ	$(F_m - F'_m)/F'_m$
	qN	$1 - (F'_m - F'_0)/(F_m - F_0)$

BIOTIC STRESS DETECTION AT LAB SCALE

Viruses

The study of the timing and location of viral diseases in host plants was one of the first applications of Chl-FI (Balachandran et al., 1994). Hence, a number of studies have also used Chl-FI to evaluate the effect of viruses on primary metabolism, linking those findings to other alterations in plant physiology. Photoinhibitory damage of symptomatic tissues but also in asymptomatic areas of the infected plants during pathogenesis has been widely demonstrated. Moreover, Chl-FI can be used for diagnostic purposes before the appearance of visible symptoms (Barón et al., 2016). It was the case of *Tobacco mosaic virus* (TMV)-infected tobacco plants (Chaerle et al., 2007). Before symptoms appeared, affected areas of infected leaves showed low Chl-F values and little quenching capacity upon exposure to actinic light. These regions subsequently showed chlorotic-mosaic symptoms induced by TMV (Balachandran et al., 1994). Zucchini cotyledons inoculated with *Cucumber mosaic virus* (CMV) also showed different regions with different intensities of Chl-F emission before symptoms appearance (Técsi et al., 1994). Authors demonstrated that regions with high ability of Chl-F quenching correlated with leaf areas where starch would accumulate 24 h later, thus concluding that those areas possessed high qP capacity. On the contrary, *Abutilon striatum* leaves infected with *Abutilon mosaic virus* showed impaired NPQ in infected tissues that accompanied symptom expansion rather than underlying alterations in plant carbohydrate status (Osmond et al., 1998; Lohaus et al., 2000). On the other hand, tobacco plants resistant to TMV displayed a presymptomatic increment of Chl-F which evolved to a lower intensity patch surrounded by a high Chl-F intensity halo. This leaf area corresponded to the region where a visible hypersensitive response (HR) developed later on (Chaerle et al., 2004). Moreover, the damage caused by the reactive oxygen species (ROS) in soybean leaves infected with *Soybean mosaic virus* spatially correlated with decreases in Φ_{PSII} , showing a negative trend of their respective relationship, as well (Aldea et al., 2006a). An spatial correlation between the Chl-FI (either increased NPQ or Chl-F at high excitation light) pattern and viral distribution was also found in asymptomatic *Nicotiana benthamiana* leaves infected with the Italian and the Spanish strains of the *Pepper mild mottle virus* (PMMoV) (Chaerle et al., 2006; Pérez-Bueno et al., 2006). This effect took place progressively in each downstream leaf invaded by PMMoV (Pineda et al., 2011). Therefore, Chl-FI proved to be an outstanding method for real-time tracking of viral movement in the host plant. In contrast, symptomatic leaves of pepper plants

harboring the L3 resistant gene and inoculated with PMMoV showed decreased values of NPQ. The inoculation of the same pepper plants with the *Obuda pepper virus* led to an increase in F_v/F_m , Φ_{PSII} , and NPQ in the areas adjacent to the infected ones (Rys et al., 2014). NPQ was also revealed as the most useful parameter to follow the infection caused by *Potato virus Y* in wild type and transgenic tobacco plants overproducing endogenous cytokinins; nevertheless, the viral-induced Chl-FI alterations were no presymptomatic in this pathosystem (Spoustova et al., 2013). Also coinciding with symptoms appearance, photosynthetic alterations in pea leaves infected by *Pea enation mosaic virus* consisted in a decrease of Φ_{PSII} together with an increase of NPQ (Kyseláková et al., 2011).

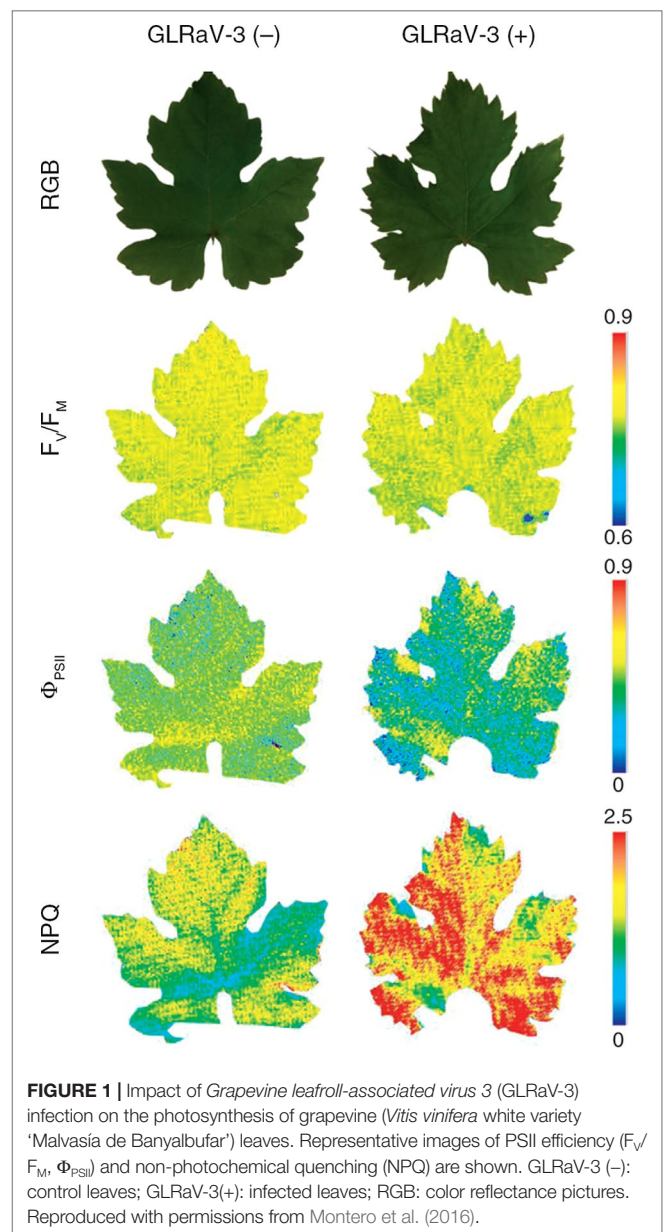
Chl-FI has also been used to assess the effect of mutations in the photosynthesis of virus-infected plants. Golden2-like (GLKs) transcription factors, with an unclear involvement in plant resistance to virus, play important roles in regulation of photosynthesis-associated nuclear genes in *Arabidopsis*, participating also in development of chloroplast. Double mutants of GLKs resulted more susceptible to CMV infection and showed decreased F_v/F_m and Φ_{PSII} when compared either to the controls or to the single mutants. These results suggested that, in *Arabidopsis*, GLK1 and GLK2 might play redundant roles in virus resistance (Han et al., 2016). Similarly, the uncoupling protein (UCP), member of the plant mitochondrial energy dissipation pathway (which coordinates cellular energy metabolism), might play a role in the resistance to *Turnip crinkle virus* (TCV) infection in *Arabidopsis*. In fact, the decline in Φ_{PSII} values registered on TCV-infected wild-type plants were lower compared to the drop recorded when measuring the same parameter in *ucp1*- or *ucp2*-deficient TCV-infected plants (Pu et al., 2016).

The combination of Chl-FI with other biochemical techniques can provide more insights about plant metabolism under viral infections. For example, metabolomics studies were carried out in combination with Chl-FI to estimate the alterations in the primary metabolism of grapevine upon infection with *Grapevine leafroll-associated virus 3* (Montero et al., 2016). The F_v/F_m , Φ_{PSII} , and NPQ parameters showed photoinhibition of PSII in infected plants (Figure 1). Moreover, the increase in NPQ correlated with a decrease in the accumulation of some photorespiratory intermediates in infected plants. Several omics have also been used along with Chl-FI to evaluate the beneficial trade-offs from viral infections against drought (Aguilar et al., 2017).

Occasionally, standard Chl-FI parameters do not always offer clear differences between healthy and infected tissues, or do so at late stages of the disease. In these cases, it is necessary to apply other mathematical tools to enhance such differences in the early stages of the infection. Combinatorial imaging analysis is an advance statistical approach rendering parameters with no physiological meaning, which in turn offers the highest contrast between treatments. As an example, combinatorial imaging revealed the infection caused by PMMoV in asymptomatic leaves of *N. benthamiana* plants earlier than standard Chl-FI parameters, even before than viral capsid can be detected by immunodetection in those leaves (Pineda et al., 2008).

Bacteria

Although bacterial diseases cause important economic losses in agriculture worldwide, fewer works have applied Chl-FI to



study the impact of bacterial infection, compared to other types of pathogens. A number of them are focused on the effect of virulent or avirulent pathovars of *Pseudomonas syringae*, causing systemic infection or HR, respectively. Soybean plants infected with an avirulent strain of *P. syringae* pv. *glycinea* showed lowered values of F_v/F_m and Φ_{PSII} , as well as an increase in NPQ, prior to the development of symptoms. However, little changes were observed in plants infected with a virulent strain (Zou et al., 2005). On the other hand, *Arabidopsis* plants displayed lower values of F_v/F_m , Φ_{PSII} , and NPQ when infected with either a virulent or an avirulent *P. syringae* pv. *tomato* (Pto) strain (Bonfig et al., 2006). The same pathosystem was analyzed by combinatorial imaging to obtain images of Chl-FI parameters with no physiological meaning, but with high-resolving power to identify infected leaf areas earlier than Chl-FI standard parameters. The symptoms

visualized by combinatorial imaging were stronger in the plants infected with the avirulent strain than in those inoculated with the virulent one. Moreover, the applied algorithms were also able to identify Chl-FI signatures characterizing early and late phases of the infection (Matouš et al., 2006; Berger et al., 2007). In bean plants, *P. syringae* pv. *phaseolicola* (Pph) causes a compatible infection, whereas Pto produces an HR. Using an inoculum concentration resembling those encountered in the field (10^4 colony forming units [cfu]·ml⁻¹), Pto-infected plants presented little Chl-FI changes respecting to the controls. However, NPQ maximized the differences between control and Pph-infected plants at 5 days post-inoculation (dpi), before symptoms appearance, in both infiltrated and non-infiltrated areas of the bean leaf. Moreover, the decrease in NPQ values in the non-infiltrated leaf areas inversely correlated to the cfu isolated from those leaf areas (Rodríguez-Moreno et al., 2008). However, when infiltrating leaves with a higher inoculum dose (10^7 cfu·ml⁻¹), alterations caused by Pto and Pph infections on bean photosynthesis could be detected at earlier time points: at 3 and 6 hours post-infection (hpi), respectively. Decreases in F_v/F_m and Φ_{PSII} and increases in NPQ were measured at those time points. At later stages of the compatible infection, NPQ started to diminish in the inoculated areas, whereas the development of chlorosis in non-inoculated zones was preceded by increases in NPQ values. It was hypothesized that as the leaf tissue is progressively colonized by the pathogen, an increment of NPQ occurs, followed by a decline in the activity of the thylakoid as

soon as the total viable count reaches a certain concentration (Pérez-Bueno et al., 2015).

The infection caused by the necrotrophic bacteria *Dickeya dadantii* has also been subject of study by Chl-FI. In the case of *N. benthamiana* plants, inoculations at high dose of inoculum seemed to overcome plant defense capacity, whereas plant inoculated at low dose did not show tissue maceration, and bacterial growth was inhibited. The extent and timing of changes in photosynthesis measured by Chl-FI parameters was dose-dependent, taking place earlier in the high-dose-infected leaves. Tissues surrounding inoculated areas of low-dose-infected leaves showed increased reversible NPQ as well as decreased values of F_v/F_m and Φ_{PSII} . Since reversible NPQ is actively controlled by the plant, it was proposed that this protective mechanism against photoinhibition was positively enhanced by the plant as part of the defense response (Pérez-Bueno et al., 2016). In the case of *D. dadantii*-melon-infected plants, Chl-FI detected decreased values of F_v/F_m and NPQ in the whole leaf. The magnitude of these changes was more pronounced upon infection with high bacterial dose (Figure 2). In combination with multicolor fluorescence imaging and thermography, data obtained by Chl-FI were used to feed classificatory algorithms able to distinguish between healthy and infected plants at high accuracy. Those mathematical models based on data from infiltrated areas were susceptible to apply to whole leaves, offering a high performance of classification (Pineda et al., 2018). An image analysis procedure for quantifying the leaf area impacted by *Xanthomonas fuscans*

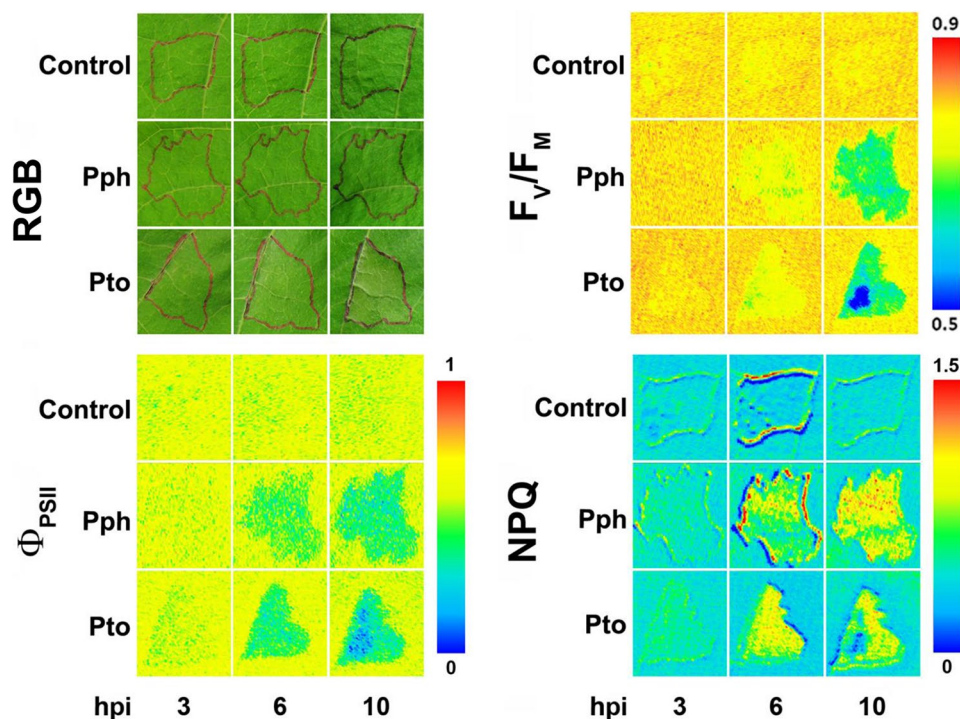


FIGURE 2 | Symptoms evolution in bean leaves infiltrated either with *Pseudomonas syringae* pv. *phaseolicola* (Pph) or pv. *tomato* (Pto) at high dose (10^7 cfu·ml⁻¹), compared with control leaves (RGB panel). Infiltrated areas are marked in black. Representative measurements of short-term effect of bacterial infection on photosynthesis, analyzed in terms of PSII efficiency (F_v/F_m and Φ_{PSII} panels) and non-photochemical quenching (NPQ panel). hpi, hours post-infection. Modified from Pérez-Bueno et al. (2015) with permissions.

subsp. *fuscans* has also been developed. F_v/F_m was the parameter used to presymptomatically diagnose the infection caused by this pathogen on bean leaves. The segmentation of F_v/F_m images aimed to quantify disease severity by a thresholding approach (Rousseau et al., 2013). On the other hand, *Xanthomonas oryzae* pv. *oryzae* infection (bacterial blight) in rice causes inhibition of photosynthesis and could be detected by a decrease in F_v/F_m , Φ_{PSII} , and F_t (Šebela et al., 2018).

PsbS, key for the NPQ mechanism, was one of the few photosynthetic proteins that rapidly decreased in abundance in cell cultures of *Arabidopsis* after treatment with a peptide derived from the bacterial motor protein flagellin (flg22). The registered decrease in NPQ values in samples treated with flg22 was dose-dependent. Thus, NPQ was proposed to be a positive regulator of pathogen-associated molecular pattern-triggered immunity (Göhre et al., 2012). Plants overexpressing bacterial outer surface protein A in their chloroplast have also been subject of study by Chl-FI. Transplastomic lines were unable to grow autotrophically and required the supply of exogenous sugars. Therefore, they suffered from photosynthesis impairment that could be measured as decreases in both F_v/F_m and Φ_{PSII} when transferred from sugar-supplemented culture medium into soil (Hennig et al., 2007).

Fungi and Oomycetes

Among the different biotic stresses, infections caused by fungi and oomycetes are the diseases most widely studied by Chl-FI. The photosynthetic performance of both oomycetes- and fungi-infected plants usually presents complex spatial and temporal patterns (Barón et al., 2016). It is so because infected leaves usually consist of regions of cells directly colonized by the pathogen surrounded by apparently healthy areas and remote regions (Scholes and Rolfe, 1996; Osmond et al., 1998; Chou et al., 2000; Meyer et al., 2001). The way fungi and oomycetes interacts with their host plant depends on the lifestyle of the pathogen: biotrophic, necrotrophic, and hemibiotrophic.

Biotrophic Fungi and Oomycetes

Typically, biotrophic organisms lower the rate of leaf photosynthesis of their compatible hosts. Oat leaves infected with the fungus *Puccinia coronata* displayed lower Φ_{PSII} values than the controls, whereas non-qP, measured as qN, increased from 8 dpi (Scholes and Rolfe, 1996). The oomycetes *Albugo candida* progressively decreased Φ_{PSII} while NPQ increased, and F_v/F_m showed no changes in *Arabidopsis* leaves (Chou et al., 2000). The oomycete *Bremia lactucae* also caused a considerable patchy decrease of F_v/F_m in infected lettuce leaf discs (Bauriegel et al., 2014), as well as an increase in NPQ and a reduction in both Φ_{PSII} and F_v/F_m , associated to a decrease in Chl content (Prokopová et al., 2010). On the other hand, changes in Chl-FI parameters caused by the fungus *Podosphaera xanthii* in melon plants cannot be attributed to alterations in Chl content of leaves (Figure 3). These changes involved a decline in Φ_{PSII} , while NPQ increased and F_v/F_m did not display any changes in *P. xanthii*-infected melon leaves (Polonio et al., 2019). This is in accordance with previous results obtained for cucumber leaves infected with *P. xanthii*, which displayed a decrease in Φ_{PSII} several days

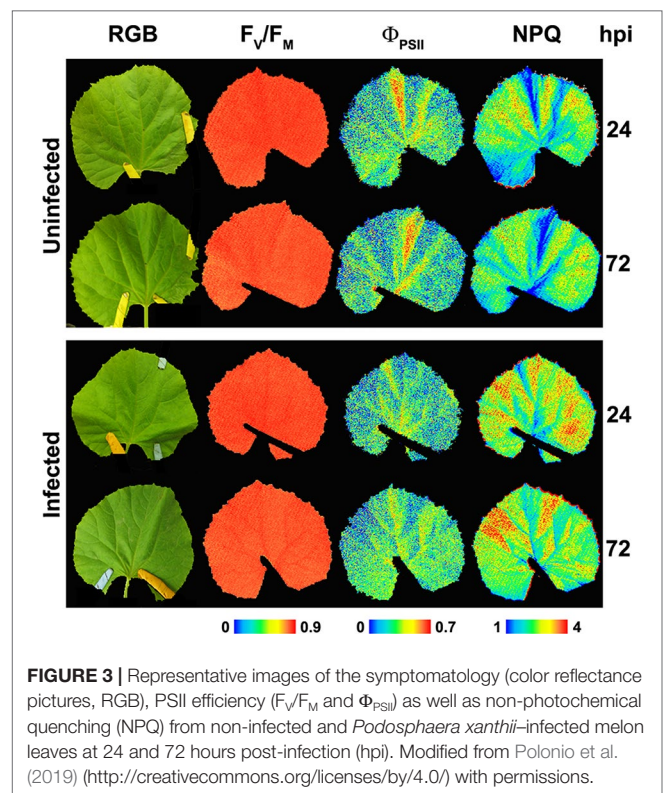


FIGURE 3 | Representative images of the symptomatology (color reflectance pictures, RGB), PSII efficiency (F_v/F_m and Φ_{PSII}) as well as non-photochemical quenching (NPQ) from non-infected and *Podosphaera xanthii*-infected melon leaves at 24 and 72 hours post-infection (hpi). Modified from Polonio et al. (2019) (<http://creativecommons.org/licenses/by/4.0/>) with permissions.

before a reduction in Chl content could be detected (Berdugo et al., 2014). The fungus *Erysiphe cichoracearum* also caused low Φ_{PSII} and high NPQ values in oak-infected leaves relative to the controls (Repka, 2002).

F_v/F_m was also used to diagnose several diseases, such as that caused by the fungus *Hemileia vastatrix* on coffee plants, since this parameter significantly correlated with visual severity of the infection (Honorato Júnior et al., 2015), and that caused by the endophytic fungus *Pestalotiopsis* spp. in cedar needles (Ning et al., 1995). Invasion of bean leaves by the rust fungus *Uromyces appendiculatus* was detected presymptomatically during the fluorescence induction kinetics as discreet areas of high Chl-F emission (coinciding with centers of subsequent lesion development) encircled by a halo of diminished emission relative to that of uninfected tissues (Peterson and Aylor, 1995). At the early stages of the *Plasmopara viticola* (oomycete)–grapevine interaction, F_v/F_m and Φ_{PSII} were identified as the most sensitive presymptomatic reporters of the infection, as their heterogeneous distribution on inoculated leaves was associated with the presence of developing mycelium (Cséfalvay et al., 2009).

The interaction of another biotrophic fungus, *Blumeria graminis*, and cereals has also been studied. In the case of wheat, this fungal infection can be presymptomatically detected by Chl-FI as a reduction in F_v/F_m (Kuckenberg et al., 2009). On the other hand, this fungus reduced Φ_{PSII} and increased NPQ, whereas F_v/F_m only diminished in the latter stage of barley leaf infection (Brugger et al., 2018). It has been suggested that development of *B. graminis* haustoria and hyphae damages chloroplast structure in barley leaves, causing inhibition of

photosynthesis (measured as Φ_{PSII}) both in cells directly below fungal colonies and in adjacent cells when compared with non-inoculated leaves (Swarbrick et al., 2006).

Necrotrophic Fungi and Oomycetes

Regarding necrotrophic fungi, the effects of *Rhizoctonia solani* in the photosynthetic performance of rice only could be detected once the symptoms appeared. Both necrotic zone and adjoining lesion areas significantly reduced the NPQ values, whereas F_v/F_m values only decayed in the lesions compared to the control tissues (Ghosh et al., 2017). Cashew seedlings inoculated with two different isolates of *Lasiodiplodia theobromae* displayed significantly lower F_v/F_m values respecting to the controls, as well as decays in Φ_{PSII} and increases in NPQ values before any visual symptoms appeared. The photosynthetic perturbations were clearly noticeable in F_v/F_m images along the borders of leaves, spreading gradually into inner regions (Muniz et al., 2014). In the *Bipolaris sorokiniana*-infected leaves of susceptible wheat plants, there was a progressive decrease of photosynthesis (measured as F_v/F_m and Φ_{PSII}) correlated to the expansion of lesions, as well as to a progressive loss of Chl (Rios et al., 2017). The impact of *Ascochyta rabiei* fungus in chickpea leaves was assessed by the impairment of Φ_{PSII} on infected leaves, since this fungus altered source/sink relationships (Esfeld et al., 1995). F_v/F_m and Φ_{PSII} showed an inhibition of photosynthesis in the direct vicinity of the *Botrytis cinerea* infection sites of tomato leaves. At the same time, the primary metabolism is activated in circular areas surrounding the infection sites together with decreased values of NPQ in such areas. However, no alterations in the primary metabolism could be detected in the rest of the leaf tissue, farther away from the infection site (Berger et al., 2004). In contrast, *B. cinerea* caused a different Chl-FI spatial pattern on ice plants: while F_v/F_m diminished only in the infected areas, NPQ increased in the non-infected regions of the leaves (Sekulska-Nalewajko et al., 2019). Chl-FI was applied to evaluate the extent of the impact caused by different strains of *Pythium irregulare* Buisman in ginseng plants. Values of F_v/F_m significantly diminished relative to the controls only for leaves inoculated with the highest pathogenic strain assayed of this oomycete (Ivanov and Bernards, 2016). Other less common Chl-FI parameters could be good indicators of disease. That was the case of F_m/F_0 , F'_v/F'_m , and F'_v/F'_0 for the detection at early stages of the infection of avocado trees by the soil-borne fungus *Rosellinia necatrix*. However, F_v/F_m decreased dramatically only when the first symptoms appeared (Granum et al., 2015).

Hemibiotrophic Fungi

The interaction of several species of the hemibiotrophic fungal genus *Colletotrichum* with their host plants has also been studied by means of Chl-FI. The infection caused by *Colletotrichum orbiculare* in *N. benthamiana* plants can be visualized as presymptomatic decreases in the parameter F_v/F_m but late in the biotrophic phase (Tung et al., 2013). Based on the measured reductions in F_v/F_m and NPQ, and increases in the efficiency of PSII (measured as Φ_{PSII} and qP), the impact of the infection by *Colletotrichum truncatum* on the photosynthetic performance of the soybean leaflets was noticeable exclusively on the necrotic vein tissue, the only tissue colonized by the pathogen (Dias et al.,

2018). Bean leaves infected with *Colletotrichum lindemuthianum* registered a decreased photosynthetic activity in terms of Φ_{PSII} in green areas only during the necrotrophic stage of the infection; such inhibition of photosynthesis was more pronounced in the dark brown necrotic lesions (Meyer et al., 2001). For the system sugar beet–*Cercospora beticola*, spots of high intensity fluorescence emission developed presymptomatically in the areas where necrotic lesions would later develop (Chaerle et al., 2004). Distribution and progression of head blight disease (caused by fungi *Fusarium* spp.) in winter wheat ears can be determined using F_v/F_m , since values of this parameter clearly diminished in the single grains gradually colonized within the spikelets (Bauriegel et al., 2010; Bauriegel et al., 2011).

Other Studies on Fungal Infections

Chl-FI has been used to distinguish between compatible and incompatible fungus/oomycete-plant interactions, or to visualize the infection effects on plants with different degrees of susceptibility to the pathogen. A pixel-wise analysis of the parameter F_v/F_m could distinguish resistant and susceptible lettuce lines against the biotrophic oomycete *B. lactucae* (Bauriegel et al., 2014). Photosynthesis was reduced during an incompatible barley–*B. graminis* interaction, accompanied by an increase in NPQ. This effect was more evident in cells straight related with attempted penetration of the biotrophic fungus but also in neighboring cells (Swarbrick et al., 2006). The distribution pattern of both Φ_{PSII} and NPQ over the entire leaf of wild-type oak infected with *E. cichoracearum* is heterogeneous when compared to those displayed by a Chl-deficient mutant of oak with high resistance to this fungus. These patterns coincided with fungal distribution in the infected leaves (Repka, 2002). The photosynthetic performance of the *B. sorokiniana*-infected leaves measured in terms of F_v/F_m and Φ_{PSII} was dramatically impaired on the most susceptible wheat cultivar compared to a less susceptible cultivar (Rios et al., 2017).

The effects of fungal phytotoxins directly applied on leaves or fruits of susceptible plants could also be assessed by Chl-FI. Based on Kautsky kinetic measurements, an experimental algorithm was proposed to identify affected and unaffected leaves of both *Brassica napus* and *Sinapis alba* plants treated with destruxins produced by the fungus *Alternaria brassicae* (Soukupová et al., 2003). The same method was used to detect apple areas treated with roseotoxins (phytotoxin produced by *Trichothecium roseum*) from non-treated regions (Žabka et al., 2006).

Some substances can confer certain protection against fungal infection, and Chl-FI has been proved to be useful to evaluate the photosynthetic performance of treated-infected plants. The protective effect of magnesium (Tatagiba et al., 2016a) and silicon (Tatagiba et al., 2016b) against *Monographella albescens* infection in rice plants was reported as a lower decrease of both qP and Φ_{PSII} in those infected plants treated with either Mg or Si relative to non-treated-infected plants. 2R,3R-butanediol (BD) is a volatile organic compound able to elicit induced systemic resistance (ISR), and thus, to delay 24 h the necrosis development caused by in *C. orbiculare* infection in *N. benthamiana* plants. Chl-FI was used to determine the levels of damage in BD-treated plants relative to those where ISR was not elicited. F_v/F_m showed that BD treatment significantly

increased the amount of healthy tissue and diminished the extent of necrotic tissue (Tung et al., 2013). F_v/F_m also reported that the treatment with the fungicides epoxiconazole and pyraclostrobin decreased the symptoms produced by *H. vastatrix* on coffee leaves, since this parameter was shown to positively correlate to symptoms severity (Honorato Júnior et al., 2015).

Pests

Pests also cause severe economic losses in crop yield around the world. It includes insects and also weeds and parasitic plants, such as the *Orobanch* genus or the *Santalaceae* family. The effect of herbivory, and parasites to a lesser extent, on host photosynthesis has been analyzed by Chl-F.

Herbivore insects devour vast amounts of plant biomass each year. However, simply considering the quantity of tissue removed may undervalue their real impact on yield production, because often insect damages affect photosynthesis in remaining leaf tissues. This “indirect” effect on primary metabolism may be considerably greater than the direct removal of leaf area (Nabity et al., 2009). The mechanisms governing the spatial patterns of photosynthesis following herbivory have been explored by Chl-FI, among other imaging techniques. In the case of *Arabidopsis* leaves affected by the first and fourth instars of the lepidopteran *Trichoplusia ni*, the measured decrease in Φ_{PSII} inversely correlated with the percentage of area removed; however, the correlation was considerably greater for the first instar. This difference in correlation slope is probably related to the different way of instars to cause photoinhibitory damage in the remaining tissues. Lower values of Φ_{PSII} and F_v/F_m , as well as increases in NPQ registered in leaves eaten by fourth instars, were circumscribed to a thin band immediately adjacent to the hole, whereas those values for leaves damaged by first instars were altered also in the areas between some of the holes (Tang et al., 2006). A deeper analysis of the effect of the first instar on *Arabidopsis* leaves revealed that photosynthetic damage (measured as lower levels of Φ_{PSII} and F_v/F_m and increased NPQ) was most severe at the edge of holes but decreased inversely with the distance from them. Moreover, in portions of the leaf where the photosynthesis was depressed, the defense-related cinnamate-4-hydroxylase gene expression was upregulated, suggesting a trade-off between primary and secondary metabolisms (Tang et al., 2009). Moreover, the results obtained by Chl-FI highlighted the potential differences between the herbivory damages caused colony-reared and wild-caught larvae of the tobacco hornworm *Manduca sexta* in the ornamental plant *Datura wrightii*. Whereas herbivory by colony-reared larvae produces no significant changes in photosynthesis, wild larvae induced a fast and spreading decrease of Φ_{PSII} within minutes, in both eaten and uneaten leaves. NPQ was increased near the damage and increased progressively in distant areas of the leaf away from the wound (Barron-Gafford et al., 2012). Both Φ_{PSII} and F_v/F_m values also resulted diminished in the case *M. sexta*-damaged *Nicotiana attenuata* leaves, but not in those leaves attacked by the *Tupiocoris notatus* mirid bugs, which displayed no alterations in the photosynthetic activity. *T. notatus* is known to render the plant more resistance to other, more damaging, herbivores (Halitschke et al., 2011). The combination of Chl-FI with other techniques also demonstrated that the inhibition of photosynthesis in *M. sexta*-damaged *N. attenuata* leaves is mediated by the jasmonic acid defense signaling pathway (Nabity et al., 2013).

Plant parasites take nutrients, including photosynthate, from their host plants. In particular, parasitic plants can be holoparasites (non-photosynthetic), such as broomrapes (*Orobanch* sp.) and witchweeds (*Striga* sp.), or hemiparasitic plants like rattle (*Rhinanthus* sp.). Parasites can affect photosynthesis in different ways, depending on the interaction established between the parasite and the host plant. Few works have analyzed such effect by single point Chl-F measurements (Strong et al., 2000; Gurney et al., 2002; Cameron et al., 2008; Rodenburg et al., 2008), and even less by Chl-FI. Rousseau et al. (2015) reported the detection of the broomrape *Orobanch* *ramose*-infested *Arabidopsis* plants by a decline in qP and NPQ. There is also a lack of Chl-FI works studying the effect of parasitic nematodes. It was the case of sugar beet showing photoinhibition (detected as a decrease in F_v/F_m) when infested by *Heterodera schachtii* (Schmitz et al., 2006).

BIOTIC STRESS DETECTION IN HIGH-THROUGHPUT PLATFORMS AND AT FIELD SCALE

Crop improvement based on plant breeding needs of accurate phenotyping (Mir et al., 2019). Thus, there is an increasing interest from research institutions to develop systems for high-throughput plant phenotyping both at greenhouse and at field scale (Roitsch et al., 2019, and references therein). Although Chl-FI provides valuable information on photosynthetic activity and general fitness of plants, this type of system is not usually used on plant phenotyping. This is partly due to some technical limitations affecting the robustness and reproducibility, as reviewed by Li et al. (2014). The Chl-F at the scale of high-throughput platforms and field can be analyzed or derived by measurements with a variety of devices that can be classified by the type of light source used—artificial or solar—and by the environment-controlled vs. natural conditions (Figure 4), as described below.

Robotized Platforms for Plant Phenotyping Under Controlled Environmental Conditions

Automatized phenotyping platforms are developing quickly in recent years. In Europe, the European Infrastructure for Multi-Scale Plant Phenomics and Simulation (EMPHASIS), under the European Plant Phenotyping Network 2020 (ERRN2020), offers 145 facilities for phenotyping of plants under controlled conditions plus lean fields and intensive fields (<https://emphasis.plant-phenotyping.eu/database>). The North American High-Throughput Phenotyping (NAPPN) counts with 20 phenotyping platforms in Canada, USA, and Mexico. In the rest of the world, the main facilities are offered by the Australian Plant Phenomics Facility and the China Plant Phenotyping Network. For more complete information about worldwide available high-throughput plant phenotyping facilities/platforms and their services, please see Tschiersch et al. (2017) and Mir et al. (2019). There is also an increasing interest on low-cost (and “do it yourself”) sensor solutions (Roitsch et al., 2019). Wang et al. (2018) reported a monitoring system under controlled environmental conditions able to perform large-area Chl-FI and multispectral reflectance

imaging that allows not only a continuous monitoring of crop physiology but also the possibility of implementing automatic diagnosis of drought, nutrition deficiency, and infection with *B. cinerea*. In spite of the interest in phenotyping plants by Chl-FI in automatized platforms under controlled environmental conditions, there is a lack of studies addressing the effects of biotic stress on host-plant photosynthesis by such approach.

Remote and Proximal Sensing for Plant Stress Detection Under Natural Environments

Active Chl-F measurements have conventionally been measured upon excitation with artificial lighting systems, generally by lamps or LEDs. However, technical limitations make very difficult the measurement of Chl-F remotely, mainly for the analysis of quenching kinetics. This problem has been partially solved by the application of systems such as: laser-imaging detection and ranging systems (LiDAR), laser-induced fluorescence transients (LIFTs), and laser-induced fluorescence spectroscopy (LIFS). Alternatively, passive methodologies based on sun-induced fluorescence (SiF) have been developed to analyze photosynthetic activity at leaf and canopy level. Finally, the analysis of hyperspectral reflectance indices correlating with Chl-F parameters seems a promising tool. These sensors can be implemented on a wide range of remote sensing systems: (i) stationary, with sensors mounted on cranes, towers, or cables; (ii) vehicle-based sensors; (iii) robotic devices; (iv) drones (unmanned aerial vehicles, i.e., UAVs) or airplanes; and (v) moreover, satellite imagery could also be used to cover very large areas. However, the use of satellite sensors has been limited to regional scales due to their

low spatial resolution, making this approach not feasible for most crops (Gago et al., 2015; Smigaj et al., 2019).

Imaging of Chlorophyll Fluorescence Excited by Artificial Light Systems

Several studies have analyzed the photochemical activity under biotic stress in experimental plots by imaging PAM fluorimeters. The infection with *Phyllosticta* fungus on *Quercus velutina* and *Cercis canadensis* trees inhibited Φ_{PSII} on areas surrounding infection points without evidence of compensation for this decrease in the remaining tissue (Aldea et al., 2006b). On the contrary, the inhibition of PSII in areas of redbud and sweetgum trees affected by *Cercospora* was counteracted by an increase in the photosynthetic efficiency in the undamaged leaf tissue and in a halo surrounding lesions (McElrone et al., 2010). The effect of herbivory on photosynthesis has been analyzed in several studies. Aldea et al. (2006b) investigated the indirect effect of herbivory on Chl-F by performing feeding trials with the Polyphemus caterpillar *Antheraea polyphemus* Cramer. This work concluded that, of all classes of damage studied, galls had the largest halos of depressed PSII activity when normalized to the size of visible injury. Nabity et al. (2012) compared the indirect effect of different types of herbivory on photosynthesis of aspen and birch trees. This work showed that the PSII activity was inhibited in the undamaged tissue and concluded that elevated ambient CO_2 was related to a decrease in the transpiration rate of leaves and could indirectly reduce the effects of herbivory on photosynthesis. On the other hand, *P. viticola* caused a decrease in FV/FM in infected spots of susceptible grapevine leaves. Symptomatic and asymptomatic regions over a leaf could be discriminated by the spatial distribution of FV/FM (Šebela et al., 2014). Furthermore, the most destructive fungus for rice crops worldwide, *Magnaporthe oryzae*, could be detected as a decrease in Φ_{PSII} and F_v (Šebela et al., 2018). Other Chl-FI devices adapted for remote sensing can be found in the literature. Such is the case of the CropReporter, a CCD camera (coupled with LEDs to induce Chl-F transients) onboard the platform Field Scanalyzer (Virlet et al., 2017). This sensor allows monitoring plant growth, morphology, physiology, and plant fitness under natural conditions.

Alternatively to lamps and LEDs, other systems excite Chl-F by laser. Saito et al. (2002) reported a method for imaging Chl content on trees based on fluorescence measured by a LiDAR system. This approach can be used to analyze spatial distribution of green tissues providing a detailed 3-D model of the canopy. Furthermore, the photosynthetic activity can be measured at the whole plant and canopy level by scanning methods that use LIFTs, as previously reviewed by Omasa et al. (2006) and Fiorani et al. (2012). A terrestrial-adapted LIFT (mounted on a telescope or on a tower above the canopies) has demonstrated its potential in remote measurements of photosynthetic traits in cottonwood and oak trees (Kolber et al., 2005); avocado trees (Rascher and Pieruschka, 2008); limes, oaks, and pines (Pieruschka et al., 2014); as well as in barley and sugar beet (Raesch et al., 2014). The results were comparable to those obtained at leaf scale by the PAM system. Moreover, Osmond et al. (2017) developed a prototype of LIFT that induces a Chl-F transient by a series of short flashes in a saturation sequence and operates from up

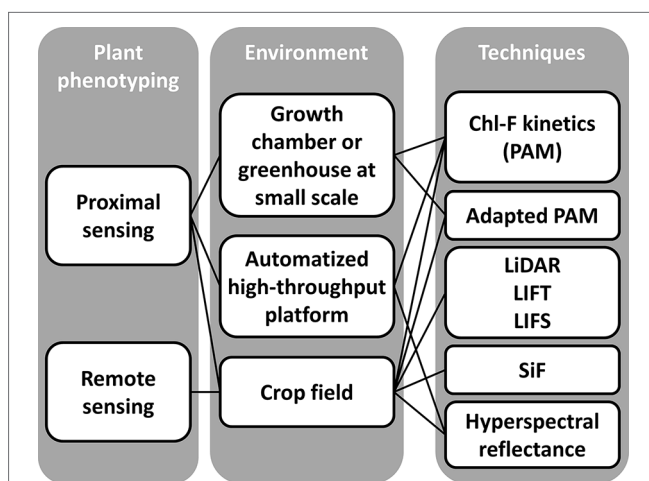


FIGURE 4 | Different approaches based on chlorophyll fluorescence imaging systems to plant phenotyping. The scales of analysis include: lab scale, high-throughput platforms under controlled environmental conditions, and field scale under natural environmental conditions. Techniques are grouped by the source of light used for the measurements: LEDs (PAM measurements), laser (LiDAR, LIFT, and LIFS), and natural light (SiF and hyperspectral reflectance on canopy surface).

to 2-m distance under ambient light, allowing the analysis of photosynthetic regulation at canopy scale during sun flecks in natural environments. More recently, a methodology using a portable LIFS system in combination with classifying algorithms allowed the presymptomatic detection of citrus trees affected by citrus greening, also called huanglongbing (Ranulfi et al., 2016). Although the use of laser-based measurements is well-established on remote sensing, the automated data processing and analysis need further development—for example, taking in account the effects of complex heterogeneous canopy structures on Chl-F parameters (Pieruschka et al., 2014; Roitsch et al., 2019).

Sun-Induced Fluorescence

A different approach for remote assessment of photosynthesis activity is based on remote measurements of steady-state Chl-F (noted either as Ft or Fs) induced by the sun, since it yields strong correlations with stomatal conductance and net CO₂ assimilation rate (Flexas et al., 2002). The SiF is retrieved from narrow spectral bands, whereas conventional PAM fluorescence is measured over broad spectral bands. Moreover, unlike PAM fluorescence, SiF is affected by environmental light but can be applied at leaf, canopy, and regional scale. The setups and methodologies for measuring SiF have been intensively reviewed by Aasen et al. (2019). The development of methods to measure steady-state SiF has been mainly focused on improving the retrieval of valid fluorescence values under natural illumination that correlate firstly with data obtained by conventional fluorimeters and secondly with parameters related to the CO₂ fixation rate.

SiF, emitted by Chl *a* in the broad-band-red and far-red regions of the spectrum near 683 and 736 nm, respectively (Joiner et al., 2016; Goulas et al., 2017), can be analyzed by hyperspectral cameras. Garzonio et al. (2017) developed an UAV system equipped with small hyperspectral cameras to measure the visible and near-infrared (VNIR) surface reflectance and SiF. This setup retrieved fluorescence in absolute units with a good spatial resolution. However, most works apply methods that can retrieve Chl-F at leaf to canopy level from data collected by high-resolution spectrometers. The Fraunhofer line depth (FLD) method, described by Plascyk and Gabriel (1975), has been used successfully to estimate SiF, demonstrating its correlation with Chl content or Φ_{PSII} (Tubuxin et al., 2015). Moreover, at seasonal time scales, SiF correlated with the electron transport rates (ETR) and constitutive heat dissipation (YNO) in avocado and orange jasmine orchards (Wyber et al., 2017). Several modifications to the method have been developed by other authors along the years. Thus, Maier et al. (2003) and Ni et al. (2015) published a modification of FLD based on three spectral bands named FLD3. Rascher et al. (2015) and Pinto et al. (2016) presented a new methodology based on FLD3 to estimate Φ_{PSII} , which was verified against the standard PAM method. SiF quantified by FLD3 was significantly associated with gross primary production (GPP) at ecosystem scale (Zarco-Tejada et al., 2013) and with leaf-level measurements of CO₂ assimilation (Zarco-Tejada et al., 2016). Indeed, Guanter et al. (2014) concluded that SiF data could contribute to improve global models for more accurate projections

of agricultural productivity and also to estimate climate impact on crop yields.

A step forward in the use of SiF for the estimation of GPP could be taken based on Goulas et al. (2017), who reported that SiF in the far red (FRSiF) yields a stronger correlation than the traditionally used SiF in the red region (RSiF) of the spectrum. Moreover, FRSiF provided a better estimation of GPP than greenness-based indices (Damm et al., 2015). These findings were corroborated by other authors (Joiner et al., 2016; Campbell et al., 2019). Similarly, Yang et al. (2018) used a singular vector decomposition method for the spectral range of 745 to 780 nm as a proxy for absorbed PAR (APAR) in rice paddies at diurnal and seasonal time scales. Also, Miao et al. (2018) found a strong and positive correlation between SiF and APAR for soybean. Nonetheless, it was suggested that only SiF correlates with ETR and the photosynthetic yield at large spatial scales (Du et al., 2017). The estimation of GPP based on SiF would need to take into account relevant environmental information to model the light use efficiency of photosynthesis (Yang et al., 2018), canopy structure, and competing energy pathways (Damm et al., 2015).

These SiF retrieval methods have been applied not only to UAV data but also to satellite data, including GOSAT, GOME-2, OCO-2, SCIAMACHY, and TanSat, as reviewed recently by Ni et al. (2019). Furthermore, the fluorescence explorer project (FLEX), currently held by the European Space Agency, is aiming to map vegetation fluorescence at high spatial resolution, leading to better insight into plant health and stress.

A different approach for stress detection could take advantage of the combination of SiF with different techniques. Rahimzadeh-Bajgiran et al. (2017) reported a FLD and laser-induced saturation pulse (FLD-LISP) method as a robust and accurate technique for the estimation of Chl-F parameters such as Φ_{PSII} , NPQ, and ETR, for several plant species. In parallel, a model based on measurements of two satellite detectors (SiF from Orbiting Carbon Observatory-2 and surface reflectance from the moderate resolution imaging spectroradiometer [MODIS]), provided a very sensitive indicator of drought (Zhang et al., 2018).

Until now, few studies have addressed the study of infections in the field by SiF. Hernández-Clemente et al. (2017) proposed a 3-D modelling approach that improved the correlation between the F_s at leaf level from ground data measurements and the image-based fluorescence inferred by FLD3. This work studied an oak forest (*Quercus ilex*) affected by water stress and *Phytophthora* infection. Their results lead to the conclusion that their model could make possible to map SiF for single-tree assessment of forest physiological condition offering the possibility of early disease detection. Raji et al. (2015) analyzed the infection of cassava plants by the *Cassava mosaic virus* by the FLD method, finding that the fluorescence ratio F687/F760 showed a good correlation with net photosynthesis rate, the Chl content, and the laser-induced Chl-F (LICF) ratio F685/F735 and that this parameter could be a good marker of early stress detection in crops and vegetation.

Reflectance Spectra for the Estimation of Chlorophyll Fluorescence Parameters

Measurements of Chl-F under natural environments are technically challenging, mainly by the difficulty of splitting fluorescence from reflectance. Strong efforts have been made to develop an alternative to Chl-F detection valid for remote sensing, based on the analysis of hyperspectral leaf reflectance spectra and derived vegetation indices (VIs). Hyperspectral reflectance is an imaging technique that allows the detection of plant stress in a non-invasive and objective way (Thomas et al., 2018).

Several VIs have been found to provide a good estimate for the efficiency of PSII on a wide range of plant species. The single ratio (SR) and the curvature index (CUR) were highly correlated with F_v/F_m (Jia et al., 2016). Peng et al. (2017) concluded that normalized difference vegetation index (NDVI) correlated with F_v/F_m only in non-stressed plants. In contrast, other authors reported no significant correlation between NDVI and Chl-F parameters (Jia et al., 2016). More promising is the estimation of Φ_{PSII} by VIs. PRI correlates positively with this Chl-F parameter at canopy level (Gamon et al., 1992; Naumann et al., 2008) and at the leaf level for different plant species (Gamon et al., 1997). The ETR could be also estimated by PRI at leaf scale; however, a PRI calibrated for the pigments content provided an even better estimation (Rahimzadeh-Bajgiran et al., 2012). Other VIs, such as the normalized multi-band drought index (NMDI) or the water band index (WBI), have also been found to correlate with F_v/F_m and Φ_{PSII} for a range of alpine sward species (Kycko et al., 2019). Furthermore, the maximum daily photosynthetic rate correlated with NDVI and SR (Gamon et al., 1995).

The capacity for energy dissipation at the PSII could also be estimated by several VIs across plant species. NPQ and the de-epoxidation state of the xanthophyll cycle (which controls NPQ) correlate negatively with PRI at canopy (Gamon et al., 1992) and leaf scale (Gamon et al., 1997; Van Gaalen et al., 2007; Rahimzadeh-Bajgiran et al., 2012; Alonso et al., 2017; Sancho-Knapik et al., 2018). More recently, the indices ΔPRI (which accounts for pigment composition in PRI) and the normalized difference spectral index (NDSI) were reported to estimate NPQ more accurately than PRI (Maimaitiyming et al., 2017; Kováč et al., 2018).

Particularly in recent years, several research groups have established correlations between new VIs and Chl-F parameters. The so-called fluorescence ratio indices R_{690}/R_{600} and R_{740}/R_{800} (being R_x the leaf reflectance at the wavelength x) were able to qualitatively track the leaf F_s in a grapevine canopy (Dobrowski et al., 2005). Zarco-Tejada et al. (2009) could retrieve the Chl-F signal from reflectance airborne measurements on olive, peach, and orange orchards, demonstrating the correlation between the retrieved Chl-F and in-field F_s measurements, the derivative index D_{702}/D_{680} (being the Dx the derivative of the reflectance at the wavelength x), and the reflectance indices R_{690}/R_{630} , $R_{761} - R_{757}$, and R_{761}/R_{757} . Similarly for rice plots, the parameters F_0 , F_m , and F_v/F_m could be monitored by the indices $(R_{680} - R_{935})/(R_{680} + R_{935})$ and R_{680}/R_{935} , while Φ_{PSII} and NPQ could be

estimated by the ratios $(R_{800} - R_{445})/(R_{800} - R_{680})$ and $(R_{780} - R_{710})/(R_{780} - R_{680})$, respectively (Zhang et al., 2011). In *Suaeda salsa* experimental plots, indices $(R_{680} - R_{935})/(R_{680} + R_{935})$ and R_{680}/R_{935} correlated with F_v/F_m , Φ_{PSII} , and qP , whereas $(R_{780} - R_{710})/(R_{780} - R_{680})$ correlated with NPQ (Zhang et al., 2012). Moreover, the first derivative of some spectral indices such as D_{705}/D_{722} and D_{730}/D_{706} strongly correlated with F_v/F_m (Jia et al., 2016). Also, indices using long-wave red edge and near-infrared reflectance (NDRE740 and CI740) probed to be adequate for the estimation of F_v/F_m (Peng et al., 2017).

The correlation between the VIs and the Chl-F parameters is however influenced by different factors (canopy structure, environmental conditions such as light, wind, etc.), limiting the scaling up from leaf to canopy level (Thomas et al., 2018). The resolution of the cameras and, in particular, the methodology for the analysis of data need to be improved in order to obtain more robust and accurate estimations of photosynthetic activity, GPP, and detection of plant stress for precision agriculture (Camino et al., 2018; Cendrero-Mateo et al., 2018).

CONCLUSIONS AND FUTURE OUTLOOK

Precision agriculture and plant breeding need of high-throughput imaging techniques to reach the main goal of a sustainable low-input management of crops. On this matter, Chl-FI is a very relevant technique, as a sensitive tool for monitoring crop performance and detection of plant stress. This approach has been applied extensively at lab scale on its own and also complemented with other imaging techniques and omics approaches. The implementation of Chl-FI to high-throughput scale, and particularly under natural light conditions, presented technical challenges partially solved by adapted imaging systems based on lamps, LEDs, or lasers. For high-throughput phenotyping, alternative techniques based on solar light might be advantageous over fluorescence imagers, obtaining high temporal and spatial resolution data. It includes the development of methodologies to retrieve SiF or to estimate photosynthetic parameters by hyperspectral reflectance as a more feasible alternative to Chl-FI in high-throughput platforms and crop fields for plant biotic stress detection and monitoring. However, up to date, there is still a lack of standardized methods to obtain Chl-F data showing high correlation with photosynthetic and crop yield traits under natural conditions. Ongoing research into this area will contribute to set up widely adopted standards that could be applied across crop species and agrosystems.

Nevertheless, the application of SiF and hyperspectral reflectance on plant phenotyping need of further research on the effects of environmental factors (i.e., incoming PAR, viewing solar geometry, direct-to-diffuse light ratios, air temperature, and wind), canopy heterogeneity, and architecture on the remote measurements. In this sense, advances have been made in the last year, developing 3D models of canopies at different spatial resolutions by a range of methodologies (Gastellu-Etcheberry et al., 2017; Janoutova et al., 2019; Roitsch et al., 2019). Particularly in the case of

hyperspectral reflectance, the applicability of spectral indices for predicting photosynthetic activity and GPP should be explored across different canopy types and temporal and spatial scales.

In the future, the routine programs to monitor crop fields should include Chl-F sensors but, most importantly, should make use of SiF and hyperspectral imagery, along with the widely used thermography to reach the final goal of a low-input highly efficient agriculture with minimal impact in the environment. Furthermore, high-throughput plant phenotyping platforms need of further development to overcome the economic constraints in their use, and to make of them easy-to-use reliable tools. Thus, low-cost and do-it-yourself platforms could be the best solution to achieve a

real impact on agricultural yields and natural environment protection across the world.

AUTHOR CONTRIBUTIONS

MP-B, MP and MB contributed to the writing up.

FUNDING

This work was supported by grants from CICE-Junta de Andalucía (P12-AGR-0370) and Ministerio de Ciencia, Innovación y Universidades (RTI2018-094652-B-I00).

REFERENCES

- Aasen, H., Van Wittenberghe, S., Medina, N. S., Damm, A., Goulas, Y., Wieneke, S., et al. (2019). Sun-induced chlorophyll fluorescence II: review of passive measurement setups, protocols, and their application at the leaf to canopy level. *Remote Sens.* 11, 33. doi: 10.3390/rs11080927
- Aguilar, E., Cutrona, C., del Toro, F. J., Vallarino, J. G., Osorio, S., Pérez-Bueno, M. L., et al. (2017). Virulence determines beneficial trade-offs in the response of virus-infected plants to drought via induction of salicylic acid. *Plant Cell Environ.* 40, 2909–2930. doi: 10.1111/pce.13028
- Aldea, M., Frank, T. D., and DeLucia, E. H. (2006a). A method for quantitative analysis of spatially variable physiological processes across leaf surfaces. *Photosynth. Res.* 90, 161–172. doi: 10.1007/s11120-006-9119-z
- Aldea, M., Hamilton, J. G., Resti, J. P., Zangerl, A. R., Berenbaum, M. R., Frank, T. D., et al. (2006b). Comparison of photosynthetic damage from arthropod herbivory and pathogen infection in understory hardwood saplings. *Oecologia* 149, 221–232. doi: 10.1007/s00442-006-0444-x
- Alonso, L., Van Wittenberghe, S., Amorós-López, J., Vila-Francés, J., Gómez-Chova, L., and Moreno, J. (2017). Diurnal cycle relationships between passive fluorescence, pri and npq of vegetation in a controlled stress experiment. *Remote Sens.* 9, 770. doi: 10.3390/rs9080770
- Baker, N. R. (2008). Chlorophyll fluorescence: a probe of photosynthesis *in vivo*. *Annu. Rev. Plant Biol.* 59, 89–113. doi: 10.1146/annurev.arplant.59.032607.092759
- Balachandran, S., Osmond, C. B., and Daley, P. F. (1994). Diagnosis of the earliest strain-specific interactions between *Tobacco mosaic virus* and chloroplasts of tobacco leaves *in vivo* by means of chlorophyll fluorescence imaging. *Plant Physiol.* 104, 1059–1065. doi: 10.1104/pp.104.3.1059
- Barón, M., Pineda, M., and Pérez-Bueno, M. L. (2016). Picturing pathogen infection in plants. *Z. Naturforsch. C. Biosci.* 71, 355–368. doi: 10.1515/znc-2016-0134
- Barron-Gafford, G. A., Rascher, U., Bronstein, J. L., Davidowitz, G., Chaszar, B., and Huxman, T. E. (2012). Herbivory of wild *Manduca sexta* causes fast down-regulation of photosynthetic efficiency in *Datura wrightii*: an early signaling cascade visualized by chlorophyll fluorescence. *Photosynth. Res.* 113, 249–260. doi: 10.1007/s11120-012-9741-x
- Bauriegel, E., Brabandt, H., Gärber, U., and Herppich, W. B. (2014). Chlorophyll fluorescence imaging to facilitate breeding of *Bremia lactucae*-resistant lettuce cultivars. *Comput. Electron. Agric.* 105, 74–82. doi: 10.1016/j.compag.2014.04.010
- Bauriegel, E., Giebel, A., and Herppich, W. B. (2010). Rapid *Fusarium* head blight detection on winter wheat ears using chlorophyll fluorescence imaging. *J. Appl. Bot. Food Qual.* 83, 196–203.
- Bauriegel, E., Giebel, A., and Herppich, W. B. (2011). Hyperspectral and chlorophyll fluorescence imaging to analyse the impact of *Fusarium culmorum* on the photosynthetic integrity of infected wheat ears. *Sensors (Basel)* 11, 3765–3779. doi: 10.3390/s110403765
- Berdugo, C. A., Zito, R., Paulus, S., and Mahlein, A. K. (2014). Fusion of sensor data for the detection and differentiation of plant diseases in cucumber. *Plant Pathol.* 63, 1344–1356. doi: 10.1111/ppa.12219
- Berger, S., Benediktyová, Z., Matouš, K., Bonfig, K., Mueller, M. J., Nedbal, L., et al. (2007). Visualization of dynamics of plant–pathogen interaction by novel combination of chlorophyll fluorescence imaging and statistical analysis: differential effects of virulent and avirulent strains of *P. syringae* and of oxylipins on *A. thaliana*. *J. Exp. Bot.* 58, 797–806. doi: 10.1093/jxb/erl208
- Berger, S., Papadopoulos, M., Schreiber, U., Kaiser, W., and Roits, T. (2004). Complex regulation of gene expression, photosynthesis and sugar levels by pathogen infection in tomato. *Physiol. Plant.* 122, 419–428. doi: 10.1111/j.1399-3054.2004.00433.x
- Bonfig, K. B., Schreiber, U., Gabler, A., Roitsch, T., and Berger, S. (2006). Infection with virulent and avirulent *P. syringae* strains differentially affects photosynthesis and sink metabolism in *Arabidopsis* leaves. *Planta* 225, 1–12. doi: 10.1007/s00425-006-0303-3
- Brugger, A., Kuska, M. T., and Mahlein, A.-K. (2018). Impact of compatible and incompatible barley—*Blumeria graminis* f. sp. *hordei* interactions on chlorophyll fluorescence parameters. *J. Plant Dis. Prot.* 125, 177–186. doi: 10.1007/s41348-017-0129-1
- Butler, W. L. (1978). Energy distribution in the photochemical apparatus of photosynthesis. *Annu. Rev. Plant Physiol.* 29, 345–378. doi: 10.1146/annurev.pp.29.060178.002021
- Cameron, D. D., Geniez, J.-M., Seel, W. E., and Irving, L. J. (2008). Suppression of host photosynthesis by the parasitic plant *Rhinanthus minor*. *Ann. Bot.* 101, 573–578. doi: 10.1093/aob/mcm324
- Camino, C., Zarco-Tejada, P., and Gonzalez-Dugo, V. (2018). Effects of heterogeneity within tree crowns on airborne-quantified SIF and the CWSI as indicators of water stress in the context of precision agriculture. *Remote Sens.* 10, 604. doi: 10.3390/rs10040604
- Campbell, P. K. E., Huemmrich, K. F., Middleton, E. M., Ward, L. A., Julitta, T., Daughtry, C. S. T., et al. (2019). Diurnal and seasonal variations in chlorophyll fluorescence associated with photosynthesis at leaf and canopy scales. *Remote Sens.* 11, 488. doi: 10.3390/rs11050488
- Cendrero-Mateo, M. P., Bennertz, S., Burkart, A., Julitta, T., Cogliati, S., Scharr, H., et al. (2018). “Sun induced fluorescence calibration and validation for field phenotyping,” in *International Geoscience and Remote Sensing Symposium (IGARSS)*, 8248–8251. doi: 10.1109/IGARSS.2018.8519174
- Cséfalvay, L., Di Gasparo, G., Matous, K., Bellin, D., Ruperti, B., and Olejnickova, J. (2009). Pre-symptomatic detection of *Plasmopara viticola* infection in grapevine leaves using chlorophyll fluorescence imaging. *Eur. J. Plant Pathol.* 125, 291–302. doi: 10.1007/s10658-009-9482-7
- Chærle, L., Hagenbeek, D., De Bruyne, E., Valcke, R., and Van der Straeten, D. (2004). Thermal and chlorophyll-fluorescence imaging distinguish plant-pathogen interactions at an early stage. *Plant Cell Physiol.* 45, 887–896. doi: 10.1093/pcp/pch097
- Chærle, L., Leinonen, I., Jones, H. G., and Van der Straeten, D. (2007). Monitoring and screening plant populations with combined thermal and chlorophyll fluorescence imaging. *J. Exp. Bot.* 58, 773–784. doi: 10.1093/jxb/erl257
- Chærle, L., Pineda, M., Romero-Aranda, R., Van der Straeten, D., and Barón, M. (2006). Robotized thermal and chlorophyll fluorescence imaging of *Pepper*

- mild mottle virus* infection in *Nicotiana benthamiana*. *Plant Cell Physiol.* 47, 1323–1336. doi: 10.1093/pcp/pcj102
- Chou, H. M., Bundock, N., Rolfe, S. A., and Scholes, J. D. (2000). Infection of *Arabidopsis thaliana* leaves with *Albugo candida* (white blister rust) causes a reprogramming of host metabolism. *Mol. Plant Pathol.* 2, 99–113. doi: 10.1046/j.1364-3703.2000.00013.x
- Damm, A., Guanter, L., Paul-Limoges, E., van der Tol, C., Hueni, A., Buchmann, N., et al. (2015). Far-red sun-induced chlorophyll fluorescence shows ecosystem-specific relationships to gross primary production: an assessment based on observational and modeling approaches. *Remote Sens. Environ.* 166, 91–105. doi: 10.1016/j.rse.2015.06.004
- Dias, C. S., Araujo, L., Alves Chaves, J. A., DaMatta, F. M., and Rodrigues, F. A. (2018). Water relation, leaf gas exchange and chlorophyll a fluorescence imaging of soybean leaves infected with *Colletotrichum truncatum*. *Plant Physiol. Biochem.* 127, 119–128. doi: 10.1016/j.plaphy.2018.03.016
- Dobrowski, S. Z., Pushnik, J. C., Zarco-Tejada, P. J., and Ustin, S. L. (2005). Simple reflectance indices track heat and water stress-induced changes in steady-state chlorophyll fluorescence at the canopy scale. *Remote Sens. Environ.* 97, 403–414. doi: 10.1016/j.rse.2005.05.006
- Du, S., Liu, L., Liu, X., and Hu, J. (2017). Response of canopy solar-induced chlorophyll fluorescence to the absorbed photosynthetically active radiation absorbed by chlorophyll. *Remote Sens.* 9, 911. doi: 10.3390/rs9090911
- Esfeld, P., Siebke, K., and Weis, E. (1995). “Local defence-related shift in the carbon metabolism in chickpea leaves induced by a fungal pathogen,” in *Photosynthesis: From Life to Biosphere*. Ed. P. Mathis (Dordrecht: Kluwer Academic Publishers), 663–666. doi: 10.1007/978-94-009-0173-5_1069
- Fiorani, F., Rascher, U., Jahnke, S., and Schurr, U. (2012). Imaging plants dynamics in heterogenic environments. *Curr. Opin. Biotechnol.* 23, 227–235. doi: 10.1016/j.copbio.2011.12.010
- Flexas, J., Escalona, J. M., Evain, S., Gulias, J., Moya, I., Osmond, C. B., et al. (2002). Steady-state chlorophyll fluorescence (Fs) measurements as a tool to follow variations of net CO₂ assimilation and stomatal conductance during water-stress in C3 plants. *Physiol. Plant.* 114, 231–240. doi: 10.1034/j.1399-3054.2002.1140209.x
- Gago, J., Douthe, C., Coopman, R. E., Gallego, P. P., Ribas-Carbo, M., Flexas, J., et al. (2015). UAVs challenge to assess water stress for sustainable agriculture. *Agric. Water Manage.* 153, 9–19. doi: 10.1016/j.agwat.2015.01.020
- Gamon, J. A., Field, C. B., Goulden, M. L., Griffin, K. L., Hartley, A. E., Joel, G., et al. (1995). Relationships between NDVI canopy structure, and photosynthesis in three Californian vegetation types. *Ecol. Appl.* 5, 28–41. doi: 10.2307/1942049
- Gamon, J. A., Peñuelas, J., and Field, C. B. (1992). A narrow-waveband spectral index that tracks diurnal changes in photosynthetic efficiency. *Remote Sens. Environ.* 41, 35–44. doi: 10.1016/0034-4257(92)90059-S
- Gamon, J. A., Serrano, L., and Surfus, J. S. (1997). The photochemical reflectance index: an optical indicator of photosynthetic radiation use efficiency across species, functional types, and nutrient levels. *Oecologia* 112, 492–501. doi: 10.1007/s004420050337
- Garzonio, R., Di Mauro, B., Colombo, R., and Cogliati, S. (2017). Surface reflectance and sun-induced fluorescence spectroscopy measurements using a small hyperspectral UAS. *Remote Sens.* 9, 472. doi: 10.3390/rs9050472
- Gastellu-Etchegorry, J., Lauret, N., Yin, T., Landier, L., Kallel, A., Malenovsky, Z., et al. (2017). DART: recent advances in remote sensing data modeling with atmosphere, polarization, and chlorophyll fluorescence. *IEEE J. Sel. Top. Appl. Earth Obs. Remote Sens.* 10, 2640–2649. doi: 10.1109/JSTARS.2017.2685528
- Ghosh, S., Kanwar, P., and Jha, G. (2017). Alterations in rice chloroplast integrity, photosynthesis and metabolome associated with pathogenesis of *Rhizoctonia solani*. *Sci. Rep.* 7, 41610. doi: 10.1038/srep41610
- Göhre, V., Jones, A. M. E., Sklenář, J., Robatzek, S., and Weber, A. P. M. (2012). Molecular crosstalk between PAMP-triggered immunity and photosynthesis. *Mol. Plant-Microbe Interact.* 25, 1083–1092. doi: 10.1094/MPMI-11-11-0301
- Goulas, Y., Fournier, A., Daumard, F., Champagne, S., Ounis, A., Marloie, O., et al. (2017). Gross primary production of a wheat canopy relates stronger to far red than to red solar-induced chlorophyll fluorescence. *Remote Sens.* 9, 97. doi: 10.3390/rs9010097
- Granum, E., Pérez-Bueno, M. L., Calderón, C. E., Ramos, C., de Vicente, A., Cazorla, F. M., et al. (2015). Metabolic responses of avocado plants to stress induced by *Rosellinia necatrix* analysed by fluorescence and thermal imaging. *Eur. J. Plant Pathol.* 142, 625–632. doi: 10.1007/s10658-015-0640-9
- Guanter, L., Zhang, Y., Jung, M., Joiner, J., Voigt, M., Berry, J. A., et al. (2014). Global and time-resolved monitoring of crop photosynthesis with chlorophyll fluorescence. *Proc. Natl. Acad. Sci.* 111, E1327–E1333. doi: 10.1073/pnas.1320008111
- Gurney, A. L., Taylor, A., Mbwaga, A., Scholes, J. D., and Press, M. C. (2002). Do maize cultivars demonstrate tolerance to the parasitic weed *Striga asiatica*? *Weed Res.* 42, 299–306. doi: 10.1046/j.1365-3180.2002.00287.x
- Halitschke, R., Hamilton, J. G., and Kessler, A. (2011). Herbivore-specific elicitation of photosynthesis by mirid bug salivary secretions in the wild tobacco *Nicotiana attenuata*. *New Phytol.* 191, 528–535. doi: 10.1111/j.1469-8137.2011.03701.x
- Han, X.-Y., Li, P.-X., Zou, L.-J., Tan, W.-r., Zheng, T., Zhang, D.-W., et al. (2016). GOLDEN2-LIKE transcription factors coordinate the tolerance to *Cucumber mosaic virus* in *Arabidopsis*. *Biochem. Biophys. Res. Commun.* 477, 626–632. doi: 10.1016/j.bbrc.2016.06.110
- Hennig, A., Bonfig, K., Roitsch, T., and Warzecha, H. (2007). Expression of the recombinant bacterial outer surface protein A in tobacco chloroplasts leads to thylakoid localization and loss of photosynthesis. *FEBS J.* 274, 5749–5758. doi: 10.1111/j.1742-4658.2007.06095.x
- Hernández-Clemente, R., North, P. R. J., Hornero, A., and Zarco-Tejada, P. J. (2017). Assessing the effects of forest health on sun-induced chlorophyll fluorescence using the FluorFLIGHT 3-D radiative transfer model to account for forest structure. *Remote Sens. Environ.* 193, 165–179. doi: 10.1016/j.rse.2017.02.012
- Honorato Júnior, J., Zambolim, L., Duarte, H. S. S., Aucique-Pérez, C. E., and Rodrigues, F. Á. (2015). Effects of epoxiconazole and pyraclostrobin fungicides in the infection process of *Hemileia vastatrix* on coffee leaves as determined by chlorophyll a fluorescence imaging. *J. Phytopathol.* 163, 968–977. doi: 10.1111/jph.12399
- Horton, P., Johnson, M. P., Perez-Bueno, M. L., Kiss, A. Z., and Ruban, A. V. (2008). Photosynthetic acclimation: does the dynamic structure and macro-organisation of photosystem II in higher plant grana membranes regulate light harvesting states? *FEBS J.* 275, 1069–1079. doi: 10.1111/j.1742-4658.2008.06263.x
- Ivanov, D. A., and Bernards, M. A. (2016). Chlorophyll fluorescence imaging as a tool to monitor the progress of a root pathogen in a perennial plant. *Planta* 243, 263–279. doi: 10.1007/s00425-015-2427-9
- Janoutova, R., Homolova, L., Malenovsky, Z., Hanus, J., Lauret, N., and Gastellu-Etchegorry, J. P. (2019). Influence of 3D spruce tree representation on accuracy of airborne and satellite forest reflectance simulated in DART. *Forests* 10, 35. doi: 10.3390/f10030292
- Jia, M., Zhou, C., Cheng, T., Tian, Y., Zhu, Y., Cao, W., et al. (2016). “Inversion of chlorophyll fluorescence parameters on vegetation indices at leaf scale,” in *2016 IEEE International Geoscience and Remote Sensing Symposium (IGARSS)*, 4359–4362. doi: 10.1109/IGARSS.2016.7730136
- Joiner, J., Yoshida, Y., Guanter, L., and Middleton, E. M. (2016). New methods for retrieval of chlorophyll red fluorescence from hyper-spectral satellite instruments: simulations and application to GOME-2 and SCIAMACHY. *Atmos. Meas. Tech.* 9, 3939–3967. doi: 10.5194/amt-9-3939-2016
- Kautsky, H., and Hirsch, A. (1931). Neue Versuche zur Kohlensäureassimilation. *Naturwissenschaften* 19, 964–964. doi: 10.1007/BF01516164
- Kolber, Z., Klimov, D., Ananyev, G., Rascher, U., Berry, J., and Osmond, B. (2005). Measuring photosynthetic parameters at a distance: laser induced fluorescence transient (LIFT) method for remote measurements of photosynthesis in terrestrial vegetation. *Photosynth. Res.* 84, 121–129. doi: 10.1007/s11120-005-5092-1
- Kováč, D., Veselovská, P., Klem, K., Večeřová, K., Ač, A., Peñuelas, J., et al. (2018). Potential of Photochemical Reflectance Index for indicating photochemistry and light use efficiency in leaves of European beech and Norway spruce trees. *Remote Sens.* 10, 1202. doi: 10.3390/rs10081202
- Kuckenberg, J., Tartachnyk, I., and Noga, G. (2009). Temporal and spatial changes of chlorophyll fluorescence as a basis for early and precise detection of leaf rust and powdery mildew infections in wheat leaves. *Precis. Agric.* 10, 34–44. doi: 10.1007/s11119-008-9082-0
- Kycko, M., Zagajewski, B., Lavender, S., and Dabija, A. (2019). *In situ* hyperspectral remote sensing for monitoring of alpine trampled and recultivated species. *Remote Sens.* 11, 1296. doi: 10.3390/rs11111296
- Kyseláková, H., Prokopová, J., Nauš, J., Novák, O., Navrátil, M., Safářová, D., et al. (2011). Photosynthetic alterations of pea leaves infected systemically by *Pea enation mosaic virus*: a coordinated decrease in efficiencies of CO₂ assimilation

- and photosystem II photochemistry. *Plant Physiol. Biochem.* 49, 1279–1289. doi: 10.1016/j.plaphy.2011.08.006
- Li, L., Zhang, Q., and Huang, D. (2014). A review of imaging techniques for plant phenotyping. *Sensors* 14, 20078–20111. doi: 10.3390/s141120078
- Lohaus, G., Heldt, H. W., and Osmond, C. B. (2000). Infection with phloem limited *Abutilon mosaic virus* causes localized carbohydrate accumulation in leaves of *Abutilon striatum*: relationships to symptom development and effects on chlorophyll fluorescence quenching during photosynthetic induction. *Plant Biol.* 2, 161–167. doi: 10.1055/s-2000-9461
- Maier, S. W., Günther, K. P., and Stellmes, M. (2003). “Sun-induced fluorescence: a new tool for precision farming,” in *Digital imaging and spectral techniques: applications to precision agriculture and crop physiology*. Eds. J. Schepers and T. Vantoi (Madison, WI: American Society of Agronomy, Crop Science Society of America, and Soil Science Society of America), 209–222. doi: 10.2134/asa specpub66.c16
- Maimaitiyiming, M., Ghulam, A., Bozzolo, A., Wilkins, J. L., and Kwasniewski, M. T. (2017). Early detection of plant physiological responses to different levels of water stress using reflectance spectroscopy. *Remote Sens.* 9, 745. doi: 10.3390/rs9070745
- Matouš, K., Benediktyova, Z., Berger, S., Roitsch, T., and Nedbal, L. (2006). Case study of combinatorial imaging: what protocol and what chlorophyll fluorescence image to use when visualizing infection of *Arabidopsis thaliana* by *Pseudomonas syringae*? *Photosynth. Res.* 90, 243–253. doi: 10.1007/s1120-006-9120-6
- Maxwell, K., and Johnson, G. N. (2000). Chlorophyll fluorescence—a practical guide. *J. Exp. Bot.* 51, 659–668. doi: 10.1093/jexbot/51.345.659
- McElrone, A. J., Hamilton, J. G., Krafnick, A. J., Aldea, M., Knepp, R. G., and DeLucia, E. H. (2010). Combined effects of elevated CO₂ and natural climatic variation on leaf spot diseases of redbud and sweetgum trees. *Environ. Pollut.* 158, 108–114. doi: 10.1016/j.envpol.2009.07.029
- Meyer, S., Saccardt, A. K., Rizza, F., and Genty, B. (2001). Inhibition of photosynthesis by *Colletotrichum lindemuthianum* in bean determined by chlorophyll fluorescence imaging. *Plant Cell Environ.* 24, 947–955. doi: 10.1046/j.0016-8025.2001.00737.x
- Miao, G., Guan, K., Yang, X., Bernacchi, C. J., Berry, J. A., DeLucia, E. H., et al. (2018). Sun-induced chlorophyll fluorescence, photosynthesis, and light use efficiency of a soybean field from seasonally continuous measurements. *J. Geophys. Res. Biogeophys.* 123, 610–623. doi: 10.1002/2017JG004180
- Mir, R. R., Reynolds, M., Pinto, F., Khan, M. A., and Bhat, M. A. (2019). High-throughput phenotyping for crop improvement in the genomics era. *Plant Sci.* 282, 60–72. doi: 10.1016/j.plantsci.2019.01.007
- Montero, R., Pérez-Bueno, M. L., Barón, M., Florez-Sarasa, I., Tohge, T., Fernie, A. R., et al. (2016). Alterations in primary and secondary metabolism in *Vitis vinifera* ‘Malvasia de Banyalbufar’ upon infection with *Grapevine leafroll associated virus 3* (GLRaV-3). *Physiol. Plant.* 157, 442–452. doi: 10.1111/ppl.12440
- Muniz, C. R., Freire, F. C. O., Viana, F. M. P., Cardoso, J. E., Sousa, C. A. F., Guedes, M. I. F., et al. (2014). Monitoring cashew seedlings during interactions with the fungus *Lasiodiplodia theobromae* using chlorophyll fluorescence imaging. *Photosynthetica* 52, 529–537. doi: 10.1007/s11099-014-0061-6
- Murchie, E. H., and Lawson, T. (2013). Chlorophyll fluorescence analysis: a guide to good practice and understanding some new applications. *J. Exp. Bot.* 64, 3983–3998. doi: 10.1093/jxb/ert208
- Nabity, P. D., Hillstrom, M. L., Lindroth, R. L., and DeLucia, E. H. (2012). Elevated CO₂ interacts with herbivory to alter chlorophyll fluorescence and leaf temperature in *Betula papyrifera* and *Populus tremuloides*. *Oecologia* 169, 905–913. doi: 10.1007/s00442-012-2261-8
- Nabity, P. D., Zavala, J. A., and DeLucia, E. H. (2009). Indirect suppression of photosynthesis on individual leaves by arthropod herbivory. *Ann. Bot.* 103, 655–663. doi: 10.1093/aob/mcn127
- Nabity, P. D., Zavala, J. A., and DeLucia, E. H. (2013). Herbivore induction of jasmonic acid and chemical defences reduce photosynthesis in *Nicotiana attenuata*. *J. Exp. Bot.* 64, 685–694. doi: 10.1093/jxb/ers364
- Naumann, J. C., Anderson, J. E., and Young, D. R. (2008). Linking physiological responses, chlorophyll fluorescence and hyperspectral imagery to detect salinity stress using the physiological reflectance index in the coastal shrub, *Myrica cerifera*. *Remote Sens. Environ.* 112, 3865–3875. doi: 10.1016/j.rse.2008.06.004
- Ni, Z., Liu, Z., Li, Z.-L., Nerry, F., Huo, H., and Li, X. (2015). Estimation of solar-induced fluorescence using the canopy reflectance index. *Int. J. Remote Sens.* 36, 5239–5256. doi: 10.1080/01431161.2015.1058987
- Ni, Z., Lu, Q., Huo, H., and Zhang, H. (2019). Estimation of chlorophyll fluorescence at different scales: a review. *Sensors* 19, 3000. doi: 10.3390/s19133000
- Ning, L., Edwards, G. E., Strobel, G. A., Daley, L. S., and Callis, J. B. (1995). Imaging fluorometer to detect pathological and physiological change in plants. *Appl. Spectrosc.* 49, 1381–1389. doi: 10.1366/0003702953965542
- Omasa, K., Hosoi, F., and Konishi, A. (2006). 3D lidar imaging for detecting and understanding plant responses and canopy structure. *J. Exp. Bot.* 58, 881–898. doi: 10.1093/jxb/erl142
- Osmond, B., Chow, W. S., Wyber, R., Zavafer, A., Keller, B., Pogson, B. J., et al. (2017). Relative functional and optical absorption cross-sections of PSII and other photosynthetic parameters monitored *in situ*, at a distance with a time resolution of a few seconds, using a prototype light induced fluorescence transient (LIFT) device. *Funct. Plant Biol.* 44, 985–1006. doi: 10.1071/FP17024
- Osmond, C. B., Daley, P. F., Badger, M. R., and Lüttge, U. (1998). Chlorophyll fluorescence quenching during photosynthetic induction in leaves of *Abutilon striatum* Dicks infected with *Abutilon mosaic virus* observed with a field-portable system. *Bot. Acta* 111, 390–397. doi: 10.1111/j.1438-8677.1998.tb00724.x
- Peng, Y., Zeng, A., Zhu, T., Fang, S., Gong, Y., Tao, Y., et al. (2017). Using remotely sensed spectral reflectance to indicate leaf photosynthetic efficiency derived from active fluorescence measurements. *J. Appl. Remote Sens.* 11, 026034. doi: 10.1117/1.JRS.11.026034
- Pérez-Bueno, M. L., Ciscato, M., VandeVen, M., García-Luque, I., Valcke, R., and Barón, M. (2006). Imaging viral infection: studies on *Nicotiana benthamiana* plants infected with the pepper mild mottle tobamovirus. *Photosynth. Res.* 90, 111–123. doi: 10.1007/s1120-006-9098-0
- Pérez-Bueno, M. L., Granum, E., Pineda, M., Flors, V., Rodríguez-Palenzuela, P., López-Solanilla, E., et al. (2016). Temporal and spatial resolution of activated plant defense responses in leaves of *Nicotiana benthamiana* infected with *Dickeya dadantii*. *Front. Plant Sci.* 6, 1209. doi: 10.3389/fpls.2015.01209
- Pérez-Bueno, M. L., Pineda, M., Díaz-Casado, E., and Barón, M. (2015). Spatial and temporal dynamics of primary and secondary metabolism in *Phaseolus vulgaris* challenged by *Pseudomonas syringae*. *Physiol. Plant.* 153, 161–174. doi: 10.1111/ppl.12237
- Peterson, R. B., and Aylor, D. E. (1995). Chlorophyll fluorescence induction in leaves of *Phaseolus vulgaris* infected with bean rust (*Uromyces appendiculatus*). *Plant Physiol.* 108, 163–171. doi: 10.1104/pp.108.1.163
- Pieruschka, R., Albrecht, H., Müller, O., Berry, J. A., Klimov, D., Kolber, Z. S., et al. (2014). Daily and seasonal dynamics of remotely sensed photosynthetic efficiency in tree canopies. *Tree Physiol.* 34, 674–685. doi: 10.1093/treephys/tpu035
- Pineda, M., Olejníčková, J., Cséfalvay, L., and Barón, M. (2011). Tracking viral movement in plants by means of chlorophyll fluorescence imaging. *J. Plant Physiol.* 168, 2035–2040. doi: 10.1016/j.jplph.2011.06.013
- Pineda, M., Pérez-Bueno, M. L., and Barón, M. (2018). Detection of bacterial infection in melon plants by classification methods based on imaging data. *Front. Plant Sci.* 9, 164. doi: 10.3389/fpls.2018.00164
- Pineda, M., Soukupová, J., Matoš, K., Nedbal, L., and Barón, M. (2008). Conventional and combinatorial chlorophyll fluorescence imaging of tobamovirus-infected plants. *Photosynthetica* 46, 441–451. doi: 10.1007/s11099-008-0076-y
- Pinto, F., Damm, A., Schickling, A., Panigada, C., Cogliati, S., Müller-Linow, M., et al. (2016). Sun-induced chlorophyll fluorescence from high-resolution imaging spectroscopy data to quantify spatio-temporal patterns of photosynthetic function in crop canopies. *Plant Cell Environ.* 39, 1500–1512. doi: 10.1111/pce.12710
- Plascyk, J. A., and Gabriel, F. C. (1975). The Fraunhofer line discriminator MKII—An airborne instrument for precise and standardized ecological luminescence measurement. *IEEE Trans. Instrum. Meas.* 24, 306–313. doi: 10.1109/TIM.1975.4314448
- Polonio, Á., Pineda, M., Bautista, R., Martínez-Cruz, J., Pérez-Bueno, M. L., Barón, M., et al. (2019). RNA-seq analysis and fluorescence imaging of melon powdery mildew disease reveal an orchestrated reprogramming of host physiology. *Sci. Rep.* 9, 7978. doi: 10.1038/s41598-019-44443-5
- Prokopová, J., Špundová, M., Sedlářová, M., Husíčková, A., Novotný, R., Doležal, K., et al. (2010). Photosynthetic responses of lettuce to downy mildew infection and cytokinin treatment. *Plant Physiol. Biochem.* 48, 716–723. doi: 10.1016/j.plaphy.2010.04.003
- Pu, X.-J., Li, Y.-N., Wei, L.-J., Xi, D.-H., and Lin, H.-H. (2016). Mitochondrial energy-dissipation pathway and cellular redox disruption compromises *Arabidopsis* resistance to *Turnip crinkle virus* infection. *Biochem. Biophys. Res. Commun.* 473, 421–427. doi: 10.1016/j.bbrc.2016.03.023

- Raesch, A. R., Muller, O., Pieruschka, R., and Rascher, U. (2014). Field observations with laser-induced fluorescence transient (LIFT) method in barley and sugar beet. *Agriculture* 4, 159–169. doi: 10.3390/agriculture4020159
- Rahimzadeh-Bajgirani, P., Munehiro, M., and Omasa, K. (2012). Relationships between the photochemical reflectance index (PRI) and chlorophyll fluorescence parameters and plant pigment indices at different leaf growth stages. *Photosynth. Res.* 113, 261–271. doi: 10.1007/s1120-012-9747-4
- Rahimzadeh-Bajgirani, P., Tubuxin, B., and Omasa, K. (2017). Estimating chlorophyll fluorescence parameters using the joint Fraunhofer line depth and laser-induced saturation pulse (FLD-LISP) method in different plant species. *Remote Sens.* 9, 599. doi: 10.3390/rs9060599
- Raji, S. N., Subhash, N., Ravi, V., Saravanan, R., Mohanan, C. N., Nita, S., et al. (2015). Detection of mosaic virus disease in cassava plants by sunlight-induced fluorescence imaging: a pilot study for proximal sensing. *Int. J. Remote Sens.* 36, 2880–2897. doi: 10.1080/01431161.2015.1049382
- Ranulfi, A. C., Cardinali, M. C. B., Kubota, T. M. K., Freitas-Astúa, J., Ferreira, E. J., Bellete, B. S., et al. (2016). Laser-induced fluorescence spectroscopy applied to early diagnosis of citrus Huanglongbing. *Biosys. Eng.* 144, 133–144. doi: 10.1016/j.biosystemseng.2016.02.010
- Rascher, U., Alonso, L., Burkart, A., Cilia, C., Cogliati, S., Colombo, R., et al. (2015). Sun-induced fluorescence—a new probe of photosynthesis: first maps from the imaging spectrometer HyPlant. *Global Change Biol.* 21, 4673–4684. doi: 10.1111/gcb.13017
- Rascher, U., and Pieruschka, R. (2008). Spatio-temporal variations of photosynthesis: the potential of optical remote sensing to better understand and scale light use efficiency and stresses of plant ecosystems. *Precis. Agric.* 9, 355–366. doi: 10.1007/s11119-008-9074-0
- Repka, V. (2002). Chlorophyll-deficient mutant in oak (*Quercus petraea* L.) displays an accelerated hypersensitive-like cell death and an enhanced resistance to powdery mildew disease. *Photosynthetica* 40, 183–193. doi: 10.1023/A:1021577521522
- Rios, J. A., Aucique-Pérez, C. E., Debona, D., Cruz Neto, L. B. M., Rios, V. S., and Rodrigues, F. A. (2017). Changes in leaf gas exchange, chlorophyll *a* fluorescence and antioxidant metabolism within wheat leaves infected by *Bipolaris sorokiniana*. *Ann. Appl. Biol.* 170, 189–203. doi: 10.1111/aab.12328
- Rodenburg, J., Bastiaans, L., Schapendonk, A. H. C. M., van der Putten, P. E. L., van Ast, A., Dingemanse, N. J., et al. (2008). CO₂-assimilation and chlorophyll fluorescence as indirect selection criteria for host tolerance against *Striga*. *Euphytica* 160, 75–87. doi: 10.1007/s10681-007-9555-7
- Rodríguez-Moreno, L., Pineda, M., Soukupová, J., Macho, A. P., Beuzón, C. R., Barón, M., et al. (2008). Early detection of bean infection by *Pseudomonas syringae* in asymptomatic leaf areas using chlorophyll fluorescence imaging. *Photosynth. Res.* 96, 27–35. doi: 10.1007/s1120-007-9278-6
- Roháček, K., and Barták, M. (1999). Technique of the modulated chlorophyll fluorescence: basic concepts, useful parameters, and some applications. *Photosynthetica* 37, 339–363. doi: 10.1023/A:1007172424619
- Roitsch, T., Cabrera-Bosquet, L., Fournier, A., Ghamkhar, K., Jiménez-Berni, J., Pinto, F., et al. (2019). Review: new sensors and data-driven approaches—a path to next generation phenomics. *Plant Sci.* 282, 2–10. doi: 10.1016/j.plantsci.2019.01.011
- Rolfe, S. A., and Scholes, J. D. (2010). Chlorophyll fluorescence imaging of plant-pathogen interactions. *Protoplasma* 247, 163–175. doi: 10.1007/s00709-010-0203-z
- Rousseau, C., Belin, E., Bove, E., Rousseau, D., Fabre, F., Berruyer, R., et al. (2013). High throughput quantitative phenotyping of plant resistance using chlorophyll fluorescence image analysis. *Plant Methods* 9, 17. doi: 10.1186/1746-4811-9-17
- Rousseau, C., Hunault, G., Gaillard, S., Bourbeillon, J., Montiel, G., Simier, P., et al. (2015). Phenoplant: a web resource for the exploration of large chlorophyll fluorescence image datasets. *Plant Methods* 11, 24. doi: 10.1186/s13007-015-0068-4
- Rys, M., Juhász, C., Surówka, E., Janeczko, A., Saja, D., Tóbiás, I., et al. (2014). Comparison of a compatible and an incompatible pepper-tobamovirus interaction by biochemical and non-invasive techniques: chlorophyll *a* fluorescence, isothermal calorimetry and FT-Raman spectroscopy. *Plant Physiol. Biochem.* 83, 267–278. doi: 10.1016/j.plaphy.2014.08.013
- Saito, Y., Kurihara, K.-J., Takahashi, H., Kobayashi, F., Kawahara, T., Nomura, A., et al. (2002). Remote estimation of the chlorophyll concentration of living trees using laser-induced fluorescence imaging LIDAR. *Opt. Rev.* 9, 37–39. doi: 10.1007/s10043-002-0037-9
- Sancho-Knapik, D., Mendoza-Herrer, Ó., Gil-Pelegrín, E., and Peguero-Pina, J. (2018). Chl fluorescence parameters and leaf reflectance indices allow monitoring changes in the physiological status of *Quercus ilex* L. Under progressive water deficit. *Forests* 9, 400. doi: 10.3390/f9070400
- Schmitz, A., Tartachnyk, I., Kiewnick, S., A. Sikora, R., and Kühbauch, W. (2006). Detection of *Heterodera schachtii* infestation in sugar beet by means of laser-induced and pulse amplitude modulated chlorophyll fluorescence. *Nematology* 8, 273–286. doi: 10.1163/15685410677998755
- Scholes, J. D., and Rolfe, S. A. (1996). Photosynthesis in localised regions of oat leaves infected with crown rust (*Puccinia coronata*): quantitative imaging of chlorophyll fluorescence. *Planta* 199, 573–582. doi: 10.1007/BF00195189
- Šebela, D., Olejníčková, J., Sotolář, R., Vrchotová, N., and Tršić, J. (2014). Towards optical detection of *Plasmopara viticola* infection in the field. *J. Plant Pathol.* 96, 309–320. doi: 10.4454/JPP.V96I2.037
- Šebela, D., Quiñones, C., Cruz, C. V., Ona, I., Olejníčková, J., and Jagdish, K. S. V. (2018). Chlorophyll fluorescence and reflectance-based non-invasive quantification of blast, bacterial blight and drought stresses in rice. *Plant Cell Physiol.* 59, 30–43. doi: 10.1093/pcp/pcx144
- Sekulski-Nalewajko, J., Kornas, A., Goclawski, J., Misalski, Z., and Kuźniak, E. (2019). Spatial referencing of chlorophyll fluorescence images for quantitative assessment of infection propagation in leaves demonstrated on the ice plant: *Botrytis cinerea* pathosystem. *Plant Methods* 15, 18. doi: 10.1186/s13007-019-0401-4
- Smigaj, M., Gaulton, R., Suarez, J. C., and Barr, S. L. (2019). Canopy temperature from an unmanned aerial vehicle as an indicator of tree stress associated with red band needle blight severity. *For. Ecol. Manage.* 433, 699–708. doi: 10.1016/j.foreco.2018.11.032
- Soukupová, J., Smatanová, S., Nedbal, L., and Jegorov, A. (2003). Plant response to destruxins visualized by imaging of chlorophyll fluorescence. *Physiol. Plant.* 118, 399–405. doi: 10.1034/j.1399-3054.2003.00119.x
- Spoustova, P., Synkova, H., Valcke, R., and Cerovska, N. (2013). Chlorophyll *a* fluorescence as a tool for a study of the *Potato virus Y* effects on photosynthesis of nontransgenic and transgenic *Pssu-ipt* tobacco. *Photosynthetica* 51, 191–201. doi: 10.1007/s11099-013-0023-4
- Strong, G. L., Bannister, P., and Burritt, D. (2000). Are mistletoes shade plants? CO₂ assimilation and chlorophyll fluorescence of temperate mistletoes and their hosts. *Ann. Bot.* 85, 511–519. doi: 10.1006/anbo.1999.1098
- Swarbrick, P. J., Schulze-Lefert, P., and Scholes, J. D. (2006). Metabolic consequences of susceptibility and resistance (race-specific and broad-spectrum) in barley leaves challenged with powdery mildew. *Plant Cell Environ.* 29, 1061–1076. doi: 10.1111/j.1365-3040.2005.01472.x
- Tang, J., Zielinski, R., Aldea, M., and DeLucia, E. (2009). Spatial association of photosynthesis and chemical defense in *Arabidopsis thaliana* following herbivory by *Trichoplusia ni*. *Physiol. Plant.* 137, 115–124. doi: 10.1111/j.1399-3054.2009.01265.x
- Tang, J. Y., Zielinski, R. E., Zangerl, A. R., Crofts, A. R., Berenbaum, M. R., and DeLucia, E. H. (2006). The differential effects of herbivory by first and fourth instars of *Trichoplusia ni* (Lepidoptera: Noctuidae) on photosynthesis in *Arabidopsis thaliana*. *J. Exp. Bot.* 57, 527–536. doi: 10.1093/jxb/erj032
- Tatagiba, S. D., Damatta, F. M., and Rodrigues, F. A. (2016a). Magnesium decreases leaf scald symptoms on rice leaves and preserves their photosynthetic performance. *Plant Physiol. Biochem.* 108, 49–56. doi: 10.1016/j.plaphy.2016.07.002
- Tatagiba, S. D., DaMatta, F. M., and Rodrigues, F. A. (2016b). Silicon partially preserves the photosynthetic performance of rice plants infected by *Monographella albescens*. *Ann. Appl. Biol.* 168, 111–121. doi: 10.1111/aab.12246
- Técsi, L. I., Maule, A. J., Smith, A. M., and Leegood, R. C. (1994). Complex, localized changes in CO₂ assimilation and starch content associated with the susceptible interaction between *Cucumber mosaic virus* and cucurbit host. *Plant J.* 5, 837–847. doi: 10.1046/j.1365-3113.1994.5060837.x
- Thomas, S., Kuska, M. T., Bohnenkamp, D., Brugger, A., Alisaac, E., Wahabzada, M., et al. (2018). Benefits of hyperspectral imaging for plant disease detection and plant protection: a technical perspective. *J. Plant Dis. Prot.* 125, 5–20. doi: 10.1007/s41348-017-0124-6
- Tschiersch, H., Junker, A., Meyer, R. C., and Altmann, T. (2017). Establishment of integrated protocols for automated high throughput kinetic chlorophyll fluorescence analyses. *Plant Methods* 13, 54. doi: 10.1186/s13007-017-0204-4

- Tubuxin, B., Rahimzadeh-Bajgiran, P., Ginnan, Y., Hosoi, F., and Omasa, K. (2015). Estimating chlorophyll content and photochemical yield of photosystem II (Φ_{PSII}) using solar-induced chlorophyll fluorescence measurements at different growing stages of attached leaves. *J. Exp. Bot.* 66, 5595–5603. doi: 10.1093/jxb/erv272
- Tung, J., Goodwin, P. H., and Hsiang, T. (2013). Chlorophyll fluorescence for quantification of fungal foliar infection and assessment of the effectiveness of an induced systemic resistance activator. *Eur. J. Plant Pathol.* 136, 301–315. doi: 10.1007/s10658-012-0164-5
- Van Gaalen, K. E., Flanagan, L. B., and Peddle, D. R. (2007). Photosynthesis, chlorophyll fluorescence and spectral reflectance in *Sphagnum* moss at varying water contents. *Oecologia* 153, 19–28. doi: 10.1007/s00442-007-0718-y
- Virlet, N., Sabermanesh, K., Sadeghi-Tehran, P., and Hawkesford, M. J. (2017). Field Scanalyzer: an automated robotic field phenotyping platform for detailed crop monitoring. *Funct. Plant Biol.* 44, 143–153. doi: 10.1071/FP16163
- Wang, H., Qian, X., Zhang, L., Xu, S., Li, H., Xia, X., et al. (2018). A method of high throughput monitoring crop physiology using chlorophyll fluorescence and multispectral imaging. *Front. Plant Sci.* 9, 407. doi: 10.3389/fpls.2018.00407
- Wyber, R., Malenovsky, Z., Ashcroft, M. B., Osmond, B., and Robinson, S. A. (2017). Do daily and seasonal trends in leaf solar induced fluorescence reflect changes in photosynthesis, growth or light exposure? *Remote Sens.* 9, 604. doi: 10.3390/rs9060604
- Yang, K., Ryu, Y., Dechant, B., Berry, J. A., Hwang, Y., Jiang, C., et al. (2018). Sun-induced chlorophyll fluorescence is more strongly related to absorbed light than to photosynthesis at half-hourly resolution in a rice paddy. *Remote Sens. Environ.* 216, 658–673. doi: 10.1016/j.rse.2018.07.008
- Žabka, M., Drastichová, K., Jegorov, A., Soukupová, J., and Nedbal, L. (2006). Direct evidence of plant-pathogenic activity of fungal metabolites of *Trichothecium roseum* on apple. *Mycopathologia* 162, 65–68. doi: 10.1007/s11046-006-0030-0
- Zarco-Tejada, P. J., Berni, J. A. J., Suarez, L., Sepulcre-Canto, G., Morales, F., and Miller, J. R. (2009). Imaging chlorophyll fluorescence with an airborne narrow-band multispectral camera for vegetation stress detection. *Remote Sens. Environ.* 113, 1262–1275. doi: 10.1016/j.rse.2009.02.016
- Zarco-Tejada, P. J., González-Dugo, M. V., and Fereres, E. (2016). Seasonal stability of chlorophyll fluorescence quantified from airborne hyperspectral imagery as an indicator of net photosynthesis in the context of precision agriculture. *Remote Sens. Environ.* 179, 89–103. doi: 10.1016/j.rse.2016.03.024
- Zarco-Tejada, P. J., Morales, A., Testi, L., and Villalobos, F. J. (2013). Spatio-temporal patterns of chlorophyll fluorescence and physiological and structural indices acquired from hyperspectral imagery as compared with carbon fluxes measured with eddy covariance. *Remote Sens. Environ.* 133, 102–115. doi: 10.1016/j.rse.2013.02.003
- Zhang, H., Hu, H., Zhang, X., Wang, K., Song, T., and Zeng, F. (2012). Detecting *Suaeda salsa* L. chlorophyll fluorescence response to salinity stress by using hyperspectral reflectance. *Acta Physiol. Plant* 342, 581–588. doi: 10.1007/s11738-011-0857-y
- Zhang, H., Zhu, L.-F., Hu, H., Zheng, K.-F., and Jin, Q.-Y. (2011). Monitoring leaf chlorophyll fluorescence with spectral reflectance in rice (*Oryza sativa* L.). *Procedia Eng.* 15, 4403–4408. doi: 10.1016/j.proeng.2011.08.827
- Zhang, Y., Joiner, J., Alemohammad, S. H., Zhou, S., and Gentine, P. (2018). A global spatially contiguous solar-induced fluorescence (CSIF) dataset using neural networks. *Biogeosciences* 15, 5779–5800. doi: 10.5194/bg-15-5779-2018
- Zou, J., Rodriguez-Zas, S., Aldea, M., Li, M., Zhu, J., Gonzalez, D. O., et al. (2005). Expression profiling soybean response to *Pseudomonas syringae* reveals new defense-related genes and rapid HR-specific downregulation of photosynthesis. *Mol. Plant-Microbe Interact.* 18, 1161–1174. doi: 10.1094/MPMI-18-1161

Conflict of Interest Statement: The authors declare that the research was conducted in the absence of any commercial or financial relationships that could be construed as a potential conflict of interest.

Copyright © 2019 Pérez-Bueno, Pineda and Barón. This is an open-access article distributed under the terms of the Creative Commons Attribution License (CC BY). The use, distribution or reproduction in other forums is permitted, provided the original author(s) and the copyright owner(s) are credited and that the original publication in this journal is cited, in accordance with accepted academic practice. No use, distribution or reproduction is permitted which does not comply with these terms.



Whole Irradiated Plant Leaves Showed Faster Photosynthetic Induction Than Individually Irradiated Leaves *via* Improved Stomatal Opening

Shunji Shimadzu¹, Mitsunori Seo², Ichiro Terashima¹ and Wataru Yamori^{1,3*}

¹ Department of Biological Sciences, Graduate School of Science, The University of Tokyo, Tokyo, Japan, ² RIKEN Center for Sustainable Resource Science, Yokohama, Japan, ³ Institute for Sustainable Agro-Ecosystem Services, The University of Tokyo, Nishitokyo, Japan

OPEN ACCESS

Edited by:

Michael Moustakas,
Aristotle University of Thessaloniki,
Greece

Reviewed by:

Xiaolei Sui,
China Agricultural University (CAU),
China
Izumi C. Mori,
Okayama University, Japan

*Correspondence:

Wataru Yamori
wataru.yamori@isas.a.u-tokyo.ac.jp

Specialty section:

This article was submitted to
Plant Abiotic Stress,
a section of the journal
Frontiers in Plant Science

Received: 15 September 2019

Accepted: 31 October 2019

Published: 28 November 2019

Citation:

Shimadzu S, Seo M, Terashima I and
Yamori W (2019) Whole Irradiated
Plant Leaves Showed Faster
Photosynthetic Induction Than
Individually Irradiated Leaves *via*
Improved Stomatal Opening.
Front. Plant Sci. 10:1512.
doi: 10.3389/fpls.2019.01512

Rapid photosynthetic induction is crucial for plants under fluctuating light conditions in a crop canopy as well as in an understory. Most previous studies have focused on photosynthetic induction responses in a single leaf, whereas the systemic responses of the whole plant have not been considered. In a natural environment, however, both single leaves and whole plants are exposed to sunlight, since the light environment is not uniform even within a given plant. In the present study, we examined whether there is any difference between the photosynthetic induction response of a leaf of a whole irradiated plant and an individually irradiated leaf in *Arabidopsis thaliana* to consider photosynthetic induction as the response of a whole plant. We used two methods, the visualization of photosynthesis and direct measurements of gas-exchange and Chl fluorescence, to demonstrate that whole irradiated plant promoted its photosynthetic induction *via* improved stomatal opening compared with individually irradiated leaf. Furthermore, using two *Arabidopsis* knockout mutants of abscisic acid transporter, *abcg25* and *abcg40*, the present study suggests that abscisic acid could be involved in this systemic response for stomatal opening, allowing plants to optimize the use of light energy at minimal cost in plants in a dynamic light environment.

Keywords: photosynthesis, photosynthetic induction, stomatal conductance, systemic signaling, abscisic acid

INTRODUCTION

Plant biomass is determined by the total incident radiation that occurs during the growing season, the light-interception efficiency of a plant, and the conversion efficiency of the intercepted radiation into biomass (Long et al., 2006; Zhu et al., 2010). The last factor, namely the conversion efficiency, is considered to be primarily determined by photosynthesis. As the light condition in a natural environment changes dynamically over time, the leaf photosynthetic rate does not always reach its steady state. Photosynthetic reactions, including stomatal opening and the enzymatic reaction, are switched off in the dark, specifically to prevent (1) water loss from stomata and (2) the unnecessary metabolism of carbon assimilation. Thus, plant leaves need some time to open their stomata and reactivate the enzymes of carbon assimilation when the irradiance increases rapidly in light-flecked environment after a prolonged period of darkness. The photosynthetic rate increases gradually over several minutes and approaches a new steady state when the light intensity on a leaf is increased

suddenly after a prolonged period of low light or darkness. This phenomenon has been termed “photosynthetic induction” (Percy, 1990), which occurs both in crop canopies and forest understories (Schurr et al., 2006).

The photosynthetic induction response can typically be divided into three phases that are highly interactive with each other: (1) photosynthetic electron transport, which is usually complete within the first 1–2 min, (2) enzyme reactions in a Calvin–Benson cycle, which often takes 5–10 min, and (3) stomatal opening, which typically takes as much as 1 h (Percy, 1990; Yamori, 2016). Recent studies have shown that cyclic electron flows around photosystem I (Yamori et al., 2016c) as well as ion channels such as KEA3, a thylakoid membrane localized K^+/H^+ antiporter (Armbruster et al., 2014; Kunz et al., 2014), and VCCN1, a voltage-dependent Cl^- channel (Herdean et al., 2016) are involved in photosynthetic induction to adjust photosynthetic light utilization in electron transport under fluctuating light conditions (for a review, see Tanaka et al., 2019). Moreover, it has been shown that Rubisco activase, an enzyme involved in Rubisco activation, is essential for photosynthetic induction in the second phase (Mott and Woodrow, 2000; Yamori et al., 2012; Carmo-Silva and Salvucci, 2013; Kaiser et al., 2016). In addition, the stomatal opening can be another factor limiting photosynthetic induction, as stomatal responses are much slower than the activation process of a Calvin cycle (Allen and Percy, 2000a; Allen and Percy, 2000b; Lawson et al., 2012; Kaiser et al., 2016).

The conversion efficiency of intercepted radiation into biomass under fluctuating light conditions is important for plant growth, especially for crops and for the survival of understory plants (Tinoco-Ojanguren and Percy, 1993; Valladares and Percy, 1997; Urban et al., 2007; Montgomery and Givnish, 2008). In particular, rapid photosynthetic induction improves the energy gain for CO_2 assimilation in dark-adapted leaves exposed to light flecks, since light flecks contribute up to 60–80% of the photosynthetically active radiation experienced by understory plants (Percy and Seemann, 1990; Leakey et al., 2003; Leakey et al., 2005). Additionally, the enhancement of photosynthetic capacity under fluctuating light has been receiving much attention, as an understanding of the physiological and genetic mechanisms behind photosynthetic induction is expected to contribute to it (Tanaka et al., 2019). Most previous studies have focused on photosynthetic induction responses in a single leaf, and the systemic responses of the whole plant have not been considered. In a natural environment, however, both single leaves and whole plants are exposed to sunlight, and light environments are not uniform even within a plant. In fact, different plant parts can communicate with one another through specific signals, which is known as systemic signaling (Karpinski et al., 1999; Bialasek et al., 2017). Previous studies have shown that the uppermost leaves, which are generally the first to receive sunlight, display faster photosynthetic induction than understory leaves (Bai et al., 2008). Photosynthetic induction in understory leaves is enhanced by the preillumination of upper leaves but not lower leaves (Hou et al., 2015). Furthermore, preillumination of a shoot apex could accelerate photosynthetic induction in distal leaves (Guo et al., 2016). These researches implied that the

photosynthetic response to fluctuating light in a single leaf would be different from that in the leaves of a whole plant.

In this study, we examined whether there is any difference between the photosynthetic induction responses of the leaf of a plant where all the leaves were irradiated (WIP, whole irradiated plant), and a leaf of a plant where all the other leaves were kept in the dark (IIL, individually irradiated leaf), in *Arabidopsis thaliana* to consider photosynthetic induction as a response of the whole plant. We also focused on abscisic acid (ABA) transport as a possible of systemic signaling mechanism in photosynthetic induction, since ABA is known to play pivotal roles in the regulation of stomatal opening/closing. Using two *Arabidopsis* knockout mutants, *abcg25*, which is an ABA exporter mediating the ABA efflux from vascular tissues (Kuromori et al., 2010) and *abcg40*, which is an ABA importer expressed in guard cells (Kang et al., 2010), we analyzed the relationship between ABA and photosynthetic induction and the effect of ABA on systemic signaling. These studies will provide a new perspective for a strategy that will enable plants to improve the light utilization efficiency of photosynthesis in crop canopies and forest understories.

MATERIAL AND METHODS

Plant Materials and Growth Conditions

The *A. thaliana* mutants, *abcg25* (SALK_063716) (Kanno et al., 2012), *abcg40-2* (SALK_005635) (Kang et al., 2010), *aba3-1* (Léon-Kloosterziel, et al., 1996), and the wild type (Col-0), were grown in soil in an environmentally controlled growth chamber. ABCG25 is localized in a plasma membrane in vascular tissue and executes ABA transport from the vasculature, ABCG40 is localized in guard cells and functions as a plasma membrane ABA uptake transporter, and ABA3-1 is impaired ABA synthesis. All the plants were grown in a 200-ml plastic pot containing soil, and each pot was supplied once a week with 100 ml of 1/500 strength nutrient solution (HYPONeX, N/P/K, 6:10:5, Hyponex Japan, Osaka, Japan). The growth chamber was operated at an air temperature of 23°C, a relative humidity of 70%, a photosynthetically active photon flux density (PPFD) of 150 $\mu\text{mol m}^{-2} \text{s}^{-1}$, with an 8-h photoperiod and a CO_2 concentration of 400 $\mu\text{mol mol}^{-1}$. The rice (*Oryza sativa* cv. Hitomebore) was grown in a 1.3-L plastic pot with 1.0 g of slow-release fertilizer (Temairazu; Co-op Chemical Co., Ltd., Tokyo, Japan). The growth chamber was also environmentally controlled and operated at a temperature of 23°C, a relative humidity of 70%, a PPFD of 500 $\mu\text{mol m}^{-2} \text{s}^{-1}$, with a 14-h photoperiod and a CO_2 concentration of 400 $\mu\text{mol mol}^{-1}$. All plants were given enough water, however, ABA-deficient mutant, *aba3-1*, was susceptible to water stress as shown previously (Finkelstein et al., 2002).

Analysis of Gas Exchange and Chlorophyll Fluorescence

Gas exchange and chlorophyll fluorescence were concurrently measured at a cuvette temperature of 25°C and a relative humidity of 70%, in fully expanded young leaves with a portable

gas exchange system LI-6400XT (Li-COR, Lincoln, NE, USA). A single leaf was clamped by the chamber of the Li-6400XT and the photosynthetic parameters were measured. First, leaves of the plants that were maintained in darkness overnight were treated with a saturating pulse to obtain maximum fluorescence. Then, the quantum yield of photosystem II [Y(II)], which reflects the photochemical efficiency of the electron transfer through photosystem II and the fraction of the oxidized photosystem II centers (qP), were obtained at $500 \mu\text{mol m}^{-2} \text{s}^{-1}$ for *A. thaliana* or $1,000 \mu\text{mol m}^{-2} \text{s}^{-1}$ for rice, as described previously (Baker, 2008). The electron transport rates (ETRs) through photosystem II were calculated using the following equation: $\text{ETR} = 0.5 \times \text{abs I} \times \text{Y(II)}$, where 0.5 is the fraction of absorbed light allocated to photosystems, and abs I refers to the absorbed irradiance taken as 0.84 of incident irradiance.

A–C_i Curve

A–C_i curve (CO₂ assimilation rate, A, versus intercellular CO₂ concentrations, C_i) analysis was performed at $500 \mu\text{mol m}^{-2} \text{s}^{-1}$ with an LI-6400XT. First, the steady-state photosynthetic rate at a CO₂ concentration of $400 \mu\text{mol mol}^{-1}$ was measured, and the CO₂ concentration was changed successively to 100, 200, 300, 400, 600, 800, 1,200, and $1,500 \mu\text{mol mol}^{-1}$. The photosynthetic rates were recorded after 5 min exposure to each CO₂ concentration.

Imaging PAM

Chlorophyll fluorescence was measured with an imaging fluorometer (IMAGING-PAM; Heinz Walz) in 4 to 6-week old plants. The plants were kept in darkness overnight, and then the photosynthetic induction response at a PPFD of $1,000 \mu\text{mol m}^{-2} \text{s}^{-1}$ was measured. The quantum yield of photosystem II [Y(II)], nonphotochemical quenching, and the fraction of oxidized photosystem II centers (qP) were analyzed.

Light Conditions for the Measurement of Photosynthetic Induction

We recorded the photosynthetic induction response in a WIP, in which all the leaves were irradiated, and in an IIL, where all the other leaves were kept in the dark. The rate of photosynthetic induction of an IIL and a WIP was compared. For the light treatment of the individual leaf, the IIL was clamped in a cuvette of the Li-6400XT while the rest of the plant remained in darkness. In contrast, for the light treatment of the whole plant, a leaf of the WIP was clamped while the rest of the plant was illuminated with the same light intensity by the same light source during the photosynthetic induction measurement (Figure 1). By using these plants, which had been kept in the dark overnight, the responses of various photosynthetic parameters to an irradiance of $500 \mu\text{mol m}^{-2} \text{s}^{-1}$ for *A. thaliana* or $1,000 \mu\text{mol m}^{-2} \text{s}^{-1}$ for rice were measured every 30 s.

Plant Growth Analysis

The plants were grown in a growth chamber at room temperature (23°C), a relative humidity of 70%, a PPFD of $150 \mu\text{mol m}^{-2} \text{s}^{-1}$ and

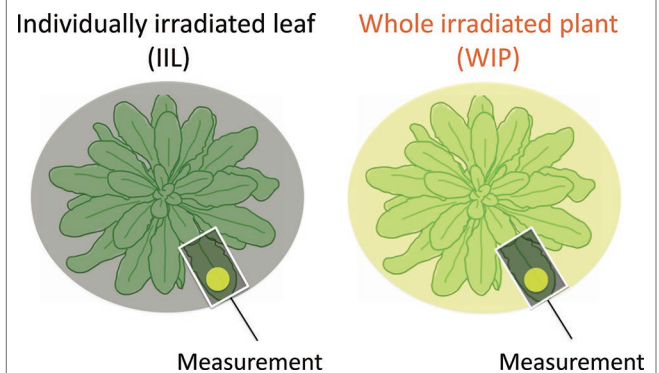


FIGURE 1 | Schematic diagram of light treatment to a leaf of a whole irradiated plant (WIP) and an individually irradiated leaf (IIL). During the measurement of the IIL, the other leaves were covered with black cloth and were kept in the dark, whereas during the measurement of the WIP, all the leaves of a plant were irradiated. Under both light conditions, the selected target leaves were similar in age.

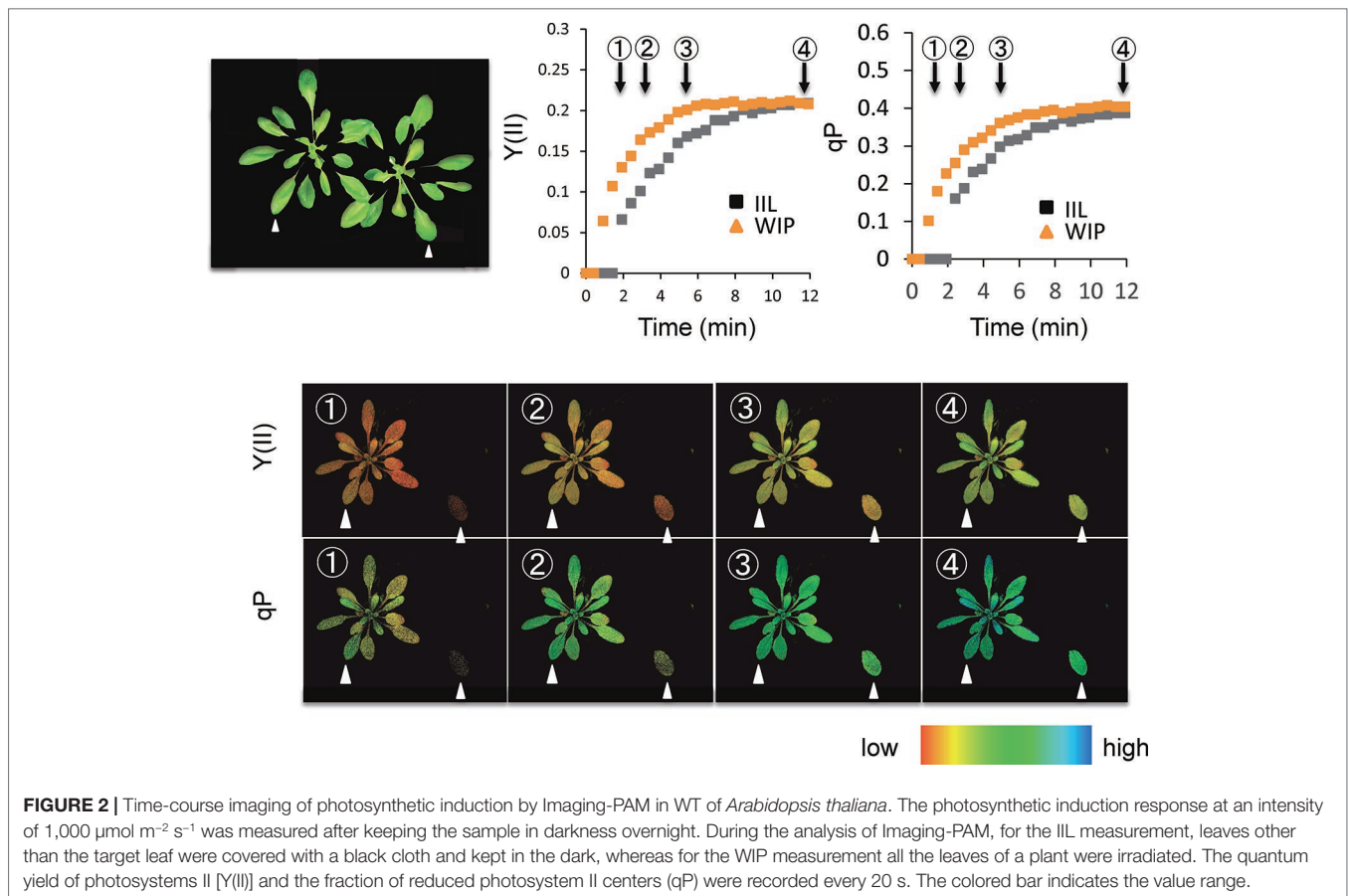
an 8-h photoperiod until 23 days after sowing. Then, the plants were transferred to either fluctuating light conditions or constant light conditions. Under both conditions, the plants were exposed to a high light intensity of $500 \mu\text{mol m}^{-2} \text{s}^{-1}$ for 4 h and a low light intensity of $60 \mu\text{mol m}^{-2} \text{s}^{-1}$ for 8 h per day. Under the constant light conditions, the plants were exposed to a low light intensity for 4 h each in the morning and evening, and to a high light intensity for 4 h around midday. On the other hand, under the fluctuating light conditions, a high light intensity for 5 min and a low light intensity for 10 min were alternated for 12 h. At 43 days after sowing, the above-ground parts of the plants were sampled and dried at 80°C for several days, and their dry weights were measured.

RESULTS

Photosynthetic Induction in IIL and WIP

Photosynthetic induction was compared between an IIL and a leaf of WIP (Figure 1). During the analysis with Imaging-PAM of *A. thaliana*, for the IIL measurement, the other leaves were covered with black cloth and were kept in the dark (Figure 2), whereas, for the WIP measurement, whole plant was irradiated during the measurement of photosynthetic induction of the targeted leaf, which was a similar age to the IIL. The WIP significantly promoted the induction of Y(II) and qP upon exposure to a high light intensity ($1,000 \mu\text{mol m}^{-2} \text{s}^{-1}$) at a CO₂ concentration of $400 \mu\text{mol mol}^{-1}$ (Figure 2), indicating that the WIP would be able to use more light energy to drive the electron transport to generate adenosine triphosphate and reduced nicotinamide adenine dinucleotide phosphate during the first few minutes after a change in light intensity.

This was supported by the concomitant measurement of gas exchange and Chl fluorescence, which showed that the WIP exhibited a faster induction of CO₂ assimilation (A) and photosynthetic ETR at a high light intensity of $500 \mu\text{mol m}^{-2} \text{s}^{-1}$ at a CO₂ concentration of $400 \mu\text{mol mol}^{-1}$ in *Arabidopsis* (Figure 3). Moreover, the steady-state A and ETR tended to be greater



in the WIP than in the IIL (Figure S1). Interestingly, the WIP significantly promoted the induction of stomatal conductance (g_s) upon exposure to a high light intensity and thus the transition to the steady-state of the intercellular CO_2 concentrations (C_i) was faster in the WIP than in the IIL. The WIP significantly shortened the time required to reach 60% (T_{60}) of the maximum A , g_s , and ETR , and the time required to reach 60% in the transition from minimum to maximum C_i (Table 1). This result was also confirmed in rice (Figure S2). In contrast, the WIP lost its effect upon exposure to a high light intensity at a high CO_2 concentration of $1,500 \mu\text{mol mol}^{-1}$, where the effect of the stomatal response on photosynthetic induction could be negligible since C_i was held above a certain level regardless of the stomatal response (Figure 3). These findings indicate that the WIP promoted its photosynthetic induction *via* an improvement in the stomatal response.

Photosynthetic Induction in ABCG Knockout Mutants

During the photosynthetic induction, the stomata opened synchronously as the CO_2 assimilation accelerated. To clarify the role of the stomata in the promotion of photosynthetic induction, and to evaluate whether ABA plays pivotal roles in the promotion of photosynthetic induction, we compared the photosynthetic induction processes at a CO_2 concentration of $400 \mu\text{mol mol}^{-1}$ of wild type (WT) and two *Arabidopsis* knockout mutants of ABA

transporter, *abcg25* and *abcg40*. Photosynthetic CO_2 response curves ($A - C_i$ curve) were similar among WT and two *abcg* mutants (Figure S3). The rate at which A and g_s approached a steady state following an increase in the irradiance was fastest in *abcg40*, intermediate in *abcg25*, and slowest in WT (Figure 4). This was supported by the time required to reach 60% (T_{60}) of the maximum A , g_s , and ETR , and the time required to reach 60% of the maximum C_i compared to the minimum upon irradiation at a CO_2 concentration of $400 \mu\text{mol mol}^{-1}$ (Table 2). The rates at which the reduction level of the plastoquinone pool ($1 - qP$) approached their steady states upon irradiation were faster in the two *abcg* mutants than in WT. These results indicate that, during photosynthetic induction, the two mutants utilized more light energy driving photosynthesis.

We also compared the photosynthetic induction process for WT, *abcg25* and *abcg40* at a high CO_2 concentration of $1,500 \mu\text{mol mol}^{-1}$ (Figure 4). The induction response of all the photosynthetic parameters (i.e., A , g_s , and ETR) showed no clear difference for WT and the two *abcg* mutants, which was supported by the T_{60} of the maximum A , g_s , and C_i at a CO_2 concentration of $1,500 \mu\text{mol mol}^{-1}$ (Table 2). These results showed that stomatal opening would actually have a great influence on the photosynthetic induction process. This was partly supported by a previous study, which reported that increases in initial g_s up to a threshold value accelerate photosynthetic induction in a knockout mutant of ABA synthesis, *aba2-1* (Kaiser et al., 2016).

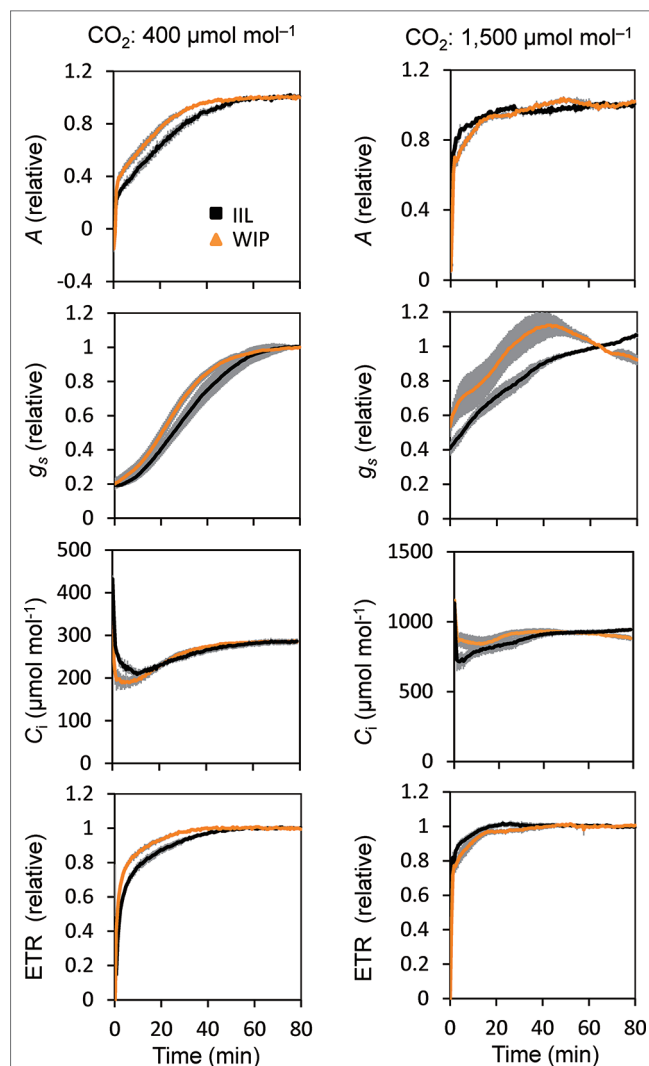


FIGURE 3 | Photosynthetic induction of IIL and WIP of *Arabidopsis* WT. CO₂ assimilation rate (*A*), stomatal conductance (*g_s*), intercellular CO₂ concentration (*C_i*), and photosynthetic electron transport rate (ETR) were simultaneously measured in an IIL or WIP, at CO₂ concentrations of 400 μmol mol⁻¹ and 1,500 μmol mol⁻¹. The leaves of plants kept in the dark overnight were used for the experiments. The photosynthetic parameters were recorded every 30 s at an irradiance of 500 μmol photons m⁻² s⁻¹ for a total of 80 min. Absolute values are shown in **Figure S1**. The data are the means ± standard errors of four biological replicates.

To further examine whether ABA is involved in the stomatal responses observed in the WIP and IIL, we compared the photosynthetic induction processes of *abcg25* and *abcg40* knockout mutants under two conditions at a CO₂ concentration of 400 μmol mol⁻¹. In the two *abcg* mutants, the induction responses of all the photosynthetic parameters (i.e., *A*, *g_s*, and ETR) were similar for the WIP and IIL (**Figure 5**, **Table 3**), although it was significantly different in WT (**Figure 3**). Taken together, these results suggest that the promotion of photosynthetic induction by whole plant irradiation is affected by stomatal responses to ABA, which are regulated by the two ABA transporters.

TABLE 1 | The time required to reach 60% (*T₆₀*) of the maximum CO₂ assimilation rate (*A*), stomatal conductance (*g_s*), the intercellular CO₂ concentrations (*C_i*), and photosynthetic electron transport rate (ETR) at a CO₂ concentration of 400 or 1,500 μmol mol⁻¹ between in a leaf of a whole irradiated plant (WIP) and an individually irradiated leaf (IIL) in WT of *Arabidopsis thaliana*.

<i>T₆₀</i> (min)	IIL	WIP
<i>A</i> ₄₀₀	18.3 ± 2.5	10.8 ± 1.8*
<i>g_s</i> ₄₀₀	37.0 ± 2.97	29.0 ± 1.73*
<i>C_i</i> ₄₀₀	32.5 ± 2.36	24.7 ± 1.25*
ETR ₄₀₀	3.53 ± 0.34	1.72 ± 0.20*
<i>A</i> ₁₅₀₀	0.95 ± 0.12	1.16 ± 0.10
ETR ₁₅₀₀	0.79 ± 0.08	0.92 ± 0.03

The values are presented as the mean ± standard deviation (*n* ≥ 4), and the asterisks next to WIP indicate significant differences between data for the IIL and WIP (Student's *t*-test, *P* < 0.05).

Plant Growth Under Fluctuating Light Conditions in *abcg* Knockout Mutants

To examine the effect of the improvement of the photosynthetic induction response on the total biomass in *abcg* knockout mutants, these mutants as well as wt and *aba3-1*, which impaired aba synthesis, were grown under both fluctuating and constant light conditions. wt and two *abcg* mutants grew almost equally under constant light conditions, whereas the plant growth of the two *abcg* knockout mutants was greater than that of wt under fluctuating light conditions where there was an alternating high light intensity of 500 μmol m⁻² s⁻¹ for 5 min and a low light intensity of 60 μmol m⁻² s⁻¹ for 10 min (**Figure 6**). growth of *aba3-1* knockout mutant was apparently suppressed both in fluctuating light conditions and constant light conditions, since drought stress could suppress its plant growth.

DISCUSSION

As light flecks are the primary energy source for plants not only in the understory but also in the crop canopy (Pearcy and Seemann, 1990; Percy and Way, 2012), rapid photosynthetic induction is crucial for plants under fluctuating light conditions. Light flecks move continuously from one leaf of a plant to another, since light flecks are usually too small to cover a whole plant in a forest understory or canopy. To date, most previous studies have focused on the photosynthetic induction responses in a single leaf, with scant attention to the systemic responses of the whole plant. Here, we used two methods, the visualization of photosynthesis with Imaging-PAM and direct measurements of gas exchange and Chl fluorescence with an Li-6400XT, to demonstrate that a leaf of a WIP promotes photosynthetic induction *via* improvement of the stomatal response in comparison with an IIL. This mechanism is important for optimizing the light utilization efficiency of photosynthesis at minimum cost in plants in a dynamic light environment. In addition, a better understanding of the photosynthetic induction response is necessary if we are to better calculate the terrestrial carbon cycle and its influence on the atmospheric CO₂ concentration and global climate change, since most photosynthetic models used for global carbon

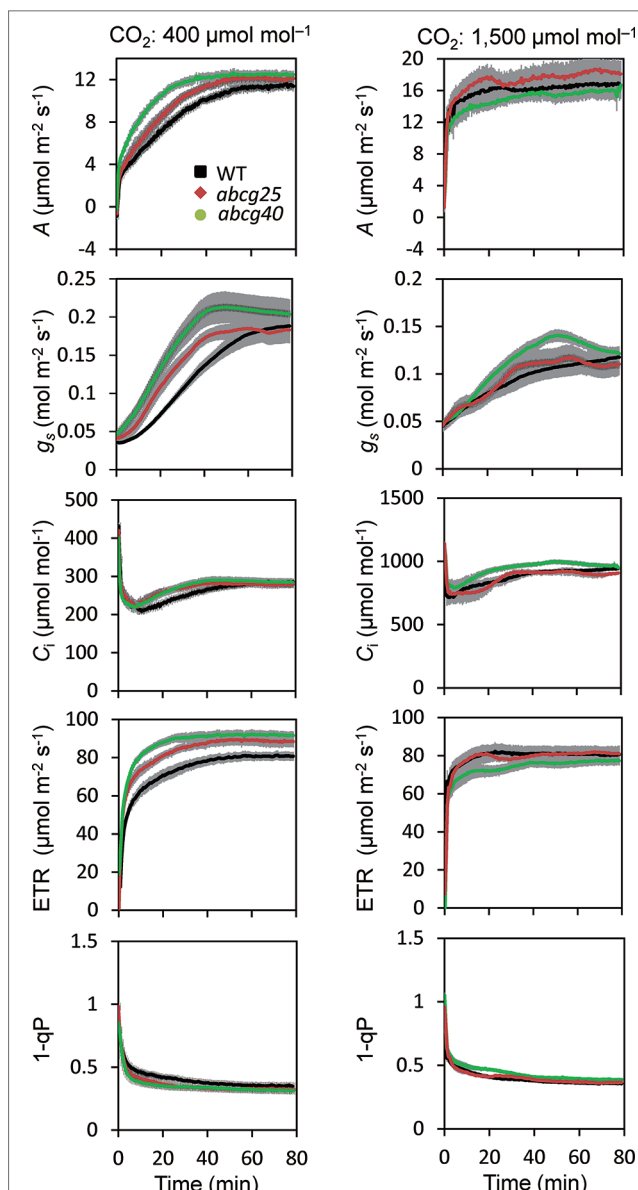


FIGURE 4 | Photosynthetic induction in ILL among WT and two *abcg* mutants. CO_2 assimilation rate (A), stomatal conductance (g_s), intercellular CO_2 concentration (C_i), photosynthetic electron transport rate (ETR), the redox state of the plastoquinone pool ($1 - qP$) were simultaneously measured at CO_2 concentrations of 400 and $1,500 \mu\text{mol mol}^{-1}$. The data are the means \pm standard errors of four biological replicates.

issues are based on steady-state photosynthesis under constant environmental conditions in single leaves.

Whole Irradiated Plants Exhibited Faster Photosynthetic Induction *via* Improved Stomatal Opening

This study showed that the photosynthetic induction time at $400 \mu\text{mol mol}^{-1} \text{CO}_2$ was shortened with a rapid increase in g_s in a WIP compared with an ILL, whereas at a high CO_2 concentration of $1,500 \mu\text{mol mol}^{-1}$, the photosynthetic induction time was shortened

TABLE 2 | The time required to reach 60% (T_{60}) of the maximum CO_2 assimilation rates (A), stomatal conductance (g_s), the intercellular CO_2 concentrations (C_i), and photosynthetic electron transport rate (ETR) at a CO_2 concentration of 400 or $1,500 \mu\text{mol mol}^{-1}$ in an individually irradiated leaf (ILL) in WT, *abcg25*, and *abcg40* knockout mutants.

T_{60} (min)	WT	<i>abcg 25</i>	<i>abcg 40</i>
A_{400}	18.3 ± 2.5 a	14.3 ± 2.6 ab	7.7 ± 1.4 b
g_{s400}	37.0 ± 2.97 a	27.6 ± 2.35 ab	24.9 ± 3.42 b
C_{i400}	32.5 ± 2.36 a	17.9 ± 0.79 b	23.6 ± 2.40 b
ETR_{400}	3.53 ± 0.34 a	2.30 ± 0.47 b	2.36 ± 0.32 ab
A_{1500}	0.95 ± 0.12 a	1.27 ± 0.09 a	1.19 ± 0.10 a
ETR_{1500}	0.79 ± 0.08 a	1.06 ± 0.08 a	1.03 ± 0.04 a

The values are presented as the mean \pm standard deviation ($n \geq 4$), and the different letters denote significant differences (Tukey–Kramer's honest significant difference test).

under both conditions and the differences in photosynthetic induction times were eliminated (**Figure 3**). These results clearly showed that the reduction in the photosynthetic induction time in a WIP was caused by the quick stomatal opening.

It has been suggested that ABA is actively synthesized in leaf vascular tissues and then transported to guard cells to close the stomata in response to water stress, although guard cell autonomous ABA biosynthesis has also been reported (Kuromori et al., 2018). *Arabidopsis ABCG25*, which encodes an ABA exporter, is expressed in vascular tissues (phloem companion cells) (Kuromori et al., 2010; Kuromori et al., 2014) whereas *ABCG40*, which encodes an ABA importer, is expressed in guard cells (Kang et al., 2010). Thus, it is expected that both *abcg25* and *abcg40* would have lower ABA concentrations in guard cells. In these mutants, photosynthetic induction time and the increase in g_s at $400 \mu\text{mol mol}^{-1} \text{CO}_2$ were almost the same for the ILL and WIP (**Figure 5, Table 3**), and also were much faster than for WT (**Tables 1 and 3**), suggesting that the reduction in the ABA levels within guard cells is involved in the stomatal opening in response to irradiation and that this process is enhanced in a WIP. It has been reported that changes in g_s induced by guard cells are linked with ABA signaling arriving in the xylem (Tardieu et al., 1992), and that there are negative correlations between the ABA concentrations in xylem sap and g_s (Tardieu et al., 1991). Although most studies have focused on ABA production in roots followed by its transport to leaves *via* transpiration (Tardieu et al., 1992), it is now recognized that ABA is also produced by local biosynthesis in leaves (Boursiac et al., 2013; Takahashi et al., 2018). The importance of ABA as a systemic signal initiating stomatal closure has also been shown (Christmann et al., 2007). Thus, the distribution of ABA in a xylem flow as well as the ABA uptake into guard cells could affect photosynthetic induction, although it is unknown how ABA transport mediated by *ABCG25* and *ABCG40* is regulated in response to light irradiation. In leaves, stomata typically close at night to limit transpiration and save water, and the stomatal response to darkness might be related to the ABA concentration in guard cells. On the assumption that a low concentration of ABA is present in xylem sap, which could close stomata at night, and that transpiration is promoted upon irradiation only in one leaf of a plant where all the other leaves are kept in the dark (ILL), ABA could be concentrated only in the leaf *via* transpiration, leading to stomatal closure. On the other

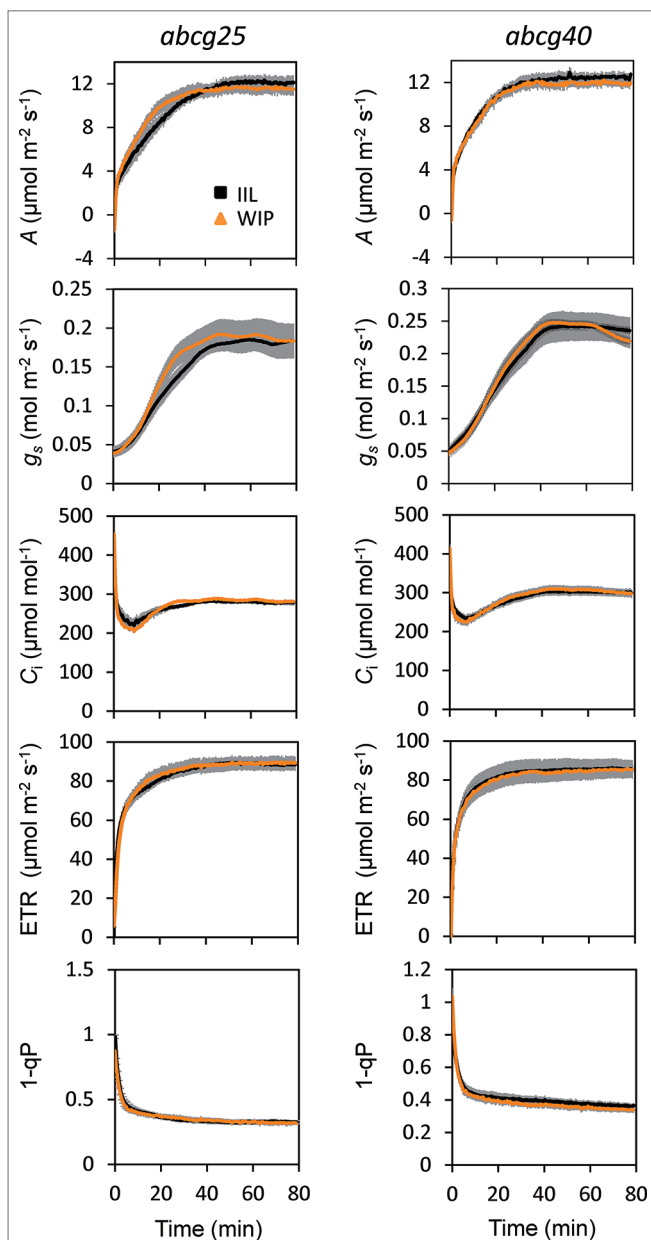


FIGURE 5 | Photosynthetic induction of IIL and WIP in two *abcg* mutants. CO_2 assimilation rate (A), stomatal conductance (g_s), intercellular CO_2 concentration (C_i), photosynthetic electron transport rate (ETR), the redox state of the plastoquinone pool ($1 - qP$) were simultaneously measured in an IIL or WIP, at a CO_2 concentration of $400 \mu\text{mol mol}^{-1}$. The leaves of plants kept in the dark overnight were used for experiments. The photosynthetic parameters were recorded every 30 s at an irradiance of $500 \mu\text{mol photons m}^{-2} \text{s}^{-1}$ until 80 min. The data are the means \pm standard errors of four biological replicates.

hand, assuming that transpiration is promoted upon irradiation of all the leaves of a plant (WIP), ABA could not be concentrated, leading to prompt stomatal opening.

In addition to ABA, several other systemic signals such as chemical signals, electrical long-distance signals, and hydraulic signals have been reported (for a review, see Huber and

TABLE 3 | The time required to reach 60% (T_{60}) of the maximum CO_2 assimilation rates (A), stomatal conductance (g_s), the intercellular CO_2 concentrations (C_i), and photosynthetic electron transport rate (ETR) at a CO_2 concentration of $400 \mu\text{mol mol}^{-1}$ in a leaf of a whole irradiated plant (WIP) and an individually irradiated leaf (IIL), and in both *abcg25* and *abcg40* knockout mutants.

T_{60} (min)		IIL	WIP
<i>abcg25</i>	A_{400}	14.3 ± 2.6	9.1 ± 1.4
	g_{s400}	27.6 ± 2.35	21.8 ± 1.57
	C_{i400}	17.9 ± 0.79	18.1 ± 2.25
	ETR_{400}	2.30 ± 0.47	2.76 ± 0.21
<i>abcg40</i>	A_{400}	7.70 ± 1.36	8.66 ± 1.68
	g_{s400}	24.9 ± 3.41	23.1 ± 1.83
	C_{i400}	23.6 ± 2.40	20.3 ± 1.93
	ETR_{400}	2.36 ± 0.32	2.39 ± 0.31

The values are presented as the mean \pm standard deviation ($n \geq 4$). There was no statistical difference between the T_{60} values for the IIL and WIP and in both *abcg25* and *abcg40* (Student's *t*-test, $P < 0.05$).

Bauerle, 2016) Recently, it was reported that the induction of photosynthesis and stomatal opening in understory leaves is enhanced by the preirradiation of upper leaves but not lower leaves, suggesting a directional signal transfer passing through the phloem (Hou et al., 2015). Another recent report showed that systemic signaling mediated by phytochrome B and auxin caused by the irradiation of the shoot apex promoted photosynthetic induction (Guo et al., 2016), as the phytohormone auxin is produced in the shoot apex and redistributed throughout the shoot by rapid phloem transport (Ljung et al., 2001) and changes in the light environment can greatly alter auxin homeostasis (Halliday et al., 2009). This systemic signaling might also be related to the differences in the photosynthetic induction of WIP and IIL observed in the present study.

Also, we cannot exclude the possibility that changes in the turgor pressure in mesophyll cells could affect stomatal opening more in a WIP than in an IIL. In general, the more stomata open, the more plants lose water by transpiration. Since a WIP promotes photosynthetic induction and stomatal opening in the entire plant, the plant would lose more water than an IIL where only a single leaf is irradiated. As the water flow in vessels would be a factor limiting the water supply to a leaf, it can be expected that the leaf water content during photosynthetic induction would be lower in a WIP than an IIL. Stomatal opening and closing takes place due to changes in the turgor pressure in guard cells. Solutes are taken in the guard cells from the neighboring epidermal and mesophyll cells, and so both the osmotic potential and water potential of the guard cells are lowered. These create a water potential gradient between the guard cells and the neighboring cells, making the water move into the guard cells, and resulting in the enlargement of the guard cells that eventually bow outwards causing the stomatal pore to open. Water is supplied from the root through the xylem vessels. Since the xylem vessels are connected to each leaf, the amount of water which the xylem vessels can supply simultaneously would be limited. The number of leaves that lose water would be higher in WIP than in IIL. In WIP, the difference in water potential could contribute to an increase in the amount of water supply itself, but it is unlikely that the same amount of water that flows into an IIL can flow into each leaf of a WIP. As

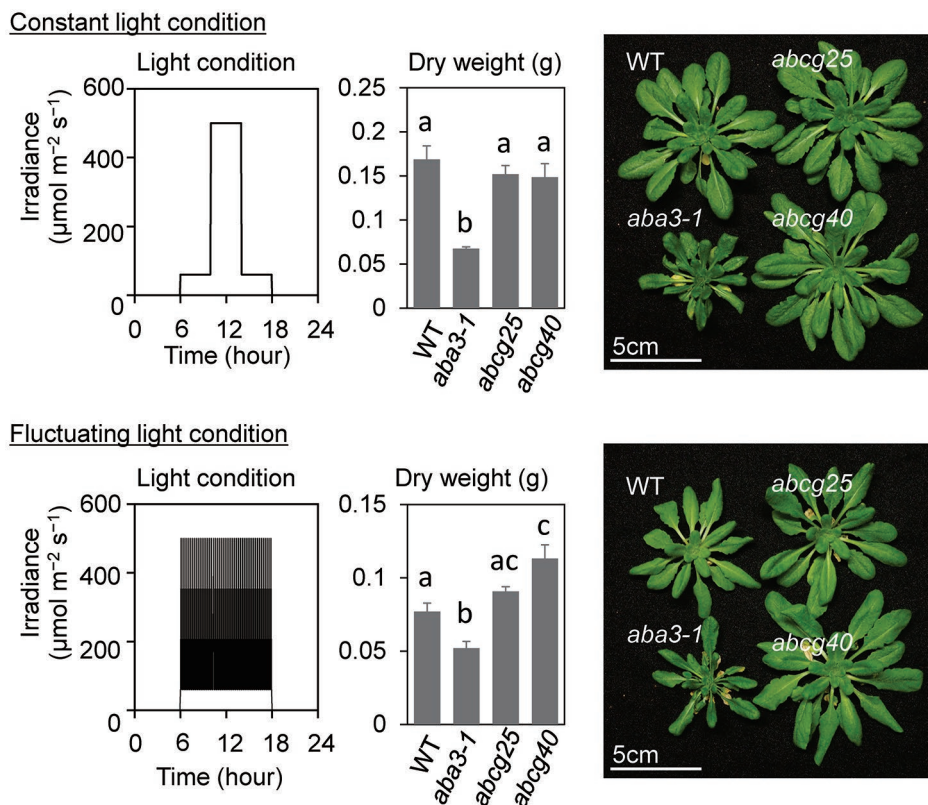


FIGURE 6 | Plant growth under constant light and fluctuating light conditions. The growth light conditions and dry weights of aerial parts of plants at 43 days after sowing (DAS) were shown with plant pictures at 43 DAS. All plants were grown under constant light until 23 DAS and were divided into two growth conditions; constant light and fluctuating light conditions. Under the constant light conditions, the plants were exposed to low light for 4 h in the morning and 4 h in the evening, and to high light for 4 h in the middle of the day, whereas, under the fluctuating light conditions, a high light for 5 min and low light for 10 min were alternated for 12 h. The data are the means \pm standard errors of four biological replicates, and the letters denote significant differences (Tukey–Kramer’s honest significant difference test).

a result, it is expected that WIP would lose more water than IIL. Assuming that the leaf water content of a WIP decreases during photosynthetic induction, it is expected that the turgor pressure in the neighboring epidermal and mesophyll cells would also decrease, resulting in the stomata opening more smoothly with less tension. Why was stomatal opening promoted in two *abcg* mutants with the WIP and IIL? There could be two possibilities: (1) ABA positively closed the stomata in the dark in WT but not in the two *abcg* mutants, (2) the leaf water content was lower because of the smaller amount of ABA in the guard cell resulting in the stomata open more smoothly. More studies are needed to clarify the specific mechanism that promoted stomatal opening more in a WIP than in an IIL.

ABA-Mediated Prompt Stomatal Response Improves Plant Biomass

Since photosynthesis is the basis for plant growth and yield (Yamori et al., 2016b), researchers have been trying to enhance photosynthetic performance to improve plant biomass and/or yield (Yamori et al., 2016a). In most studies, the target has been to improve leaf photosynthesis under constant conditions (Wang et al., 2014; Simkin et al., 2017). However, in natural

environments, various environmental factors, especially light, change dynamically over time (Percy et al., 1990; Percy, 1990; Yamori, 2016). Therefore, we should explore strategies for optimizing photosynthesis and plant growth in natural environments. Recent work has shown that stomatal conductance, at the onset of a sudden light increase, plays a major role in photosynthetic induction from an analysis of *aba2-1* mutant in *A. thaliana* (Kaiser et al., 2016). Additionally, it was recently reported that acceleration of stomatal opening and closing caused by introduction of synthetic, blue light-gated K^+ channel to guard cells enhanced plant growth in *A. thaliana* in the fluctuating light conditions (Papanatsiou et al., 2019).

The present study showed that the photosynthetic induction time at $400 \mu\text{mol mol}^{-1} \text{CO}_2$ was shortened in *abcg25* and *abcg40* with a rapid increase in g_s (Figure 5), whereas at a high CO_2 concentration of $1,500 \mu\text{mol mol}^{-1}$, the photosynthetic induction time was shortened under both conditions, and the differences in the photosynthetic induction time were eliminated (Figure 6 and Table 2). These results clearly showed that the shortening of the photosynthetic induction time was due to the high C_i levels caused by the quick stomatal opening upon irradiation. Since the amount of ABA transported to a guard cell was estimated to be lower in *abcg25* and *abcg40* than in WT, the lower ABA concentration

consequently promoted stomatal opening upon irradiation, leading to improved photosynthetic induction. Moreover, the plant growth under fluctuating light in the two *abcg* mutants was greater than in WT, indicating that rapid induction improved the efficiency of the total photosynthesis during plant growth. As it has been reported that there are several transporters for ABA (Kuromori et al., 2018), we concluded that an improvement in the stomatal response caused by a slight impairment of the ABA transport could promote a photosynthetic response to a repeated fluctuating light and thus improve the plant biomass under long-term fluctuating light conditions with well-controlled relative humidity. We propose that a consideration of stomatal conductance will be promising approach in terms of improving photosynthesis in natural environments where irradiance always fluctuates.

DATA AVAILABILITY STATEMENT

All datasets generated for this study are included in the article/supplementary material.

REFERENCES

- Allen, M. T., and Pearcy, R. W. (2000a). Stomatal behavior and photosynthetic performance under dynamic light regimes in a seasonally dry tropical rain forest. *Oecologia* 122, 470–478. doi: 10.1007/s004420050968
- Allen, M. T., and Pearcy, R. W. (2000b). Stomatal versus biochemical limitations to dynamic photosynthetic performance in four tropical rainforest shrub species. *Oecologia* 122, 479–486. doi: 10.1007/s004420050969
- Armbruster, U., Carrillo, L. R., Venema, K., Pavlovic, L., Schmidtman, E., Kornfeld, A. et al. (2014). Ion antiport accelerates photosynthetic acclimation in fluctuating light environments. *Nat. Commun.* 5, 5439. doi: 10.1038/ncomms6439
- Bai, F. W., Anderson, W. A., and Moo-Young, M. (2008). Ethanol fermentation technologies from sugar and starch feedstocks. *Biotechnol. Adv.* 26, 89–105. doi: 10.1016/j.biotechadv.2007.09.002
- Baker, N. R. (2008). Chlorophyll fluorescence: a probe of photosynthesis in vivo. *Annu. Rev. Plant Biol.* 59, 89–113. doi: 10.1146/annurev.arplant.59.032607.092759
- Białecka, M., Górecka, M., Mittler, R., and Karpiński, S. (2017). Evidence for the involvement of electrical, calcium and ROS signaling in the systemic regulation of non-photochemical quenching and photosynthesis. *Plant Cell Physiol.* 58, 207–215. doi: 10.1093/pcp/pcw232
- Boursiac, Y., Lérans, S., Corratgé-Faillie, C., Gojon, A., Krouk, G., and Lacombe, B. (2013). ABA transport and transporters. *Trends Plant Sci.* 18, 325–333. doi: 10.1016/j.tplants.2013.01.007
- Carmo-Silva, A. E., and Salvucci, M. E. (2013). The regulatory properties of Rubisco activase differ among species and affect photosynthetic induction during light transitions. *Plant Physiol.* 161, 1645–1655. doi: 10.1104/pp.112.213348
- Christmann, A., Weiler, E. W., Steudle, E., and Grill, E. (2007). A hydraulic signal in root-to-shoot signalling of water shortage. *Plant J.* 52, 167–174. doi: 10.1111/j.1365-313X.2007.03234.x
- Finkelstein, R. R., Gampala, S. S., and Rock, C. D. (2002). Absciscic acid signaling in seeds and seedlings. *Plant Cell* 14 (suppl 1), S15–S45. doi: 10.1105/tpc.010441
- Guo, Z., Wang, F., Xiang, X., Ahammed, G. J., Wang, M., Onac, E. et al. (2016). Systemic induction of photosynthesis via illumination of the shoot apex is mediated sequentially by phytochrome B, auxin and hydrogen peroxide in Tomato. *Plant Physiol.* 172, 1259–1272. doi: 10.1104/pp.16.01202
- Halliday, K. J., Martínez-García, J. F., and Josse, E. M. (2009). Integration of light and auxin signaling. *Cold Spring Harbor Perspect. In Biol.* 1, a001586. doi: 10.1101/cshperspect.a001586

AUTHOR CONTRIBUTIONS

All authors conceived and designed the experiments. SS and WY performed the experiments. SS analysed the data and prepared figures and graphs. SS and WY prepared the manuscript, and all the members contributed extensively to its finalization.

FUNDING

This study was partly supported by Japan Society for the Promotion of Science (JSPS) [KAKENHI Grant Number: 16H06552, 18H02185, and 18KK0170 (to WY)] and by Ichimura foundation for new technology to WY.

SUPPLEMENTARY MATERIAL

The Supplementary Material for this article can be found online at: <https://www.frontiersin.org/articles/10.3389/fpls.2019.01512/full#supplementary-material>

- Herdean, A., Teardo, E., Nilsson, A. K., Pfeil, B. E., Johansson, O. N., Ünneper, R. et al. (2016). A voltage-dependent chloride channel fine-tunes photosynthesis in plants. *Nat. Commun.* 7, 11654. doi: 10.1038/ncomms11654
- Hou, F., Jin, L. Q., Zhang, Z. S., and Gao, H. Y. (2015). Systemic signaling in photosynthetic induction of *Rumex K-1* (*Rumex patientia* × *Rumex tianschaisicus*) leaves. *Plant Cell Environ.* 38, 685–692. doi: 10.1111/pce.12427
- Huber, A. E., and Bauerle, T. L. (2016). Long-distance plant signaling pathways in response to multiple stressors: the gap in knowledge. *J. Exp. Bot.* 67, 2063–2079. doi: 10.1093/jxb/erw099
- Kaiser, E., Morales, A., Harbinson, J., Heuvelink, E., Prinzenberg, A. E., and Marcelis, L. F. (2016). Metabolic and diffusional limitations of photosynthesis in fluctuating irradiance in *Arabidopsis thaliana*. *Sci. Rep.* 6, 31252. doi: 10.1038/srep31252
- Kang, J., Hwang, J. U., Lee, M., Kim, Y. Y., Assmann, S. M., Martinoia, E. et al. (2010). PDR-type ABC transporter mediates cellular uptake of the phytohormone abscisic acid. *Proc. Natl. Acad. Sci. U.S.A.* 107, 2355–2360. doi: 10.1073/pnas.0909222107
- Kanno, Y., Hanada, A., Chiba, Y., Ichikawa, T., Nakazawa, M., Matsui, M. et al. (2012). Identification of an abscisic acid transporter by functional screening using the receptor complex as a sensor. *Proc. Natl. Acad. Sci. U.S.A.* 109, 9653–9658. doi: 10.1073/pnas.1203567109
- Karpinski, S., Reynolds, H., Karpinska, B., Wingsle, G., Creissen, G., and Mullineaux, P. (1999). Systemic signaling and acclimation in response to excess excitation energy in *Arabidopsis*. *Science* 284, 654–657. doi: 10.1126/science.284.5414.654
- Kunz, H. H., Gierth, M., Herdean, A., Satoh-Cruz, M., Kramer, D. M., Spetea, C. et al. (2014). Plastidial transporters KEA1, -2, and -3 are essential for chloroplast osmoregulation, integrity, and pH regulation in *Arabidopsis*. *Proc. Natl. Acad. Sci. U.S.A.* 111, 7480–7485. doi: 10.1073/pnas.1323899111
- Kuromori, T., Miyaji, T., Yabuuchi, H., Shimizu, H., Sugimoto, E., Kamiya, A. et al. (2010). ABC transporter AtABCG25 is involved in abscisic acid transport and responses. *Proc. Natl. Acad. Sci. U.S.A.* 107, 2361–2366. doi: 10.1073/pnas.0912516107
- Kuromori, T., Sugimoto, E., and Shinozaki, K. (2014). Intertissue signal transfer of abscisic acid from vascular cells to guard cells. *Plant Physiol.* 164, 1587–1592. doi: 10.1104/pp.114.235556
- Kuromori, T., Seo, M., and Shinozaki, K. (2018). ABA transport and plant water stress responses. *Trends Plant Sci.* 23, 513–522. doi: 10.1016/j.tplants.2018.04.001
- Lawson, T., Kramer, D. M., and Raines, C. A. (2012). Improving yield by exploiting mechanisms underlying natural variation of photosynthesis. *Curr. Opin. Biotechnol.* 23, 215–220. doi: 10.1016/j.copbio

- Leakey, A. D. B., Press, M. C., and Scholes, J. D. (2003). High-temperature inhibition of photosynthesis is greater under sunflecks than uniform irradiance in a tropical rain forest tree seedling. *Plant Cell Environ.* 26, 1681–1690. doi: 10.1046/j.1365-3040.2003.01086.x
- Leakey, A. D. B., Scholes, J. D., and Press, M. C. (2005). Physiological and ecological significance of sunflecks for dipterocarp seedlings. *J. Exp. Bot.* 56, 469–482. doi: 10.1093/jxb/eri055
- Léon-Kloosterziel, K. M., Gil, M. A., Ruijs, G. J., Jacobsen, S. E., Olszewski, N. E., Schwartz, S. H. et al. (1996). Isolation and characterization of abscisic acid-deficient Arabidopsis mutants at two new loci. *Plant*. 10, 655–661. doi: 10.1046/j.1365-313x.1996.10040655.x
- Ljung, K., Östin, A., Lioussanne, L., and Sandberg, G. (2001). Developmental regulation of indole-3-acetic acid turnover in Scots pine seedlings. *Plant Physiol.* 125, 464–475. doi: 10.1104/pp.125.1.464
- Long, S. P., ZHU, X. G., Naidu, S. L., and Ort, D. R. (2006). Can improvement in photosynthesis increase crop yields? *Plant Cell Environ.* 29, 315–330. doi: 10.1111/j.1365-3040.2005.01493.x
- Montgomery, R. A., and Givnish, T. J. (2008). Adaptive radiation of photosynthetic physiology in the Hawaiian lobeliads: dynamic photosynthetic responses. *Oecologia* 155, 455. doi: 10.1007/s00442-007-0936-3
- Mott, K. A., and Woodrow, I. E. (2000). Modelling the role of Rubisco activase in limiting non-steady-state photosynthesis. *J. Exp. Bot.* 51, 399–406. doi: 10.1093/jxb/51.suppl_1.399
- Papanatsiou, M., Petersen, J., Henderson, L., Wang, Y., Christie, J. M., and Blatt, M. R. (2019). Optogenetic manipulation of stomatal kinetics improves carbon assimilation, water use, and growth. *Science* 363, 1456–1459. doi: 10.1126/science.aaw0046
- Pearcy, R. W., and Seemann, J. R. (1990). Photosynthetic induction state of leaves in a soybean canopy in relation to light regulation of ribulose-1,5-bisphosphate carboxylase and stomatal conductance. *Plant Physiol.* 94, 628–633. doi: 10.1104/pp.94.2.628
- Pearcy, R. W., and Way, D. A. (2012). Two decades of sunfleck research: looking back to move forward. *Tree Physiol.* 32, 1059–1061. doi: 10.1093/treephys/tps084
- Pearcy, R. W., Roden, J. S., and Gamon, J. A. (1990). Sunfleck dynamics in relation to canopy structure in a soybean (*Glycine max* (L.) Merr.) canopy. *Agric. For. Meteorol.* 52, 359–372. doi: 10.1016/0168-1923(90)90092-K
- Pearcy, R. W. (1990). Sunflecks and photosynthesis in plant canopies. *Annu. Rev. Plant Physiol.* 41, 421–453. doi: 10.1146/annurev.pp.41.060190.002225
- Schurr, U., Walter, A., and Rascher, U. (2006). Functional dynamics of plant growth and photosynthesis—from steady-state to dynamics—from homogeneity to heterogeneity. *Plant Cell Environ.* 29, 340–352. doi: 10.1111/j.1365-3040.2005.01490.x
- Simkin, A. J., McAusland, L., Lawson, T., and Raines, C. A. (2017). Overexpression of the RieskeFeS protein increases electron transport rates and biomass yield. *Plant Physiol.* 175, 135–145. doi: 10.1104/pp.17.00622
- Takahashi, F., Suzuki, T., Osakabe, Y., Betsuyaku, S., Kondo, Y., Dohmae, N. et al. (2018). A small peptide modulates stomatal control via abscisic acid in long-distance signaling. *Nature* 556, 235. doi: 10.1038/s41586-018-0009-2
- Tanaka, Y., Adachi, S., and Yamori, W. (2019). Natural genetic variation of the photosynthetic induction response to fluctuating light environment. *Curr. Opin. Plant Biol.* 49, 52–59. doi: 10.1016/j.pbi.2019.04.010
- Tardieu, F., Katerji, N., Bethenod, O., Zhang, J., and Davies, W. J. (1991). Maize stomatal conductance in the field: its relationship with soil and plant water potentials, mechanical constraints and ABA concentration in the xylem sap. *Plant Cell Environ.* 14, 121–126. doi: 10.1111/j.1365-3040.1991.tb01378.x
- Tardieu, F., Zhang, J., Katerji, N., Bethenod, O., Palmer, S., and Davies, W. J. (1992). Xylem ABA controls the stomatal conductance of field-grown maize subjected to soil compaction or soil drying. *Plant Cell Environ.* 15, 193–197. doi: 10.1111/j.1365-3040.1992.tb01473.x
- Tinoco-Ojanguren, C., and Pearcy, R. W. (1993). Stomatal dynamics and its importance to carbon gain in two rainforest Piper species. *Oecologia* 94, 395–402. doi: 10.1007/BF00317115
- Urban, O., Košvancová, M., Marek, M. V., and Lichtenthaler, H. K. (2007). Induction of photosynthesis and importance of limitations during the induction phase in sun and shade leaves of five ecologically contrasting tree species from the temperate zone. *Tree Physiol.* 27, 1207–1215. doi: 10.1093/treephys/27.8.1207
- Valladares, F., and Pearcy, R. W. (1997). Interactions between water stress, sunshade acclimation, heat tolerance and photoinhibition in the sclerophyll *Heteromeles arbutifolia*. *Plant Cell Environ.* 20, 25–36. doi: 10.1046/j.1365-3040.1997.d01-8.x
- Wang, Y., Noguchi, K., Ono, N., Inoue, S., Terashima, I., and Kinoshita, T. (2014). Overexpression of plasma membrane H⁺-ATPase in guard cells promotes light-induced stomatal opening and enhances plant growth. *Proc. Natl. Acad. Sci. U.S.A.* 111, 533–538. doi: 10.1073/pnas.1305438111
- Yamori, W., Masumoto, C., Fukayama, H., and Makino, A. (2012). Rubisco activase is a key regulator of non-steady-state photosynthesis at any leaf temperature and, to a lesser extent, of steady-state photosynthesis at high temperature. *Plant J.* 71, 871–880. doi: 10.1111/j.1365-313X.2012.05041.x
- Yamori, W., Irving, L. J., Adachi, S., and Busch, F. A. (2016a). “Strategies for optimizing photosynthesis with biotechnology to improve crop yield,” in *Handbook of Photosynthesis*. (Florida, CRC Press), 741–760. doi: 10.1201/b19498-55
- Yamori, W., Kondo, E., Sugiura, D., Terashima, I., Suzuki, Y., and Makino, A. (2016b). Enhanced leaf photosynthesis as a target to increase grain yield: Insights from transgenic rice lines with variable Rieske FeS protein content in the Cytochrome b₆/f complex. *Plant Cell Environ.* 39, 80–87. doi: 10.1111/pce.12594
- Yamori, W., Makino, A., and Shikanai, T. (2016c). A physiological role of cyclic electron transport around photosystem I in sustaining photosynthesis under fluctuating light in rice. *Sci. Rep.* 6, 20147. doi: 10.1038/srep20147
- Yamori, W. (2016). Photosynthetic response to fluctuating environments and photoprotective strategies under abiotic stress. *J. Plant Res.* 129, 379–395. doi: 10.1007/s10265-016-0816-1
- Zhu, X. G., Long, S. P., and Ort, D. R. (2010). Improving photosynthetic efficiency for greater yield. *Annu. Rev. Plant Biol.* 61, 235–261. doi: 10.1146/annurev-arplant-042809-112206

Conflict of Interest: The authors declare that the research was conducted in the absence of any commercial or financial relationships that could be construed as a potential conflict of interest.

Copyright © 2019 Shimadzu, Seo, Terashima and Yamori. This is an open-access article distributed under the terms of the Creative Commons Attribution License (CC BY). The use, distribution or reproduction in other forums is permitted, provided the original author(s) and the copyright owner(s) are credited and that the original publication in this journal is cited, in accordance with accepted academic practice. No use, distribution or reproduction is permitted which does not comply with these terms.



Novel Action Targets of Natural Product Gliotoxin in Photosynthetic Apparatus

Yanjing Guo¹, Jing Cheng¹, Yuping Lu¹, He Wang¹, Yazhi Gao¹, Jiale Shi¹, Cancan Yin¹, Xiaoxiong Wang¹, Shiguo Chen^{1*}, Reto Jörg Strasser^{1,2} and Sheng Qiang^{1*}

¹ Weed Research Laboratory, Nanjing Agricultural University, Nanjing, China, ² Bioenergetics Laboratory, University of Geneva, Geneva, Switzerland

OPEN ACCESS

Edited by:

Michael Moustakas,
Aristotle University of Thessaloniki,
Greece

Reviewed by:

Marek Zivcak,
Slovak University of Agriculture,
Slovakia

Rajagopal Subramanyam,
University of Hyderabad,
India

*Correspondence:

Shiguo Chen
chenshg@njau.edu.cn
Sheng Qiang
wrf@njau.edu.cn

Specialty section:

This article was submitted to
Plant Abiotic Stress,
a section of the journal
Frontiers in Plant Science

Received: 16 August 2019

Accepted: 29 November 2019

Published: 17 January 2020

Citation:

Guo Y, Cheng J, Lu Y, Wang H, Gao Y,
Shi J, Yin C, Wang X, Chen S,
Strasser RJ and Qiang S (2020) Novel
Action Targets of Natural Product
Gliotoxin in Photosynthetic Apparatus.
Front. Plant Sci. 10:1688.
doi: 10.3389/fpls.2019.01688

Gliotoxin (GT) is a fungal secondary metabolite that has attracted great interest due to its high biological activity since it was discovered by the 1930s. It exhibits a unique structure that contains a N-C = O group as the characteristics of the classical PSII inhibitor. However, GT's phytotoxicity, herbicidal activity and primary action targets in plants remain hidden. Here, it is found that GT can cause brown or white leaf spot of various monocotyledonous and dicotyledonous plants, being regarded as a potential herbicidal agent. The multiple sites of GT action are located in two photosystems. GT decreases the rate of oxygen evolution of PSII with an I_{50} value of 60 μ M. Chlorophyll fluorescence data from *Chlamydomonas reinhardtii* cells and spinach thylakoids implicate that GT affects both PSII electron transport at the acceptor side and the reduction rate of PSI end electron acceptors' pool. The major direct action target of GT is the plastoquinone Q_B-site of the D1 protein in PSII, where GT inserts in the Q_B binding niche by replacing native plastoquinone (PQ) and then interrupts electron flow beyond plastoquinone Q_A. This leads to severe inactivation of PSII RCs and a significant decrease of PSII overall photosynthetic activity. Based on the simulated modeling of GT docking to the D1 protein of spinach, it is proposed that GT binds to the-Q_B-site through two hydrogen bonds between GT and D1-Ser264 and D1-His252. A hydrogen bond is formed between the aromatic hydroxyl oxygen of GT and the residue Ser264 in the D1 protein. The 4-carbonyl group of GT provides another hydrogen bond to the residue D1-His252. So, it is concluded that GT is a novel natural PSII inhibitor. In the future, GT may have the potential for development into a bioherbicide or being utilized as a lead compound to design more new derivatives.

Keywords: chlorophyll a fluorescence (OJIP) transient, mycotoxin, action target, D1 protein, binding model

INTRODUCTION

Gliotoxin (GT), an alkaloid with a molecular mass of 326 Da, is the most important and well-known epipolythiodioxypiperazine (ETP)-type mycotoxin with biological active internal disulfide bridge (Smith et al., 2016). Since it was discovered by the 1930s, GT has been isolated from various fungal species, including *Trichoderma*, *Aspergillus fumigatus*, *Eurotium chevalieri*, *Neosartorya pseudofischeri*, some *Penicillium* spp., and *Acremonium* spp. Numerous studies show that GT

processes medicinal properties, including immunosuppressive, antitumor, antibacterial, and antiviral activity. However, it was discarded from clinical practice for its toxicity. GT is also recognized for an antibiotic substance involved in biological control of plant disease because it can cause cytoplasmic leakage, inhibit the germination of sporangia and mycelia growth of some plant pathogenic fungi (Scharf et al., 2016). Several GT-producing strains of *Trichoderma virens* have been successfully commercialized as biopesticides and widely used in agriculture (Lumsden and Walter, 2003; Khan et al., 2011).

Previous references indicated that GT has multiple cellular effects because of its different action targets. Early in 1968, it was found that GT can prevent viral RNA replication due to the specific inhibition of reverse transcriptase (Miller et al., 1968). In eukaryotic cells, GT has been proven as inhibitor of several enzymes such as farnesyltransferase, geranylgeranyltransferase, nicotinamide adenine dinucleotide phosphate (NADPH) oxidase, alcohol-dehydrogenases, and nuclear factor- κ B, causing apoptosis and necrosis in various cell types (Vigushin et al., 2004; Kim and Park, 2016; Scharf et al., 2016; Arias et al., 2018). Further evidence revealed that necrotic cell death induced by GT in murine thymocytes is associated with activation of a redox active calcium channel in the plasma membrane (Hurne et al., 2002). The inhibition of proteasome activity is one of the putative molecular targets of GT-mediated apoptosis in immune cells (Kroll et al., 1999; Dolan et al., 2015; Li et al., 2018). Based on the fact that the disulfide bridge of GT allows the cross linking with proteins and generates reactive oxygen species (ROS) through the redox cycling between reduced and oxidized forms, ROS is believed to be also responsible for DNA damage and apoptosis in cells of immune system (Harms et al., 2015; Nouri et al., 2015). Additionally, it is proposed that GT can perturb microfilament structure and induce cell detachment (Jordan and Pedersen, 1986). Recent work demonstrated that GT can target integrins to induce anoikis on lung epithelial cells (Haun et al., 2018).

However, at present very little attention is paid to the phytotoxicity of GT. It was reported that GT is inhibitory to root growth of clover and mustard accompanied by reduction in percentage germination of seeds (Wright, 1951). Similarly, GT shows potent growth inhibition against lettuce seedlings (Furuta et al., 1984; Haraguchi et al., 1992). Haraguchi et al. (1996; 1997) discovered that GT inhibits growth of cultured tobacco cells and pea seedling roots through the interference with the biosynthesis of branched-chain amino acids by reducing acetolactate synthase (ALS) activity. ALS is one of the targets of commercial herbicides. This means GT is possibly used to develop directly as a potential bioherbicide or design more novel derivatives as a template in the future. However, GT's herbicidal activity, multiple primary action targets, and mechanistic details of certain physiological effects on plants are unclear.

The goal of this study is to evaluate the herbicidal activity of GT, probe its action targets on two photosystems, and tests two hypotheses as following. Firstly, GT can cause leaf lesion of various plant species, possessing excellent herbicidal activity. Secondly, GT is a novel natural photosynthetic inhibitor,

decreasing PSII activity by binding to D1 protein. To prove these hypotheses, here phytotoxicity of GT to 10 different plant species was determined, and then chlorophyll (Chl) *a* fluorescence technique as an expeditious tool was utilized to identify and localize effects of GT on two photosystems. Finally, based on the structural information available from atrazine- and DCMU- binding to the reaction center of purple bacteria, a simulated modeling of GT interacting with the reaction center of spinach was constructed. Identification of the detailed molecular action targets of GT may help to design high-affinity GT-based derivatives, which is important for developing future new bio-based herbicides.

MATERIALS AND METHODS

Plants and Chemicals

Ten species of plants (Table 1) were cultured in soil from seed for about 2 months in the greenhouse at 20–25 °C and illuminated for 12 h with approximate 200 $\mu\text{mol m}^{-2}\text{s}^{-1}$ white light.

The green alga, *Chlamydomonas reinhardtii*, was obtained from the Freshwater Algae Culture Collection at the Institute of Hydrobiology (FACHB-collection 2221, Chinese Academy of Science, China). Cells were grown at 25°C in liquid Tris-acetate-phosphate medium, shaken 3 to 4 times per day, under about 100 $\mu\text{mol m}^{-2}\text{s}^{-1}$ white light (day/night, 12 h/12 h). The experiments were done with 3-day old cultures during their logarithmic growth phase (Gao et al., 2018).

Gliotoxin (CAS No. 7562-61-0), diuron (CAS No. 330-54-1, DCMU, 3-(3,4-Dichlorophenyl)-1,1-dimethylurea), methyl viologen (CAS No. 75365-73-0, MV, 1,1'-dimethyl-4,4'-bipyridinium-dichloride), and dimethyl sulphoxide (CAS No. 67-68-5, DMSO) were obtained from Sigma-Aldrich, and other common chemical reagents used in this work were purchased from Amresco. The Gliotoxin, DCMU and MV stock solutions were prepared in 100% DMSO and diluted in distilled water as required. The final concentration of DMSO in every experiment was less than 1% (v/v).

Phytotoxicity Assay

The detached-intact leaves from 10 species of plants were rinsed with sterilized water, subsequently blotted-dry with sterile paper, and then placed in Petri dishes with wet filter paper. Leaves were punctured using a needle from their margin on the abaxial side. A 10 μl of 1% DMSO (mock) or GT solution at different concentrations (100, 500, and 1,000 μM) was dripped onto the punctured wound of leaves. All Petri dishes were placed in a growth chamber for 96 h at 25°C under around 200 $\mu\text{mol m}^{-2}\text{s}^{-1}$ white light (day/night, 12h/12h). The diameter of leaf lesions was measured with calipers. Each mean value was obtained from at least fifteen leaf samples.

Measurement of PSII Oxygen Evolution Rate

The rate of oxygen evolution of PSII was measured using a Clark type oxygen electrode (Hansatech Instruments Ltd., King's Lynn,

TABLE 1 | Formulae and explanation of the technical data of the OJIP curves and the selected JIP-test parameters used in this study^a.**Technical fluorescence parameters**

F_t	fluorescence at time t after onset of actinic illumination
$F_O \cong F_{20\mu s}$	minimal fluorescence, when all PSII RCs are open
$F_L \equiv F_{150\mu s}$	fluorescence intensity at the L-step (150 μs) of OJIP
$F_K \equiv F_{300\mu s}$	fluorescence intensity at the K-step (300 μs) of OJIP
$F_J \equiv F_{2ms}$	fluorescence intensity at the J-step (2 ms) of OJIP
$F_I \equiv F_{30ms}$	fluorescence intensity at the I-step (30 ms) of OJIP
$F_P (= F_M)$	maximal recorded fluorescence intensity, at the peak P of OJIP
$F_v \equiv F_t - F_O$	variable fluorescence at time t
$F_v \equiv F_M - F_O$	maximal variable fluorescence
t_{FM}	time (in ms) to reach the maximal fluorescence intensity F_M
$V_t \equiv (F_t - F_O)/(F_M - F_O)$	relative variable fluorescence at time t
$V_K = (F_K - F_O)/(F_M - F_O)$	relative variable fluorescence at the K-step
$V_J = (F_J - F_O)/(F_M - F_O)$	relative variable fluorescence at the J-step
$W_t \equiv (F_t - F_O)/(F_J - F_O)$	relative variable fluorescence F_v to the amplitude $F_J - F_O$
$W_{OK} = (F_t - F_O)/(F_K - F_O)$	ratio of variable fluorescence $F_t - F_O$ to the amplitude $F_K - F_O$
$W_{OJ} = (F_t - F_O)/(F_J - F_O)$	ratio of variable fluorescence $F_t - F_O$ to the amplitude $F_J - F_O$
$W_{OI} = (F_t - F_O)/(F_I - F_O)$	ratio of variable fluorescence $F_t - F_O$ to the amplitude $F_I - F_O$
$W_{IP} = (F_t - F_I)/(F_P - F_I)$	ratio of variable fluorescence $F_t - F_I$ to the amplitude $F_P - F_I$
$M_0 \equiv 4(F_{270\mu s} - F_O)/(F_M - F_O)$	approximated initial slope (in ms^{-1}) of the fluorescence transient normalized on the maximal variable fluorescence F_v
$S_m \equiv Area/(F_M - F_O)$	normalized total complementary area above the O-J-I-P transient (reflecting multiple-turnover Q_A reduction events)
$S_s = V_J/M_0$	normalized total complementary area corresponding only to the O-J phase (reflecting single-turnover Q_A reduction events)

Quantum efficiencies or flux ratios

$\Phi_{PO} = PHI(P_O) = TR_O/ABS = 1 - F_O/F_M$	maximum quantum yield for primary photochemistry
$\Psi_{EO} = PSI_O = ET_O/TR_O = 1 - V_J$	probability that an electron moves further than Q_A
$\Phi_{EO} = PHI(E_O) = ET_O/ABS = (1 - F_O/F_M) (1 - V_J)$	quantum yield for electron transport (ET)
$\Phi_{DO} = PHI(D_O) = 1 - \Phi_{PO} = F_O/F_M$	quantum yield (at $t = 0$) of energy dissipation
$\Phi_{RO} = RE_O/ABS = \Phi_{PO} \cdot \Psi_{EO} \cdot \delta_{RO} = \Phi_{PO} \cdot (1 - V_J)$	quantum yield for reduction of the end electron acceptors at the PSI acceptor side (RE)

$$\delta_{RO} = RE_O/ET_O = (1 - V_J)/(1 - V_J)$$

$$\gamma_{RC} = Chl_{RC}/Chl_{total} = RC/(ABS + RC)$$

Phenomenological energy fluxes (per excited leaf cross-section-CS)

$ABS/CS = Chl/CS$	absorption flux per CS
$TR_O/CS = \Phi_{PO} \cdot (ABS/CS)$	trapped energy flux per CS
$ET_O/CS = \Phi_{PO} \cdot \Psi_{EO} \cdot (ABS/CS)$	electron transport flux per CS

Density of RCs

$RC/CS = \Phi_{PO} \cdot (V_J/M_0) \cdot (ABS/CS)$	Q_A -reducing RCs per CS
$Q_A\text{-reducing centers} = (RC/RC_{reference}) \cdot (ABS/ABS_{reference}) = [(RC/CS)_{treatment}/(RC/CS)_{control}] \cdot [(ABS/CS)_{treatment}/(ABS/CS)_{control}]$	The fraction of Q_A -reducing reaction centers
$Non\text{-}Q_A\text{-reducing centers} = 1 - Q_A\text{-reducing centers}$	The fraction of non- Q_A -reducing reaction centers, also so-called heat sink centers or silent centers

$$S_m/t_{FM} = [RC_{open}/(RC_{close} + RC_{open})]_{av} = [Q_A/Q_{A(tot)}]_{av}$$

$$R_J = [\Psi_{EO}(\text{control}) - \Psi_{EO}(\text{treatment})]/\Psi_{EO}(\text{control}) = [V_J(\text{treatment}) - V_J(\text{control})]/[1 - V_J(\text{control})]$$

Performance indexes

$$PI_{ABS} \equiv \frac{\gamma_{RC}}{1 - \gamma_{RC}} \cdot \frac{\Phi_{PO}}{1 - \Phi_{PO}} \cdot \frac{\Psi_{EO}}{1 - \Psi_{EO}}$$

$$PI_{total} \equiv PI_{ABS} \cdot \frac{\delta_{RO}}{1 - \delta_{RO}}$$

maximum quantum yield for primary photochemistry
probability that an electron moves further than Q_A
quantum yield for electron transport (ET)
quantum yield (at $t = 0$) of energy dissipation
quantum yield for reduction of the end electron acceptors at the PSI acceptor side (RE)
probability that an electron is transported from the reduced intersystem electron acceptors to the final electron acceptors of PSI
probability that a PSII Chl molecule functions as RC

absorption flux per CS
trapped energy flux per CS
electron transport flux per CS

Q_A -reducing RCs per CS
The fraction of Q_A -reducing reaction centers

The fraction of non- Q_A -reducing reaction centers, also so-called heat sink centers or silent centers
average fraction of open RCs of PSII in the time span between 0 to t_{FM}
number of PSII RCs with Q_B -site filled by PSII inhibitor

performance index (potential) for energy conservation from photons absorbed by PSII to the reduction of intersystem electron acceptors
performance index (potential) for energy conservation from photons absorbed by PSII to the reduction of PSI end acceptors

^aSubscript "O" (or "o" when written after another subscript) indicates that the parameter refers to the onset of illumination, when all RCs are assumed to be open.

UK) according to Chen et al. (2007). *C. reinhardtii* cells were resuspended in Buffer A with a 0.65 A_{750} , and then GT and DCMU were individually added into 2 ml suspensions with the indicated concentrations. After the cells were incubated for 3 h in darkness at 25°C, treated-cells containing 45 μg chlorophylls were added into the reaction medium including 50 mM Hepes-KOH buffer (7.6), 4 mM $K_3Fe(CN)_6$, 5 mM NH_4Cl , 1 mM p-Phenylenediamine. Cells were illuminated with 400 μmol photons $m^{-2} s^{-1}$ red actinic light. The rate of oxygen evolution

was measured during the first three minutes after onset of illumination.

Chl a Fluorescence Imaging

Chl *a* fluorescence imaging was determined using a pulse-modulated Imaging-PAM M-series fluorometer (MAXI-version, Heinz Walz GmbH, Effeltrich, Germany) in three independent experiments (Gao et al., 2018). *C. reinhardtii* cells were harvested and resuspended in Buffer A (20 mM HEPES-

KOH pH 7.5, 350 mM sucrose, and 2.0 mM MgCl_2) with a 0.65 A_{750} . 200 μl of cell suspensions with 1% DMSO (mock), GT (10, 50, and 100 μM) were added into the 96-well black microtiter plate, incubating for 2.5 h under 100 $\mu\text{mol m}^{-2} \text{s}^{-1}$ white light at 25°C. Subsequently, the samples were placed under the imaging system camera for 0.5 h dark-adaptation after focusing of the camera. Images of fluorescence were recorded at 0.25 $\mu\text{mol m}^{-2} \text{s}^{-1}$ measuring light, 110 $\mu\text{mol m}^{-2} \text{s}^{-1}$ actinic light, and 6,000 $\mu\text{mol m}^{-2} \text{s}^{-1}$ saturation pulse light. In the absence of actinic illumination, on application of a weak measuring light and saturation pulse, the minimum fluorescence yield (F_0) and the maximum fluorescence yield (F_M) were determined respectively, from which the F_V/F_M was calculated. The fluorescence yield (F_S) was determined after the addition of actinic light. During 315 s of actinic illumination, the maximum fluorescence yield in the light-adapted state (F_M') was determined during the repeated saturation pulse light for 0.8 s at intervals of 20 s. The electron transport rate (ETR), effective quantum yield (Yield), and photochemical quenching coefficient (qP) were also calculated automatically based on F_0 , F_M , F_S , and F_M' .

Chl *a* Fluorescence Rise Kinetics OJIP and the Modulated 820 Nm Reflection (MR_{820})

Chl *a* fluorescence rise kinetics OJIP were measured with a Handy PEA instrument (Plant Efficiency Analyser, Hansatech Instruments Ltd., King's Lynn, UK). Samples were always kept in darkness for 0.5 h before the measurements and were illuminated with continuous red light (650 nm peak wavelength, 3,500 $\mu\text{mol photons m}^{-2} \text{s}^{-1}$ maximum light intensity). The experiment was repeated three times with at least 15 repetitions. For *C. reinhardtii*, 1 ml of cells in Buffer A with 0.65 A_{750} were treated with 1% DMSO (mock), GT (10, 50, and 100 μM) and 1 μM DCMU for 2.5 h under 100 $\mu\text{mol m}^{-2} \text{s}^{-1}$ white light at 25°C. The samples were collected by centrifugation and resuspended in 20 μl Buffer A. After 0.5 h dark-adaptation, 20 μl suspensions were filtered onto glass microfiber filter (diameter 25 mm, GF/C, Whatman), and then positioned immediately above the PEA sensor head by a leaf clip to obtained the fluorescence data. For thylakoids of spinach (*Spinacea oleracea*), thylakoids were isolated according to the method of Chen et al. (2008). Before the fluorescence OJIP curves measurements, 1% DMSO (mock), GT (50, 100, 200, and 400 μM) and 1 μM DCMU were added to thylakoid suspensions with 100 $\mu\text{g Chl ml}^{-1}$ and incubated for 0.5 h in complete darkness at 25 °C.

The fluorescence rise kinetics OJIP curves were analyzed by the JIP-test based on the model of "Theory of Energy Fluxes in Biomembranes" (Strasser et al., 2004). The JIP-test defines the specific (per reaction center, RC) and the phenomenological (per excited cross-section, CS) energy fluxes of the absorbed light by the antenna pigments (ABS), the maximum energy trapping (TR_0), the electron transport beyond Q_A^- (ET_0) and dissipation (DI_0). Various JIP-test parameters used in this study are listed in Table 1.

The MR_{820} signal measurements of *C. reinhardtii* cells were performed using a Multifunctional-PEA fluorometer (Hansatech Instruments Ltd., King's Lynn, UK). Further technical details

were described in a reference by Gao et al. (2018). The raw data were transferred to the computer and the numerical processing of the MR_{820} signals were carried out by the in-house software M-PEA data Analyzer v.5.1.

Modeling of GT in the Q_B -Binding Site

Based on the assumption that the D1 protein is an equivalent of the L-subunit, the coordinates of the L-subunit of purple photosynthetic bacterial *Rhodospseudomonas viridis* obtained from Protein Data Bank (PDB entry 1PRC) were used as the templates for the D1 protein. The amino acid sequence information of target protein D1 of *C. reinhardtii* (Reference Sequence: NP_958413.1) and *S. oleracea* (Reference Sequence: NP_054912.1) was obtained from NCBI. Docking was performed with DS-CDocker implemented in Discovery Studio (version 3.5, BIOVIA, America). The modeling started from the crystal structure alignment of complexes of the bacterial *Rps. viridis* RC with atrazine (Lancaster and Michel, 1999; PDB entry 5PRC) and the crystal structure alignment of *S. oleracea* D1 protein (PDB entry 3JCU). The atrazine binding environment in the bacterial RC or atrazine, DCMU and toxin GT binding environment in *S. oleracea* D1 was further refined by molecular dynamics simulations. The structures of three ligands were constructed using ChemBioDraw Ultra 14.0 software (CambridgeSoft, America). The ligand structures were energetically minimized using MM2 energy minimizations in Chem3D Pro 14.0 (CambridgeSoft, America). All bound water and ligands were eliminated from the protein, and the polar hydrogens were added to the proteins in the processes of the above energy minimization and molecular refinement.

RESULTS AND DISCUSSION

GT Caused Leaf Lesion of Various Monocotyledonous and Dicotyledonous Plants

It was proved that GT possesses growth inhibiting bioactivity (Wright, 1951; Furuta et al., 1984; Haraguchi et al., 1992; Haraguchi et al., 1996; Haraguchi et al., 1997). To further examine the phytotoxicity of GT to different plants, the leaf lesion formation was monitored. As shown in Figure 1, the ratio of lesions in the leaf blades of ten plant species exhibited a concentration-dependent increase after 96 h treatment with 100, 500, and 1,000 μM GT. The white leaf spot was observed in GT-treated five plants including *Digitaria sanguinalis*, *Microstegium vimineum*, *Zea mays*, *Oryza sativa*, and *Nicotiana tabacum*. GT caused brown leaf spot in another five plants including *Solidago Canadensis*, *Ageratina adenophora*, *Youngia japonica*, *Oxalis corniculata*, and *Gossypium barbadense*. In the case of 1% DMSO treatment (mock), no visible damage was found in the leaf blades in these ten plants. Such chlorosis or necrosis symptoms indicate that GT led to chlorophyll breakup and cell death.

To further access pathogenicity level of GT, these ten plant species were classified into three categories according to the

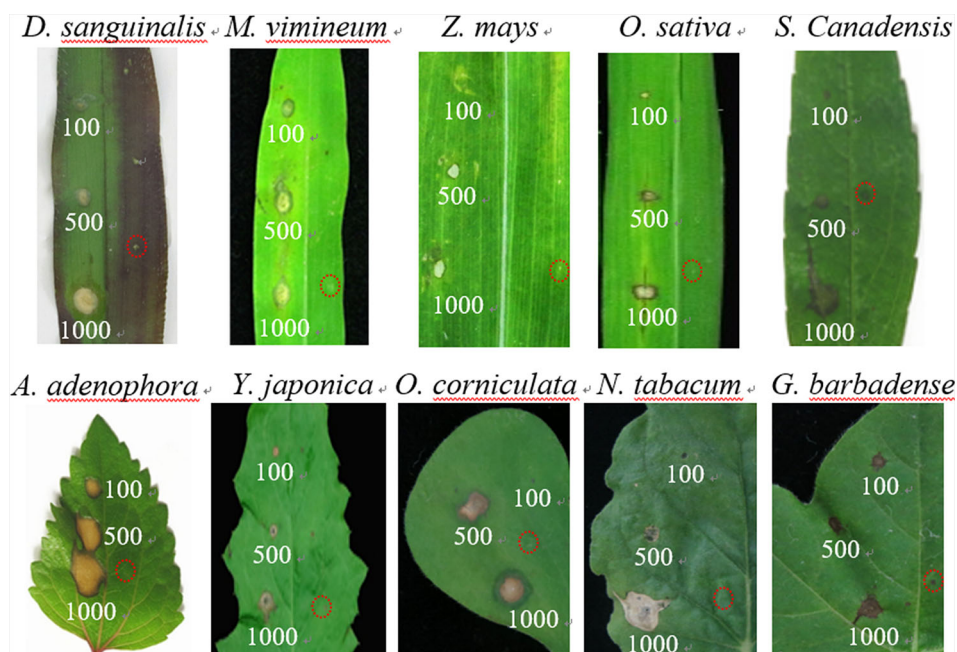


FIGURE 1 | Disease development of the detached-leaves with Gliotoxin (GT). Leaves from 10 different plant species were treated without (1% DMSO as control, red circles on the right side) or with GT at various concentrations (100, 500, and 1,000 μM). Lesion photographs were taken at 96 h. Lesion diameter and pathogenicity level were analyzed in **Table 2**.

diameter of leaf lesions (**Table 2**). At 100 μM GT, *A. adenophora* leaves showed highly susceptible, where the diameter of the developed necrotic lesion in leaf blades was more than 3.0 mm. For lower susceptible *D. sanguinalis*, their leaves formed chlorotic lesions of less than 1.0 mm in diameter. The left eight species belonged to moderately susceptible category with leaf lesions between 1.0 and 3.0 mm in diameter, including monocotyledonous (e.g., *M. vimineum*, *Z. mays*, and *O. sativa*), and dicotyledonous plants (e.g., *S. canadensis*, *Y. japonica*, *O. corniculata*, *N. tabacum* and *G. barbadense*). Based on such standard, *D. sanguinalis*, *O. sativa*, *G. barbadense* leaves still show moderate pathogenicity level at higher concentrations of 500 even 1000 μM GT. Obviously, GT has good phytotoxicity to various monocotyledonous and dicotyledonous plants, leading to leaf lesion formation. It is also suggested that GT can damage photosynthetic tissues because chlorotic or necrotic lesions are evidence of chlorophyll destruction and cell death.

GT Decreased the Oxygen Evolution Rate of *C. reinhardtii*

Influence of GT and DCMU on the rate of O_2 evolution of *C. reinhardtii* cells is shown in **Figure 2**. DCMU inhibits O_2 evolution much faster and at lower concentrations compared with GT. Almost 100% decrease in O_2 evolution was observed in the case of 1 μM DCMU treatment. GT also caused a negative concentration-dependent effect on O_2 evolution. More than 58% decrease in the O_2 evolution rate had occurred when *C.*

reinhardtii cells were exposed to 100 μM GT comparable to mock-treatment. The I_{50} (the concentration producing 50% inhibition) value of GT for the inhibition of O_2 evolution *in vivo* was calculated to be around 60 μM . Clearly, GT is a weaker photosynthetic inhibitor relative to DCMU as an excellent photosynthetic inhibiting herbicide.

GT Inhibited Photosynthetic Activity of *C. reinhardtii*

Chlorophyll fluorescence is an indicator of plant photosynthetic activity. To test the effect of GT on photosynthesis of *C. reinhardtii*, the Imaging-PAM chlorophyll fluorometer was used to monitor the change of GT-induced fluorescence image parameters. As in **Figure 3A**, the representative color-coded images of four parameters, F_0 (when all PSII reaction centers are open after dark adaptation), F_V/F_M (the maximal PSII quantum yield), qP (the coefficient of photochemical quenching), and Yield (the effective PSII quantum yield), are shown after *C. reinhardtii* cells were treated with different concentrations of GT. It is observed that images of F_0 kept relatively stable in the presence of GT, images of F_V/F_M and Yield as well as qP also did not been affected in the case of 10 and 50 μM GT treatment. At 100 μM GT-treated *C. reinhardtii* cells, images of F_V/F_M and Yield faded from blue for mock to green, images of qP became purple colors from white colors. The results are strongly supported by the values of fluorescence parameters F_V/F_M , Yield and qP (**Figure 3B**). About 36% and 38% decrease in F_V/F_M

TABLE 2 | Phytotoxicity of Gliotoxin (GT) to various plants^a.

Family	Plant species	GT concentration (μM)	Lesion diameter (mm)	Pathogenicity level ^b
Gramineae	<i>Digitaria sanguinalis</i>	100	0.61 ± 0.15	+
		500	2.24 ± 0.16	++
		1,000	2.59 ± 0.09	++
	<i>Microstegium vimineum</i>	100	2.49 ± 0.13	++
		500	3.06 ± 0.10	+++
		1,000	4.23 ± 0.66	+++
	<i>Zea mays</i> Linn	100	2.10 ± 0.16	++
		500	3.60 ± 0.83	+++
		1,000	5.49 ± 0.29	+++
	<i>Oryza sativa</i>	100	1.29 ± 0.09	++
		500	2.09 ± 0.07	++
		1,000	2.10 ± 0.07	++
Compositae	<i>Solidago Canadensis</i>	100	2.10 ± 0.67	++
		500	3.19 ± 1.51	+++
		1,000	3.60 ± 0.69	+++
	<i>Ageratina adenophora</i>	100	3.88 ± 0.34	+++
		500	5.94 ± 1.17	+++
		1,000	7.25 ± 1.69	+++
	<i>Youngia japonica</i>	100	1.68 ± 0.13	++
		500	3.04 ± 0.21	+++
		1,000	3.78 ± 0.22	+++
	Oxalidaceae	<i>Oxalis corniculata</i> L	100	2.55 ± 0.08
500			3.79 ± 0.24	+++
1,000			4.20 ± 0.29	+++
Solanaceae	<i>Nicotiana tabacum</i> L.	100	1.58 ± 0.10	++
		500	2.87 ± 0.60	++
		1,000	4.84 ± 2.05	+++
Malvaceae	<i>Gossypium barbadense</i>	100	1.63 ± 0.18	++
		500	1.96 ± 0.11	++
		1,000	2.61 ± 0.17	++

^aThe detached-intact leaves from different plant species are rinsed with sterilized water, subsequently dried and placed in Petri dishes with wet filter paper. The leaves were lightly punctured using a needle from the leaf margin on the abaxial side. Ten microliter of GT solution was dripped onto the punctured wound. All Petri dishes were placed in the growth chamber for 96 h at 25°C under around 200 μmol m⁻² s⁻¹ white light (day/night, 12 h/12 h). Diameter of leaf lesion was measured with calipers. Each value is the average of three independent experiments. ^b +, ++, +++ denotes leaf lesion diameter 0 to <1.0 mm, 1.0 to <3.0 mm, and ≥3.0 mm, respectively.

F_M and Yield, respectively, was observed relative to mock-treatment after 100 μM GT treatment, suggesting high concentration of GT declined the quantum efficiency of light energy transfer in PSII. The value of qP was 0.86 for mock-treatment, and was 0.60 for 100 μM GT-treatment. qP denotes the proportion of excitons captured by open traps and being concerted to chemical energy in the PSII reaction center (Krause and Weis, 1991). In addition, the parameter ETR, expressing the apparent rate of photosynthetic electron transport, exhibited a rapid concentration-dependent decrease by increasing of GT concentration (Figure 3B). After *C. Reinhardtii* cells were incubated by 10, 50, and 100 μM GT, the mean of ETR was declined by around 29%, 52%, and 100% by comparison with mock-treatment, respectively. The I_{50} value for ETR is about 50 μM, which is closed to the I_{50} value for O_2 evolution rate. An approximately linear lower in ETR and O_2 evolution rate indicates that the inhibition of PSII electron transport should be the important action site of GT on photosynthetic apparatus. Considering above results, it is concluded that GT can affect

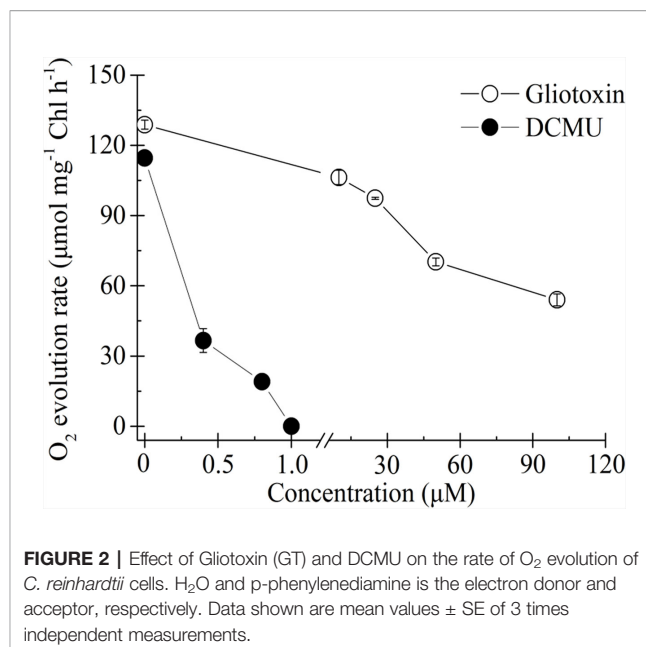


FIGURE 2 | Effect of Gliotoxin (GT) and DCMU on the rate of O_2 evolution of *C. reinhardtii* cells. H_2O and p-phenylenediamine is the electron donor and acceptor, respectively. Data shown are mean values ± SE of 3 times independent measurements.

photosynthesis of *C. Reinhardtii* mainly due to inhibiting PSII electron transport.

Action Sites of GT on Photosystem II and Photosystem I of *C. reinhardtii*

In the last two decades, fast chlorophyll a fluorescence rise kinetics OJIP and JIP-test analysis has been widely used to probe the structure, conformation and function of the photosynthetic apparatus (Strasser et al., 1995; Strasser et al., 2004). To further investigate the precise action sites of GT on photosynthesis, the fluorescence rise kinetics OJIP of *C. reinhardtii* cells were measured after GT treatment for 3 h with different concentrations (Figure 4).

As shown in Figure 4A, the fluorescence rise OJIP curve of mock-treatment is a typical polyphasic O-J-I-P shape. GT and DCMU treatment led to a distinct change of the fluorescence rise OJIP curve of *C. reinhardtii* cells. After 1 μM DCMU treatment, the biggest change of fluorescence rise OJIP curve is that the J-step increased quickly equal to the P level (F_M). A rapid rise of the level of J-step is a result of the large accumulation of Q_A^- in PSII RCs, which attributes to the interruption of the electron flow from Q_A to Q_B (Strasser and Govindjee, 1992; Strasser et al., 2004). For GT, it is observed that the variable Chl fluorescence intensity (F_t) and F_M decreased significantly, and the I- and P-steps disappeared gradually by increasing treatment concentration. A decrease in F_M might be relative to the quenching of fluorescence, which is resulted from the presence of an oxidized plastoquinone pool or to the damage of the structure and function of PSII antennae (Tóth et al., 2005).

For investigation of the detailed effect of GT on Chl a fluorescence rise kinetics OJIP properties, the fluorescence curves were double normalized by F_0 and F_M , and presented as relative variable fluorescence V_t (top) and $\Delta V_t = V_{t(treated)} - V_{t(control)}$ (bottom) versus logarithmic time scale (Figure 4B, the

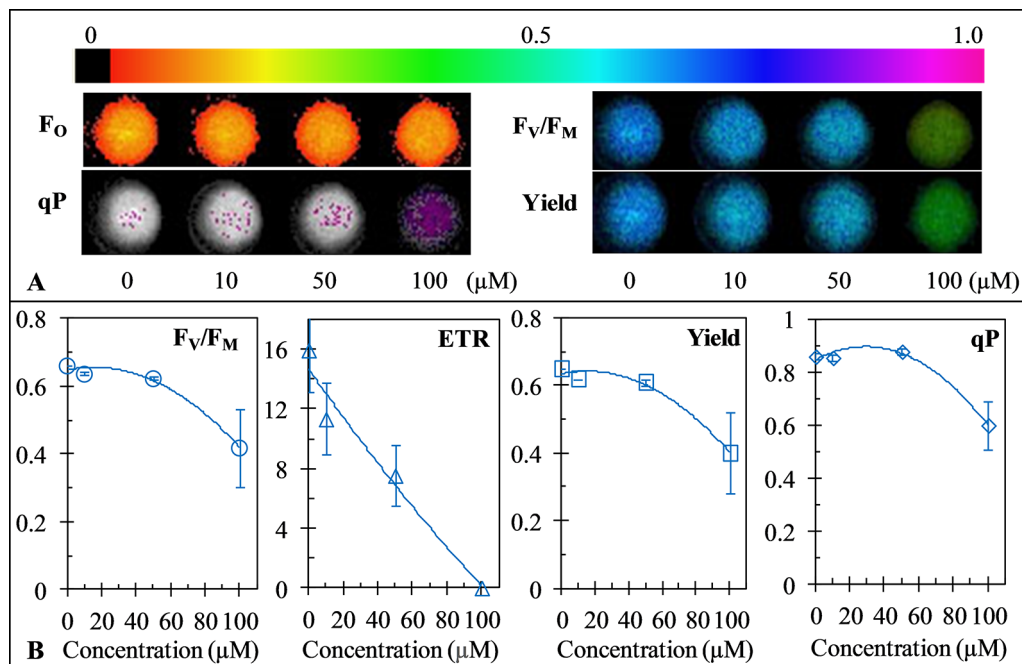


FIGURE 3 | Effect of Gliotoxin (GT) on color fluorescence imaging (A) the value of the maximum quantum yield of PSII (F_v/F_m), electron transport rate (ETR), Yield and qP (B) of *C. reinhardtii* cells. Fluorescence images were indicated by color code in the order of black (0) through red, orange, yellow, green, blue, violet to purple (1). The number codes above images are marked from 0 to 1, showing the changes. Each value is the average \pm SE of three independent experiments.

“control” is the mock-treated samples). This allows to find richer information that usually were hidden in the actual fluorescence rise kinetics curve. The data from the V_t and ΔV_t show that the most major effect of GT on the fluorescence rise kinetics is a rapid increase of the J-peak. This is equivalent to the DCMU behavior. To analyze GT-treated cells for events, reflected in the OK, OJ, OI, and IP phase, other normalizations of the fluorescence rise kinetics were also conducted (Figures 4C–F). In Figure 4C, the fluorescence rise kinetics data were double normalized by F_0 and F_K as W_{OK} (top) and plotted with $\Delta W_{OK} = W_{OK(treated)} - W_{OK(control)}$ (bottom) to show L-band. The L-band is an indicator of the energetic connectivity or grouping of the PSII units, being higher when connectivity or grouping probability is lower (Strasser et al., 2004). Our data reveal that L-band is low sensitive to different concentration of GT. In Figure 4D, the fluorescence rise kinetics normalized by F_0 and F_J as W_{OJ} in the linear time scale from 10 μ s to 2 ms is presented. No clear effect on the OJ phase was observed after *C. reinhardtii* cells were incubated by GT. Based on the $\Delta W_{OJ} = W_{OJ(treated)} - W_{OJ(control)}$, it is seen that GT just caused a very slight negative influence on the K-band (Figure 4D). The OJ phase is largely driven by primary photochemistry, the JP phase is dominated by the biochemical reaction (Strasser et al., 2004). So, it seems reasonable that the mainly influence of GT is on the biochemical reaction after Q_A not the primary photochemical reaction. Figure 4E shows that the fluorescence rise kinetics were double normalized by F_0 and F_I as W_{OI} . The J-peak of GT-

treated curves exhibited a significant increase compared with that of mock. At the same time, the W_{OI} (only the part ≥ 1 is shown), in the linear 30–530 ms time range, was also plotted in the insert in Figure 4F. The I-step reflects the kinetic bottleneck of the electron chain between PQH_2 and cytochrome (cyt) b_6f (Strasser et al., 2010). The IP phase is related to electron flow through PSI and inactive ferredoxin-NADP⁺-reductase (FNR) at the acceptor side of PSI (Schansker et al., 2005). It reflects the electron flow from PQ pool to the end electron acceptors at the PSI acceptor side. For each W_{OI} curve, the maximal amplitude of the fluorescence rise from I- to P-step reflects the size of the pool of the end electron acceptors at PSI acceptor side (Yusuf et al., 2010; Chen et al., 2016). It is demonstrated that GT resulted in a decrease of this pool size since the W_{OI} (≥ 1) curves of GT-treated samples have smaller IP amplitude compared to mock. To further assess the effect of GT on the IP phase, the fluorescence data were normalized by F_I and F_P , as $W_{IP} = (F_I - F_t)/(F_P - F_t)$, and plotted in a linear time scale from 30 to 530 ms (Figure 4F). Yusuf et al. (2010) suggested that the reduction rate of PSI end electron acceptors' pool in different treatments can be estimated by the half-time, which is the time point at $W_{IP} = 0.5$ (half rise of the curves). A bigger (or less) value of the half-time means a lower (or higher) conduction rate. Here, it is observed that GT caused a distinct increase of the half times relative to mock. This indicates that GT can decline the rate of the reduction of the end electron acceptors on PSI possibly or/and inactivate FNR.

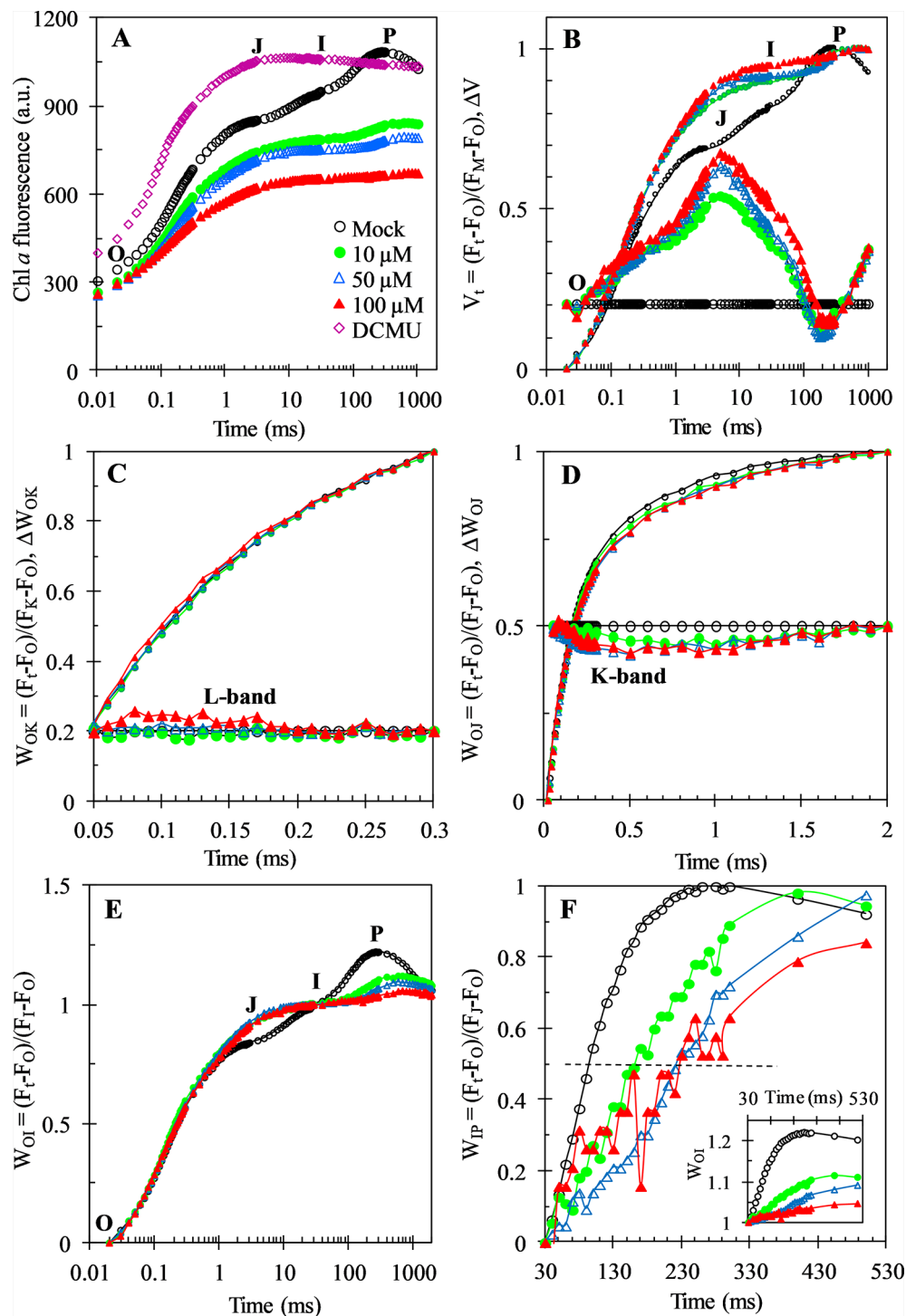


FIGURE 4 | Chl *a* fluorescence rise kinetics of *C. reinhardtii* cells treated with 1% DMSO (mock), DCMU (1 μ M), and Gliotoxin (GT) at the indicated concentrations. **(A)** Raw fluorescence rise kinetics. **(B)** Fluorescence rise kinetics normalized by F_0 and F_M as $V_t = (F_t - F_0)/(F_M - F_0)$ (top), and $\Delta V_t = V_{t(\text{treated})} - V_{t(\text{control})}$ (bottom). **(C)** Fluorescence rise kinetics normalized by F_0 and F_K as $W_{OK} = (F_t - F_0)/(F_K - F_0)$ (top), and the difference kinetics $\Delta W_{OK} = W_{OK(\text{treated})} - W_{OK(\text{control})}$ (bottom). **(D)** Fluorescence rise kinetics normalized by F_0 and F_J as $W_{OJ} = (F_t - F_0)/(F_J - F_0)$ (top), and the difference kinetics $\Delta W_{OJ} = W_{OJ(\text{treated})} - W_{OJ(\text{control})}$ (bottom). **(E)** Fluorescence rise kinetics normalized by F_0 and F_I as $W_{OI} = (F_t - F_0)/(F_I - F_0)$. **(F)** Fluorescence rise kinetics normalized by F_I and F_P as $W_{IP} = (F_t - F_I)/(F_P - F_I)$ and $W_{OI} (\geq 1)$ in the insert, the half-times are shown by the crossing of the curves with the horizontal dashed line drawn at $W_{IP} = 0.5$ (half rise). Each curve is the average of 30 measurements.

In **Figure 5**, several representative JIP-test parameters are presented for further analysis of the behavior of GT-treated *C. reinhardtii* cells. In these parameters, V_K (relative variable fluorescence at the K-step) and V_J (relative variable fluorescence at the J-step) increased after GT treatment. However, combining with the stable parameter F_K/F_J , it's clear that the increase of V_K is caused by the increase of F_J . Actually, GT has no significant influence on the K-step. It has been suggested that the K-step is a signal of the inactivation of the oxygen-evolving-complex (OEC) (Strasser et al., 2004). Thus, the major impact of GT is a rise of the J-step level, suggesting a large accumulation of Q_A^- occurred in PSII RCs due to inhibition of PSII electron transfer activity. In fact, it is seen that all parameters involved electron transport, ET_0/CS (electron transport flux per CS), ϕ_{E_0} (the quantum yield for PSII electron transport), and ψ_{E_0} (the probability that a trapped exciton moves an electron into the electron transport chain beyond Q_A), show dramatic reduction in the presence of GT. However, GT can't inhibit entirely PSII electron transport activity *in vivo*. At 100 μM GT, ϕ_{E_0} and ψ_{E_0} just decreased by around 56% and 43% relative to the mock (Figure 5). Since GT blocked PSII electron transfer further than Q_A , inactivation events of PSII RCs are expected to happen. Data from **Figure 5** show that the number of active PSII RCs per cross-section (RC/CS) decreased quickly after GT treatment. S_m/t_{FM} , expressing the

average fraction of open RCs of PSII in the time interval from 0 to t_{FM} (Strasser et al., 2004), is shown. By increasing treatment concentration, an approximately linearly sharply decrease of S_m/t_{FM} is observed. The S_m/t_{FM} ratio of GT-treated cells was about 54% (10 μM), 62% (50 μM), and 74% (100 μM) lower than that of mock, respectively. This means that GT caused the faster closure of PSII RCs. The fraction of Q_A -reducing centers were also calculated according to the reference (Chen et al., 2014), as follow: Q_A reducing centers = $[(RC/CS)_{treatment}/(RC/CS)_{control}] \cdot [(ABS/CS)_{treatment}/(ABS/CS)_{control}]$. It is found that the fraction of Q_A -reducing centers reduced quickly after 3 h treatment of GT with different concentrations (Figure 5). The data indicate that GT inactivated indeed the RCs of PSII *in vivo*. In contrast with Q_A -reducing centers, GT treatment increased the fraction of non- Q_A -reducing centers (data not shown). Non- Q_A -reducing centers, also so-called heat sink centers, are radiators and often are used to protect the system from over excitation and over reduction which would create dangerous ROS (Strasser et al., 2004; Chen et al., 2014).

In addition, the maximum quantum yield of PSII primary photochemistry (ϕ_{P_0}) shows a slight decrease after *C. reinhardtii* cells were treated with GT *in vivo*. The value of two parameters, ABS/CS and TR_0/CS decreased greatly. ABS/CS refers to the total absorption flux per PSII cross-section, and can be taken as a measure for an average antenna size or chlorophyll

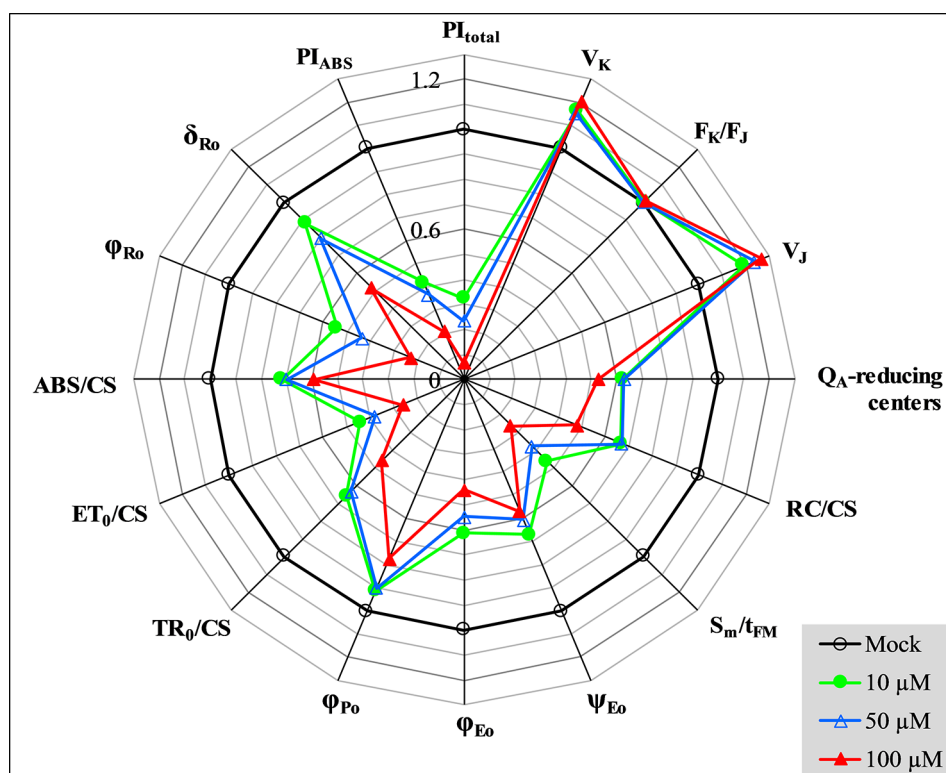


FIGURE 5 | Spider plot presentation of selected parameters derived from JIP-test quantifying PSII behavior of *C. reinhardtii* cells treated with various concentrations of GT. Each parameter is expressed as fraction relatively to the values of the control (mock, back regular circle with value 100% = 1).

concentration (Srivastava et al., 1998; Strasser et al., 2004). TR_0/CS expresses the trapped energy flux per PSII cross-section, reflecting the specific rate of the exciton trapped by open RCs (Strasser et al., 2004). A significant decrease of ABS/CS and TR_0/CS indicates that GT not only lowered the chlorophyll concentration, but damaged the conformation of the antenna pigment assemblies and reduced the efficiency of light energy transfer between antenna pigment molecules and from those to the PSII RCs. This might be also a possibility for decreasing of the variable Chl fluorescence intensity (F_i) and the F_M value. With respect to the performance index PI_{ABS} , the parameter is a product of the three independent parameters Φ_{Po} , Ψ_{Eo} , and γ_{RC} . Here, γ_{RC} is the fraction of RC chlorophyll in relation to total chlorophyll (Strasser et al., 2004; **Table 1**). So, PI_{ABS} is extremely sensitive to different stresses, expressing the overall photosynthetic activity of PSII (Strasser et al., 2004). When cells were exposed to 10, 50, and 100 μM GT, the value of PI_{ABS} decreased by 58%, 63%, and 79% compared to the mock, respectively. It is proved that GT can strongly inhibit PSII photosynthetic activity of *C. reinhardtii*. Moreover, PI_{ABS} is much higher sensitive to GT treatment than these three parameters (Φ_{Po} , Ψ_{Eo} , and γ_{RC}) that contribute to this index and even PSII O_2 evolution rate (**Figures 2 and 5**). This might be interpreted by the reason that the inhibition of PSII electron transfer activity is the dominant factor not the only one for the decrease of the overall photosynthetic activity of PSII after GT treatment.

After *C. reinhardtii* cells were treated with various concentrations of GT, both Φ_{Ro} and δ_{Ro} show a significant decrease. The value of Φ_{Ro} reduced to 54% (10 μM), 44% (50 μM), and 23% (100 μM) of the mock, respectively (**Figure 5**). For 10 μM and 50 μM GT treated cells, δ_{Ro} only lowered 12% and 20%. Under 100 μM GT treatment, δ_{Ro} has 48% distinct decrease. Φ_{Ro} is the product of Φ_{Po} , Ψ_{Eo} , and δ_{Ro} , expressing that the quantum yield for the reduction of the end electron acceptors at the PSI acceptor side (Strasser et al., 2010). Here, δ_{Ro} is given as $\delta_{Ro} = RE_0/ET_0 = (1-V_I)/(1-V_J)$. δ_{Ro} is used as the probability that an electron is transported from the reduced intersystem electron acceptors to final electron acceptors of PSI (Strasser et al., 2010). A significant decrease of Φ_{Ro} and δ_{Ro} suggests that GT inhibits the reduction of the end acceptors at the PSI electron acceptor side. This is well in agreement with that GT-treated cells have a smaller IP amplitude during Chl fluorescence transient (**Figure 4F**). Ceppi et al. (2012) suggested that the IP amplitude is a semiquantitative indicator for relative changes in the PSI content. A smaller IP amplitude is related to a loss of PSI content (Oukarroum et al., 2009; Ceppi et al., 2012). A decrease of PSI content is due to increased level of PSI produced oxygen radicals (Mittler, 2002; Oukarroum et al., 2009). A block of electron flow on the acceptor side of PSI will divert electrons from the PSI acceptor side, that normally goes to carbon fixation path, to reduce O_2 generating ROS (Chen et al., 2012). Another possible explanation for the decrease in IP amplitude would seem to be a loss of cyt b_6/f complexes. Because the loss of cyt b_6/f complexes could make the rate limitation posed by the re-oxidation of PQH₂ stronger and as a

consequence shift the I-step up. This could also lead to a smaller IP amplitude not directly relative to a loss of PSI (Ceppi et al., 2012). The performance index PI_{total} incorporates two parameters PI_{ABS} and δ_{Ro} , reflecting the whole photosynthetic activity of two photosystems (Strasser et al., 2010). Here, PI_{total} is the most sensitive JIP-test parameter. After cells were treated with 10, 50, and 100 μM GT, PI_{total} declined to about 33%, 24%, and 7% of mock.

Fluorescence rise from I- to P-step lasts normally from around 30 to 200 ms and is shown to parallel the re-reduction of plastocyanin (PC^+) and PSI reaction center (P_{700}^+) (Strasser et al., 2010). Here, in order to further confirm the effect of GT on PSI, the modulated reflection at 820 nm (MR) of *C. reinhardtii* cells was determined. As shown in **Figure 6A**, a typical MR signal curve exhibits two phases: a fast decrease phase between MR_0 (about 0.7 ms) and MR_{min} (about 10–200 ms), and a slow increase phase between MR_{min} (about 10–200 ms) and MR_{max} (about 1–2 s). The fast phase corresponds to the accumulation of PC^+ and P_{700}^+ . The transitory steady state of MR kinetics at the end of the fast phase, MR_{min} , appears due to the accumulation of PSII initiates electron transfer to PC^+ and P_{700}^+ just compensates the further oxidation of PC and P_{700} by PSI activity. In other words, at the MR_{min} point the non-cycle electron flow through PSII and PSI achieved the balance level. Once the reduction rate overcomes the oxidation rate, the slow MR phase comes out. The slow phase corresponds to the net re-reduction of PC^+ and P_{700}^+ by the intersystem electron carriers (Strasser et al., 2010; Goltsev et al., 2012). At 100 μM GT, 1 μM DCMU, and 200 μM MV, a similar the fast phase of MR/ MR_0 kinetics of cells was observed compared to mock, reflecting no effect on the capability of P_{700} to get oxidized. For MV as a PSI herbicide, it gets electrons from PSI electron transport chain at the nearly same rate as PSII is pumping them to the PSI (Schansker et al., 2005). Therefore, the MR signal of MV-treated cells remained the steady same level as the MR_{min} after the end of the fast MR phase (**Figure 6B**). However, the slow MR phase of DCMU-treated cells was losing, suggesting the complete disconnection of two photosystems (**Figure 6B**). In the presence of DCMU, the fast MR phase continued to go down, revealing a further more oxidation of PC and P_{700} . This is because that DCMU can prevent entirely PSII electron flow from reaching the PC and P_{700} and oxidating them (Schansker et al., 2003). A smaller slow MR phase reveals a lower rate of the net re-reduction of PC^+ and P_{700}^+ in the case of GT with 100 and 200 μM . Obviously, unlike DCMU, GT could not completely inhibit electron flow from PQ at PSII acceptor side to PC^+ and P_{700}^+ since the slow MR phase did not disappear. At higher concentration of 200 μM GT, a pronounced decrease of the fast MR phase was also observed, indicating the capability of P_{700} to get oxidized was markedly decreased (**Figure 6B**). Considering the decrease in the IP amplitude of OJIP curve, it is suggested that GT cause a loss of PSI active contents and disconnection of two photosystems.

On the basis of above analysis of *C. reinhardtii* cells *in vivo*, it is concluded that the major action site of GT is the acceptor side of PSII, blocking electron transfer further than Q_A and then inactivating PSII RCs. In addition, GT can also destroy the

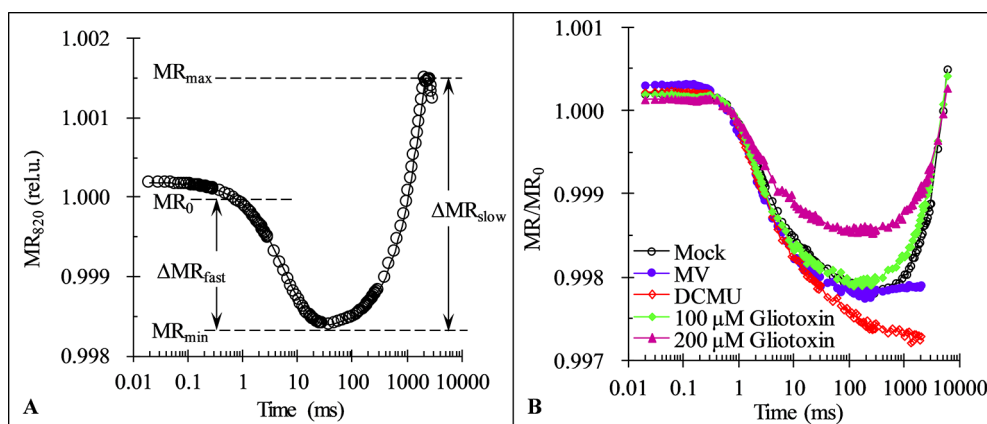


FIGURE 6 | Effect of Gliotoxin (GT) on the kinetics of modulated reflection at 820 nm (MR). **(A)** A graphical definition of the characteristic parameters of the MR kinetics. Here, MR_0 is the value at the onset of the actinic illumination (taken at 0.7 ms, the first reliable MR measurement), MR_{min} is the minimal signal reached during the fast phase between 0.7 ms and 10–200 ms, MR_{max} is the maximal signal reached by the end of the slow phase (usually taken at 1 to 2 s). **(B)** The MR induction curves of *C. reinhardtii* cells treated with 1% DMSO (mock), MV (200 μ M), DCMU (1 μ M), and GT (100, 200 μ M). The plotted values are expressed by the MR/MR_0 ratio. Each curve is the average of 30 measurements.

antenna pigment assemblies and damage the reduction of the end acceptors at the PSI acceptor side.

Effects of GT on Photosystem II and Photosystem I of Spinach Thylakoids

To more in-depth investigate the direct action sites of GT on two photosystems, Chl fluorescence rise kinetics OJIP of spinach thylakoids were measured and analyzed. As *C. reinhardtii* cells *in vivo*, the best biggest change of the fluorescence rise OJIP curves of GT-treated thylakoids is a significant rise of the J-step level (**Figures 7A, B**). A similar effect of GT is also found on JIP-test parameters including Φ_{P_0} , ET_0/CS , Φ_{E_0} , Ψ_{E_0} , S_m/t_{FM} , PI_{ABS} , Φ_{R_0} , and δ_{R_0} (**Figures 5 and 7C**). Moreover, the J-step level (V_J), PI_{ABS} , and S_m/t_{FM} are linearly related to Φ_{E_0} by increasing of GT concentration (**Figure 7E**). Such results further prove that GT mainly inhibits the PSII overall activity by inactivating PSII RCs due to interruption of PSII electron transfer beyond Q_A at the acceptor side. Concerning the values of δ_{R_0} , the inhibition of the reduction of the end acceptors at the PSI electron acceptor side is another action site of GT at high concentration above 100 μ M. The conclusion is consistent with the previous analysis of the MR_{820} kinetics. However, unlike *C. reinhardtii* cells, evidence from ABS/CS and TR_0/CS shows that no remarkable direct influence on the chlorophyll concentration and antenna pigment assemblies of PSII was observed in GT-treated spinach thylakoids (**Figure 7C**). Another expression ABS/RC, being taken a calculated average amount of chlorophyll which channels excitation energy into RC (Srivastava et al., 1998), also did not respond to different concentrations of GT treatment. Consequently, it is assumed that the damage of PSII antenna pigment assemblies in GT-treated *C. reinhardtii* cells *in vivo* might be an indirect effect of ROS production attributed to

inactivation of PSII RCs and inhibition of the reduction of the end acceptors at the PSI acceptor side. It is further supported by the evidence from SDS-PAGE of thylakoid membrane proteins. After 50, 100, 200, and 400 μ M GT treatment, the content of major PSI and PSII polypeptides, including PSI core peptide PsaA/B, D1/D2 dimer, PSII core antenna chl-binding protein (CP47, CP43, and CP29) and OEC 33 kD, did not show remarkable differences compared with the mock and DCMU treatment (see **Figure S1**). It is indicated that GT does not alter directly thylakoid polypeptide composition.

Previous evidence has tangibly demonstrated that PSII inhibiting herbicides lead to inactivation of PSII RCs for blocking electron flow beyond Q_A due to the Q_B -site of D1 protein occupying by herbicide molecules (Lazár et al., 1998; Oettmeier, 1999). Based on the JIP-test, the parameter R_j is derived, which represents the number of PSII RCs with Q_B -site filled by PSII inhibitor (**Table 1**; Lazár et al., 1998; Chen et al., 2014). The data in **Figure 7D** show that the value of R_j increases with the increasing concentration of GT. After spinach thylakoids were incubated with GT for 0.5 h, the amount of PSII RCs with Q_B -site filled by GT was about 24% (50 μ M), 28% (100 μ M), 42% (200 μ M), and 60% (400 μ M), respectively. There is a visible concentration-dependent enhancement of GT bound to PSII RCs. A highly negative correlation between S_m/t_{FM} (average fraction of open PSII RCs) and R_j was observed in the presence of GT (**Figure 7F**). This suggests that GT-caused severe closure of PSII RCs is because of an enhancement of the number of PSII RCs with the Q_B -site filled with GT.

Obviously, one of the most important primary action sites of GT is perhaps the Q_B -site of PSII RCs. GT decreases the photosynthetic activity by inhibiting electron flow beyond Q_A at the acceptor side of PSII for its binding to the PSII RCs with Q_B -site.

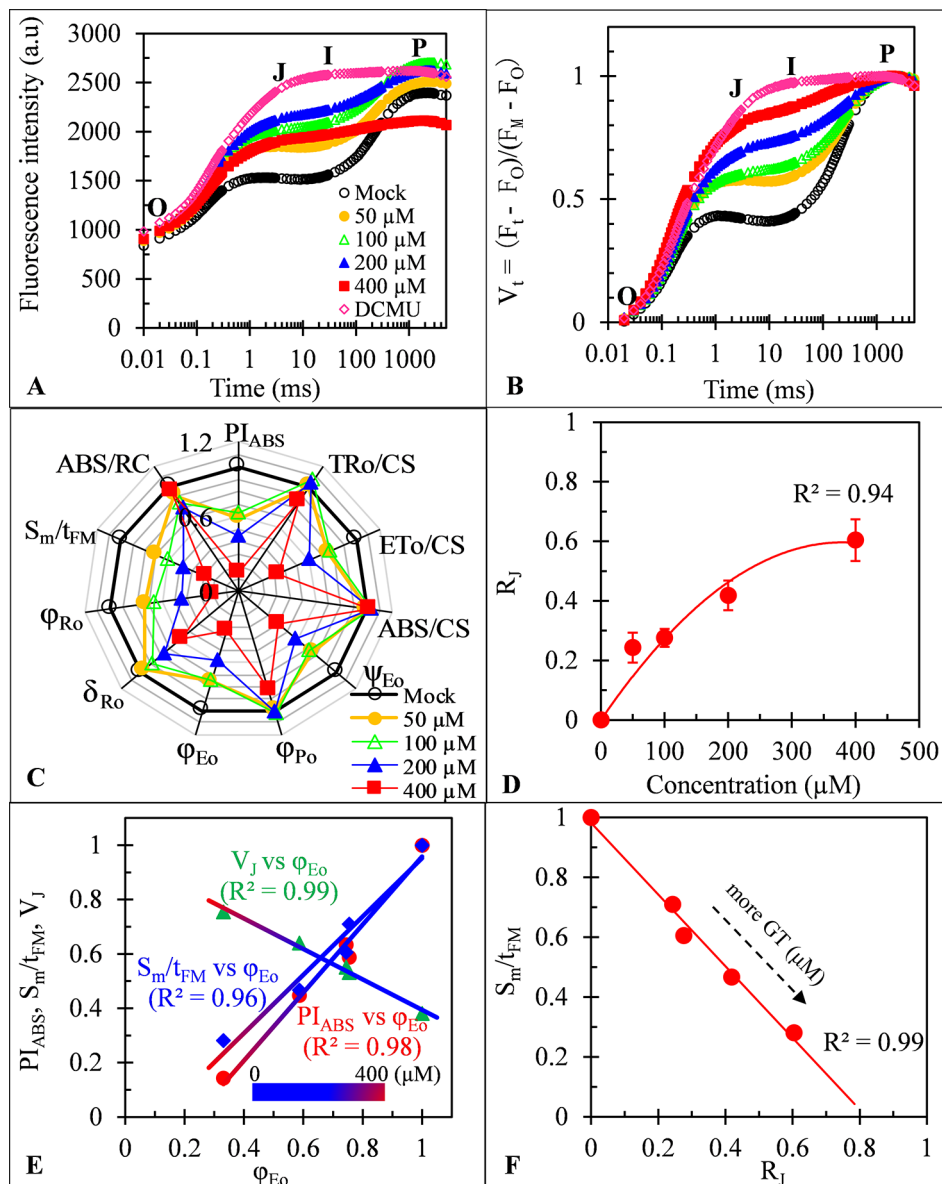


FIGURE 7 | Effect of Gliotoxin (GT) on spinach thylakoids. **(A)** Raw fluorescence rise kinetics of thylakoids treated with 1% DMSO (mock), DCMU (1 μ M), and GT at the indicated concentrations for 0.5 h. **(B)** Fluorescence rise kinetics normalized by F_0 and F_M as $V_t = (F_t - F_0)/(F_M - F_0)$. **(C)** Radar plot presenting the JIP-test parameters from thylakoids with different concentrations of GT. **(D)** The concentration-dependent change of R_j . The parameter R_j reflects the number of PSII RCs with their Q_B site filled by PSII inhibitors (here is GT). **(E)** Analysis of the correlation for V_j , PI_{ABS} , and S_m/t_{FM} versus ϕ_{E_0} of spinach thylakoids treated with GT at different concentration (mock, 50, 100, 200, and 400 μ M). **(F)** Analysis of the linear relationship between S_m/t_{FM} and R_j after spinach thylakoids were treated with GT. Each value is the average of 30 measurements.

GT Binding Niche At the Q_B -Site of the D1 Protein

Generally, herbicides that target PSII interrupt linear electron transport at the acceptor side of PSII by replacing with native PQ for the Q_B -site of D1 protein (Oettmeier, 1999). The D1 protein in higher plant is called L-subunit protein in the photosynthetic bacteria. It contains five trans-membrane α -helices and several short nonmembrane helices between the transmembrane helices

(Xiong et al., 1996; Kamiya and Shen, 2003). The Q_B -site just falls between the helices IV and V of the D1 protein from phenylalanine (Phe211) to leucine (Leu275), which is also called the site of PSII herbicide binding (Xiong et al., 1996; Ke, 2001; Trebst, 2008).

Above evidence from Chl fluorescence rise kinetics shows that GT may be like DCMU to inhibit PSII electron transfer beyond Q_A by occupying the Q_B -site. In order to get further proof to

support this hypothesis, GT was modeled its position in the Q_B-site at spinach D1 protein using Discovery Studio version 3.5. Meanwhile, to ensure reliability of this method, the simulated modeling of classical herbicide atrazine and DCMU binding to the Q_B-site was also established based on the available experimental and theoretical data. First, the standard modeling of atrazine to the Q_B-site was simulated according to the crystal structure information of complexes of the bacterial *Rps. viridis* RC with atrazine (5PRC) and spinach D1 protein (3JCU). It is found that a hydrogen bond can be formed between N-3 of the atrazine ring system and Ile224 of the L-subunit. A second hydrogen bridge between the ethylamino hydrogen (NH) of atrazine and Ser223 of the L-subunit is observed (**Figures 8A, B, Table 3**). Furthermore, Phe216 of the L-subunit is involved in

atrazine binding by both π -electron systems (**Figures 8A, B**). In addition, four residues, L-His190, L-Asn213, L-Tyr222, and L-Gly225 of the ligand with atrazine are also identified. The results are quite matched with previous studies from X-ray crystal and resistance mutant reports (Oettmeier, 1999; Lancaster and Michel, 1999). **Figure 8C** depicts a homology sequence comparison between the L-subunit from *Rps. viridis* and the D1 protein from *C. reinhardtii* and spinach. The counterparts of L-Phe216, L-Ser223, and L-Ile224 in the L-subunit, as atrazine binding residues, are just D1-Phe255, D1-Ser264, and D1-Asn266 in the D1 protein. Thereinto, D1-Ser264 is the most important for atrazine resistance (Oettmeier, 1999). In modeling of atrazine docking to the D1 protein of spinach (3JCU), D1-Ser264 and D1-His252 are defined as the active sites

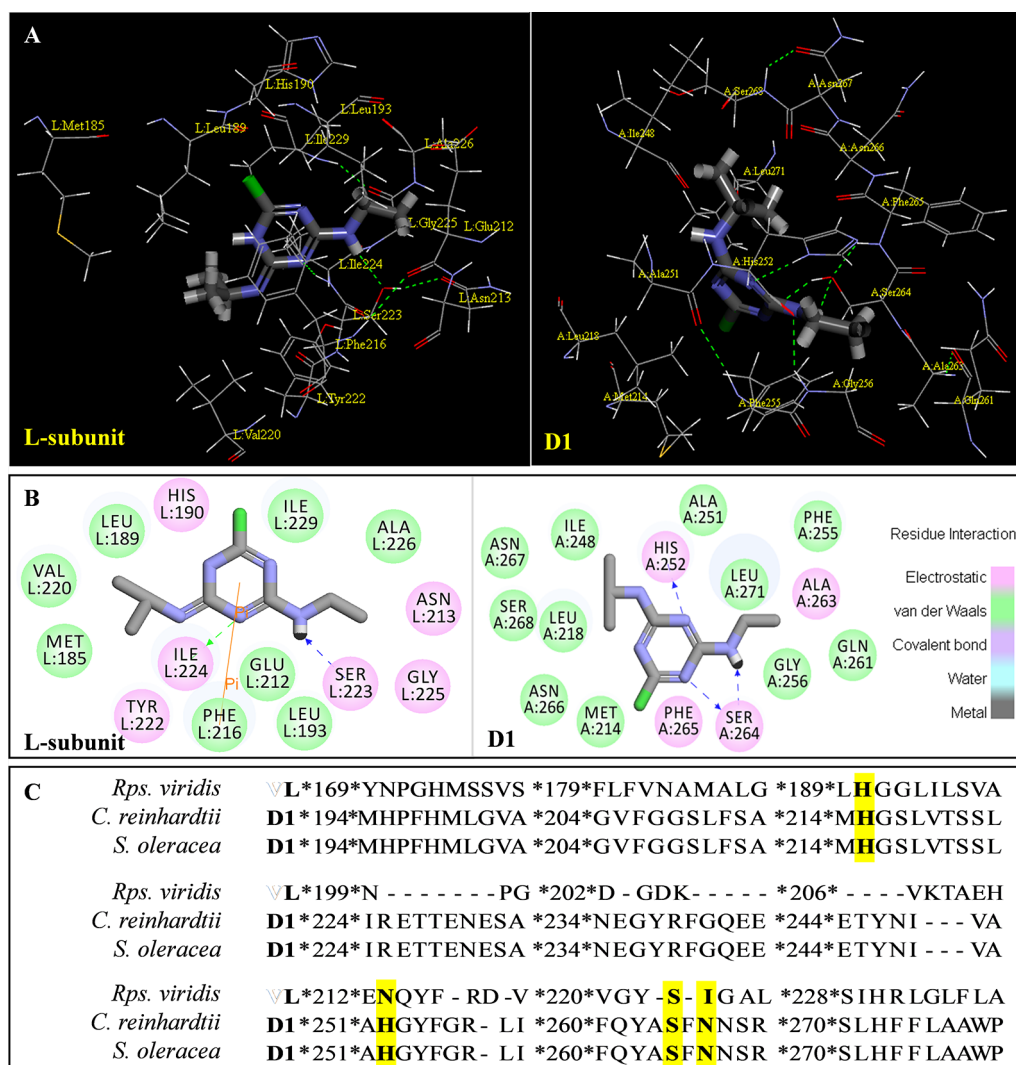
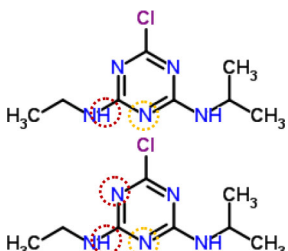
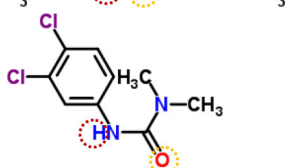



FIGURE 8 | The simulated modeling of atrazine binding to the Q_B-site. **(A)** Stereo view of atrazine binding environment of the L-subunit of *Rps. viridis* (left) and the D1 protein of *S. oleracea* (right). **(B)** Hydrogen bonding interactions for atrazine binding to the Q_B niche. Here, carbon atoms are shown in grey, nitrogen atoms in blue, oxygen in red, chlorine in green, and hydrogen atoms in white. The possible hydrogen bonds are indicated by dashed lines. **(C)** Sequence alignment of the D1 protein of *C. reinhardtii* and *S. oleracea* with the L-subunit of the *Rps. viridis* RC. The bacterial L-subunit sequences are in upper case and the D1 sequence is in lower case.

TABLE 3 | Possible hydrogen bonding interactions for atrazine, DCMU and Gliotoxin (GT) binding to the L-subunit of *Rh. viridis* or the D1 protein of *S. oleracea*. The circle refers to the predicted atom position providing hydrogen bond with the indicated amino acid residue.

Com.	Mol. Formula	Chemical Structure	Binding target	Hydrogen Bound Position
atrazine	$C_8H_{14}ClN_5$		L-subunit	L – Ser223 ↓ NH
				D1 – Ser264 D1 – His252
				N – NH –, N –
DCMU	$C_9H_{10}Cl_2N_2O$		D1	D1 – His252 = O –
				NH –
gliotoxin	$C_{13}H_{14}N_2O_4S_2$		D1	D1 – His252 = O –
				HO –

(Figures 8A, B). D1-Ser264 interacting with atrazine is the same as L-Ser223 in the L-subunit. Interestingly, N-1 of the atrazine ring system also provides a weak hydrogen bond to D1-Ser264. Another hydrogen bond is formed between N-3 of the atrazine ring system and D1-His252 not D1-Asn266 corresponding L-Ile224 in the L-subunit.

The binding modeling of the D1 protein from spinach (3JCU) docking with DCMU is also presented in Figure 9. The D1-Ser264 provides a hydrogen bond to the amide hydrogen of DCMU. Another hydrogen bond is found between the carbonyl group of DCMU and D1-His252 (Figure 9, Table 3). Previous modeling has shown that the protein binding environment for DCMU is overlapping with that for Q_B . The residues that appear to coordinate DCMU binding are D1-Phe211, D1-Met214, D1-His215, D1-Val219, D1-Phe232, D1-Tyr246, D1-Ala251, D1-His252, D1-Gly256, D1-Ala263, D1-Ser264, D1-Phe265, D1-Asn266, and D1-Leu271 (Xiong et al., 1996). It is predicted that DCMU orients itself preferentially towards D1-Ser264 by a hydrogen bond (Trebst, 1987; Xiong et al., 1996).

The modeling of GT docking to the Q_B -site was built on the basis of the available crystal structure alignment of spinach D1 protein (3JCU) through energy minimization and molecular dynamics simulations (Figure 9). In the modeling, D1 residues identified to be more likely related to the binding of GT are D1-Tyr246, D1-Ile248, D1-Val249, D1-Ala251, D1-His252, D1-S264, D1-Phe265, D1-Asn266, and D1-Ser268. Here, it is predicted that hydrogen bonds are formed between D1-Ser264 and the aromatic hydroxyl oxygen of GT, and between D1-His252 and the 4-carbonyl group of GT. This exhibits somewhat different from DCMU. Additionally, the residues, D1-Met214, D1-His215, D1-Leu218, D1-Val219, D1-Phe255, D1-Asn267, and D1-His272, are also found within the van der Waals contact sphere with GT. However, to further identify amino acids in the

target which participate in GT binding, more experimental data based on the site directed mutant and X-ray structure are needed in the future.

It is well known that all PSII inhibitors share the same binding site on the D1 protein. However, each inhibitor has its characteristic orientation in the D1 protein. PSII inhibitors can be grouped into two families, the classical type with ureas and triazine, and the phenol type with ioxynil and dinoseb (Trebst, 1987). The ureas/triazine family inhibitors have the common structure group $N-C = X$, where X signifies N or O. They are more closely oriented toward D1-Ser264 in the Q_B binding niche. The phenolic inhibitors contain the aromatic hydroxyl group bearing nitro and/or halogen and/or nitrile substituent, binding to the Q_B -site via D1-His215 (Oettmeier et al., 1982; Trebst, 1987). GT belongs to the first family since it possesses the common characteristics group $N-C = O$ like ureas/triazine type PSII inhibitors. The protein-binding environment of GT appears to be consistent with most existing data of the classical PSII inhibitors.

CONCLUSIONS

Above all presentations reveal that GT has excellent herbicidal potentiality attributed to its multiple effects on photosynthetic apparatus. The main action of GT is the arrest of photosynthesis by blocking electron flow beyond Q_A at the acceptor side of PSII and then inactivating PSII RCs. The primary direct target of GT is the Q_B -site of the D1 protein in PSII. Based on the modeling of GT docking to the D1 protein, it is assumed that GT binds to the Q_B -site by the hydrogen bonds between the aromatic hydroxyl oxygen of GT and the residue D1-Ser264, and between the 4-carbonyl group of GT and the residue D1-His252. It is clear that GT is a novel natural PSII inhibitor with the characteristics group

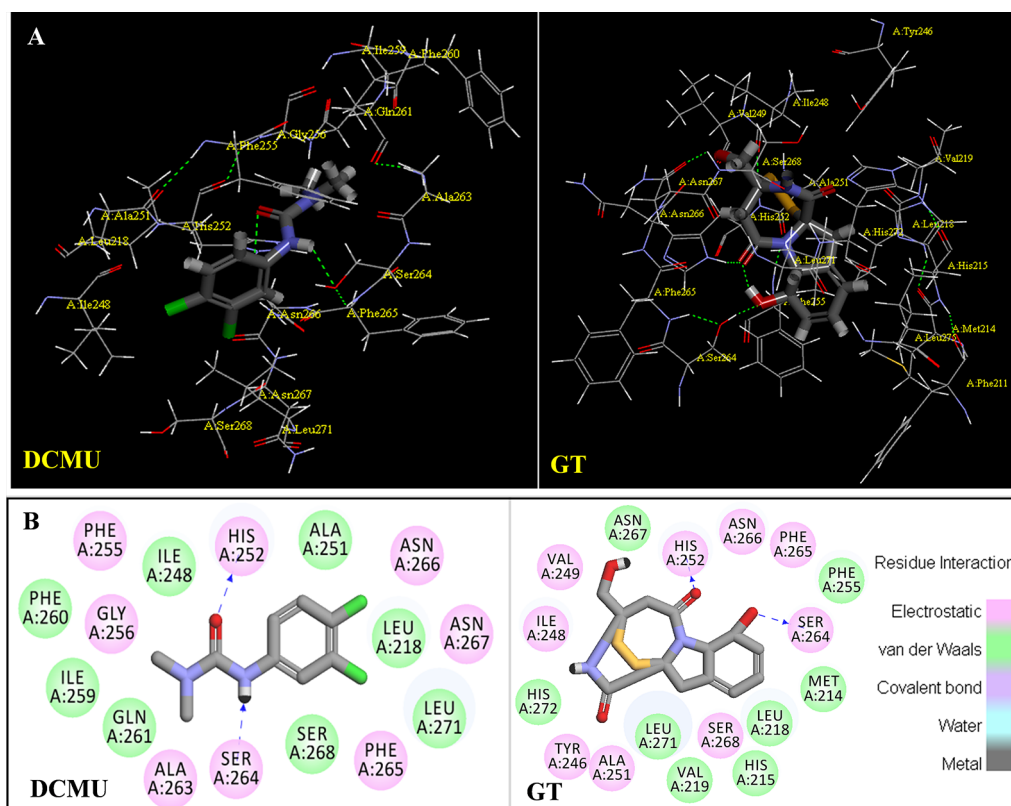


FIGURE 9 | The simulated modeling of DCMU and Gliotoxin (GT) binding to the D1 protein of *S. oleracea*. **(A)** Stereo view of DCMU (left) and GT (right) binding environment of *S. oleracea* D1 protein. **(B)** Hydrogen bonding interactions for DCMU (left) and GT (right) binding to the D1 protein. Here, carbon atoms are shown in grey, nitrogen atoms in blue, oxygen in red, chlorine in green, and hydrogen atoms in white. The possible hydrogen bonds are indicated by dashed lines.

N-C = O. Additionally, GT at high concentration can also inhibit PSI activity by decreasing the reduction of the end acceptors at the PSI acceptor side. So, it is concluded that GT may be an interesting structural framework of a potential photosynthetic inhibitor. However, further studies are needed to clarify and confirm the actual binding site for GT in PSII and PSI.

DATA AVAILABILITY STATEMENT

All datasets generated for this study are included in the article/**Supplementary Material**.

AUTHOR CONTRIBUTIONS

SC and SQ designed research. TGu, JC, YL, HW, YGa, JS, CY, and XW performed experiments. SC, YGu, JC, and RS analyzed data and wrote the paper.

ACKNOWLEDGMENTS

This work was supported by the National Key Research and Development Program (2017YFD0201300), the Foreign Expert

Project (G20190010118) and the Fundamental Research Funds for the Central Universities (KYZZ01530). The authors also wish to thank Bernal E. Valverde (Investigación y Desarrollo en Agricultura Tropical, Costa Rica) for helpful comments and improving the manuscript.

SUPPLEMENTARY MATERIAL

The Supplementary Material for this article can be found online at: <https://www.frontiersin.org/articles/10.3389/fpls.2019.01688/full#supplementary-material>

FIGURE S1 | SDS-PAGE analysis of spinach thylakoid polypeptides after GT treatment. Thylakoids with $100 \mu\text{g Chl ml}^{-1}$ were treated with 1% DMSO, $1 \mu\text{M}$ DCMU and different concentrations of GT for 0.5 h in the dark at 25°C . Thylakoid membrane proteins were separated by gel electrophoresis. A total protein containing $15 \mu\text{g}$ chlorophylls was loaded onto the gel for each sample. SDS-PAGE containing 6 M urea was used with a slab gel containing 4% (stacking) and 12% (resolving) acrylamide. From left to right: marker (Thermo Scientific PageRuler Prestained Protein Ladder, No. 26616) (1), 1% DMSO (mock, 2), $50 \mu\text{M}$ GT (3), $100 \mu\text{M}$ GT (4), $200 \mu\text{M}$ GT (5), $400 \mu\text{M}$ GT (6), $1 \mu\text{M}$ DCMU (7) and water (8). CP and OEC indicate Chl a/b binding protein and oxygen evolving complex 33 kD, respectively. The similar result was repeated at least 3 times.

REFERENCES

- Arias, M., Santiago, L., Vidal-García, M., Redrado, S., Lanuza, P., Comas, L., et al. (2018). Preparations for invasion: modulation of host lung immunity during Pulmonary Aspergillosis by gliotoxin and other fungal secondary metabolites. *Front. Immunol.* 9, 2549. doi: 10.3389/fimmu.2018.02549
- Ceppi, M. G., Oukarroum, A., Ççiek, N., Strasser, R. J., and Schansker, G. (2012). The IP amplitude of the fluorescence rise OJIP is sensitive to changes in the photosystem I content of leaves: a study on plants exposed to magnesium and sulfate deficiencies, drought stress and salt stress. *Physiol. Plant* 144, 277–288. doi: 10.1111/j.1399-3054.2011.01549.x
- Chen, S., Xu, X., Dai, X., Yang, C., and Qiang, S. (2007). Identification of tenuazonic acid as a novel type of natural photosystem II inhibitor binding in QB-site of *Chlamydomonas reinhardtii*. *Biochim. Biophys. Acta* 1767, 306–318. doi: 10.1016/j.bbabi.2007.02.007
- Chen, S., Yin, C., Dai, X., Qiang, S., and Xu, X. (2008). Action of tenuazonic acid, a natural phytotoxin, on photosystem II of spinach. *Environ. Exp. Bot.* 62, 279–289. doi: 10.1016/j.envexpbot.2007.10.002
- Chen, S., Yin, C., Strasser, R. J., Govindjee, J., Yang, C., and Qiang, S. (2012). Reactive oxygen species from chloroplasts contribute to 3-acetyl-5-isopropyltetramic acid-induced leaf necrosis of *Arabidopsis thaliana*. *Plant Physiol. Biochem.* 52, 38–51. doi: 10.1016/j.plaphy.2011.11.004
- Chen, S., Strasser, R. J., and Qiang, S. (2014). In vivo assessment of effect of phytotoxin tenuazonic acid on PSII reaction centers. *Plant Physiol. Biochem.* 84, 10–21. doi: 10.1016/j.plaphy.2014.09.004
- Chen, S., Yang, J., Zhang, M., Strasser, R. J., and Qiang, S. (2016). Classification and characteristics of heat tolerance in *Ageratina adenophora* populations using fast chlorophyll a fluorescence rise O-J-I-P. *Environ. Exp. Bot.* 122, 126–140. doi: 10.1016/j.envexpbot.2015.09.011
- Dolan, S. K., O’Keeffe, G., Jones, G. W., and Doyle, S. (2015). Resistance is not futile: gliotoxin biosynthesis, functionality and utility. *Trends Microbiol.* 23, 419–428. doi: 10.1016/j.tim.2015.02.005
- Furuta, T., Kigane, T., and Suganoya, Y. (1984). Isolation of gliotoxin as lettuce seedling growth inhibit substance from the culture broth of *Aspergillus fumigatus* Fres. *Bull. Fac. Agric. Tamagawa Univ.* 24, 16–25.
- Gao, Y., Liu, W., Wang, X., Yang, L., Han, S., Chen, S., et al. (2018). Comparative phytotoxicity of usnic acid, salicylic acid, cinnamic acid and benzoic acid on photosynthetic apparatus of *Chlamydomonas reinhardtii*. *Plant Physiol. Biochem.* 128, 1–12. doi: 10.1016/j.plaphy.2018.04.037
- Goltsev, V., Zaharieva, I., Chernev, P., Kouzmanova, M., Kalaji, H. M., Yordanov, I., et al. (2012). Drought-induced modifications of photosynthetic electron transport in intact leaves: analysis and use of neural networks as a tool for a rapid non-invasive estimation. *Biochim. Biophys. Acta* 1817, 1490–1498. doi: 10.1016/j.bbabi.2012.04.018
- Haraguchi, H., Hamatani, Y., Shibata, K., and Hashimoto, K. (1992). An inhibitor of acetolactate synthase from a microbe. *Biosci. Biotechnol. Biochem.* 56, 2085–2086. doi: 10.1271/bbb.562085
- Haraguchi, H., Hamatani, Y., Hamada, M., and Fujii-Techino, A. (1996). Effect of gliotoxin on growth and branched-chain amino acid biosynthesis in plants. *Phytochemistry* 42, 645–648. doi: 10.1016/0031-9422(95)00982-5
- Haraguchi, H., Yamano, K., Kusunoki, N., and Fukuda, A. (1997). Effect of gliotoxin and related compounds on acetolactate synthase. *J. Agric. Food Chem.* 45, 2784–2787. doi: 10.1021/jf960842a
- Harms, H., Orlikova, B., Ji, S., Nesaee-Mosaferan, D., Konig, G. M., and Diederich, M. (2015). Epipolythiodiketopiperazines from the marine derived fungus *Dichotomomyces cepjii* with NF- κ B inhibitory potential. *Mar. Drugs* 13, 4949–4966. doi: 10.3390/md13084949
- Haun, F., Neumann, S., Peintner, L., Wieland, K., Habicht, J., Schwan, C., et al. (2018). Identification of a novel ankois signalling pathway using the fungal virulence factor gliotoxin. *Nat. Commun.* 9, 3524. doi: 10.1038/s41467-018-05850-w
- Hurne, A. M., Chai, C. L. L., Moerman, K., and Waring, P. (2002). Influx of calcium through a redox-sensitive plasma membrane channel in thymocytes causes early necrotic cell death induced by the epipolythiodioxopiperazine toxins. *J. Biol. Chem.* 277, 31631. doi: 10.1074/jbc.M201699200
- Jordan, T. W., and Pedersen, J. S. (1986). Sporidesmin and gliotoxin induce cell detachment and perturb microfilament structure in cultured liver cells. *J. Cell Sci.* 85, 33–46. doi: 10.1083/jcb.103.31129
- Kamiya, N., and Shen, J. R. (2003). Crystal structure of oxygen-evolving photosystem II from *Thermosynechococcus vulcanus* at 3.7-Å resolution. *Proc. Natl. Acad. Sci. U.S.A.* 100, 98–103. doi: 10.1073/pnas.0135651100
- Ke, B. (2001). “The stable primary electron acceptor QA and the second electron acceptor QB,” in *Photosynthesis: Photobiochemistry and Photobiophysics*. Ed. B. Ke (New York-Boston-Dordrecht-London-Moscow: Kluwer Academic Publishers), 289–304.
- Khan, M. R., Arshad Anwer, M., and Shahid, S. (2011). Management of gray mold of chickpea, *Botrytis cinerea* with bacterial and fungal biopesticides using different modes of inoculation and application. *Biol. Control* 57, 13–23. doi: 10.1016/j.biocontrol.2011.01.004
- Kim, Y., and Park, S. J. (2016). Gliotoxin from the marine fungus *Aspergillus fumigatus* induces apoptosis in HT1080 fibrosarcoma cells by downregulating NF- κ B. *Fish. Aquat. Sci.* 19, 35. doi: 10.1186/s41240-016-0036-6
- Krause, G. H., and Weis, E. (1991). Chlorophyll fluorescence and photosynthesis: the basics. *Annu. Rev. Plant Physiol. Plant Mol. Biol.* 42, 313–349. doi: 10.1146/annurev.pp.42.060191.001525
- Kroll, M., Arenzana-Seisdedos, F., Bachelier, F., Thomas, D., Friguet, B., and Conconi, M. (1999). The secondary fungal metabolite gliotoxin targets proteolytic activities of the proteasome. *Chem. Biol.* 6, 689–698. doi: 10.1016/s1074-5521(00)80016-2
- Lancaster, C. R. D., and Michel, H. (1999). Refined crystal structures of reaction centres from *Rhodospseudomonas viridis* in complexes with the herbicide atrazine and two chiral atrazine derivatives also lead to a new model of the bound carotenoid. *J. Mol. Biol.* 286, 883–898. doi: 10.1006/jmbi.19982532
- Lazar, D., Brokeš, M., Nauš, J., and Dvorák, L. (1998). Mathematical modeling of 3-(3',4'-dichlorophenyl)-1,1-dimethylurea action in plant leaves. *J. Theor. Biol.* 191, 79–86. doi: 10.1006/jtbi.19970566
- Li, J., Zhang, Y., Santos, B. D. S. D., Wang, F., Ma, Y., Perez, C., et al. (2018). Epithiodiketopiperazines inhibit protein degradation by targeting proteasome deubiquitinase Rpn11. *Cell Chem. Biol.* 25, 1350–1358. doi: 10.1016/j.chembiol.2018.07.012
- Lumsden, R. D., and Walter, J. F. (2003). “Development of the biocontrol fungus *Gliocladium virens*: risk assessment and approval for horticultural use,” in *Biological Control: Benefits and Risks*. Eds. H. M. T. Hokkanen and J. M. Lynch (Cambridge, UK: Cambridge University Press), 263–269.
- Miller, P. A., Milstrey, K. P., and Trown, P. W. (1968). Specific inhibition of viral ribonucleic acid replication by Gliotoxin. *Science* 159, 431–432. doi: 10.1126/science.159.3813.431
- Mittler, R. (2002). Oxidative stress, antioxidants and stress tolerance. *Trends Plant Sci.* 7, 405–410. doi: 10.1016/S1360-1385(02)02312-9
- Nouri, M. A., Al-Halbosi, M. M. F., Dheeb, B. I., and Hashim, A. J. (2015). *Aquat. J. King Saud Univ. Sci.* 27, 193–197. doi: 10.1016/j.jksus.2014.12.005
- Oettmeier, W., Masson, K., and Johanningmeier, U. (1982). Evidence for two different herbicide-binding proteins at the reducing side of photosystem II. *Biochim. Biophys. Acta* 679, 376–383. doi: 10.1016/0005-2728(82)90157-8
- Oettmeier, W. (1999). Herbicide resistance and supersensitivity in photosystem II. *CMLS. Cell. Mol. Life Sci.* 55, 1255–1277. doi: 10.1007/s000180050370
- Oukarroum, A., Schansker, G., and Strasser, R. J. (2009). Drought stress effects on photosystem I content and photosystem II thermostability analyzed using Chl a fluorescence kinetics in barley varieties differing in their drought tolerance. *Physiol. Plant* 137, 188–199. doi: 10.1111/j.1399-3054.2009.01273.x
- Schansker, G., Srivastava, A., Govindjee, J., and Strasser, R. J. (2003). Characterization of the 820-nm transmission signal paralleling the chlorophyll a fluorescence rise (OJIP) in pea leaves. *Funct. Plant Biol.* 30, 785–796. doi: 10.1071/FP03032
- Schansker, G., Tóth, S. Z., and Strasser, R. J. (2005). Methylviologen and dibromothymoquinone treatments of pea leaves reveal the role of photosystem I in the Chl a fluorescence rise OJIP. *Biochim. Biophys. Acta* 1706, 250–261. doi: 10.1016/j.bbabi.2004.11.006
- Scharf, D. H., Brakhage, A. A., and Mukherjee, P. K. (2016). Gliotoxin—bane or boon? *Environ. Microbiol.* 18, 1096–1109. doi: 10.1111/1462-2920.13080

- Smith, E. B., Dolan, S. K., Fitzpatrick, D. A., Doyle, S., and Jones, G. W. (2016). Towards understanding the gliotoxin detoxification mechanism: in vivo thiomethylation protects yeast from gliotoxin cytotoxicity. *Microb. Cell* 3, 120–125. doi: 10.15698/mic2016.03.485
- Srivastava, A., Jüttner, F., and Strasser, R. J. (1998). Action of the allelochemical, fischerellin A, on photosystem II. *Biochim. Biophys. Acta* 1364, 326–336. doi: 10.1016/S0005-2728(98)00014-0
- Strasser, R. J., and Govindjee, (1992). “The Fo and the O-J-I-P Fluorescence Rise in Higher Plants and Algae,” in *Regulation of Chloroplast Biogenesis*. Ed. J. H. Argyroudi-Akoyunoglou (New York: Plenum Press), 423–426.
- Strasser, R. J., Srivastava, A., and Govindjee, (1995). Polyphasic chlorophyll a fluorescence transient in plants and cyanobacteria. *Photochem. Photobiol.* 61, 32e42. doi: 10.1111/j.1751-1097.1995.tb09240.x
- Strasser, R. J., Tsimilli-Michael, M., and Srivastava, A. (2004). “Analysis of the Chlorophyll a Fluorescence Transient,” in *Chlorophyll Fluorescence: A Signature of Photosynthesis*. Eds. G. C. Papageorgiou and Govindjee, (Netherlands: Kluwer Academic Publishers), 321–362.
- Strasser, R. J., Tsimilli-Michael, M., Qiang, S., and Goltsev, V. (2010). Simultaneous in vivo recording of prompt and delayed fluorescence and 820-nm reflection changes during drying and after rehydration of the resurrection plant *Haberlea rhodopensis*. *Biochim. Biophys. Acta* 1797, 1313–1326. doi: 10.1016/j.bbabi.2010.03.008
- Tóth, S. Z., Schansker, G., and Strasser, R. J. (2005). In intact leaves, the maximum fluorescence level (FM) is independent of the redox state of the plastoquinone pool: A DCMU-inhibition study. *Biochim. Biophys. Acta* 1708, 275–282. doi: 10.1016/j.bbabi.2005.03.012
- Trebst, A. (1987). The three-dimensional structure of the herbicide binding niche on the reaction center polypeptides of photosystem II. *Z. Naturforsch.* 42C, 742–750. doi: 10.1515/znc-1987-0616
- Trebst, A. (2008). “The mode of action of triazine herbicides in plants,” in *The Triazine Herbicides 50 years Revolutionizing Agriculture*. Eds. H. M. LeBaron, J. E. McFarland and O. C. Burnside (San Diego: Elsevier), 101–110.
- Vigushin, D. M., Mirsaidi, N., Brooke, G., Sun, C., Pace, P., Inman, L., et al. (2004). Gliotoxin is a dual inhibitor of farnesyltransferase and geranylgeranyltransferase I with antitumor activity against breast cancer in vivo. *Med. Oncol.* 21, 21–30. doi: 10.1385/mo:21:1:21
- Wright, J. M. (1951). Phytotoxic effects of some antibiotics. *Ann. Bot.* 15, 493–499. doi: 10.1093/oxfordjournals.aob.a083294
- Xiong, J., Jee, G., and Subramaniam, S. (1996). Modeling of the D1/D2 proteins and cofactors of the photosystem II reaction center: Implications for herbicide and bicarbonate binding. *Protein Sci.* 5, 2054–2073. doi: 10.1002/pro.5560051012
- Yusuf, M. A., Kumar, D., Rajwanshi, R., Strasser, R. J., Tsimilli-Michael, M., Govindjee, et al. (2010). Overexpression of g-tocopherol methyl transferase gene in transgenic *Brassica juncea* plants alleviates abiotic stress: physiological and chlorophyll a fluorescence measurements. *Biochim. Biophys. Acta* 1797, 1428–1438. doi: 10.1016/j.bbabi.2010.02.002

Conflict of Interest: The authors declare that the research was conducted in the absence of any commercial or financial relationships that could be construed as a potential conflict of interest.

Copyright © 2020 Guo, Cheng, Lu, Wang, Gao, Shi, Yin, Wang, Chen, Strasser and Qiang. This is an open-access article distributed under the terms of the Creative Commons Attribution License (CC BY). The use, distribution or reproduction in other forums is permitted, provided the original author(s) and the copyright owner(s) are credited and that the original publication in this journal is cited, in accordance with accepted academic practice. No use, distribution or reproduction is permitted which does not comply with these terms.



Hydrogen Peroxide Production by the Spot-Like Mode Action of Bisphenol A

Ioannis-Dimosthenis S. Adamakis^{1*}, Ilektra Sperdoulis², Eleftherios P. Eleftheriou³ and Michael Moustakas^{3*}

¹ Department of Botany, Faculty of Biology, National and Kapodistrian University of Athens, Athens, Greece, ² Institute of Plant Breeding and Genetic Resources, Hellenic Agricultural Organization Demeter, Thessaloniki, Greece, ³ Department of Botany, Aristotle University of Thessaloniki, Thessaloniki, Greece

OPEN ACCESS

Edited by:

Vasileios Fotopoulos,
Cyprus University of Technology,
Cyprus

Reviewed by:

Qing Zhou,
Jiangnan University, China
Manuel Joaquín Reigosa-Roger,
University of Vigo, Spain

*Correspondence:

Ioannis-Dimosthenis S. Adamakis
iadamaki@biol.uoa.gr
Michael Moustakas
moustak@bio.auth.gr

Specialty section:

This article was submitted to
Plant Abiotic Stress,
a section of the journal
Frontiers in Plant Science

Received: 09 April 2020

Accepted: 23 July 2020

Published: 05 August 2020

Citation:

Adamakis I-D, Sperdoulis I,
Eleftheriou EP and Moustakas M
(2020) Hydrogen Peroxide
Production by the Spot-Like Mode
Action of Bisphenol A.
Front. Plant Sci. 11:1196.
doi: 10.3389/fpls.2020.01196

Bisphenol A (BPA), an intermediate chemical used for synthesizing polycarbonate plastics, has now become a wide spread organic pollutant. It percolates from a variety of sources, and plants are among the first organisms to encounter, absorb, and metabolize it, while its toxic effects are not yet fully known. Therefore, we experimentally studied the effects of aqueous BPA solutions (50 and 100 mg L⁻¹, for 6, 12, and 24 h) on photosystem II (PSII) functionality and evaluated the role of reactive oxygen species (ROS) on detached leaves of the model plant *Arabidopsis thaliana*. Chlorophyll fluorescence imaging analysis revealed a spatiotemporal heterogeneity in the quantum yields of light energy partitioning at PSII in *Arabidopsis* leaves exposed to BPA. Under low light PSII function was negatively influenced only at the spot-affected BPA zone in a dose- and time-dependent manner, while at the whole leaf only the maximum photochemical efficiency (Fv/Fm) was negatively affected. However, under high light all PSII photosynthetic parameters measured were negatively affected by BPA application, in a time-dependent manner. The affected leaf areas by the spot-like mode of BPA action showed reduced chlorophyll autofluorescence and increased accumulation of hydrogen peroxide (H₂O₂). When H₂O₂ was scavenged via N-acetylcysteine under BPA exposure, PSII functionality was suspended, while H₂O₂ scavenging under non-stress had more detrimental effects on PSII function than BPA alone. It can be concluded that the necrotic death-like spots under BPA exposure could be due to ROS accumulation, but also H₂O₂ generation seems to play a role in the leaf response against BPA-related stress conditions.

Keywords: bisphenol A, chlorophyll fluorescence imaging, plastoquinone pool, signaling molecule, H₂O₂ scavenger, photosystem II functionality, necrotic death-like spot, reactive oxygen species

INTRODUCTION

Plants are sessile organisms, specially affected by changes in their environment and therefore unavoidably prone to many stress-factors. So, plants have evolved an extensive range of mechanisms for acclimation and adaptation (van Loon, 2016). Numerous studies have confirmed that some of these mechanisms include reactive oxygen species (ROS) formation (Garg and Manchanda, 2009;

Foyer, 2018; Huang et al., 2019). These molecules were traditionally related to wide-range damaging of cellular macromolecules (i.e., nucleic acids, lipids, proteins, etc.), which probably could result in cell death and even whole organism collapse (Potters et al., 2010). Nonetheless, decades of thorough research gathered substantial evidence to support that ROS-mediated responses are orchestrated and regulated under a tight genetic control. Hence, in plants, ROS roles in early signaling events initiated by various environmental stimuli have been established (Noctor et al., 2018; Huang et al., 2019). These stimuli could include extreme temperatures (Awasthi et al., 2015), drought (Laxa et al., 2019), heavy metals (Eleftheriou et al., 2015), nanoparticles (Sperdouli et al., 2019), and organic pollutants (Christou et al., 2018).

One such organic pollutant is bisphenol A (2,2-bis(4-hydroxyphenyl)propane; BPA), a chemical stabilizer widely applied in the industrial manufacture of plastic materials (Lin et al., 2017). As plastic commodities deteriorate, BPA can escape and pollute the environment (Xu et al., 2011). This pollution seems to be harmful, since, BPA belongs to the xenoestrogen substance family and by acting as an endocrine disruptor can cause several human health issues (Jalal et al., 2018; Abraham and Chakraborty, 2019). While extensive research has been conducted about BPA effects on humans/animals, scientific data regarding the toxic effects of BPA on plants have been accumulating only in recent years (Xiao et al., 2020). Although plants can absorb and metabolize BPA, at the same time BPA could deteriorate their cellular/physiological status (Zhang et al., 2017). It has been shown that experimentally applied concentrations of BPA (mg/L) negatively affected the growth of many important crops, e.g., soybean (Qui et al., 2013; Zhang et al., 2016; Jiao et al., 2017; Li X. et al., 2018; Zhang et al., 2018; Xiao et al., 2019), pea (Adamakis et al., 2013), wheat (Adamakis et al., 2019), maize (Stavropoulou et al., 2018), rice (Ali et al., 2016), cucumber (Li Y. T. et al., 2018) and onion (Adamakis et al., 2019); also of non-cultivated plants such as the Cephalonian fir (Adamakis et al., 2016) and the model plant *Arabidopsis thaliana* (Pan et al., 2013; Tian et al., 2014; Frejd et al., 2016; Ali et al., 2017; Rapala et al., 2017; Bahmani et al., 2020). Growth reduction effects have interestingly been found to occur also after environmentally relevant concentrations ($\mu\text{g/L}$) applied on cultivated crops, e.g., cabbage and tomato (Staples et al., 2010), native plants such as oat (Staples et al., 2010) and seagrasses (Adamakis et al., 2018; Malea et al., 2020).

BPA-derived growth defects have been linked to either cytoskeletal derangement (Adamakis et al., 2013; Adamakis et al., 2016; Adamakis et al., 2018; Stavropoulou et al., 2018; Adamakis et al., 2019), hormonal imbalance (Frejd et al., 2016; Li X. et al., 2018; Bahmani et al., 2020), deterioration of the photosynthetic machinery (Jiao et al., 2017; Kim et al., 2018; Li Y. T. et al., 2018) or ROS production (Wang et al., 2015; Ali et al., 2016; Zhang et al., 2018; Xiao et al., 2019). It could therefore be concluded that BPA effects in plants are pleiotropic (Xiao et al., 2020). However, the increased demand for BPA and focus on BPA research over the past years (Shafei et al., 2018), has gathered significant amount of evidence indicating that the

induction of ROS is the start of a cascade of BPA-induced cellular effects. As such, ROS contribute significantly to BPA toxic and carcinogenic potential (Moura et al., 2010). Specifically for plants, BPA effects on photosynthesis have been linked to ROS production (Li Y. T. et al., 2018), but fascinatingly a protective role for ROS in the plant response against BPA has been also proposed (Zhang et al., 2018), a phenomenon also observed in animal models (Guo et al., 2017; Durovcova et al., 2018) under BPA exposure.

It is evident that any change or imbalance in the function of the chloroplast will affect directly or/and indirectly the other cellular functions of the plant cell (Bobik and Burch-Smith, 2015). Earlier studies have suggested that the redox state of the plastoquinone (PQ) pool initiates plant acclimation and is of unique significance for antioxidant defense and signaling (Hüner et al., 2012). Consequently, it can be hypothesized that BPA stress in plants, like in animals (Moura et al., 2010), could be initially sensed *via* ROS-production; then the associated changes in the chloroplast oxidoreduction homeostasis synergistically with other signaling pathways could induce physiological or/and molecular adaptive responses. In order to test this hypothesis and provide novel insights into mechanisms of BPA effects to plant physiological functions such as photosynthesis, we experimentally studied the effects of BPA aqueous solutions on several parameters of photosystem II (PSII) functionality in detached leaves of the model plant *Arabidopsis thaliana*. In particular, we investigated whether the BPA-induced hydrogen peroxide (H_2O_2) in combination with the H_2O_2 scavenger, N-acetylcysteine, has a positive or negative action on the selected photosynthetic parameters.

MATERIALS AND METHODS

Plant Material and Growth Conditions

Arabidopsis thaliana (L.) Heynh. (Col-0) seeds, obtained from Nottingham Arabidopsis Stock Centre (NASC), were bleach surface sterilized and after being imbibed at 4°C for 24 h were sown directly on soil. Emerged seedlings were left to grow at a $22 \pm 1^\circ\text{C}$ temperature and a 16-h/8-h light/dark cycle at $120 \mu\text{mol photons m}^{-2} \text{s}^{-1}$ light intensity and $60 \pm 5\%$ day/night humidity for 4 weeks. Rosette leaves 8 from 4-week-old plants were cut and further on processed.

BPA and NAC Treatments

Detached leaves of *A. thaliana* maintained in Petri dishes on filter paper soaked with distilled water were considered as controls. Four to five leaves per experiment were treated with aqueous 50 and 100 mg L^{-1} (0.2 and 0.4 mM) BPA solutions, prepared from a stock solution of 200 mg L^{-1} at 21.5°C , pH 7.0 (Staples et al., 1998; Adamakis et al., 2013; Adamakis et al., 2019), soaked on filter paper in Petri dishes, for 6, 12 and 24 h. Each treatment has been done in triplicate.

N-acetylcysteine (NAC) is a ROS scavenger capable of interacting with H_2O_2 (Aruoma et al., 1989; Zafarullah et al., 2003; Ezeriņa et al., 2018). We applied NAC on detached *A.*

thaliana leaves to evaluate the result of H_2O_2 scavenging in combination with BPA action. Leaves were treated with either 500 μM NAC (Muranaka et al., 2013; Livanos et al., 2016; Colak et al., 2019) or with 50 mg L^{-1} (0.2 mM) BPA plus 500 μM NAC or with 50 mg L^{-1} BPA alone for 24 h. All treatments were performed with three independent biological replicates.

Hydrogen Peroxide Imaging Detection

H_2O_2 detection in *A. thaliana* leaves was implemented as described earlier (Moustaka et al., 2015). Briefly, leaves were incubated for 30 min with 25 μM 2', 7'-dichlorofluorescein diacetate ($\text{H}_2\text{DCF-DA}$, Sigma) in 10 mM Tris-HCl (pH 7.4) in dark. The leaves were observed under a Zeiss AxioImager.Z2 fluorescence microscope at excitation and emission wavelengths of 480 and 530 nm, respectively (Moustaka et al., 2015). An AxioCam MRC 5 camera attached to the microscope captured the images. Autofluorescence signal interference was also checked (Moustaka et al., 2018). All treatments were performed with three independent biological replicates.

Chlorophyll Fluorescence Imaging Analysis

A modulated chlorophyll fluorescence system (Imaging PAM M-Series system, Heinz Walz Instruments, Effeltrich, Germany) was used to evaluate the spatiotemporal effects of BPA on PSII photochemistry. Chlorophyll fluorescence in dark-adapted (for 20 min) detached *A. thaliana* leaves was measured at room temperature as described previously (Moustaka et al., 2015). Two light intensities were used for chlorophyll fluorescence measurements, a low light intensity (140 $\mu\text{mol photons m}^{-2} \text{s}^{-1}$) that was similar to the growth light and a high light intensity (1000 $\mu\text{mol photons m}^{-2} \text{s}^{-1}$). Color-coded images are presented of dark adapted leaves of (a) the maximum photochemical efficiency (F_v/F_m), and after 5 min of illumination, (b) the effective quantum yield of PSII photochemistry (Φ_{PSII}) that estimates the efficiency by which light absorbed by PSII is used for photochemistry, (c) the quantum yield of regulated non-photochemical energy loss in PSII (Φ_{NPQ}), (d) the quantum yield of non-regulated energy loss in PSII (Φ_{NO}), and (e) the photochemical quenching (q_p), a measure of the fraction of open PSII reaction centers, that is the redox state of the plastoquinone (PQ) pool. Nine to fourteen areas of interest (AOIs) were selected in each leaf so as to have representative areas of the whole leaf.

Statistical Analyses

Statistically significant differences were evaluated for the chlorophyll fluorescence parameters of Control Whole Leaves (CWL), BPA treated Whole Leaves (BWL), Spot BPA zone (SPB), Spot Surrounding Area (SSA) and the Rest of the Leaf (RL), that is the leaf area that remains if the Spot BPA zone (SPB) and the Spot Surrounding Area (SSA) are subtracted from the BPA-treated Whole Leaves (BWL). The measured chlorophyll fluorescence parameters were analyzed by t-test at a level of $P < 0.05$ (StatView computer package, Abacus Concepts, Inc Berkley, CA, USA). Data are presented as means from three independent experiments.

RESULTS

We evaluated the effects of 50 and 100 mg L^{-1} BPA treatments for 6, 12 and 24 h on the chlorophyll fluorescence parameters F_v/F_m , Φ_{PSII} , Φ_{NPQ} , Φ_{NO} , and q_p in order to evaluate BPA effects on PSII functionality. Color-coded images after 20 min dark adaptation of F_v/F_m , and after 5 min illumination (140 $\mu\text{mol photons m}^{-2} \text{s}^{-1}$) for Φ_{PSII} , Φ_{NPQ} , Φ_{NO} , and q_p , of either control (leaves maintained in Petri dishes on soaked filter paper with distilled water) or of BPA treated leaves (maintained in Petri dishes on soaked filter paper with 50 and 100 mg L^{-1} aqueous BPA solution) for 6 h are presented in **Figure 1**. We observed a spot-like mode of action of BPA after 6 h treatment with 100 mg L^{-1} that could not be observed after 6 h treatment with 50 mg L^{-1} (**Figure 1**). However, the spot-like mode of BPA action was visible after 12 and 24 h treatment with 50 mg L^{-1} under both low light (**Figure 2**) and high light (**Figure 3**) intensities.

After 6 h treatment with 50 mg L^{-1} BPA Φ_{PSII} values of the mid vein AOIs (arrows) increased compared to their corresponding controls, while Φ_{NO} values of the mid vein AOIs decreased compared to their corresponding controls (**Figure 1**). In addition, the fraction of open PSII reaction centers (q_p) of the mid vein AOIs (arrows) increased, compared to their corresponding controls (**Figure 1**). After 6 h treatment with 100 mg L^{-1} BPA, the same pattern as 50 mg L^{-1} BPA treatment was observed for Φ_{PSII} and Φ_{NO} values but only for the lower mid vein AOI, while q_p values increased for both the mid vein AOIs (arrows) (**Figure 1**). This treatment (100 mg L^{-1} BPA, 6 h) decreased significantly F_v/F_m value of the whole leaf and mid vein AOIs (arrows) compared to the control values (**Figure 1**).

Under 12 and 24 h treatments with 50 mg L^{-1} BPA the fraction of open PSII reaction centers (q_p) of the whole leaf increased (with the exception of the spot like affected AOI) compared to control (**Figure 2**). Exposure to high light (1000 $\mu\text{mol photons m}^{-2} \text{s}^{-1}$) of *Arabidopsis* leaves resulted in increased leaf heterogeneity under non-stressed conditions of the chlorophyll fluorescence parameters Φ_{PSII} , Φ_{NPQ} , and q_p as was evidenced from the whole leaf color-coded images and the increased standard deviation (**Figure 3**). After 12 h treatment with 50 mg L^{-1} BPA, whole leaf Φ_{PSII} value under high light decreased significantly, with the spot like affected AOI to have Φ_{PSII} value 0, and all the reaction centers (q_p) closed (**Figure 3**).

The effects of BPA treatment on the allocation of the absorbed light energy in *A. thaliana* leaves are presented in **Figure 4**. We estimated the fraction of the absorbed light energy that is used for photochemistry (Φ_{PSII}) (**Figures 4A–C**), the fraction that is lost by regulated heat dissipation (Φ_{NPQ}) (**Figures 4D–F**), and the fraction of non-regulated energy loss (Φ_{NO}) (**Figures 4G–I**). These three quantum yields (Φ_{PSII} , Φ_{NPQ} , and Φ_{NO}) add up to unity. After 6 h treatment with 50 mg L^{-1} , Φ_{PSII} values of BPA-treated whole leaves (BWL) increased 6% compared to control (CWL), without any significant difference at the BPA zone (SPB) and the surrounding area (SSA) compared to CWL, but with a significant increased (7%) value at the rest of the leaf (RL) (**Figure 4A**). After 12 and 24 h treatment, Φ_{PSII} values at the spot BPA zone (SPB) decreased (64% and 86% respectively),

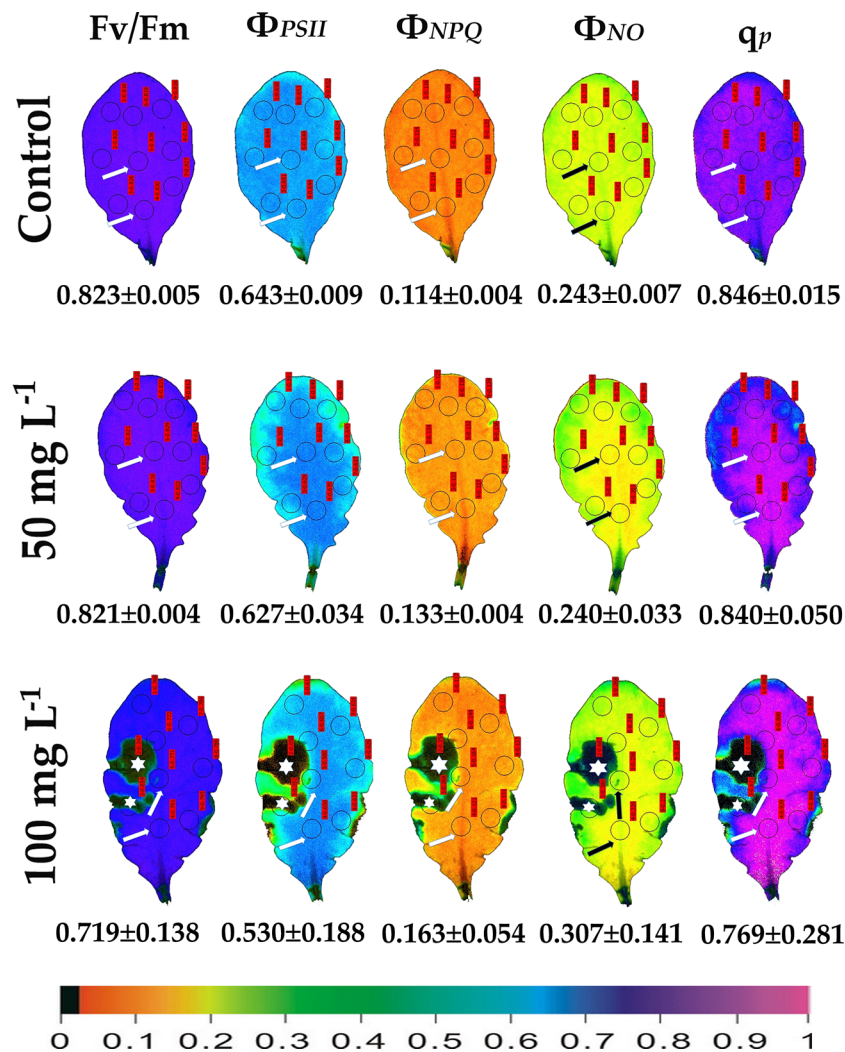


FIGURE 1 | Color-coded images of the chlorophyll fluorescence parameters Fv/Fm acquired after dark adaptation, and of Φ_{PSII} , Φ_{NPQ} , Φ_{NO} , and q_p , acquired with $140 \mu\text{mol photons m}^{-2} \text{s}^{-1}$ light intensity, after exposure to 0 (control), 50 and 100 mg L^{-1} BPA for 6 h. The color code depicted at the bottom of the images ranges from black (pixel values 0.0) to purple (1.0). Nine areas of interest (AOIs) are shown in each image together with the average value (\pm SD) of the whole leaf for each photosynthetic parameter. Arrows in the images point at the mid vein AOIs that were not affected or affected (negatively or positively) by the BPA application. Asterisks on the images note the AOIs that were negatively affected by the BPA application.

while at the rest of the leaf (RL) increased (7% and 5% respectively) compared to CWL (Figures 4B, C, respectively). Φ_{NPQ} values did not change after 6 h treatment with 50 mg L^{-1} BPA at all evaluated zones (Figure 4D), but increased significantly (114%) at the SPB after 12 h treatment (Figure 4E), while decreased significantly (21%) at the same zone after 24 h treatment compared to CWL (Figure 4F). Φ_{NO} values did not change after 6 h treatment with 50 mg L^{-1} at the spot BPA zone (SPB) compared to CWL (Figure 4G), but after 12 and 24 h treatment increased significantly (66% and 173% respectively) at the same zone compared to CWL (Figures 4H, I, respectively). At the rest of the leaf (RL) after 12 h treatment Φ_{NO} decreased (8%) (Figure 4H), while after 24 h treatment remained unchanged (Figure 4I) compared to CWL.

The maximum photochemical efficiency (Fv/Fm) was the only chlorophyll fluorescence parameter that was negatively affected in a dose- and time-dependent manner in the BPA-treated whole leaves (BWL) and not only at the spot BPA zone (SPB) (Figures 5A–C), as was observed at the other measured parameters (Figure 4). The redox state of the plastoquinone (PQ) pool (q_p), a measure of the fraction of open PSII reaction centers, increased after 6, 12 and 24 h treatment in BPA-treated whole leaves (BWL) and the rest of the leaf (RL) (Figures 5D–F).

Exposure of *A. thaliana* leaves to 50 mg L^{-1} BPA plus $500 \mu\text{M}$ NAC for 24 h eliminated whole leaf Φ_{PSII} and Φ_{NPQ} having as a consequence only Φ_{NO} to occur, and all the reaction centers to be closed (Figure 6). Exposure of leaves to $500 \mu\text{M}$ NAC alone for 24 h resulted in milder effects on chlorophyll fluorescence

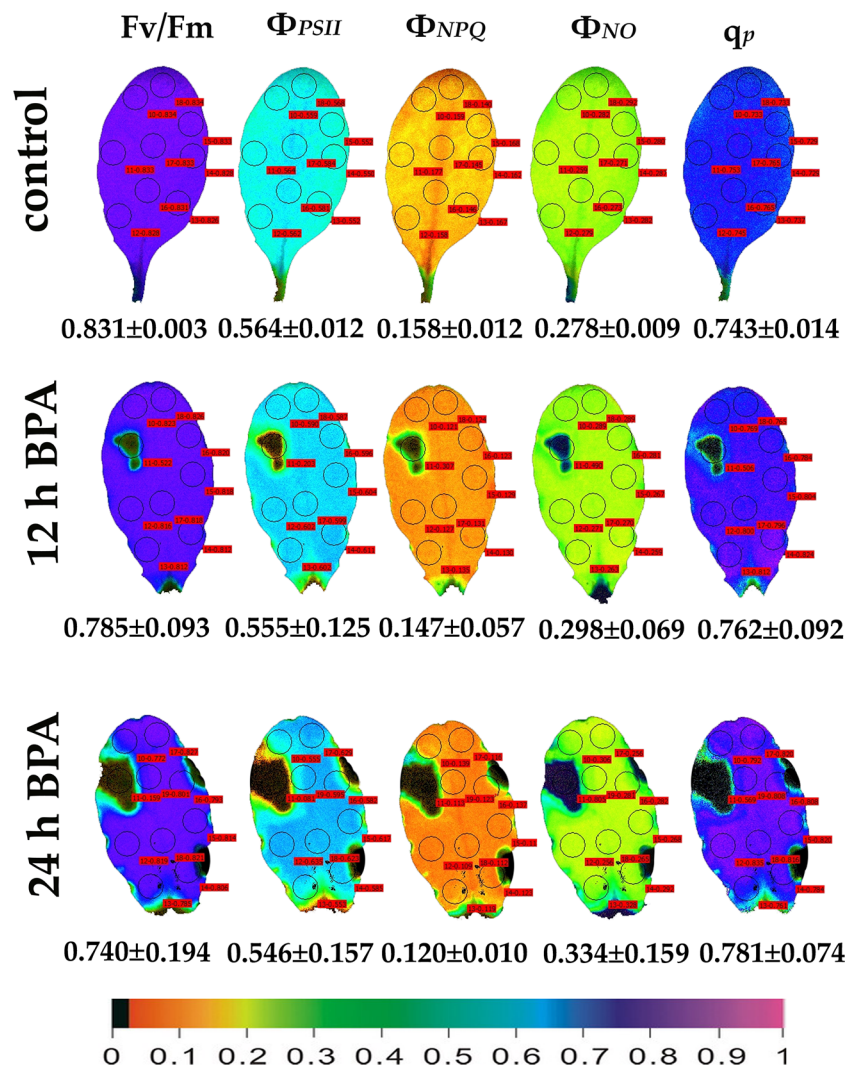


FIGURE 2 | Color-coded images of the chlorophyll fluorescence parameters Fv/Fm acquired after dark adaptation and of Φ_{PSII} , Φ_{NPQ} , Φ_{NO} , and q_p , acquired with 140 $\mu\text{mol photons m}^{-2} \text{ s}^{-1}$ light intensity, after exposure to 0 (control) and 50 mg L^{-1} BPA for 12 and 24 h. The color code depicted at the bottom of the images ranges from black (pixel values 0.0) to purple (1.0). Nine or ten AOIs are shown in each image together with the average value (\pm SD) of the whole leaf for each photosynthetic parameter.

parameters (**Figure 6**). However, a 68% reduction of the maximum photochemical efficiency (Fv/Fm), a 78% reduction in the absorbed PSII light that is used for photochemistry (Φ_{PSII}) and a 62% reduction in the photoprotective energy dissipation as heat (Φ_{NPQ}) occurred. As a result, a 2.8-fold increase in the quantum yield of non-regulated energy loss in PSII (Φ_{NO}) occurred and a 64% reduction in the fraction of open PSII reaction centers (q_p) (**Figure 6**). Twenty-four h treatment with 50 mg L^{-1} BPA alone had milder effects on chlorophyll fluorescence parameters from all the treatments (**Figure 6**).

Leaf spot BPA areas, negatively affected by BPA (asterisks in **Figure 1** and **Figures 2, 3, 6**), showed highly increased chlorophyll fluorescence heterogeneity compared to the rest leaf, with a reduced fraction of open PSII reaction centers (q_p) and an increased non-regulated energy loss (Φ_{NO}). In those

areas chlorophyll autofluorescence loss coexisted with an increased H_2O_2 production as was shown after H_2DCFDA staining (**Figures 7D–I**), a phenomenon not present in control leaves stained with H_2DCFDA (**Figures 7A–C**).

DISCUSSION

ROS production (especially H_2O_2) stimulated by BPA has been linked with the PSII photoinhibition observed under BPA treatments (Qui et al., 2013; Li Y. T. et al., 2018). BPA seems to affect the electron transport between PSII and PSI (Qiu et al., 2013), but it does not exert a direct PSII damage (Li Y. T. et al., 2018), since the block of ETR by BPA under high light is attributed to CO_2 fixation inhibition (Li Y. T. et al., 2018).

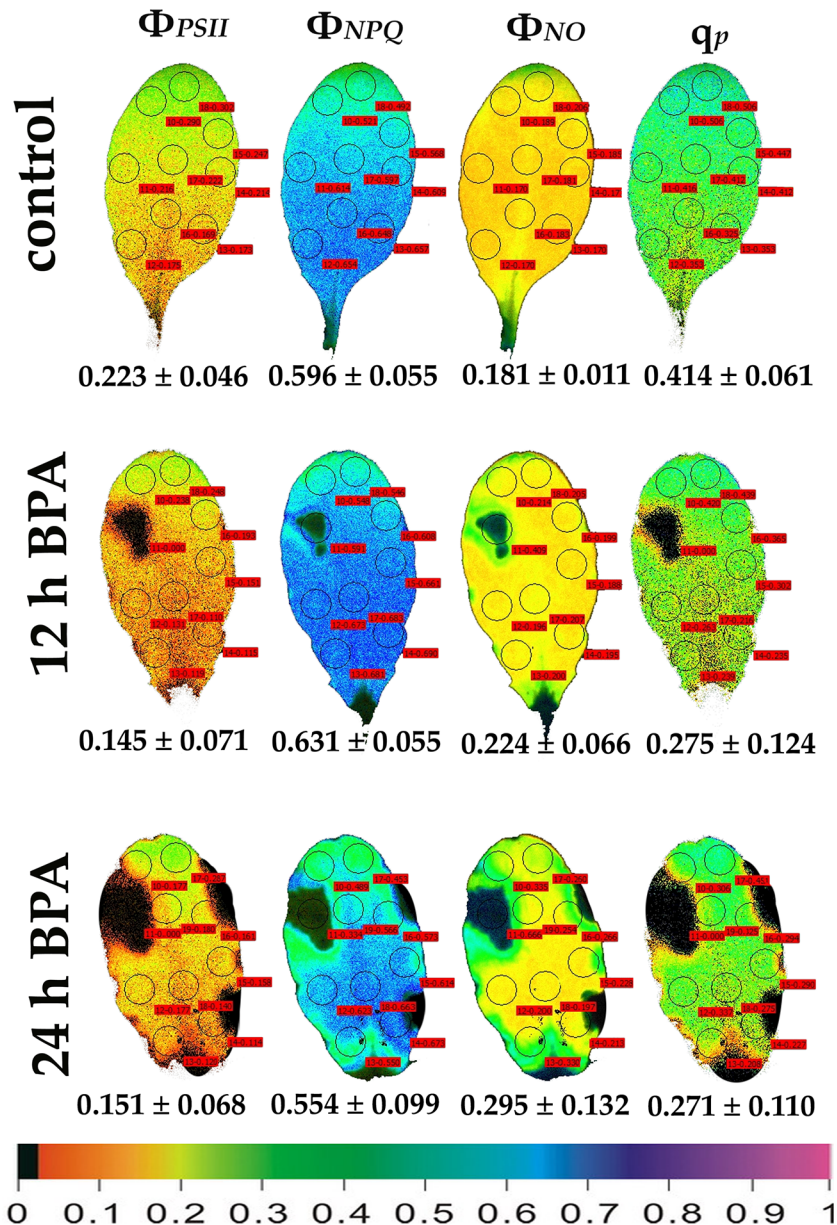


FIGURE 3 | Color-coded images of the chlorophyll fluorescence parameters Φ_{PSII} , Φ_{NPQ} , Φ_{NO} , and q_p , acquired with $1000 \mu\text{mol photons m}^{-2} \text{s}^{-1}$ light intensity, after exposure to 0 (control) and 50 mg L^{-1} BPA for 12 and 24 h. The color code depicted at the bottom of the images ranges from black (pixel values 0.0) to purple (1.0). Nine or ten AOIs are shown in each image together with the average value (\pm SD) of the whole leaf for each photosynthetic parameter.

Moreover, in soybean BPA-treated seedlings, the inhibition of growth was related to the decrease in photosynthesis due to a decrease in the content of chlorophyll, the net photosynthetic rate and changes in the chlorophyll fluorescence parameters F_v/F_m , Φ_{PSII} , and ETR that were decreased, compared to the control (Qiu et al., 2013). In the present study, under low light, PSII function was negatively influenced only at the spot affected BPA zone in a dose- and time-dependent manner, while at the whole leaf only the maximum photochemical efficiency (F_v/F_m) was negatively affected (Figures 4, 5). This BPA induced decrease in

F_v/F_m suggests photoinhibition of PSII caused by ROS through inhibition of CO_2 assimilation and over-reduction of ETR that increased ROS (H_2O_2) generation inhibiting the repair of photodamaged PSII (Li Y. T. et al., 2018). In our experiments, under high light all PSII photosynthetic parameters (Φ_{PSII} , Φ_{NPQ} , Φ_{NO} , and q_p) were negatively affected by BPA application, in a time-dependent manner (Figure 3), also in detached leaves directly exposed to BPA aqueous solutions. Increased BPA concentration (100 mg L^{-1} BPA, 6 h exposure q_p image, Figure 1) or high light exposure (50 mg L^{-1} BPA, 12 and 24 h exposure

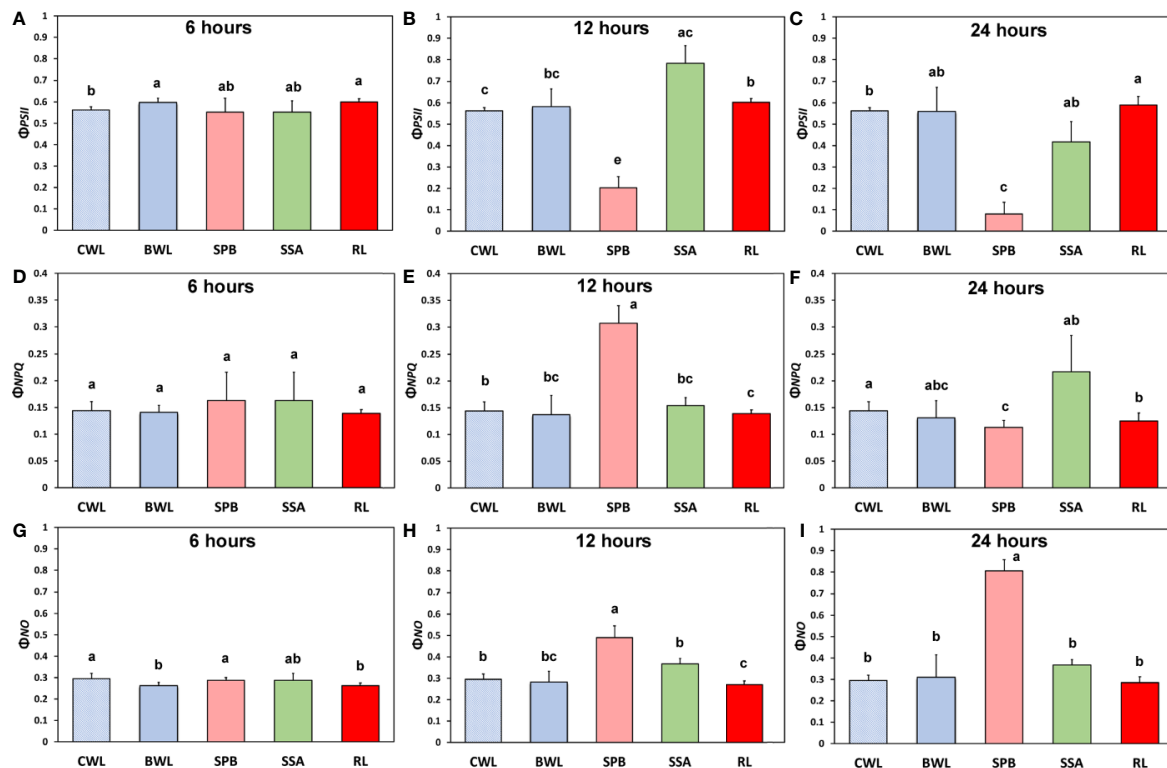


FIGURE 4 | The effects of 50 mg L⁻¹ BPA on the effective quantum yield of photochemical energy conversion in PSII (Φ_{PSII}) after 6-h (A), 12-h (B), and 24-h exposures (C); the quantum yield of regulated non-photochemical energy loss in PSII (Φ_{NPQ}) after 6 h (D), 12 h (E) and 24 h exposure (F); and the quantum yield of non-regulated energy loss in PSII (Φ_{NO}) after 6-h (G), 12-h (H), and 24-h exposures (I), all measured at 140 $\mu\text{mol photons m}^{-2} \text{s}^{-1}$ in *Arabidopsis thaliana* leaves. Symbol explanation: Control Whole Leaves (CWL) maintained in Petri dishes on filter paper soaked with distilled water and considered as controls; BPA treated whole leaves (BWL) maintained in Petri dishes on filter paper soaked with 50 mg L⁻¹ BPA; spot BPA zone (SPB) the spot like zone that was affected by BPA; spot surrounding area (SSA); Rest of the Leaf (RL), that is the leaf area that remains if the Spot BPA zone (SPB) and the spot surrounding area (SSA) are subtracted from the BPA-treated Whole Leaves (BWL). Error bars on columns are standard deviations based on three independent biological replicates under all treatments. Columns under the same time treatment with the same letter are statistically not different ($P < 0.05$).

q_p images, **Figure 3**) resulted to necrotic death-like spots in leaves, probably caused by increased H₂O₂ accumulation visible in a spot-like manner (**Figure 7**).

Using the H₂DCFDA staining we observed an increased H₂O₂ accumulation, in spots in the leaf periphery (**Figure 7**) under BPA treatments. BPA-induced H₂O₂, could be a toxic ROS able to cause damage to a variety of cellular structures but in parallel can act as a potent signaling molecule involved in BPA stress response, as it has been demonstrated in a plethora of physiological functions (Foyer and Shigeoka, 2011; Petrov and Breusegem, 2012; Foyer and Noctor, 2013; Moustaka et al., 2015; Moustakas et al., 2016). H₂O₂ enters the cell through aquaporins and regulates physiological and cellular processes (Foyer, 2020; Wu et al., 2020). Still, H₂O₂ can diffuse through leaf veins to act as a long-distance regulator molecule activating the antioxidant defense during stress in plants (Wilson et al., 2006; Mittler et al., 2011; Petrov and Breusegem, 2012; Moustaka et al., 2015; Moustakas et al., 2017; Antonoglou et al., 2018; Spirdouli et al., 2019). Since H₂O₂ travels through veins faster than from cell to cell, it seems logic why at 6 h treatments with 50 and 100

mg L⁻¹ BPA the fraction of open PSII reaction centers (q_p) of the mid veins AOIs (arrows) were those areas that increased first, compared to their corresponding controls (**Figure 1**), while just at longer treatments (12 and 24 h with 50 mg L⁻¹ BPA) whole leaf q_p values increased (with the exception of the spot like affected AOIs) compared to controls (**Figure 2**). However, the exposure of *A. thaliana* leaves to high light and 50 mg L⁻¹ BPA (12 and 24 h treatment) (**Figure 3**) decreased the effective quantum yield of PSII (Φ_{PSII}) and over-reduced the redox state of PQ pool closing a fraction of open PSII reaction centers (q_p) (Murabakshina et al., 2010; Foyer and Shigeoka, 2011; Mignolet-Spuyt et al., 2016; Moustaka et al., 2018). In agreement to our results, Li et al. (2018b) have noticed that, under high light the BPA treatment changed similarly Φ_{PSII} and q_p , and concluded that the decrease in Φ_{PSII} was mainly due to the decline in q_p rather than to the decrease in the efficiency of open PSII centers to utilize the absorbed light (Fv/Fm).

The spatiotemporal pattern of BPA effects on *A. thaliana* treated leaves points out to the differential defense response of each cell to BPA stress as it has been shown for other abiotic

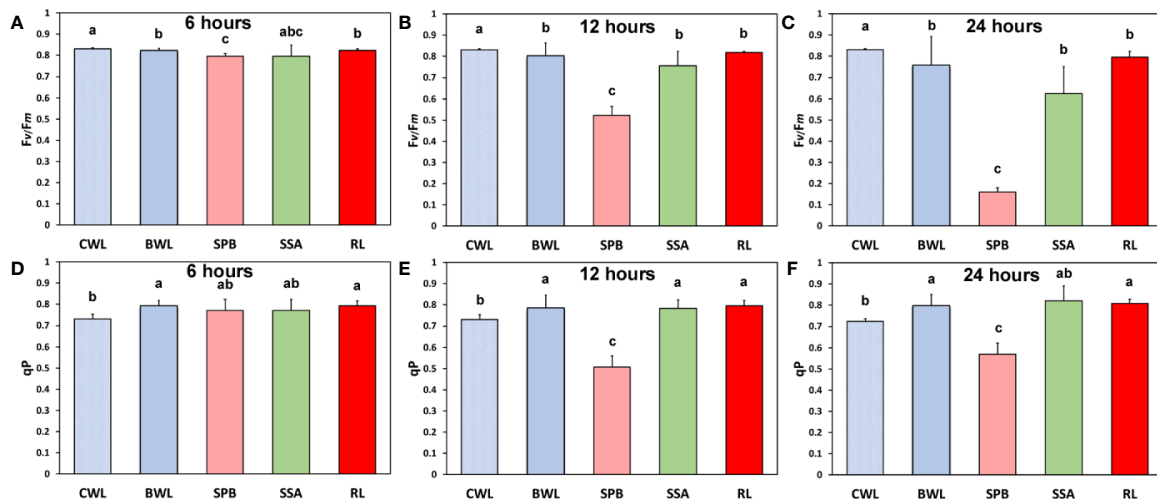


FIGURE 5 | The effects of 50 mg L⁻¹ BPA on the maximum photochemical efficiency (Fv/Fm) after 6-h (A), 12-h (B), and 24-h exposure (C), and the redox state of the plastoquinone (PQ) pool (qp), a measure of the fraction of open PSII reaction centers after 6-h (D), 12-h (E), and 24-h exposures (F), all measured at 140 μmol photons m⁻² s⁻¹ in *Arabidopsis thaliana* leaves. Symbol explanation: control whole leaves (CWL) maintained in Petri dishes on filter paper soaked with distilled water and considered as controls; BPA-treated whole leaves (BWL) maintained in Petri dishes on filter paper soaked with 50 mg L⁻¹ BPA; spot BPA zone (SPB) the spot like zone that was affected by BPA; spot surrounding area (SSA); rest of the leaf (RL), that is the leaf area that remains if the spot BPA zone (SPB) and the spot surrounding area (SSA) are subtracted from the BPA-treated whole leaves (BWL). Error bars on columns are standard deviations based on three independent biological replicates under all treatments. Columns under the same time treatment with the same letter are statistically not different ($P < 0.05$).

stress factors, e.g., drought (Sperdouli and Moustakas, 2012), hypoxia (Stasolla et al., 2019), paraquat (Moustakas et al., 2016), and heavy metals as Zn (Moustakas et al., 2019a), or Cd (Moustakas et al., 2019b). This can be due to the fact that plant cells have to defend themselves independently since they lack specialized cells and effective plant defense strongly relies in each single cell (Ruano and Scheuring, 2020).

In an earlier study, BPA residual concentrations had a negative correlation with H₂O₂ levels, i.e., an increase in H₂O₂ seemed to reduce BPA levels inside the plant tissue (Zhang et al., 2018). These results allowed to speculate that BPA could either be a direct target of ROS, and therefore subjected to oxidation (Reis et al., 2014) or ROS molecules could activate a cascade of secondary metabolic reactions degrading BPA (Noureddin et al., 2004) and finally the ROS-activated antioxidant enzymes could destroy BPA (Kang and Kondo, 2006). So in soybean roots, H₂O₂ initiated accumulation offered a protection against BPA (Zhang et al., 2018). Likewise, in our experimental system if BPA-induced H₂O₂ accumulation (Figure 7) is hindered, with NAC application (Figure 6), leaf photosynthesis is utterly being interrupted ($\Phi_{NO}=1$; Figure 6). Therefore, this H₂O₂ production could be necessary for promoting signaling events that could assist the plant to alleviate BPA-stress. NAC is a strong ROS scavenger (Zafarullah et al., 2003) since the SH group of NAC is able to donate an H-atom or an electron. Numerous researchers have used it as a mean to reduce either the stress-induced or naturally occurring H₂O₂ (Livanos et al., 2012; Muranaka et al., 2013; Sun et al., 2014; Livanos et al., 2016; Adamakis and Eleftheriou, 2019; Colak et al., 2019). Generally, NAC is being considered not toxic for plants and the environment even when

applied in high concentrations for large periods of time (i.e., Sun et al., 2014), able to alleviate oxidative stress induced by several stressors, e.g., heavy metals (Sun et al., 2014; Colak et al., 2019). However, when used to diminish naturally occurring ROS several cellular defects have been noticed. For instance, when NAC was applied in wheat or *A. thaliana* roots, microtubule organization was affected (Livanos et al., 2012) while cytokinesis failed to be accomplished (Livanos et al., 2016). The above indicated that ROS is an important factor enrolled in the microtubule assembly and cell division completion (Livanos et al., 2012; Livanos et al., 2016). Expanding the beneficial role of both naturally occurring and BPA-induced H₂O₂, we here noticed that ROS seem to have also pivotal role in the light reactions of photosynthesis. This comes as no surprise since the electron transport between PSII and PSI is a major source of ROS, which are considered more as signaling molecules rather than damaging ones (Hajiboland, 2014; Foyer et al., 2017). The role of chloroplast antioxidants, that often have overlying or interrelating functions, is not to totally eliminate O₂^{•-}, H₂O₂ and ¹O₂, but rather to achieve an appropriate balance between production and subtraction so that to match with the operation of photosynthesis and permit an efficient spread of signals to the nucleus (Foyer, 2018). When NAC diminished these naturally occurring ROS (Figure 6), all of the PSII photosynthetic parameters (Φ_{PSII} , Φ_{NPQ} , Φ_{NO} , and q_p) were severely affected, indicating the importance of naturally occurring ROS in PSII photochemistry. Now it is well established that ROS are a necessary part of subcellular and intercellular communication in plants and that some of their signaling functions require ROS-metabolizing systems (Noctor et al., 2018).

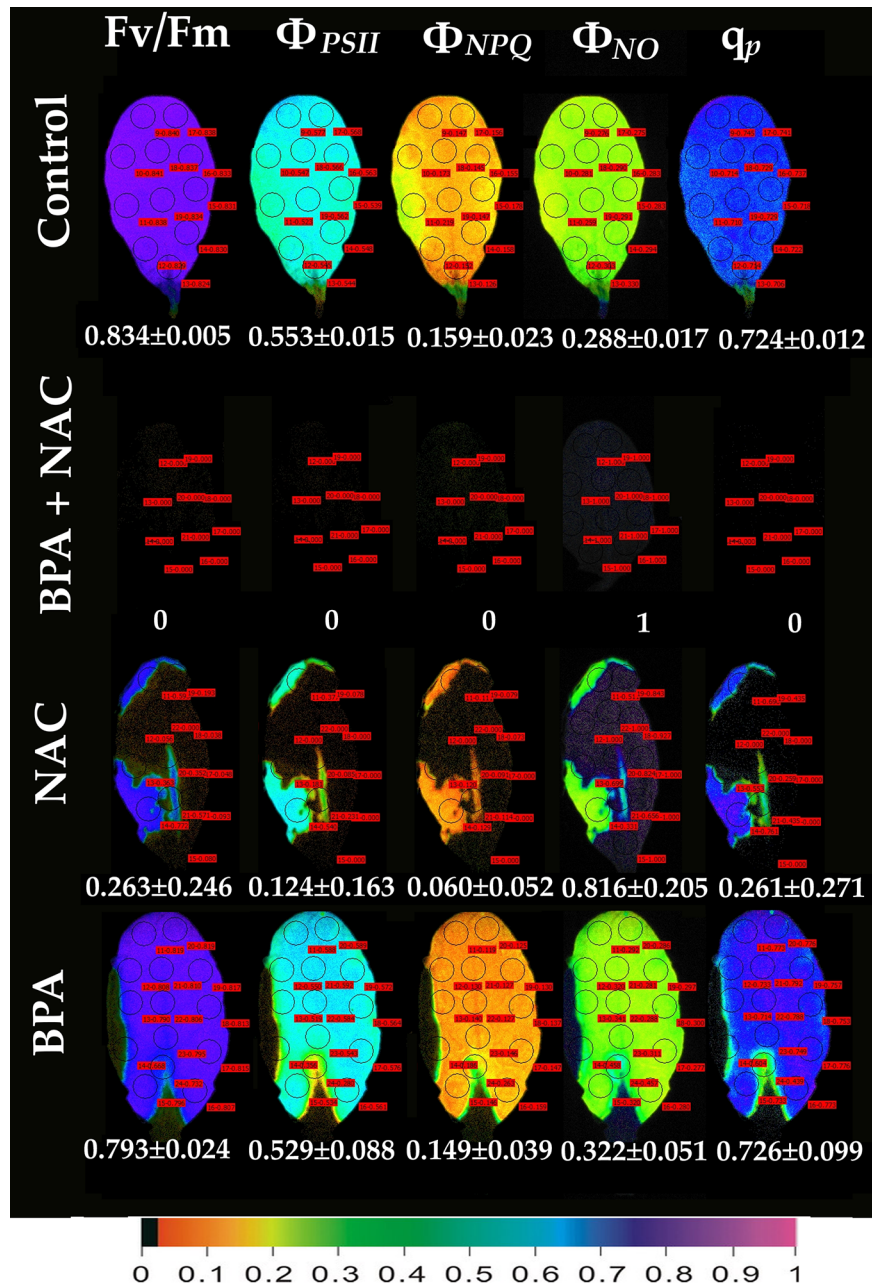


FIGURE 6 | Color-coded images of the chlorophyll fluorescence parameters F_v/F_m , Φ_{PSII} , Φ_{NPQ} , Φ_{NO} , and q_p , after exposure of *Arabidopsis thaliana* leaves to 0 (control), or 50 mg L⁻¹ BPA plus 500 μM NAC, or 500 μM NAC alone, or only 50 mg L⁻¹ BPA, for 24 h. The color code depicted at the bottom of the images ranges from black (pixel values 0.0) to purple (1.0). Ten to fourteen AOIs are shown in each image together with the average value (± SD) of the whole leaf for each photosynthetic parameter.

Our results confirm the view that ROS-removing systems are considering ROS as beneficial molecules that regulate damaging ROS below dangerous levels (Noctor et al., 2018). So, one can easily conclude, that ROS seem to play a pivotal role in plant response against BPA toxicity (Zhang et al., 2018), as we observed in BPA-affected leaves of *A. thaliana*. While the

concept that animal and plant cells need to remove ROS production to avoid extreme and permanent oxidation was the dominant view in the literature, the opinion is now shifting towards recognition of a positive role of ROS as well (Noctor and Foyer, 2016; Foyer et al., 2017). ROS generation can activate the plant's defense mechanisms in order to cope with the oxidative

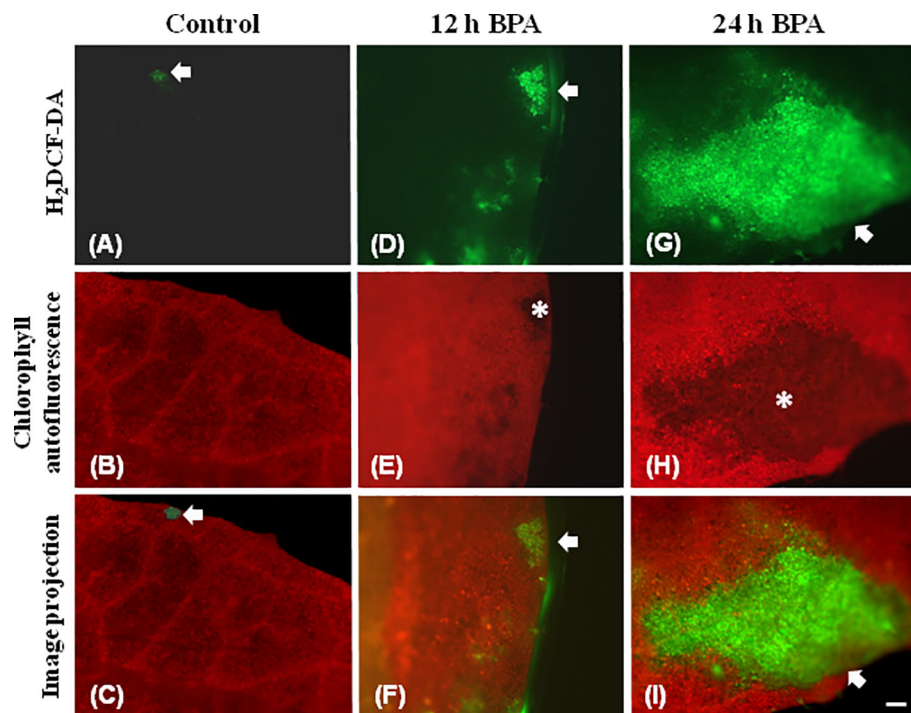


FIGURE 7 | Chlorophyll autofluorescence images (red) and after H₂DCF-DA staining, indicating H₂O₂ production (green) in untreated leaves (control) (A–C), 12 h (D–F), and 24 h (G–I) exposure to 50 mg L^{−1} BPA. In untreated leaves (A–C) very weak H₂DCF-DA staining was detected (A, C, arrows), while leaf margin areas exhibited strong chlorophyll autofluorescence (B). BPA-treated leaves exhibit reduced chlorophyll autofluorescence areas (E, H, asterisks) that coincide with time-dependent increased production of H₂O₂ (arrows in D, F, G, I). Bar, 100 μm.

stress damage and are essential for redox sensing, signaling and regulation (Petrov et al., 2015; Foyer, 2018; Malea et al., 2019). Plants have developed during the course of evolution numerous ROS-generating pathways tightly accomplishing plant function and development (Noctor et al., 2018). Therefore, the necrotic death-like spots under BPA exposure could be due to ROS accumulation, but H₂O₂ production has dual function in plants playing also a protective role in BPA-induced stress. A crucial ROS role in the photochemical reactions of photosynthesis is further on confirmed.

DATA AVAILABILITY STATEMENT

All datasets presented in this study are included in the article/supplementary material.

REFERENCES

- Abraham, A., and Chakraborty, P. (2019). A review on sources and health impacts of bisphenol A. *Rev. Environ. Health* 35, 201–210. doi: 10.1515/reveh-2019-0034 eISSN 2191-0308, ISSN 0048-7554.
- Adamakis, I.-D. S., and Eleftheriou, E. P. (2019). Structural evidence of programmed cell death induction by tungsten in root tip cells of *Pisum sativum*. *Plants* 8, 62. doi: 10.3390/plants8030062
- Adamakis, I. D. S., Panteris, E., Cherianidou, A., and Eleftheriou, E. P. (2013). Effects of bisphenol A on the microtubule arrays in root meristematic cells of

AUTHOR CONTRIBUTIONS

I-DA and MM conceived and designed the experiments, I-DA and IS performed the experiments, I-DA, EE, and MM wrote the original draft of the manuscript. All authors contributed to the article and approved the submitted version.

ACKNOWLEDGMENTS

The authors would like to thank Emmanuel Panteris (Department of Botany, School of Biology, Aristotle University of Thessaloniki) for critical reading of the manuscript. The authors would also like to express our thanks to the reviewers whose constructive suggestions helped us to improve substantially our research work.

Pisum sativum L. *Mutat. Res. Genet. Toxicol. Environ. Mutagen.* 750, 111–120. doi: 10.1016/j.mrgentox.2012.10.012

Adamakis, I. D. S., Panteris, E., and Eleftheriou, E. P. (2016). Bisphenol A disrupts microtubules and induces multipolar spindles in dividing root tip cells of the gymnosperm *Abies cephalonica*. *Chemosphere* 149, 202–210. doi: 10.1016/j.chemosphere.2016.01.082

Adamakis, I.-D. S., Malea, P., and Panteris, E. (2018). The effects of Bisphenol A on the seagrass *Cymodocea nodosa*: Leaf elongation impairment and cytoskeleton disturbance. *Ecotoxicol. Environ. Saf.* 157, 431–440. doi: 10.1016/j.ecoenv.2018.04.005

- Adamakis, I. D. S., Panteris, E., and Eleftheriou, E. P. (2019). Tubulin acetylation mediates bisphenol A effects on the microtubule arrays of *Allium cepa* and *Triticum turgidum*. *Biomolecules* 9, 1–15. doi: 10.3390/biom9050185
- Ali, I., Liu, B., Farooq, M. A., Islam, F., Azizullah, A., Yu, C., et al. (2016). Toxicological effects of bisphenol A on growth and antioxidant defense system in *Oryza sativa* as revealed by ultrastructure analysis. *Ecotoxicol. Environ. Saf.* 124, 277–284. doi: 10.1016/j.ecoenv.2015.10.027
- Ali, I., Jan, M., Wakeel, A., Azizullah, A., Liu, B., Islam, F., et al. (2017). Biochemical responses and ultrastructural changes in ethylene insensitive mutants of *Arabidopsis thaliana* subjected to bisphenol A exposure. *Ecotoxicol. Environ. Saf.* 144, 62–71. doi: 10.1016/j.ecoenv.2017.06.015
- Antonoglou, O., Moustaka, J., Adamakis, I. D., Sperdoui, I., Pantazaki, A., Moustakas, M., et al. (2018). Nanobass CuZn nanoparticles as foliar spray non phytotoxic fungicides. *ACS Appl. Mater. Interf.* 10, 4450–4461. doi: 10.1021/acsami.7b17017
- Aruoma, O. I., Halliwell, B., Hoey, B. M., and Butler, J. (1989). The antioxidant action of N-acetylcysteine: Its reaction with hydrogen peroxide, hydroxyl radical, superoxide, and hypochlorous acid. *Free Radic. Biol. Med.* 6, 593–597. doi: 10.1016/0891-5849(89)90066-X
- Awasthi, R., Bhandari, K., and Nayyar, H. (2015). Temperature stress and redox homeostasis in agricultural crops. *Front. Environ. Sci.* 3, 11. doi: 10.3389/fenvs.2015.00011
- Bahmani, R., Kim, D. G., Modareszadeh, M., Thompson, A. J., Park, J. H., Yoo, H. H., et al. (2020). The mechanism of root growth inhibition by the endocrine disruptor bisphenol A (BPA). *Environ. Pollut.* 257, 113516. doi: 10.1016/j.envpol.2019.113516
- Bobik, K., and Burch-Smith, T. M. (2015). Chloroplast signaling within, between and beyond cells. *Front. Plant Sci.* 6, 1–26. doi: 10.3389/fpls.2015.00781
- Christou, A., Michael, C., Fatta-Kassinos, D., and Fotopoulos, V. (2018). Can the pharmaceutically active compounds released in agroecosystems be considered as emerging plant stressors? *Environ. Int.* 114, 360–364. doi: 10.1016/j.envint.2018.03.003
- Colak, N., Torun, H., Gruz, J., Strnad, M., and Ayaz, F. A. (2019). Exogenous N-Acetylcysteine alleviates heavy metal stress by promoting phenolic acids to support antioxidant defence systems in wheat roots. *Ecotoxicol. Environ. Saf.* 181, 49–59. doi: 10.1016/j.ecoenv.2019.05.052
- Durovcova, I., Spackova, J., Puskar, M., Galova, E., and Sevcovicova, A. (2018). Bisphenol A as an environmental pollutant with dual genotoxic and DNA-protective effects. *Neuroendocrinol. Lett.* 39 (4), 294–298.
- Eleftheriou, E. P., Adamakis, I. D. S., Panteris, E., and Fatsiou, M. (2015). Chromium-induced ultrastructural changes and oxidative stress in roots of *Arabidopsis thaliana*. *Int. J. Mol. Sci.* 16, 15852–15871. doi: 10.3390/ijms160715852
- Ezerina, D., Takano, Y., Hanaoka, K., Urano, Y., and Dick, T. P. (2018). N-acetyl cysteine functions as a fast-acting antioxidant by triggering intracellular H₂S and sulfane sulfur production. *Cell Chem. Biol.* 25, 447–459.e4. doi: 10.1016/j.chembiol.2018.01.011
- Foyer, C. H., and Noctor, G. (2013). Redox signaling in plants. *Antioxid. Redox Signal.* 18, 2087–2090. doi: 10.1089/ars.2013.5278
- Foyer, C. H., and Shigeoka, S. (2011). Understanding oxidative stress and antioxidant functions to enhance photosynthesis. *Plant Physiol.* 155, 93–100. doi: 10.1104/pp.110.166181
- Foyer, C. H., Ruban, A. V., and Noctor, G. (2017). Viewing oxidative stress through the lens of oxidative signalling rather than damage. *Biochem. J.* 474, 877–883. doi: 10.1042/BCJ20160814
- Foyer, C. H. (2018). Reactive oxygen species, oxidative signaling and the regulation of photosynthesis. *Environ. Exp. Bot.* 154, 134–142. doi: 10.1016/j.envexpbot.2018.05.003
- Foyer, C. H. (2020). Making sense of hydrogen peroxide signals. *Nature* 578, 518–519. doi: 10.1038/d41586-020-00403-y
- Frejd, D., Dunaway, K., Hill, J., Van Maanen, J., and Carlson, C. (2016). The genomic and morphological effects of bisphenol A on *Arabidopsis thaliana*. *PLoS One* 11, 1–10. doi: 10.1371/journal.pone.0163028
- Garg, N., and Manchanda, G. (2009). ROS generation in plants: Boon or bane? *Plant Biosyst.* 143, 81–96. doi: 10.1080/11263500802633626
- Guo, J., Zhao, M. H., Shin, K. T., Niu, Y. J., Ahn, Y. D., Kim, N. H., et al. (2017). The possible molecular mechanisms of bisphenol A action on porcine early embryonic development. *Sci. Rep.* 7, 1–9. doi: 10.1038/s41598-017-09282-2
- Hajiboland, R. (2014). “Reactive oxygen species and photosynthesis,” in *Oxidative Damage to Plants. Antioxidant Networks and Signaling*. Ed. P. Ahmad (San Diego, CA, USA: Academic Press), 1–63.
- Huang, H., Ullah, F., Zhou, D. X., Yi, M., and Zhao, Y. (2019). Mechanisms of ROS regulation of plant development and stress responses. *Front. Plant Sci.* 10, 1–10. doi: 10.3389/fpls.2019.00800
- Hüner, N. P. A., Bode, R., Dahal, K., Hollis, L., Rosso, D., Krol, M., et al. (2012). Chloroplast redox imbalance governs phenotypic plasticity: the “grand design of photosynthesis” revisited. *Front. Plant Sci.* 3, 255. doi: 10.3389/fpls.2012.00255
- Jalal, N., Surendranath, A. R., Pathak, J. L., Yu, S., and Chung, C. Y. (2018). Bisphenol A (BPA) the mighty and the mutagenic. *Toxicol. Rep.* 5, 76–84. doi: 10.1016/j.toxrep.2017.12.013
- Jiao, L., Ding, H., Wang, L., Zhou, Q., and Huang, X. (2017). Bisphenol A effects on the chlorophyll contents in soybean at different growth stages. *Environ. Pollut.* 223, 426–434. doi: 10.1016/j.envpol.2017.01.042
- Kang, J. H., and Kondo, F. (2006). Distribution and biodegradation of bisphenol A in water hyacinth. *Bull. Environ. Contam. Toxicol.* 77, 500–507. doi: 10.1007/s00128-006-1092-x
- Kim, D., Kwak, J. I., and An, Y. J. (2018). Effects of bisphenol A in soil on growth, photosynthesis activity, and genistein levels in crop plants (*Vigna radiata*). *Chemosphere* 209, 875–882. doi: 10.1016/j.chemosphere.2018.06.146
- Laxa, M., Liebthal, M., Telman, W., Chibani, K., and Dietz, K. J. (2019). The role of the plant antioxidant system in drought tolerance. *Antioxidants* 8, 94. doi: 10.3390/antiox8040094
- Li, X., Wang, L., Wang, S., Yang, Q., Zhou, Q., and Huang, X. (2018). A preliminary analysis of the effects of bisphenol A on the plant root growth via changes in endogenous plant hormones. *Ecotoxicol. Environ. Saf.* 150, 152–158. doi: 10.1016/j.ecoenv.2017.12.031
- Li, Y. T., Liang, Y., Li, Y. N., Che, X. K., Zhao, S. J., Zhang, Z. S., et al. (2018). Mechanisms by which Bisphenol A affect the photosynthetic apparatus in cucumber (*Cucumis sativus* L.) leaves. *Sci. Rep.* 8, 4253. doi: 10.1038/s41598-018-22486-4
- Lin, Z., Wang, L., Jia, Y., Zhang, Y., Dong, Q., and Huang, C. (2017). A Study on environmental bisphenol A pollution in plastics industry areas. *Water Air Soil Pollut.* 228, 98. doi: 10.1007/s11270-017-3277-9
- Livanos, P., Galatis, B., Quader, H., and Apostolakis, P. (2012). Disturbance of reactive oxygen species homeostasis induces atypical tubulin polymer formation and affects mitosis in root-tip cells of *Triticum turgidum* and *Arabidopsis thaliana*. *Cytoskeleton* 69, 1–21. doi: 10.1002/cm.20538
- Livanos, P., Galatis, B., and Apostolakis, P. (2016). Deliberate ROS production and auxin synergistically trigger the asymmetrical division generating the subsidiary cells in *Zea mays* stomatal complexes. *Protoplasma* 253, 1081–1099. doi: 10.1007/s00709-015-0866-6
- Malea, P., Charitonidou, K., Sperdoui, I., Mylona, Z., and Moustakas, M. (2019). Zinc uptake, photosynthetic efficiency and oxidative stress in the seagrass *Cymodocea nodosa* exposed to ZnO nanoparticles. *Materials* 12, 2101. doi: 10.3390/ma12132101
- Malea, P., Kokkinidi, D., Kevrekidou, A., and Adamakis, I. D. S. (2020). Environmentally relevant bisphenol A concentrations effects on the seagrass *Cymodocea nodosa* different parts elongation: perceptive assessors of toxicity. *Environ. Sci. Pollut. Res.* 27, 267–279. doi: 10.1007/s11356-019-07443-6
- Mignolet-Spruyt, L., Xu, E., Idänheimo, N., Hoeberichts, F. A., Mhlenbock, P., Brosché, M., et al. (2016). Spreading the news: subcellular and organellar reactive oxygen species production and signaling. *J. Exp. Bot.* 67, 3831–3844. doi: 10.1093/jxb/erw080
- Mittler, R., Vanderauwera, S., Suzuki, N., Miller, G., Tognetti, V. B., Vandepoele, K., et al. (2011). ROS signaling: the new wave? *Trends Plant Sci.* 16, 300–309. doi: 10.1016/j.tplants.2011.03.007
- Moura, M., De, dos Santos, L. S., and Van Houten, B. (2010). Mitochondrial dysfunction in neurodegenerative diseases and cancer. *Environ. Mol. Mutagen.* 405, 391–405. doi: 10.1002/em.20575
- Moustaka, J., Tanou, G., Adamakis, I. D., Eleftheriou, E. P., and Moustakas, M. (2015). Leaf age dependent photoprotective and antioxidative mechanisms to paraquat-induced oxidative stress in *Arabidopsis thaliana*. *Int. J. Mol. Sci.* 16, 13989–14006. doi: 10.3390/ijms160613989
- Moustaka, J., Panteris, E., Adamakis, I. D. S., Tanou, G., Giannakoula, A., Eleftheriou, E. P., et al. (2018). High anthocyanin accumulation in poinsettia

- leaves is accompanied by thylakoid membrane unstacking, acting as a photoprotective mechanism, to prevent ROS formation. *Environ. Exp. Bot.* 154, 44–55. doi: 10.1016/j.envexpbot.2018.01.006
- Moustakas, M., Malea, P., Zafeirakoglou, A., and Sperdouli, I. (2016). Photochemical changes and oxidative damage in the aquatic macrophyte *Cymodocea nodosa* exposed to paraquat-induced oxidative stress. *Pest. Biochem. Physiol.* 126, 28–34. doi: 10.1016/j.pestbp.2015.07.003
- Moustakas, M., Malea, P., Haritonidou, K., and Sperdouli, I. (2017). Copper bioaccumulation, photosystem II functioning and oxidative stress in the seagrass *Cymodocea nodosa* exposed to copper oxide nanoparticles. *Environ. Sci. Pollut. Res.* 24, 16007–16018. doi: 10.1007/s11356-017-9174-3
- Moustakas, M., Bayçu, G., Gevrek-Kürtüm, N., Moustaka, J., Csáti, I., and Rognes, S. E. (2019a). Spatiotemporal heterogeneity of photosystem II function during acclimation to zinc exposure and mineral nutrition changes in the hyperaccumulator *Noccaea caerulea*. *Environ. Sci. Pollut. Res.* 26, 6613–6624. doi: 10.1007/s11356-019-04126-0
- Moustakas, M., Hanć, A., Dobrikova, A., Sperdouli, I., Adamakis, I. D. S., and Apostolova, E. (2019b). Spatial heterogeneity of cadmium effects on *Salvia sclarea* leaves revealed by chlorophyll fluorescence imaging analysis and laser ablation inductively coupled plasma mass spectrometry. *Materials* 12, 2953. doi: 10.3390/ma12182953
- Mubarakshina, M. M., Ivanov, B. N., Naydov, I. A., Hillier, W., Badger, M. R., and Krieger-Liszka, A. (2010). Production and diffusion of chloroplastic H₂O₂ and its implication to signalling. *J. Exp. Bot.* 61, 3577–3587. doi: 10.1093/jxb/erq171
- Muranaka, L. S., Giorgiano, T. E., Takita, M. A., Forim, M. R., Silva, L. F. C., Coletta-Filho, H. D., et al. (2013). N-Acetylcysteine in agriculture, a novel use for an old molecule: focus on controlling the plant–pathogen. *Xylella fastidiosa*. *PLoS One* 8, e72937. doi: 10.1371/journal.pone.0072937
- Noctor, G., and Foyer, C. H. (2016). Intracellular redox compartmentation and ROS-related communication in regulation and signaling. *Plant Physiol.* 171, 1581–1592. doi: 10.1104/pp.16.00346
- Noctor, G., Reichheld, J. P., and Foyer, C. H. (2018). ROS-related redox regulation and signaling in plants. *Semin. Cell Dev. Biol.* 80, 3–12. doi: 10.1016/j.semcdb.2017.07.013
- Noureddin, M. I., Furumoto, T., Ishida, Y., and Fukui, H. (2004). Absorption and metabolism of bisphenol A, a possible endocrine disruptor, in the aquatic edible plant, water convolvulus (*Ipomoea aquatica*). *Biosci. Biotechnol. Biochem.* 68, 1398–1402. doi: 10.1271/bbb.68.1398
- Pan, W. J., Xiong, C., Wu, Q. P., Liu, J. X., Liao, H. M., Chen, W., et al. (2013). Effect of BPA on the germination, root development, seedling growth and leaf differentiation under different light conditions in *Arabidopsis thaliana*. *Chemosphere* 93, 2585–2592. doi: 10.1016/j.chemosphere.2013.09.081
- Petrov, V. D., and Van Breusegem, F. (2012). Hydrogen peroxide—a central hub for information flow in plant cells. *AoB Plants* 2012, pls014. doi: 10.1093/aobpla/pls014
- Petrov, V., Hille, J., Mueller-Roeber, B., and Gechev, T. S. (2015). ROS-mediated abiotic stress-induced programmed cell death in plants. *Front. Plant Sci.* 6, 69. doi: 10.3389/fpls.2015.00069
- Potters, G., Horemans, N., and Jansen, M. A. K. (2010). The cellular redox state in plant stress biology - A charging concept. *Plant Physiol. Biochem.* 48, 292–300. doi: 10.1016/j.plaphy.2009.12.007
- Qiu, Z., Wang, L., and Zhou, Q. (2013). Effects of bisphenol A on growth, photosynthesis and chlorophyll fluorescence in above-ground organs of soybean seedlings. *Chemosphere* 90, 1274–1280. doi: 10.1016/j.chemosphere.2012.09.085
- Rapala, M., Pluciński, B., and Jedynak, P. (2017). The effect of bisphenol A on growth, pigment composition and photosystem II activity of *Arabidopsis thaliana*. *Acta Biochim. Pol.* 64, 407–413. doi: 10.18388/abp.2017_1626
- Reis, A. R., Tabai, K., and Sakakibara, Y. (2014). Oxidation mechanism and overall removal rates of endocrine disrupting chemicals by aquatic plants. *J. Hazard Mater.* 265, 79–88. doi: 10.1016/j.jhazmat.2013.11.042
- Ruano, G., and Scheuring, D. (2020). Plant cells under attack: Unconventional endomembrane trafficking during plant defense. *Plants* 9, 389. doi: 10.3390/plants9030389
- Shafei, A., Ramzy, M. M., Hegazy, A. I., Husseny, A. K., EL-hadary, U. G., Taha, M. M., et al. (2018). The molecular mechanisms of action of the endocrine disrupting chemical bisphenol A in the development of cancer. *Gene* 647, 235–243. doi: 10.1016/j.gene.2018.01.016
- Sperdouli, I., and Moustakas, M. (2012). Spatio-temporal heterogeneity in *Arabidopsis thaliana* leaves under drought stress. *Plant Biol.* 14, 118–128. doi: 10.1111/j.1438-8677.2011.00473.x
- Sperdouli, I., Moustaka, J., Antonoglou, O., Adamakis, I.-D. S., Dendrinou-Samara, C., and Moustakas, M. (2019). Leaf age-dependent effects of foliar-sprayed CuZn nanoparticles on photosynthetic efficiency and ROS generation in *Arabidopsis thaliana*. *Mater. (Basel)* 12, 2498. doi: 10.3390/ma12152498
- Staples, C. A., Dorn, P. B., Klečka, G. M., O'Block, S. T., and Harris, L. R. (1998). A review of the environmental fate, effects and exposures of bisphenol A. *Chemosphere* 36, 2149–2173. doi: 10.1016/S0045-6535(97)10133-3
- Staples, C., Friederich, U. R. S., Hall, T., Klečka, G., Mihaich, E., Ortego, L., et al. (2010). Estimating potential risks to terrestrial invertebrates and plants exposed to bisphenol A in soil amended with activated sludge biosolids. *Environ. Toxicol. Chem.* 29, 467–475. doi: 10.1002/etc.49
- Stasolla, C., Huang, S., Hill, R. D., and Igamberdiev, A. U. (2019). Spatio-temporal expression of phytochrome: a determining factor in the NO specification of cell fate. *J. Exp. Bot.* 70, 4365–4377. doi: 10.1093/jxb/erz084
- Stavropoulou, K., Adamakis, I.-D. S., Panteris, E., Arseni, E.-M., and Eleftheriou, E. P. (2018). Disruption of actin filaments in *Zea mays* by bisphenol A depends on their crosstalk with microtubules. *Chemosphere* 195, 653–665. doi: 10.1016/j.chemosphere.2017.12.099
- Sun, H., Zhang, X., He, X., Ahmed, I. M., Cao, F., Zhang, G., et al. (2014). N-Acetyl-cysteine alleviates Cd toxicity and reduces Cd uptake in the two barley genotypes differing in Cd tolerance. *Plant Growth Regul.* 74, 93–105. doi: 10.1007/s10725-014-9906-z
- Tian, Y. S., Jin, X. F., Fu, X. Y., Zhao, W., Han, H. J., Zhu, B., et al. (2014). Microarray analysis of differentially expressed gene responses to Bisphenol A in *Arabidopsis*. *J. Toxicol. Sci.* 39, 671–679. doi: 10.2131/jts.39.671
- van Loon, L. C. (2016). The Intelligent Behavior of Plants. *Trends Plant Sci.* 21, 286–294. doi: 10.1016/j.tplants.2015.11.009
- Wang, Q., Wang, L., Han, R., Yang, L., Zhou, Q., and Huang, X. (2015). Effects of bisphenol A on antioxidant system in soybean seedling roots. *Environ. Toxicol. Chem.* 34, 1127–1133. doi: 10.1002/etc.2904
- Wilson, K. E., Ivanov, A. G., Öquist, G., Grodzinski, B., Sarhan, F., and Huner, N. P. A. (2006). Energy balance, organellar redox status, and acclimation to environmental stress. *Can. J. Bot.* 84, 1355–1370. doi: 10.1139/B06-098
- Wu, F., Chi, Y., Jiang, Z., Xu, Y., Xie, L., Huang, F., et al. (2020). Hydrogen peroxide sensor HPCA1 is an LRR receptor kinase in *Arabidopsis*. *Nature* 578, 577–581. doi: 10.1038/s41586-020-2032-3
- Xiao, C., Wang, L., Hu, D., Zhou, Q., and Huang, X. (2019). Effects of exogenous bisphenol A on the function of mitochondria in root cells of soybean (*Glycine max* L.) seedlings. *Chemosphere* 222, 619–627. doi: 10.1016/j.chemosphere.2019.01.195
- Xiao, C., Wang, L., Zhou, Q., and Huang, X. (2020). Hazards of bisphenol A (BPA) exposure: A systematic review of plant toxicology studies. *J. Hazard Mater.* 384, 121488. doi: 10.1016/j.jhazmat.2019.121488
- Xu, S. Y., Zhang, H., He, P. J., and Shao, L. M. (2011). Leaching behaviour of bisphenol A from municipal solid waste under landfill environment. *Environ. Technol.* 32, 1269–1277. doi: 10.1080/09593330.2010.535175
- Zafarullah, M., Li, W. Q., Sylvester, J., and Ahmad, M. (2003). Molecular mechanisms of N-acetylcysteine actions. *Cell. Mol. Life Sci.* 60, 6–20. doi: 10.1007/s000180300001
- Zhang, J., Li, X., Zhou, L., Wang, L., Zhou, Q., and Huang, X. (2016). Analysis of effects of a new environmental pollutant, bisphenol A, on antioxidant systems in soybean roots at different growth stages. *Sci. Rep.* 6, 1–10. doi: 10.1038/srep23782
- Zhang, C., Feng, Y., Liu, Y. W., Chang, H. Q., Li, Z. J., and Xue, J. M. (2017). Uptake and translocation of organic pollutants in plants: A review. *J. Integr. Agric.* 16, 1659–1668. doi: 10.1016/S2095-3119(16)61590-3
- Zhang, J., Wang, L., Zhou, Q., and Huang, X. (2018). Reactive oxygen species initiate a protective response in plant roots to stress induced by environmental bisphenol A. *Ecotoxicol. Environ. Saf.* 154, 197–205. doi: 10.1016/j.ecoenv.2018.02.020

Conflict of Interest: The authors declare that the research was conducted in the absence of any commercial or financial relationships that could be construed as a potential conflict of interest.

Copyright © 2020 Adamakis, Sperdouli, Eleftheriou and Moustakas. This is an open-access article distributed under the terms of the Creative Commons Attribution License (CC BY). The use, distribution or reproduction in other forums is permitted, provided the original author(s) and the copyright owner(s) are credited and that the original publication in this journal is cited, in accordance with accepted academic practice. No use, distribution or reproduction is permitted which does not comply with these terms.



Phenotypic Variation of *Botrytis cinerea* Isolates Is Influenced by Spectral Light Quality

Lijuan Meng, Hanna Mestdagh, Maarten Ameye, Kris Audenaert, Monica Höfte and Marie-Christine Van Labeke*

Department of Plants and Crops, Faculty of Bioscience Engineering, Ghent University, Ghent, Belgium

OPEN ACCESS

Edited by:

Lucia Guidi,
University of Pisa, Italy

Reviewed by:

Marco Landi,
University of Pisa, Italy
Mario Serrano,
National Autonomous University of
Mexico, Mexico

*Correspondence:

Marie-Christine Van Labeke
MarieChristine.VanLabeke@UGent.be

Specialty section:

This article was submitted to
Plant Pathogen Interactions,
a section of the journal
Frontiers in Plant Science

Received: 30 April 2020

Accepted: 28 July 2020

Published: 13 August 2020

Citation:

Meng L, Mestdagh H, Ameye M,
Audenaert K, Höfte M and
Van Labeke M-C (2020) Phenotypic
Variation of *Botrytis cinerea* Isolates Is
Influenced by Spectral Light Quality.
Front. Plant Sci. 11:1233.
doi: 10.3389/fpls.2020.01233

Botrytis cinerea, a fungal pathogen that causes gray mold, displays a high degree of phenotypic diversity. Light emitting diodes (LEDs) with specific light spectrum are increasingly used as lighting resource for plant greenhouse production. The chosen light spectrum can also have an effect on the pathogens in this production system. In this study, we investigated the phenological diversity in 15 *B. cinerea* isolates upon different light treatments. Daylight, darkness, and LED lights with different wavelengths (white, blue, red, blue+red) were chosen as treatments. The 15 *Botrytis* isolates differed in their mycelial growth rate, conidia production, and sclerotia formation. Light quality had a limited effect on growth rate. All isolates sporulated under daylight treatment, red light resulted in lower sporulation, while white, blue, and blue+red light inhibited sclerotia formation in all isolates, and sporulation in most, but not all isolates. Pathogenicity of the *Botrytis* isolates was studied on 2-week-old strawberry (*Fragaria* × *ananassa* ‘Elsanta’) leaves grown under white, blue, and red LED lights. The isolates differed in virulence on strawberry leaves, and this was positively correlated to oxalic acid production by *B. cinerea* *in vitro*. Red LED light improved leaf basal resistance to all the tested *Botrytis* isolates. Blue light pretreatment resulted in decreased leaf resistance to some isolates. Furthermore, we used image analysis to quantify the virulence of the different *Botrytis* isolates based on changes in photosynthetic performance of the strawberry leaves: chlorophyll fluorescence (F_v/F_m), chlorophyll index (ChlIdx) and anthocyanin content (modified anthocyanin reflection index, mArIdx). F_v/F_m showed a strong negative correlation with disease severity and can be an indicator for the early detection of gray mold on strawberry leaves.

Keywords: gray mold, phenotypic variability, pathogenicity, strawberry, red light, image-based early detection

INTRODUCTION

Botrytis cinerea Pers.:Fr the causal agent of gray mold disease is a filamentous, heterothallic fungus with a necrotrophic life style (Alfonso et al., 2000). This pathogen has a wide host range and infects more than 1,000 plant species worldwide including vegetables, ornamentals, and fruits, leading to important yield and quality losses (Elad et al., 2016). *B. cinerea* is a highly versatile pathogen. As a necrotroph, it can extract nutrients from dead or senescent plant material, but it can also infect living tissues *via* direct penetration or through natural openings or wounds (Williamson et al., 2007).

Additionally, it can also grow saprophytically. *Botrytis* can be isolated from different plant species in nature and infection can be reproduced in the laboratory on a wide range of hosts. Yet, a certain degree of host specialization exists in this pathogen (Thompson and Latorre, 1999; Muñoz et al., 2002). For example, Cotoras and Silva (2005) reported that *B. cinerea* strains isolated from tomato were more virulent on tomato leaves than isolates from grapes. Furthermore, a study of 490 isolates from open-field crops by microsatellite loci suggested the occurrence of host-specific divergence of *B. cinerea* in perennial hosts (Asadollahi et al., 2013).

B. cinerea isolates show phenotypic and genetic variability. Differences in colony morphology, mycelial growth, sporulation intensity, sclerotia formation, and pathogenicity have been described (Di Lenna et al., 1981; Martinez et al., 2003; Khazaeli et al., 2010; Pande et al., 2010; Kuzmanovska et al., 2012; Kumari et al., 2014). *B. cinerea* produces a battery of extracellular enzymes, including pectinases and pectin methylesterases (Reignault et al., 1994). *Botrytis* isolates with different pathogenic capabilities on various host produced different amounts of extracellular pectic enzymes (Di Lenna et al., 1981). High genetic diversity in *B. cinerea* populations has been revealed using a multiplicity of molecular techniques, such as PCR detection of transposable elements (Martinez et al., 2008), restriction fragment length polymorphism (RFLP) analysis of PCR-amplified loci (Baraldi et al., 2002; Muñoz et al., 2002), PCR amplification of microsatellite loci (Isenegger et al., 2008; Asadollahi et al., 2013), and randomly amplified polymorphic DNA (RAPD) analysis (Alfonso et al., 2000; Pande et al., 2010). Disease control is difficult because the pathogen has a broad host range and it can survive as mycelium and/or conidia or as sclerotia for extended periods. In addition, *B. cinerea* isolates differ in their sensitivity to fungicides and fungicide resistance is quickly obtained (Kretschmer and Hahn, 2008).

B. cinerea has 11 photoreceptors including 2 cryptochromes, 4 LOVs (light, oxygen, voltage), 2 opsins, and 3 phytochromes to respond to different light conditions varying from near-UV, blue, green, red, and far-red light (Schumacher, 2017). Blue light is sensed by the proteins that bind flavin *via* LOV or FAD (flavin adenine dinucleotide) domains such as BcWCL1 and BcWCL2 (the orthologs of white collar complex in *B. cinerea*), and BcVVD1 (the orthologs of vivid in *B. cinerea*) (Rodríguez-Romero et al., 2010). BcWCL1 interacts with BcWCL2 in the nuclei, forming the white collar complex (WCC), which is required to respond to white light (Schumacher, 2012). Opsins are transmembrane proteins using retinal to sense green light, and phytochromes are histidine kinases using bilin to perceive red/far-red light (Rodríguez-Romero et al., 2010). Based on the light perception by these photoreceptors, *B. cinerea* senses surrounding light as a decision-tool for morphogenesis, as a guide for directed growth, as a stress factor for protection, and also as a time giver for the circadian clock (Schumacher, 2017). Studies have described the impact of light on mycelial growth, conidiation, sclerotial development, and tropic response, however, unclear results have been reported caused by *B.*

cinerea isolate variability and different experimental conditions (Schumacher, 2017).

Strawberry (*Fragaria × ananassa*) is an important soft fruit crop that is popular all over the world. Gray mold is a serious disease in strawberry production and leads to important economic losses (Debode et al., 2015; Petrasch et al., 2019). *B. cinerea* can infect all plant parts of strawberry including leaves, fruits, flowers, petioles, and stems at every growth stage (Williamson et al., 2007; Petrasch et al., 2019). In year-round greenhouse strawberry production, light emitting diodes (LED) are increasingly applied to increase the day length as well as the light intensity in winter. LED lighting offers the possibility of spectral modulation thus influencing both morphology and metabolite content of the leaves. Commercial LED lamps typically combine blue and red wavelengths as these are highly absorbed by chlorophyll and thus promote photosynthesis and biomass production (Okamoto et al., 1996). Application of LED lighting also opens the possibility to increase the strawberry's resistance to *B. cinerea*. Indeed, we previously showed that leaves that develop under monochromatic red light are more resistant to *Botrytis* infection compared to white, blue, and blue+red lights (Meng et al., 2019). Yet, in aforementioned study only one *Botrytis* strain was investigated. Hence, the investigation of the diversity in light-response of different *B. cinerea* isolates is of importance for the LED light application in greenhouse production.

Given the facts described above, we hypothesized that *B. cinerea* isolates will differentially respond to different light qualities. Therefore, we investigated the light-modulated phenotypic diversity of 15 *B. cinerea* isolates. We characterized their pathogenicity on strawberry leaves under white, blue, and red LED lights and hypothesized that a pretreatment of leaves with red light would reduce disease susceptibility irrespective of the isolate. To assess the virulence of the different *Botrytis* isolates on strawberry leaves in an objective way, we investigated the potential of image-based early detection to quantify changes in the photosynthetic performance of the leaves (quantum efficiency of photosystem II, chlorophyll index) and/or leaf defense compounds (modified anthocyanin reflection index).

MATERIALS AND METHODS

Botrytis cinerea Isolates

Fifteen *B. cinerea* isolates were used in this study (Table 1). Four *B. cinerea* isolates (B1, B2, B6, and B7) are well-documented laboratory strains. Eleven gray mold isolates were collected from tomato, lettuce, apple, and grape in Belgium. Purified isolates were cultivated on potato dextrose agar (PDA, Becton, Dickinson, and Company) and subjected to long-term storage in 20% glycerol at -80°C .

Light Quality Treatments to Study *Botrytis* Phenotypes

To investigate mycelial growth, sporulation, and sclerotia production, the 15 *B. cinerea* isolates were grown on PDA under different spectral light qualities at 20°C . Six different

TABLE 1 | *Botrytis cinerea* isolates used in this study.

<i>Botrytis</i> iso-lates*	Host plant	Origin/geographic origin	References
B1 (R16)	Grape	Result of the crossing SAS56×SAS405	(Faretra and Pollastro, 1991)
B2 (Bd90)	Grape	Bordeaux (France)	(Reignault et al., 1994)
B3	Lettuce	Belgium, 2018	this study
B4	Tomato	Belgium, 2018	this study
B5	Lettuce	Belgium, 2018	this study
B6 (B05.10)	Grape	Haploid strain resulted from a treatment with benomyl in Germany	(Quidde et al., 1998)
B7 (A336)	Grape	mutant of Bd90, from Bordeaux (France)	(Hamada et al., 1994)
B8	Lettuce	Belgium, 2018	this study
B9	Lettuce	Belgium, 2018	this study
B10	Apple	Belgium, 2018	this study
B11	Grape	Belgium, 2018	this study
B12	Lettuce	Belgium, 2018	this study
B13	Tomato	Belgium, 2018	this study
B14	Lettuce	Belgium, 2018	this study
B15	Lettuce	Belgium, 2018	this study

*Alternative names are indicated between brackets.

light regimes were established using 1) daylight, 2) white LEDs (300–800 nm, 29% B, 39% G, 27% R, and 5% FR, Philips, the Netherlands), 3) blue LEDs (400–500 nm, peak at 460 nm), 4) red LEDs (600–700 nm, peak at 660 nm), 5) red + blue LEDs (75/25%, peak at 660 nm and 460 nm) (**Supplementary Figure 1**) and (6) dark as control. A photoperiod of 16 h and a photon flux density of $40 \mu\text{mol m}^{-2} \text{s}^{-1}$ were provided by the LEDs. Natural daylight was provided at a lab bench (18°C), with a natural day length of 15 h and average photosynthetic photon flux density (PPFD) of $10 \mu\text{mol m}^{-2} \text{s}^{-1}$. The spectral light distribution and the light intensity were measured using a spectroradiometer (JAZ-ULM-200, Ocean Optics, US).

Mycelial plugs with 6 mm in diameter were inoculated in the center of Petri dishes (90 mm in diameter). The Petri dishes were assigned to one of the six light treatments. Six replicates per isolate and per light treatment were used. The radial growth per colony was measured daily on two perpendicular axes for 5 days or until it reached the edge of the plate. The growth rate (cm day^{-1}) was calculated as the average growth length increase per day.

To assess the sporulation and sclerotia production, PDA plates inoculated with 6 mm-mycelial plugs remained under the six light treatments for 15 days. Sporulation and sclerotia production were assessed visually and by microscopy. The class system was set as: class 0 (no spores/sclerotia formation); class I; (very few spores/sclerotia formation); class II (sparse sporulation/sclerotia formation); class III (average amount spores/sclerotia formation); class IV (many spores/sclerotia formation); class V (abundant formation of spores/sclerotia). The classification system for sclerotia is illustrated in **Supplementary Figure 2**. This was repeated three times with six replicates each time ($n = 18$).

Oxalic Acid Detection Assay

Plugs of *B. cinerea* isolates were inoculated on complete medium (Canessa et al., 2013) and always maintained in the dark at 24°C. This pH-indicating medium contains 0.1% bromothymol blue as indicator, and the medium color changes from green to yellow when an acid compound such as oxalic acid is produced. Medium acidification was evaluated after 7 days by its effect on the medium pH. The pH was measured on the outside of the yellow circle using a flat pH electrode (SF113, VWR, Germany) which can test the pH directly *via* the surface of the medium. Four measurements were conducted for each plate and averaged, this was done in four replications per isolate.

Pathogenicity Test on Strawberry

Strawberry (*Fragaria × ananassa* ‘Elsanta’) leaves that developed under different light qualities were used for the pathogenicity tests with the 15 *B. cinerea* isolates. The plants were potted in peat substrate (Van Israel nv, Belgium) and raised in a growth chamber with 70% relative humidity at 20°C. The growth chamber was equipped with three light qualities: white (W, 300–800 nm, Philips, the Netherlands), blue (B, peak at 460 nm, Philips, the Netherlands), and red (R, peak at 660 nm, Philips, the Netherlands) LED lights (**Supplementary Figure 1**). A photoperiod of 16 h with the photosynthetic photon flux density at $100 \mu\text{mol m}^{-2} \text{s}^{-1}$ was provided. The plants were fertilized with Soluplant (N:P:K:Ca 19-8-16-4, Haifa, the Netherlands, EC=1.5 dS/m, pH=5.7) three times per week.

All the 15 isolates were tested on strawberry leaves grown under white LED light, and a subset of 10 isolates was tested on leaves that developed under blue and red LED lights. *Botrytis* isolates were cultivated on PDA in Petri dishes. After 7–10 days, conidia were washed from the plates with $\frac{1}{4}$ potato dextrose broth (PDB) solution containing 0.01% (v/v) Tween 20. After removing the mycelium fragments, spore titers were determined microscopically using a Thoma counting chamber. A final concentration of 5×10^5 spore ml^{-1} was used for inoculation. Leaf discs of 1-cm in diameter from 2-week-old strawberry leaves were cut the day before inoculation and placed in disposable 24-well plates with water. Each leaf disc was inoculated with 10 μl droplets of conidial suspension on the adaxial leaf surface. Incubation was at 22°C under dark conditions. Disease symptoms were scored after 3 days. A 0–3 ordinal rating scale was employed for disease rating and disease index was calculated. Six leaf discs per leaf with four biological replicates were used in this study.

Image Analysis

Non-invasive spectral phenotyping was applied to monitor the strawberry disease development by a platform that allows to visualize diverse physiological traits in real time, based on specific absorption, reflection, and fluorescence patterns in visible and near-infrared (NIR) wavelengths. The central part of the platform comprises a 3CCD 6 Mp—16 bit camera mounted on a Cartesian coordinate robot, equipped with 12 optical interference filters (CropReporter, PhenoVation B.V., Wageningen, the Netherlands).

This multispectral imaging platform was used daily to record the lesion development of inoculated leaf discs floating in 24-well plates (24 replicates per light quality treatment and *Botrytis* isolate) from the day of inoculation until 4 days post-inoculation (dpi).

RGB (red green blue) images, reflectance spectra to calculate the anthocyanin index and chlorophyll index and the minimal fluorescence, F_0 , and the maximum fluorescence, F_m , are captured by the camera. Images obtained from the phenotyping platform were processed via the “Data Analysis Software” program (PhenoVation B.V., Wageningen, the Netherlands).

The modified anthocyanin reflectance index (mAriIdx) was determined using following formula (Gitelson et al., 2009):

$$\text{mAriIdx} = \left(\frac{1}{\rho_{550\text{nm}}} - \frac{1}{\rho_{710\text{nm}}} \right) \rho_{770\text{nm}}$$

The chlorophyll index (ChlIdx) was calculated using following formula (Gitelson et al., 2009):

$$\text{ChlIdx} = \left(\frac{\rho_{770\text{nm}}}{\rho_{710\text{nm}}} - 1 \right)$$

where ρ_{550} is the reflectance in the first spectral band, which is maximally sensitive to anthocyanin content; ρ_{710} the reflectance in the second spectral band, which is maximally sensitive to chlorophyll content but not sensitive to anthocyanin content; and ρ_{770} the reflectance of the third spectral band, which compensates for leaf thickness and density.

The maximum quantum efficiency of photosystem II (F_v/F_m) was calculated using following formula (Baker, 2008):

$$F_v/F_m = (F_m - F_0)/F_m$$

Between measurements, the 24-well plates were placed in the dark allowing immediate quantification of the minimal (F_0), then saturating red light flashes of $3,000 \mu\text{mol m}^{-2} \text{s}^{-1}$ were given. This allows the imaging of the OJIP induction curve at 12 images per second at a resolution of 1.5 Mp. This resolution gives the optimal signal to noise with respect to the detail in the image (PhenoVation B.V., Wageningen, the Netherlands). From the F_0 and F_m image measurements based on the OJIP induction curve the variable fluorescence F_v/F_m is calculated (Björkman and Demmig, 1987; Kalaji et al., 2014). This yields images of F_v/F_m and from these images corresponding average values including standard deviation of the whole image are calculated (imaging software and algorithms by PhenoVation B.V., Wageningen, the Netherlands).

Statistical Analysis

Data were tested for normal distribution using the Kolmogorov–Smirnov test and for homoscedasticity of variances using Levene’s test. The mycelial growth rate and disease rating among *B. cinerea* isolates were compared by the non-parametric Kruskal–Wallis test with Dunn test as the *post hoc* test. The effect of light quality on mycelial growth rate was analyzed by one-way ANOVA. If significant differences were found, the Tukey test ($p \leq 0.05$) was

carried out to establish significant differences between means, here a Bonferroni correction was applied when $n \geq 10$. The virulence of the *Botrytis* isolates assessed by the multispectral camera (F_v/F_m , ChlIdx, mAriIdx) were analyzed by one-way ANOVA for each light quality. As the light pretreatment affects both chlorophyll and polyphenol content (Meng et al., 2019), the effects of the light quality pretreatments were analyzed by ANCOVA using the images at the start (day 0) as covariate, adjusted means were calculated using Bonferroni for confidence interval adjustment. All assumptions for performing ANCOVA including homogeneity of regression slopes were checked. All analyses were performed using SPSS version 26 (SPSS Inc., Chicago, USA).

RESULTS

Phenotypic Characterization of *B. cinerea* Isolates

Significant differences in the mycelial growth rate were observed between the 15 *B. cinerea* isolates, this for the dark control treatment (Figure 1, Supplementary Table 1). B12 resulted in the lowest growth rate (0.45 cm day^{-1}) while B2 and B8 had a \pm three-fold higher growth rate (respectively 1.31 and 1.32 cm day^{-1}).

Light conditions greatly influenced the growth rate of *B. cinerea* (Figure 2, Supplementary Table 1). For the isolates B2, B3, B4, B5, B7, B12, and B14, the mycelial growth was considerable higher under LED lights (white, blue, red, blue+red) compared to the dark and daylight treatment. The spectral quality of the LED treatment did not affect the growth rate of B2, B5, B7, B9, B10, B12, B13, and B15. However, compared to white LED light, a significant increase was observed in the growth rate of B8 under blue light, while red light enhanced the growth rate of B1, B11, and B14. The combination blue+red, decreased the mycelial growth of B3 and B11 considerably, while an increase was observed in B1. Additionally, B1 was the only isolate where the highest growth rate was observed in the dark while all other isolates had higher or equal growth rates than the dark treatment.

Sporulation and sclerotia formation varied among the 15 *B. cinerea* isolates, and both were considerably affected by the light treatments used in this study (Figure 3). The 15 isolates were grouped according to the presence/absence of sporulation and of sclerotia formation under the light treatments (Figure 3). Four groups were defined based on their sporulation response. A first group clusters two lettuce and two tomato isolates (B3, B4, B13, B15) as they only produced spores under daylight and red LED light. A second group, including three lettuce and one grape isolate (B5, B8, B10, B14) sporulated in dark condition as well as under daylight and red light. The third group (grape isolates B2 and B11) developed spores under daylight, red and blue light. The fourth group, including grape and lettuce isolates (B1, B6, B9, and B12) exhibited great variability in sporulation compared to the other isolates under the considered light conditions. Finally, the

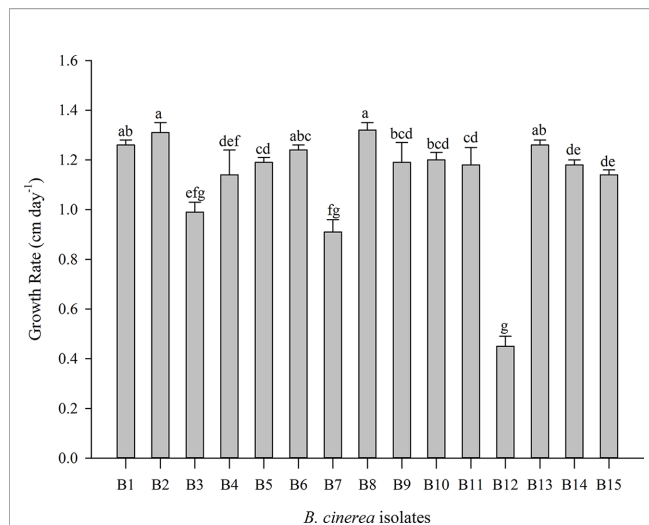


FIGURE 1 | Mycelial growth rate of 15 *Botrytis cinerea* isolates in dark condition. Data are presented as mean of six replicates with standard deviation. Different letters indicate statistical differences among *B. cinerea* isolates based on Kruskal-Wallis test with Bonferroni correction (Dunn test, $p \leq 0.0033$).

nonpathogenic mutant B7 (A366) forms a fifth group and produced spores in all six treatments.

No sclerotia formation was observed under white, blue, and blue+red LED lights, this for all isolates. Three groups could be distinguished based on the formation of sclerotia in dark, under daylight or under red light (**Figure 3**). No sclerotia were produced in B6 (B05.10) and B7 (A366) irrespectively the light or dark treatment, resulting in a first group. B1 (R16) formed a second group with only sclerotia formation in the dark. The third group is formed by the remaining twelve isolates including lettuce, tomato, apple, and grape isolates, as they all produced sclerotia under dark, daylight, and red LEDs.

Oxalic acid formation can be indicative as a virulence factor for *Botrytis* (Williamson et al., 2007; Sun et al., 2019). Media acidification due to organic acid formation was strongest for B4, B6, B12, B13, and B15, resulting in a decrease of more than 1.5 pH units compared to a non-inoculated control. The nonpathogenic mutant B7 (A366) did not acidify the medium in comparison to the control. All other isolates caused an intermediate acidification reducing the medium with 1.0 pH unit in comparison to the control (**Figure 4**). White, blue, and red LED irradiation had no significant effect on media acidification caused by different *Botrytis* isolates (data are not shown).

Inoculation Assays on Strawberry Leaves

First, 14 *Botrytis* isolates were tested by spore inoculation on white LED light-developed strawberry leaves. B6 could not be included because of its poor sporulation (**Figure 5**). Different degrees of virulence on strawberry leaves were observed between these 14 isolates. B4, B10, B13, and B15 were the most virulent, followed by B1, B2, B3, B5, B9, and B14. An intermediate

virulence was observed for B8, B11, and B12. As expected, strawberry leaves were hardly infected by the non-pathogenic B7 (A366) strain.

Second, ten *Botrytis* isolates were tested on strawberry leaves that were developed under blue and red LED lights. The isolates showed significant variations in their virulence (**Supplementary Figures 3A, B**). B7 (A366) was again the least aggressive, while B1, B2, and B13 were the most aggressive isolates and B15 resulted in moderate disease rating on the leaves that had developed either under blue or red light. Strawberry leaves that originated from red light were more resistant against the tested *Botrytis* isolates compared to leaves from white or blue light (**Figure 6**). Blue-light-developed leaves were more susceptibility to B1, B2, B9, B12, B13, while no remarkable difference was noted for isolates B3, B8, B10, B15, when compared to white-light-developed leaves. The isolate B7 (A366) also remained non-virulent on blue or red light-developed leaves (**Supplementary Figures 3A, B**).

Overall, B8 (lettuce isolate) was the least aggressive *Botrytis* isolate on strawberry leaves irrespectively of light treatments, while B13 (tomato isolate) was the most aggressive one. Interestingly, B15 (lettuce isolate) resulted in the strongest disease symptoms on leaves from white light, however, blue- and red-light developed leaves displayed moderate resistance to B15.

Image-Based Assessment of Botrytis Infection on Strawberry Leaves

For the image-based assessments of the progress rate of the disease after spore inoculation, changes in both chlorophyll fluorescence imaging (F_v/F_m) and stress indices (ChlIdx and mAriIdx) were assessed during 5 days (**Figure 7, Supplementary Figures 4-6**). The phenotyping of the plant resistance is shown from 0 to 4 dpi for three representative *Botrytis* isolates: the non-pathogenic B7 strain, the intermediate aggressive B12, and the most aggressive B13 isolate as determined by visual scoring on white-light-developed leaves (**Figure 5**). The non-pathogenic B7 displayed a minor but significant decrease in F_v/F_m from 0.755 at 0 dpi to 0.637 at 4 dpi and hardly any change in ChlIdx and mAriIdx (**Figure 7A**). For B12 a strong decline was observed in F_v/F_m from 3 dpi on, with values decreasing from 0.755 at 0 dpi to 0.263 at 4 dpi. Correspondingly, also ChlIdx displayed a significant decrease, while mAriIdx increased considerably from 0 to 4 dpi (**Figure 7B**). The isolates B8, B9, B11, and B14 showed similar temporal changes as the intermediate aggressive isolate B12 for F_v/F_m , ChlIdx, and mAriIdx, except for the mAriIdx of B14 (**Supplementary Figure 4**).

The most virulent isolate B13 caused the greatest decrease of F_v/F_m , this was already very strong at 3 dpi, while values further decreased to 0.172 at 4 dpi. Simultaneously a clear decrease in ChlIdx and increase in mAriIdx was found (**Figure 7C**). B1, B2, B3, B4, B10, and B15 grouped with B13 based on their virulence on strawberry leaves and they caused the same trends in F_v/F_m and ChlIdx. However, no significant increase was observed in mAriIdx for B1, B3, and B15.

The *Botrytis* isolates resulted in considerable variations in F_v/F_m , ChlIdx, and mAriIdx of the inoculated leaves at 4 dpi, this for

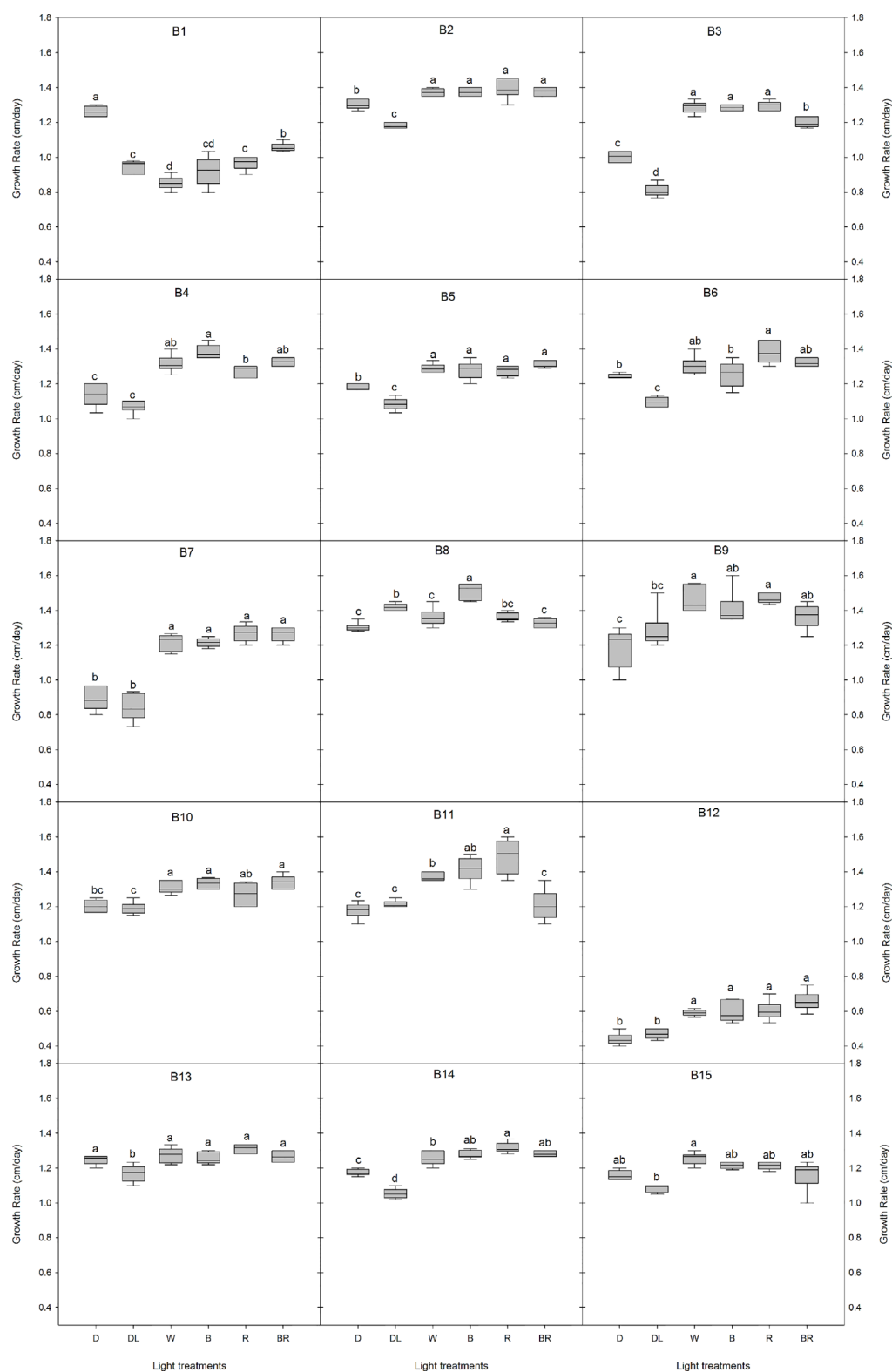


FIGURE 2 | Effects of light quality on the growth rate of 15 *Botrytis cinerea* isolates. Six light treatments were analyzed namely dark (D), daylight (DL), white (W), blue (B), red (R), and blue+red (BR). Different letters indicate statistical differences between light treatments for each isolate based on Tukey's test ($p \leq 0.05$), except for B2 and B15 where a non-parametric Kruskal-Wallis followed by a *post-hoc* Dunn's test ($p \leq 0.05$) was performed.



FIGURE 3 | Classification of sporulation and sclerotia formation in the 15 *Botrytis cinerea* isolates after 15 days under six light treatments: dark, daylight, white, blue, red, and blue+red LED, and classification based on F_v/F_m values at 4 dpi from infection in white-light-leaves. Classes of sporulation and sclerotia presented are from three replications with six plates for each replicate ($n = 18$). The classes of sporulation and sclerotia formation are: class 0 (no spores/sclerotia formation); class I (very few spores/sclerotia formation); class II (sporulation/sclerotia formation sparse); class III (average amount of spores/sclerotia formation); class IV (many spores/sclerotia formation); class V (abundant spore/sclerotia formation). The class of virulence is based on the significant letters of F_v/F_m at 4 dpi (**Table 2**) with exclusion of B6 which is indicated by a light gray color. The classes are: class I (significant letters starting with a); class II (significant letters starting with b); class III (significant letters starting with c); class IV (significant letters starting with d); class V (significant letters starting with e). These classes are shown in colors (see the color bar).

all the pre-inoculation light quality regimes of the leaves (**Table 2**).

Leaves inoculated with the nonpathogenic strain B7 (A366) maintained the highest level of F_v/F_m and ChlIIdx, while the

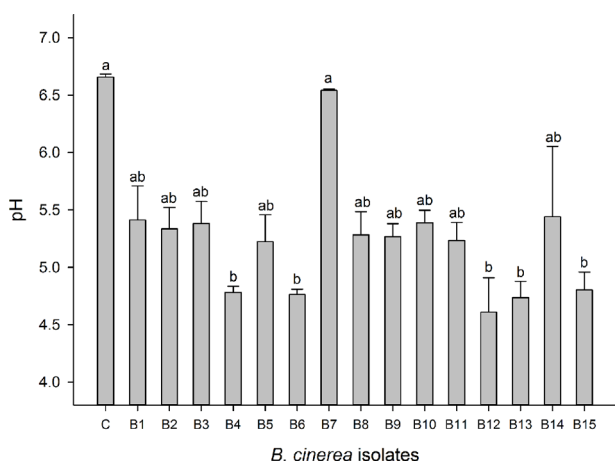
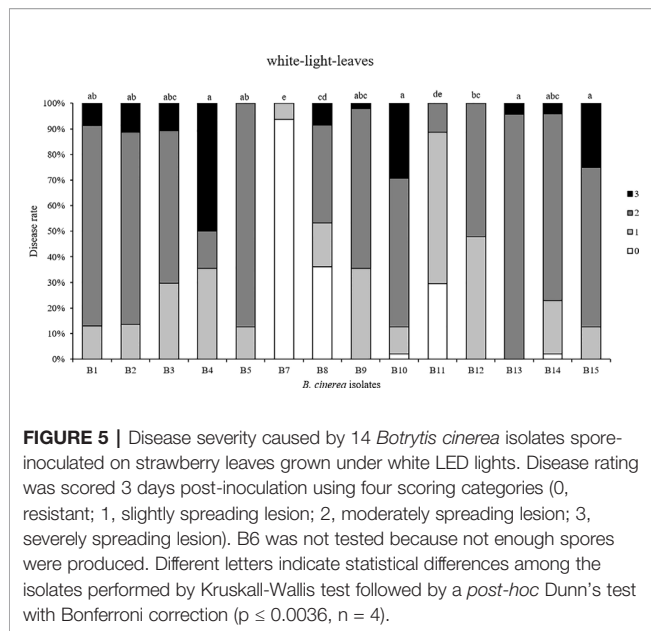


FIGURE 4 | Oxalic acid production of *Botrytis cinerea* isolates was assessed based on changes in the medium pH. Control treatment (C) is medium without *Botrytis* inoculation. Data are shown as means \pm SE ($n=4$). Different letters indicate statistical differences between *B. cinerea* isolates. Non-parametric Kruskal-Wallis followed by a *post-hoc* Dunn's test was performed with $p \leq 0.05$.

lowest levels of mArIIdx were observed, this irrespective of the light quality treatments. Leaf inoculation with the virulent B13 resulted in the strongest decrease of F_v/F_m for white-light-leaves, but not for the other light quality pretreatments. Here, F_v/F_m was lowest after B12 inoculation of leaves grown under both blue and red light. Leaf yellowing and chlorophyll content, assessed by ChlIIdx was lowest after B15 inoculation of white-light-leaves, B10 inoculation of blue-light-developed leaves, and B1 inoculation of red-light-developed leaves. Increase of anthocyanins (mArIIdx) was highest in both B9 and B13 in white-light-developed leaves, and in B12 in both blue- and red-light leaves (**Table 2**).

Light pretreatment effects are thus clearly present and these effects are shown in **Table 3**. Overall red pretreated leaves have a significant higher F_v/F_m ($p < 0.001$) and ChlIIdx ($p < 0.001$), while no difference between blue and white pretreated leaves is found. Only for strains B1 and B13 this positive effect of red light to maintain higher F_v/F_m levels was not observed, while this was the case of B2 with respect to ChlIIdx. Overall no significant effect of light pretreatment was found for mArIIdx ($p = 0.41$), indeed only for 3 out of 10 isolates an effect of light pretreatment of the leaves was present, in B1 and B7 mArIIdx increased significantly while for B9 a significant decrease was found.

Additionally, overall comparison of anthocyanins with respect to the different light qualities (**Supplementary Table 2**) or more specifically for three representative *B. cinerea* isolates (**Supplementary Table 3**) were performed from 0 to 4 dpi. Blue light-developed leaves resulted in significant lower basal



anthocyanin levels compared to leaves developed under white and red lights (Supplementary Table 2). A higher anthocyanin content was observed in *Botrytis* isolates with higher virulence (Supplementary Table 3).

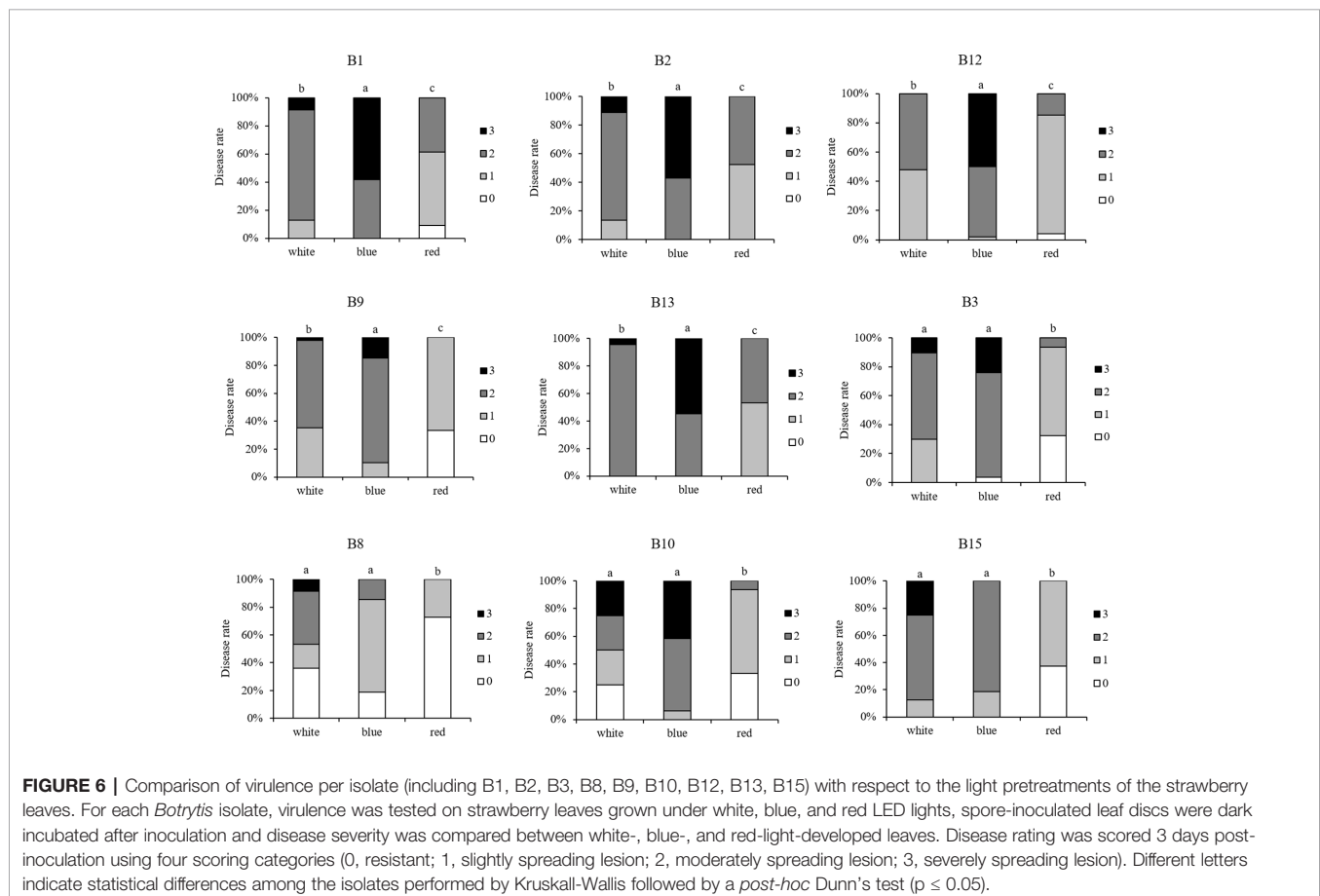
As virulence of the isolates differed, correlations between the disease index and F_v/F_m , ChlIdx, and mArIdx were explored (Figure 8). High correlations between disease index and F_v/F_m were found, this irrespective of the light quality pretreatment (all $r \geq 0.978$, Figure 8A). Stress indices resulted in lower though still significant correlations between the disease index and ChlIdx although the correlation was lowest for red pretreated leaves ($r > 0.917$ for leaves from white light and blue light, while r is 0.824 for leaves from red light, Figure 8B). Correlations between disease index and mArIdx were much lower ($r < 0.699$, Figure 8C).

We also checked the correlations between F_v/F_m and phenotypic characteristics of the different isolates such as growth rate (Figure 1) and medium acidification (Figure 4). Virulence and medium acidification were highly correlated (Supplementary Figure 7A), while no correlation between virulence and mycelial growth rate was observed (Supplementary Figure 7B).

DISCUSSION

Phenotypic Variability of *Botrytis cinerea* Isolates Is Influenced by Light Quality

The 15 *Botrytis* isolates in this study differed in their mycelial growth rate and in their ability to reproduce by conidia or form



sclerotia (**Figures 1–3, Supplementary Table 1**). This intraspecies variation in *B. cinerea* is well documented (Martinez et al., 2003; Mirzaei et al., 2009) and can be influenced by environmental factors. As *Botrytis* is an important pathogen in greenhouse plant production, changes in the greenhouse environment might also lead to phenotypic variations. Here, we specifically focused on the increasing application of monochromatic red and blue light and its combination in lighting strategies with LED. Indeed, *B. cinerea*, possesses 11 photoreceptors to sense the surrounding light environment, which triggers various photoresponses influencing vegetative growth, sporulation, germination of spores, and sclerotia formation (Schumacher, 2017). Generally, the short UV A and B (300–420 nm) wavelengths retard the mycelial growth of *B. cinerea* (Tan and Epton, 1973). Here, the shortest wavelength we investigated was monochromatic blue light (460 nm) though this wavelength did not retard the growth rate of the studied isolates, in comparison to the full-spectrum white light. Light quality had a limited effect on the growth rate. Canessa et al. (2013) found that light reduced the daily growth rate of B05.10 (= B6) and attributed this to light-induced stress. It seems that our applied lower light intensities did not induce this light stress except for the strain B1 which showed the highest mycelial growth rate under dark condition. The reduced mycelial growth rate under daylight might be explained by the lower temperature (18°C while 20°C in the climate rooms) as indicated by Tan and Epton (1973).

Early studies showed that sporulation happens exclusively in light, it is strongly stimulated by near-UV light and slightly stimulated by red light, while blue light is ineffective (Tan and Epton, 1973). This light-dependent effect on sporulation was later confirmed for strain B05.10 (= B6) by Canessa et al. (2013) where broad spectrum light (400–720 nm) induced sporulation but blue light inhibited the formation of conidiophores. Also in our research all isolates sporulated under full spectrum daylight (from class I to class V). Monochromatic red light resulted in similar or lower sporulation in most isolates (12 out of the 15), this coincides with the slight stimulation of sporulation by red light reported by Tan and Epton (1973). Sporulation under white LEDs was low, only B1 and B7 sporulated under this light source (both class II) although the light spectrum is very similar to daylight. However, daylight is rich in far-red light (700–800 nm, **Supplementary Figure 1**), which promotes sporulation (Tan, 1975).

Here, the capacity of blue light to inhibit sporulation was only observed in 9 of the 15 isolates. Blue light stimulated sporulation in B6 (B05.10) and two other grape isolates (B2 and B11), in the nonpathogenic strain B7 (A366), and in two lettuce isolates (B9 and B12). The fact that B05.10 (= B6) produced very few spores (class I) under blue light but also hardly sporulated under daylight, might indicate that despite its genetic stability (Canessa et al., 2013) the strain has mutated. This is also supported by the fact that this strain did not form sclerotia in the dark. Adding red light (600–700 nm) to the blue spectrum did not enhance sporulation as only three isolates sporulated under these conditions. Stewart and Long (1987) reported that

Botrytis strains could also show varying degrees of sporulation in the dark. This is also confirmed in our study where 8 out of 15 isolates sporulated in the dark. Although blind strains that exhibit the same phenotype under light and darkness are found in nature, this was not the case for our field collections. Only B7, the nonpathogenic mutant A366 produced conidia under each light quality as well as under dark condition and, as described by Kunz et al. (2006), was not able to form sclerotia.

Early studies indicated that sclerotia formation for survival exclusively occurs in cultures in constant darkness. Yet, this can be affected by small broad light dosages. Less sclerotia were formed when irradiated for 30 min compared to 15 min, and none were observed when irradiated for more than 60 min. Furthermore, sclerotia formation was found to be promoted by red and infrared light (Tan and Epton, 1973). In this study, blue, blue+red, and white lights inhibited sclerotia formation in the 15 *B. cinerea* isolates. This inhibition is due to the blue light fraction as under red light sclerotia were formed in 12 out of the 15 isolates. In this study also daylight at a very low light fluence (10 $\mu\text{mol m}^{-2} \text{s}^{-1}$) induced sclerotia promotion which can be caused by the enrichment of the longer wavelengths (red light or the far-red light) in the indoor daylight spectrum (Tan and Epton, 1973).

It is clear that phenotypic responses of *B. cinerea* isolates to light quality are very diverse and sometimes conflicting with earlier publications. These conflicting results might be due to the fact that limited strains were studied though probably also light intensity might be an interacting factor with light quality. Also day length effects cannot be excluded, most studies apply a photoperiod of 12 h while in this research a photoperiod of 16 h, based on greenhouse lighting duration was applied.

Virulence Variation in *Botrytis cinerea*

B. cinerea isolates in this study displayed significant variations in their virulence. Virulence diversity in *B. cinerea* isolates has been studied in various locations and on various plants around the world (Kerssies et al., 1997; Martinez et al., 2005; Mirzaei et al., 2009; Kumari et al., 2014). Variation in virulence of *B. cinerea* is often due to differences in cell wall degrading enzymatic activities and in the secretion of other virulence factors such as oxalic acid (Derckel et al., 1999). Higher oxalic acid accumulation leads to higher aggressiveness of the pathogen and reversely, lower secretion of oxalic acid is associated with lower virulence (Kunz et al., 2006; Sun et al., 2019). Various degrees of medium acidification caused by oxalic acid production of *B. cinerea* isolates were also observed in this study (**Figure 4**). B4, B13, and B15 with highest virulence on strawberry leaves secreted more oxalic acid. In contrast, B7 (A336), the nonpathogenic mutant, showed no oxalic acid production and did not cause disease. Medium acidification and virulence were highly correlated (**Supplementary Figure 7A**). Yet also other virulence factors such as cell wall degrading enzymes, toxins, and secondary metabolites (Sharma and Kapoor, 2017) can explain differences in virulence. However, it seems that *B. cinerea* isolates with strong virulence favored less sporulation and produced more sclerotia (**Figure 3**).

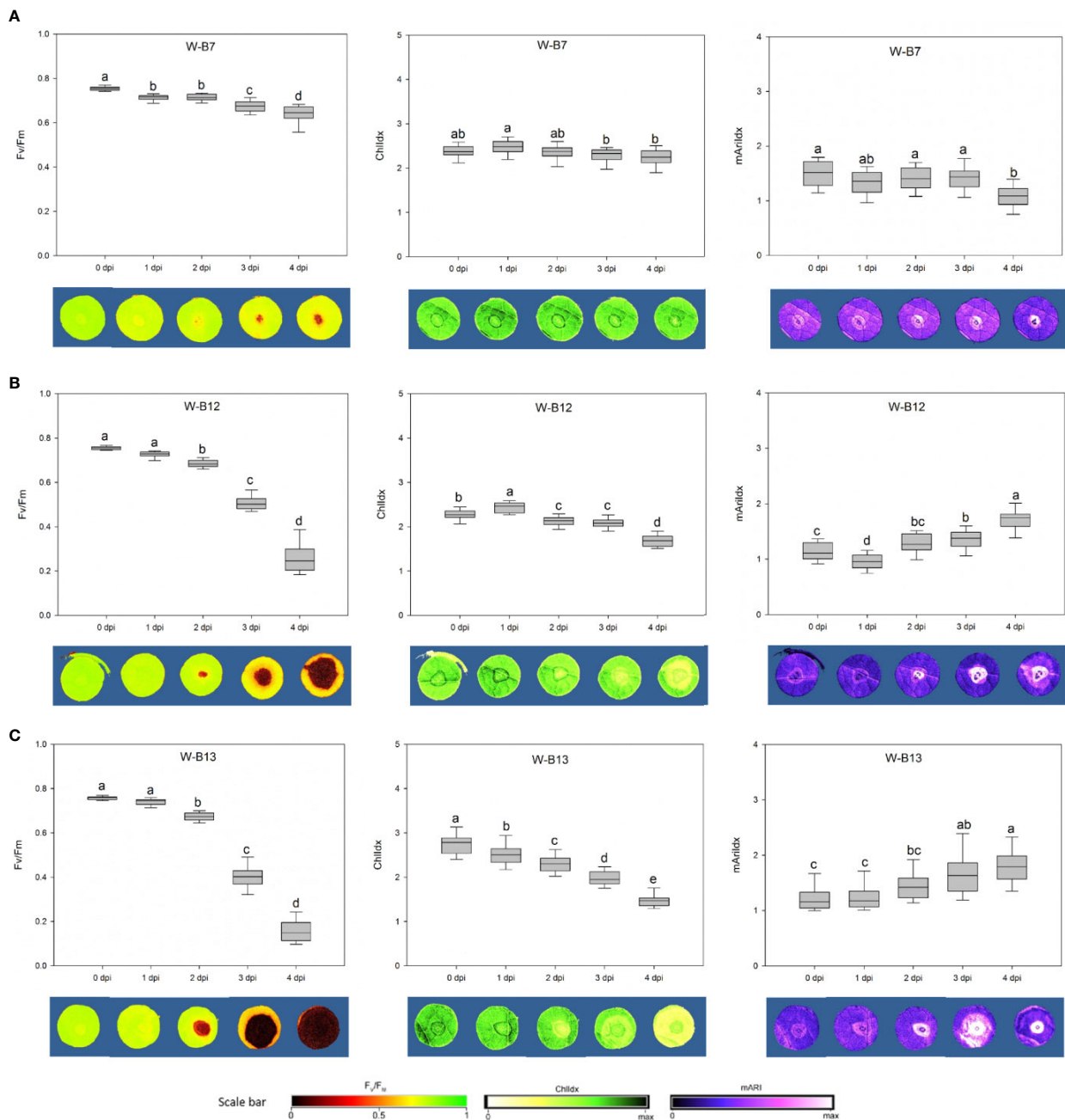


FIGURE 7 | The variations of F_v/F_m , Chlxd, and mArldx from 0 to 4 dpi caused by *Botrytis cinerea* isolates B7 (A), B12 (B), and B13 (C) were correlated with the development of disease lesion on white-light-leaves. The corresponding images are presented underneath the figures. Disease lesion led to darker F_v/F_m image with lower value, yellower Chlxd image with lower value, and brighter mArldx image with higher level. One-way ANOVA was applied for the statistical analysis (Tukey test, $p \leq 0.05$), and data are shown by box plots with median. Different letters indicates significant differences among the time points.

Strawberry Leaves Developed Under Red Light Displayed Enhanced Resistance to *Botrytis cinerea* Isolates

Higher resistance to all the tested *B. cinerea* isolates (except for the non-pathogenic B7) was found in strawberry leaves grown under red LEDs (Figure 6). Meng et al. (2019) showed that red

LED light increased strawberry leaf basal resistance against R16 (B1 in this study). Resistance improvement by red light was associated with lower hydrogen peroxide levels in the red-light-developed leaves of strawberry (Meng et al., 2019). It might also be linked to phytochrome modulated defense signaling where low R:FR ratios repress the jasmonate response to *Botrytis*

TABLE 2 | Effect of inoculation with different *Botrytis* isolates at 4 dpi on F_v/F_m , ChlDx, and mArldx in strawberry leaves grown under white, blue, and red LED lights.

Botrytis isolates	White			Blue			Red		
	F_v/F_m	ChlDx	mArldx	F_v/F_m	ChlDx	mArldx	F_v/F_m	ChlDx	mArldx
B1	0.266 ± 0.129 ^{cde}	1.635 ± 0.357 ^{bode}	1.590 ± 0.234 ^{ab}	0.199 ± 0.188 ^{de}	1.478 ± 0.420 ^{cd}	1.456 ± 0.323 ^b	0.342 ± 0.130 ^d	22.072 ± 0.389 ^c	1.860 ± 0.439 ^{ab}
B2	0.318 ± 0.169 ^{bcd}	1.780 ± 0.375 ^{bc}	1.826 ± 0.504 ^{ab}	0.148 ± 0.097 ^{de}	1.383 ± 0.275 ^{cd}	1.628 ± 0.339 ^{ab}	0.376 ± 0.157 ^{cd}	2.130 ± 0.372 ^{bc}	1.761 ± 0.376 ^{abc}
B3	0.218 ± 0.066 ^{de}	1.517 ± 0.183 ^{cde}	1.648 ± 0.200 ^{ab}	0.350 ± 0.248 ^{bc}	1.887 ± 0.522 ^{ab}	1.519 ± 0.458 ^b	0.498 ± 0.153 ^{bc}	2.263 ± 0.300 ^{bc}	1.435 ± 0.379 ^{bc}
B4	0.223 ± 0.116 ^{de}	1.441 ± 0.264 ^{de}	1.567 ± 0.348 ^{ab}	*	*	*	*	*	*
B5	0.275 ± 0.067 ^{cde}	1.647 ± 0.153 ^{abc}	1.820 ± 0.423 ^{ab}	*	*	*	*	*	*
B7	0.637 ± 0.042 ^a	2.243 ± 0.194 ^a	1.095 ± 0.280 ^c	0.599 ± 0.038 ^a	2.166 ± 0.209 ^a	0.841 ± 0.214 ^c	0.712 ± 0.022 ^a	2.765 ± 0.275 ^a	1.320 ± 0.314 ^c
B8	0.373 ± 0.203 ^{bc}	1.719 ± 0.368 ^{bcd}	1.457 ± 0.269 ^{abc}	0.377 ± 0.098 ^b	1.685 ± 0.218 ^{bc}	1.289 ± 0.220 ^{bc}	0.586 ± 0.074 ^{ab}	2.434 ± 0.254 ^{ab}	1.340 ± 0.229 ^c
B9	0.301 ± 0.095 ^{cde}	1.795 ± 0.198 ^{bc}	1.845 ± 0.245 ^a	0.206 ± 0.082 ^{cde}	1.600 ± 0.135 ^{bcd}	1.603 ± 0.206 ^{ab}	0.502 ± 0.102 ^{bc}	2.390 ± 0.293 ^{bc}	1.365 ± 0.259 ^c
B10	0.210 ± 0.109 ^{de}	1.511 ± 0.384 ^{cde}	1.722 ± 0.507 ^{ab}	0.192 ± 0.073 ^{de}	1.335 ± 0.222 ^d	1.497 ± 0.418 ^b	0.559 ± 0.102 ^b	2.349 ± 0.368 ^{bc}	1.478 ± 0.394 ^{abc}
B11	0.444 ± 0.090 ^b	1.881 ± 0.187 ^b	1.523 ± 0.213 ^{abc}	*	*	*	*	*	*
B12	0.263 ± 0.071 ^{cde}	1.686 ± 0.131 ^{bode}	1.736 ± 0.298 ^{ab}	0.095 ± 0.038 ^e	1.573 ± 0.161 ^{bcd}	2.017 ± 0.394 ^a	0.354 ± 0.071 ^d	2.149 ± 0.207 ^{bc}	1.908 ± 0.302 ^a
B13	0.173 ± 0.108 ^e	1.489 ± 0.178 ^{cde}	1.839 ± 0.425 ^a	0.192 ± 0.149 ^{de}	1.559 ± 0.338 ^{bcd}	1.668 ± 0.711 ^{ab}	0.387 ± 0.176 ^{cd}	2.078 ± 0.318 ^{bc}	1.736 ± 0.635 ^{abc}
B14	0.375 ± 0.080 ^{bc}	1.806 ± 0.240 ^{bc}	1.440 ± 0.320 ^{abc}	*	*	*	*	*	*
B15	0.222 ± 0.109 ^{de}	1.378 ± 0.282 ^e	1.400 ± 0.490 ^{bc}	0.280 ± 0.069 ^{bcd}	1.545 ± 0.177 ^{cd}	1.605 ± 0.445 ^{ab}	0.544 ± 0.082 ^b	2.367 ± 0.211 ^{dbc}	1.491 ± 0.353 ^{abc}

The statistical analysis was conducted by one-way ANOVA with Bonferroni correction ($p=0.0036$ for white-light leaves, and $p=0.005$ for blue- and red-light-leaves) followed by Tukey's test. Data were collected from approximate 24 leaf discs of 4 replicates at 4 dpi and presented as mean ± S.D. Significant differences between *B. cinerea* isolates were indicated with different letters. * means that the isolates were not tested on blue- or red-light-leaves.

(Cerrudo et al., 2012; Ballaré, 2014). In contrast blue-light-developed leaves were more susceptible to some of the isolates, including B1, B2, B9, B12, and B13 (**Figure 6**) and had lower level of anthocyanins compared to leaves grown under white and red lights (**Supplementary Table 2**). Here, both the increased hydrogen peroxide level as well as the reduced anthocyanin level might explain the increased susceptibility (Bassolino et al., 2013; Meng et al., 2019).

F_v/F_m Is the Best Indicator for Early Detection of *Botrytis cinerea* on Strawberry Leaves

Virulence of the *Botrytis* isolates on strawberry leaves derived from different light quality pretreatments was also assessed by imaging. The decrease in F_v/F_m synchronized with the development of lesion size, which was visualized on fluorescence images in dark red (**Figure 7**, **Supplementary Figures 4** and **5**). Strong correlations between F_v/F_m and disease index were observed in strawberry leaves derived from white ($r = 0.985$), blue ($r = 0.97$), and red ($r = 0.978$) LEDs (**Figure 8**).

F_v/F_m responded well to the development of *Botrytis* disease in strawberry leaves. Both biotic and abiotic stress factors decrease the efficiency of photosynthesis and suppress the variable fluorescence of dark-adapted chlorophyll-containing leaves correspondingly. F_v/F_m decreases along with the increasing effect of stresses (Rolfe and Scholes, 2010; Gorbe and Calatayud, 2012). This reduction in F_v/F_m suggests destructive changes in chloroplasts and photosystem II caused by *B. cinerea* infection. Here ChlDx was clearly not as sensitive as F_v/F_m , only at higher disease indices (> 50%) this parameter decreased. Furthermore, F_v/F_m could discriminate virulence of the *B. cinerea* isolates. Higher virulence resulted in a stronger decrease in F_v/F_m , and lower virulence in smaller F_v/F_m reduction. In this study, the infectious symptom by *B. cinerea* were predominantly observed at 2 dpi based on chlorophyll fluorescence image. Chaerle et al. (2007) also showed that chlorophyll fluorescence imaging can be used for early detection of *Botrytis* infection. Autofluorescence signals (F_{440}/F_{740}) after *Botrytis* inoculation on grape berries could only be recorded 4 days after infection (Bélanger et al., 2011), which is a delay of 2 days in comparison with F_v/F_m and 1 day in comparison with ChlDx response.

Anthocyanins are water-soluble pigments responsible for the red colors in leaves. Different abiotic stresses enhance the biosynthesis of anthocyanins in leaves, and anthocyanins act as antioxidant and reactive oxygen scavengers (Landi et al., 2015). Heim et al. (1983) described that zones of anthocyanin accumulation often surround restricted lesions where a plant disease has been successfully contained, whereas low anthocyanin levels often occur in susceptible combinations of maize. Additionally, anthocyanins levels are negatively correlated with the susceptibility to *B. cinerea* in tomato fruit (Bassolino et al., 2013). *B. cinerea* infection causes hydrogen peroxide accumulation which leads to the accumulation of anthocyanin at the infectious site (Chalker-Scott, 1999; Govrin and Levine, 2000). In this study, foliar anthocyanins are

TABLE 3 | Effect of light quality on the virulence of the *B. cinerea* isolates assessed by chlorophyll fluorescence imaging (F_v/F_m) and image-based indices (Chlldx, and mArildx) at 4 dpi.

Botrytis isolates	F_v/F_m			Chlldx			mArildx		
	White	Blue	Red	White	Blue	Red	White	Blue	Red
B1	0.234a	0.385a	0.349a	1.613a	1.053b	1.832a	1.598ab	1.432b	1.818a
B2	0.299ab	0.108b	0.413a	1.786a	1.441a	1.842a	1.816a	1.626a	1.749a
B3	0.215b	0.508a	0.514a	1.510b	1.913a	2.225a	1.633a	1.526a	1.452a
B7	0.639b	0.592c	0.714a	2.327ab	2.230b	2.542a	0.978b	1.019ab	1.261a
B8	0.395b	0.379b	0.577a	1.724b	1.647b	2.376a	1.464a	1.290a	1.342a
B9	0.306b	0.208c	0.498a	1.882b	1.596c	2.264a	1.779a	1.702a	1.374b
B10	0.207b	0.182bc	0.558a	1.541b	1.342b	2.336a	1.686a	1.604a	1.486a
B12	0.235b	0.075c	0.356a	1.716ab	1.581b	1.974a	1.735a	2.045a	1.826a
B13	0.176a	0.204a	0.312a	1.490b	1.572b	2.164a	1.875a	1.663a	1.763a
B15	0.189c	0.306b	0.545a	1.449b	1.545b	2.597a	1.379 a	1.598a	1.486a

The assessment was performed for strawberry leaves that developed respectively under full spectrum white LED light (white), monochromatic blue LED (blue), and monochromatic red LED (red) light. As light quality influences metabolite levels in the leaves, ANCOVA was performed and adjusted means were calculated with Bonferroni as confidence interval adjustment and the covariates are the values of F_v/F_m , Chlldx, and mArildx at 0 dpi. Data are means of 24 replicates. Different letters indicate significant differences for each isolate between the light treatments per parameter.

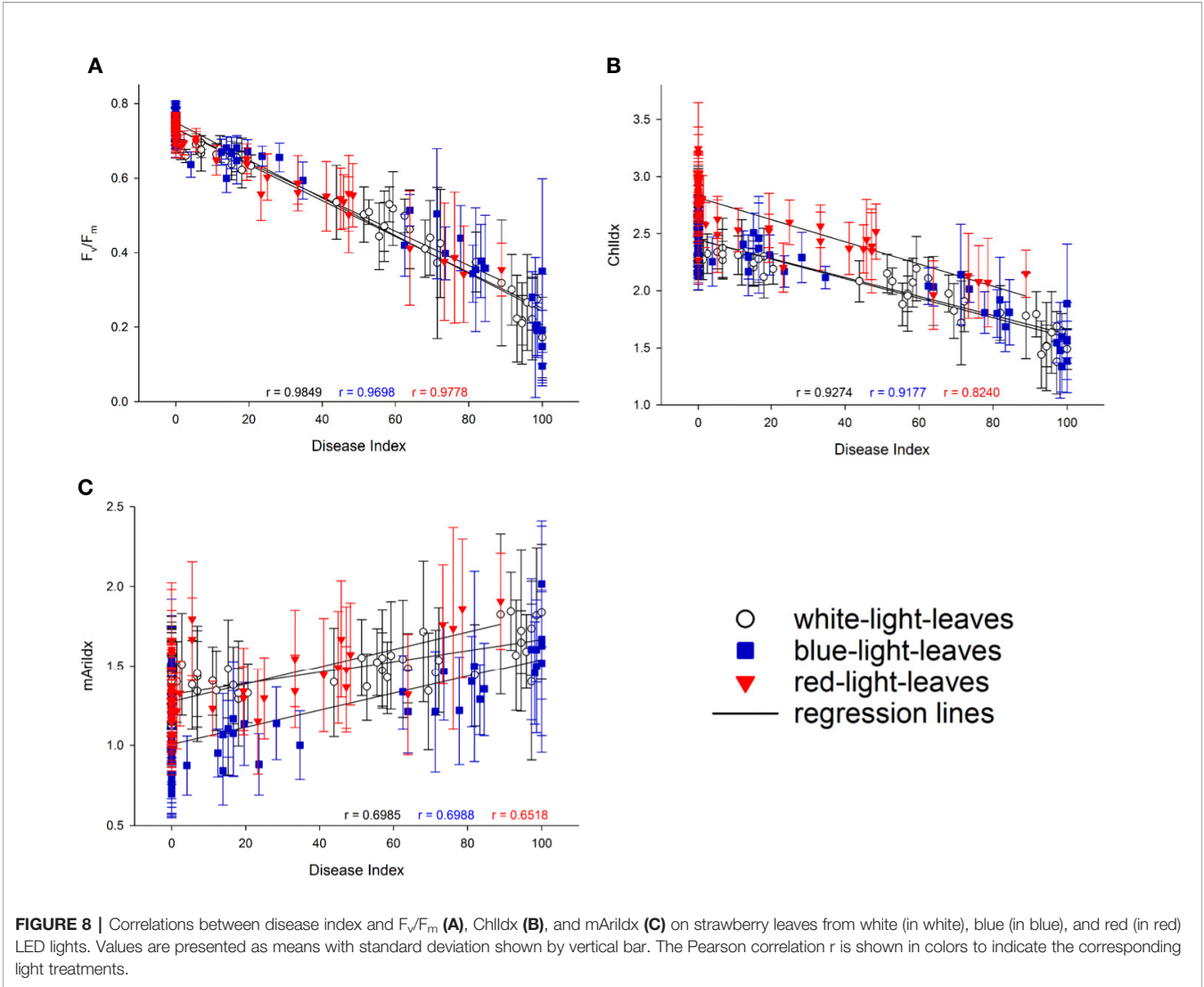


FIGURE 8 | Correlations between disease index and F_v/F_m (A), Chlldx (B), and mArildx (C) on strawberry leaves from white (in white), blue (in blue), and red (in red) LED lights. Values are presented as means with standard deviation shown by vertical bar. The Pearson correlation r is shown in colors to indicate the corresponding light treatments.

indicated by mArIIdx. Along with the pathogen invasion, anthocyanins accumulated at the infectious site as visualized in **Figure 7** and **Supplementary Figures 4** and **5**. Despite the antioxidative role of anthocyanins responding to stresses, few study focuses on its development along with pathogen infection by imaging technology. Here the blue-light-leaves which had an increased susceptibility to *Botrytis*, showed significant lower basal anthocyanin level compared to leaves derived from white and red lights (**Supplementary Table 2**). On the other hand, *B. cinerea* isolates with higher virulence induced a higher anthocyanin content (**Supplementary Table 3**), this was due to the higher accumulation of hydrogen peroxide caused by *Botrytis* infection. Furthermore, weaker correlations between *Botrytis* disease index and anthocyanin level are observed, compared to F_v/F_m and ChlIdx. Therefore, it seems that ArIIdx is more a supporting observation, but less useful for the early detection.

Horticultural Implications

B. cinerea causes significant losses in plant greenhouse production, storage, shipping, and marketing, which makes control of gray mold very important (Michailides and Elmer, 2000; Karchani-Balma et al., 2008; González et al., 2009). To control this pathogen cultural, chemical, and biological methods, as well as plant resistance breeding are used (Pande et al., 2006). However, the complexity and variability of this pathogen are reasons that make control difficult (Mirzaei et al., 2009). Awareness of the existence of pathogen variability together with the new insights in photobiological responses of both pathogen and plants may contribute to more efficient non-chemical methods of control. Here it is confirmed that red LED irradiance improved leaf resistance not only to one *B. cinerea* strain, but to all tested isolates in this study. Therefore, red LEDs have potential to be used in plant production system to control gray mold but this should be further investigated in greenhouse conditions. Moreover, effects of red LED irradiance on *Botrytis* infections on strawberry flowers and fruits need to be assessed.

Many biotic stress symptoms start as spots or patches within a crop. Such symptoms could be discovered with imaging techniques at an early stage, when no visible symptoms are yet apparent. The possibility of early stress detection allows timely treatment to prevent pathogen spread within the crop and greenhouse, which would result in limited yield loss and reduced chemicals usage. Today robots equipped with sensors are under investigation in greenhouse production. A UV-Robot with UV-C radiation is developed to control powdery mildew in horticulture (Mazar et al., 2018). This could also be equipped with imaging sensors, as early detection of disease is beneficial from both economic and environmental perspectives. In this study we evaluated imaging sensors in a highly controlled environment, without interference from other environmental factors such as wind, fluctuating light intensities, and temperature. Moreover, in horticultural production systems, not only environmental factors change in a dynamic way but also crop-dependent factors such as leaf morphology and orientation, leaf waxes and hairs, and leaf density might influence the response. Therefore, the potential of early detection of gray mold by chlorophyll fluorescence imaging

in horticulture needs further validation in a greenhouse environment (Gorbe and Calatayud, 2012; Mahlein, 2016).

CONCLUSION

Here it is clearly shown that *B. cinerea* isolates differently respond to different light qualities in phenotypes such as mycelial growth, sporulation, and sclerotia formation. Despite differences in virulence, red light considerably improved leaf basal resistance against all the tested *B. cinerea* isolates, while blue light pretreatment increased leaf susceptibility to some of them. Disease development caused by different *B. cinerea* isolates is highly correlated with F_v/F_m (maximal PSII quantum efficiency), meaning that this indicator can be used to objectively quantify *B. cinerea* disease severity and may also be useful for early detection of plant stress related to gray mold infection. Overall, red LED light has potential to control gray mold in greenhouse production, and image sensors could be developed into a new technology for early disease detection.

DATA AVAILABILITY STATEMENT

The raw data supporting the conclusions of this article will be made available by the authors, without undue reservation.

AUTHOR CONTRIBUTIONS

LM, HM, MH, and M-CL conceived and designed the experiments. HM performed the experiments of light quality effects on phenotypic variations in the 15 *Botrytis* isolates. LM conducted the experiments of pathogenic test of *Botrytis* isolates on strawberry leaves developed under white, blue, and red LED lights and of imaging from the phenotyping platform. MA and KA guided the experiments on the phenotyping platform and image data analysis. LM analyzed the data and drafted the manuscript. HM, MA, KA, MH, and M-CL critically revised the manuscript. LM, MH, and M-CL reviewed and approved the final manuscript.

FUNDING

The first author has a grant of the China Scholarship Council (CSC).

SUPPLEMENTARY MATERIAL

The Supplementary Material for this article can be found online at: <https://www.frontiersin.org/articles/10.3389/fpls.2020.01233/full#supplementary-material>

REFERENCES

- Alfonso, C., Raposo, R., and Melgarejo, P. (2000). Genetic diversity in Botrytis cinerea populations on vegetable crops in greenhouses in south-eastern Spain. *Plant Pathol.* 49 (2), 243–251. doi: 10.1046/j.1365-3059.2000.00452.x
- Asadollahi, M., Fekete, E., Karaffa, L., Flippini, M., árnyasi, M., Esmaeili, M., et al. (2013). Comparison of Botrytis cinerea populations isolated from two open-field cultivated host plants. *Microbiol. Res.* 168 (6), 379–388. doi: 10.1016/j.micres.2012.12.008
- Baker, N. R. (2008). Chlorophyll Fluorescence: A Probe of Photosynthesis In Vivo. *Annu. Rev. Plant Biol.* 59 (1), 89–113. doi: 10.1146/annurev.arplant.59.032607.092759
- Ballaré, C. L. (2014). Light regulation of plant defense. *Annu. Rev. Plant Biol.* 65, 335–363. doi: 10.1146/annurev-arplant-050213-040145
- Baraldi, E., Bertolini, P., Chierici, E., Truffelli, B., and Luiselli, D. (2002). Genetic diversity between Botrytis cinerea isolates from unstored and cold stored kiwi fruit. *J. Phytopathol.* 150 (11–12), 629–635. doi: 10.1046/j.1439-0434.2002.00809.x
- Bassolino, L., Zhang, Y., Schoonbeek, H. J., Kiferle, C., Perata, P., and Martin, C. (2013). Accumulation of anthocyanins in tomato skin extends shelf life. *New Phytol.* 200 (3), 650–655. doi: 10.1111/nph.12524
- Bélanger, M. C., Roger, J. M., Cartolaro, P., and Fermaud, M. (2011). Autofluorescence of grape berries following Botrytis cinerea infection. *Int. J. Remote Sens.* 32 (14), 3835–3849. doi: 10.1080/01431161003782064
- Björkman, O., and Demmig, B. (1987). Photon yield of O₂ evolution and chlorophyll fluorescence characteristics at 77 K among vascular plants of diverse origins. *Planta* 170 (4), 489–504. doi: 10.1007/BF00402983
- Canessa, P., Schumacher, J., Hevia, M. A., Tudzynski, P., and Larrondo, L. F. (2013). Assessing the effects of light on differentiation and virulence of the plant pathogen botrytis cinerea: Characterization of the white collar complex. *PLoS One* 8 (12), e84223. doi: 10.1371/journal.pone.0084223
- Cerrudo, I., Keller, M. M., Cargnel, M. D., Demkura, P. V., de Wit, M., Patitucci, M. S., et al. (2012). Low red/far-red ratios reduce Arabidopsis resistance to Botrytis cinerea and jasmonate responses via a COI1-JAZ10-dependent, salicylic acid-independent mechanism. *Plant Physiol.* 158 (4), 2042–2052. doi: 10.1104/pp.112.193359
- Chaerle, L., Hagenbeek, D., Vanrobaeys, X., and Van Der Straeten, D. (2007). Early detection of nutrient and biotic stress in Phaseolus vulgaris. *Int. J. Remote Sens.* 28 (16), 3479–3492. doi: 10.1080/01431160601024259
- Chalker-Scott, L. (1999). Environmental significance of anthocyanins in plant stress responses. *Photochem. Photobiol.* 70 (1), 1–9. doi: 10.1111/j.1751-1097.1999.tb01944.x
- Cotoras, M., and Silva, E. (2005). Differences in the initial events of infection of Botrytis cinerea strains isolated from tomato and grape. *Mycologia* 97 (2), 485–492. doi: 10.3852/mycologia.97.2.485
- Debode, J., Van Hemelrijck, W., Xu, X. M., Maes, M., Creemers, P., and Heungens, K. (2015). Latent entry and spread of Colletotrichum acutatum (species complex) in strawberry fields. *Plant Pathol.* 64 (2), 385–395. doi: 10.1111/ppa.12247
- Derckel, J. P., Baillieux, F., Manteau, S., Audran, J. C., Haye, B., Lambert, B., et al. (1999). Differential induction of grapevine defenses by two strains of Botrytis cinerea. *Phytopathology* 89 (3), 197–203. doi: 10.1094/PHYTO.1999.89.3.197
- Di Lenna, P., Marciano, P., and Magro, P. (1981). Comparative Investigation on Morphological and Physiological Features of Three Isolates of Botrytis cinerea. *J. Phytopathol.* 100 (3), 203–211. doi: 10.1111/j.1439-0434.1981.tb03293.x
- Elad, Y., Pertot, I., Cotes Prado, A. M., and Stewart, A. (2016). *Plant hosts of Botrytis spp. Botrytis - the fungus, the pathogen and its management in agricultural systems*. Switzerland: Springer International Publishing. doi: 10.1007/978-3-319-23371-0_20
- Faretra, F., and Pollastro, S. (1991). Genetics of resistance to benzimidazole and dicarboximide fungicides in isolates of Botryotinia fuckeliana (Botrytis cinerea). *Mycol. Res.* 95 (8), 943–951. doi: 10.1111/j.1365-3059.1993.tb02933.x
- Gitelson, A. A., Chivkunova, O. B., and Merzlyak, M. N. (2009). Nondestructive estimation of anthocyanins and chlorophylls in anthocyanic leaves. *Am. J. Bot.* 96 (10), 1861–1868. doi: 10.3732/ajb.0800395
- González, G., Moya, M., Sandoval, C., and Herrera, R. (2009). Genetic diversity in Chilean strawberry (Fragaria chiloensis): differential response to Botrytis cinerea infection. *Spanish J. Agric. Res.* 7 (4), 886. doi: 10.5424/sjar/2009074-1102
- Gorbe, E., and Calatayud, A. (2012). Applications of chlorophyll fluorescence imaging technique in horticultural research: A review. *Sci. Hortic.* 138, 24–35. doi: 10.1016/j.scienta.2012.02.002
- Govrin, E. M., and Levine, A. (2000). The hypersensitive response facilitates plant infection by the necrotrophic pathogen Botrytis cinerea. *Curr. Biol.* 10, 751–757. doi: 10.1016/S0960-9822(00)00560-1
- Hamada, W., Reignault, P., Bompeix, G., and Boccara, M. (1994). Transformation of Botrytis cinerea with the hygromycin B resistance gene, hph. *Curr. Genet.* 26 (3), 251–255. doi: 10.1007/BF00309556
- Heim, D., Nicholson, R. L., Pascholati, S. F., Hagerman, A. E., and Billett, W. (1983). Etiolated Maize Mesocotyls: A Tool for Investigating Disease Interactions. *Phytopathology* 73, 424–428. doi: 10.1094/phyto-73-424
- Isenegger, D. A., MacLeod, W. J., Ford, R., and Taylor, P. W. J. (2008). Genotypic diversity and migration of clonal lineages of Botrytis cinerea from chickpea fields of Bangladesh inferred by microsatellite markers. *Plant Pathol.* 57 (5), 967–973. doi: 10.1111/j.1365-3059.2008.01885.x
- Kalaji, H. M., Schansker, G., Ladle, R. J., Goltsev, V., Bosa, K., Allakhverdiev, S.II, et al. (2014). Frequently asked questions about *in vivo* chlorophyll fluorescence: Practical issues. *Photosyn. Res.* 122 (2), 121–158. doi: 10.1007/s11120-014-0024-6
- Karchani-Balma, S., Gautier, A., Raies, A., and Fournier, E. (2008). Geography, plants, and growing systems shape the genetic structure of Tunisian Botrytis cinerea populations. *Phytopathology* 98 (12), 1271–1279. doi: 10.1094/PHYTO-98-12-1271
- Kerssies, A., Bosker-van Zessen, A.II, Wagemakers, C. A. M., and Van Kan, J. A. L. (1997). Variation in pathogenicity and DNA polymorphism among Botrytis cinerea isolates sampled inside and outside a glasshouse. *Plant Dis.* 81 (7), 781–786. doi: 10.1094/PDIS.1997.81.7.781
- Khazaeli, P., Zamanizadeh, H., Morid, B., and Bayat, H. (2010). Morphological and Molecular Identification of Botrytis Cinerea Causal Agent of Gray Mold in Rose Greenhouses in Central Regions of Iran. *Int. J. Agric. Sci. Res.* 1 (1), 20–24.
- Kretschmer, M., and Hahn, M. (2008). Fungicide resistance and genetic diversity of Botrytis cinerea isolates from a vineyard in Germany. *J. Plant Dis. Prot.* 115 (5), 214–219. doi: 10.1007/bf03356266
- Kumari, S., Tayal, P., Sharma, E., and Kapoor, R. (2014). Analyses of genetic and pathogenic variability among Botrytis cinerea isolates. *Microbiol. Res.* 169 (11), 862–872. doi: 10.1016/j.micres.2014.02.012
- Kunz, C., Vandelle, E., Rolland, S., Poinssot, B., Bruel, C., Cimerman, A., et al. (2006). Characterization of a new, nonpathogenic mutant of Botrytis cinerea with impaired plant colonization capacity. *New Phytol.* 170 (3), 537–550. doi: 10.1111/j.1469-8137.2006.01682.x
- Kuzmanovska, B., Rusevski, R., Jankuloski, L., Jankulovska, M., Ivic, D., and Bandoz, K. (2012). Phenotypic and genetic characterization of Botrytis cinerea isolates from tomato. *Genetika* 44 (3), 633–647. doi: 10.2298/GENSER1203663K
- Landi, M., Tattini, M., and Gould, K. S. (2015). Multiple functional roles of anthocyanins in plant-environment interactions. *Environ. Exp. Bot.* 119, 4–17. doi: 10.1016/j.envexpbot.2015.05.012
- Mahlein, A.-K. (2016). Present and Future Trends in Plant Disease Detection. *Plant Dis.* 100 (2), 1–11. doi: 10.1007/s13398-014-0173-7.2
- Martinez, F., Blancard, D., Lecomte, P., Levis, C., Dubos, B., and Fermaud, M. (2003). Phenotypic differences between vacuola and transposon subpopulations of Botrytis cinerea. *Eur. J. Plant Pathol.* 109 (5), 479–488. doi: 10.1023/A:1024222206991
- Martinez, F., Dubos, B., and Fermaud, M. (2005). The role of saprotrophy and virulence in the population dynamics of Botrytis cinerea in vineyards. *Phytopathology* 95 (6), 692–700. doi: 10.1094/PHYTO-95-0692
- Martinez, F., Corio-Costet, M. F., Levis, C., Coarer, M., and Fermaud, M. (2008). New PCR primers applied to characterize distribution of Botrytis cinerea populations in french vineyards. *Vitis - J. Grapevine Res.* 47 (4), 217–226. doi: 10.5073/vitis.2008.47.217-226
- Mazar, M., Sahnoun, M., Bettayeb, B., and Klement, N. (2018). Optimization of Robotized Tasks for the UV-C Treatment of Diseases in Horticulture. *Int. Conf. Afr. Fed. Oper. Res. Soc.* 1–4.
- Meng, L., Höfte, M., and Van Labeke, M.-C. (2019). Leaf age and light quality influence the basal resistance against Botrytis cinerea in strawberry leaves. *Environ. Exp. Bot.* 157, 35–45. doi: 10.1016/j.envexpbot.2018.09.025
- Michailides, T. J., and Elmer, P. A. G. (2000). Botrytis gray mold of Kiwifruit caused by Botrytis cinerea in the United States and New Zealand. *Plant Dis.* 84 (3), 208–223. doi: 10.1094/PDIS.2000.84.3.208

- Mirzaei, S., Mohammadi Goltapeh, E., Shams-Bakhsh, M., Safaie, N., and Chaichi, M. (2009). Genetic and phenotypic diversity among botrytis cinerea isolates in Iran. *J. Phytopathol.* 157 (7–8), 474–482. doi: 10.1111/j.1439-0434.2008.01518.x
- Muñoz, G., Hinrichsen, P., Brygoo, Y., and Giraud, T. (2002). Genetic characterisation of Botrytis cinerea populations in Chile. *Mycol. Res.* 106 (5), 594–601. doi: 10.1017/S0953756202005981
- Okamoto, K., Yanagi, T., Takita, S., Tanaka, M., Higuchi, T., Ushida, Y., et al. (1996). Development of plant growth apparatus using blue and red LED as artificial light source. *Acta Hort.* 440, 111–116. doi: 10.17660/ActaHortic.1996.440.20
- Pande, S., Galloway, J., Gaur, P. M., Siddique, K. H. M., Tripathi, H. S., Taylor, P., et al. (2006). Botrytis grey mould of chickpea: A review of biology, epidemiology, and disease management. *Aust. J. Agric. Res.* 57 (11), 1137–1150. doi: 10.1071/AR06120
- Pande, S., Sharma, M., Kishore, G. K., Shivram, L., and Mangala, U. N. (2010). Characterization of Botrytis cinerea isolates from chickpea: DNA polymorphisms, cultural, morphological and virulence characteristics. *Afr. J. Biotechnol.* 9 (46), 7961–7967. doi: 10.5897/ajb10.1361
- Petrash, S., Knapp, S. J., van Kan, J. A. L., and Blanco-Ulate, B. (2019). Grey mould of strawberry, a devastating disease caused by the ubiquitous necrotrophic fungal pathogen Botrytis cinerea. *Mol. Plant Pathol.* 20 (6), 877–892. doi: 10.1111/mpp.12794
- Quidde, T., Osbourn, A. E., and Tudzynski, P. (1998). Detoxification of α -tomatine by Botrytis cinerea. *Physiol. Mol. Plant Pathol.* 52 (3), 151–165. doi: 10.1006/pmpp.1998.0142
- Reignault, P., Mercier, M., Bompeix, G., and Boccara, M. (1994). Pectin methylesterase from Botrytis cinerea: Physiological, biochemical and immunochemical studies. *Microbiology* 140 (12), 3249–3255. doi: 10.1099/13500872-140-12-3249
- Rodriguez-Romero, J., Hedtke, M., Kastner, C., Uller, S., and Fischer, R. (2010). Fungi, Hidden in Soil or Up in the Air: Light Makes a Difference. *Annu. Rev. Microbiol.* 64, 585–610. doi: 10.1146/annurev.micro.112408.134000
- Rolfe, S. A., and Scholes, J. D. (2010). Chlorophyll fluorescence imaging of plant-pathogen interactions. *Protoplasma* 247 (3), 163–175. doi: 10.1007/s00709-010-0203-z
- Schumacher, J. (2012). Tools for Botrytis cinerea: New expression vectors make the gray mold fungus more accessible to cell biology approaches. *Fungal Genet. Biol.* 49 (6), 483–497. doi: 10.1016/j.fgb.2012.03.005
- Schumacher, J. (2017). How light affects the life of Botrytis. *Fungal Genet. Biol.* 106, 26–41. doi: 10.1016/j.fgb.2017.06.002
- Sharma, E., and Kapoor, R. (2017). Insights into the molecular interplay of virulence factors in Botrytis cinerea. *Australas. Plant Pathol.* 46 (6), 551–561. doi: 10.1007/s13313-017-0519-7
- Stewart, T. M., and Long, P. G. (1987). Sporulation of Botrytis cinerea in the dark. *New Z. J. Exp. Agric.* 15 (3), 389–392. doi: 10.1080/03015521.1987.10425587
- Sun, G., Feng, C., Zhang, A., Zhang, Y., Chang, D., Wang, Y., et al. (2019). The dual role of oxalic acid on the resistance of tomato against Botrytis cinerea. *World J. Microbiol. Biotechnol.* 35 (2), 1–7. doi: 10.1007/s11274-019-2603-3
- Tan, K. K., and Epton, H. A. S. (1973). Effect of light on the growth and sporulation of Botrytis cinerea. *Trans. Br. Mycol. Soc.* 61 (1), 145–157. doi: 10.1016/S0007-1536(73)80096-8
- Tan, B. K. K. (1975). Interaction of near-ultraviolet, blue, red, and far-red light in sporulation of Botrytis cinerea. *Trans. Br. Mycol. Soc.* 64 (2), 215–222. doi: 10.1016/S0007-1536(75)80105-7
- Thompson, J. R., and Latorre, B. A. (1999). Characterization of Botrytis cinerea from table grapes in Chile using RAPD-PCR. *Plant Dis.* 83 (12), 1090–1094. doi: 10.1094/PDIS.1999.83.12.1090
- Williamson, B., Tudzynski, B., Tudzynski, P., and Van Kan, J. A. L. (2007). Botrytis cinerea: The cause of grey mould disease. *Mol. Plant Pathol.* 8 (5), 561–580. doi: 10.1111/j.1364-3703.2007.00417.x

Conflict of Interest: The authors declare that the research was conducted in the absence of any commercial or financial relationships that could be construed as a potential conflict of interest.

Copyright © 2020 Meng, Mestdagh, Ameye, Audenaert, Höfte and Van Labeke. This is an open-access article distributed under the terms of the Creative Commons Attribution License (CC BY). The use, distribution or reproduction in other forums is permitted, provided the original author(s) and the copyright owner(s) are credited and that the original publication in this journal is cited, in accordance with accepted academic practice. No use, distribution or reproduction is permitted which does not comply with these terms.



Combined Proteome and Transcriptome Analysis of Heat-Primed Azalea Reveals New Insights Into Plant Heat Acclimation Memory

Xiuyun Wang¹, Zheng Li¹, Bing Liu¹, Hong Zhou¹, Mohamed S. Elmongy^{1,2} and Yiping Xia^{1*}

¹ Genomics and Genetic Engineering Laboratory of Ornamental Plants, Department of Horticulture, College of Agriculture and Biotechnology, Zhejiang University, Hangzhou, China, ² Department of Vegetable and Floriculture, Faculty of Agriculture, Mansoura University, Mansoura, Egypt

OPEN ACCESS

Edited by:

Lucia Guidi,
University of Pisa, Italy

Reviewed by:

Klára Kosová,
Crop Research Institute (CRI), Czechia
Eduardo Zabaleta,
CONICET Mar del Plata, Argentina

*Correspondence:

Yiping Xia
ypxia@zju.edu.cn

Specialty section:

This article was submitted to
Plant Abiotic Stress,
a section of the journal
Frontiers in Plant Science

Received: 31 March 2020

Accepted: 05 August 2020

Published: 19 August 2020

Citation:

Wang X, Li Z, Liu B, Zhou H,
Elmongy MS and Xia Y (2020)
Combined Proteome and
Transcriptome Analysis of Heat-
Primed Azalea Reveals New Insights
Into Plant Heat Acclimation Memory.
Front. Plant Sci. 11:1278.
doi: 10.3389/fpls.2020.01278

Plants can obtain superinduction of defense against unpredictable challenges based on prior acclimation, but the mechanisms involved in the acclimation memory are little known. The objective of this study was to characterize mechanisms of heat acclimation memory in *Rhododendron hainanense*, a thermotolerant wild species of azalea. Pretreatment of a 2-d recovery (25/18°C, day/night) after heat acclimation (37°C, 1 h) (AR-pt) did not weaken but enhanced acquired thermotolerance in *R. hainanense* with less damaged phenotype, net photosynthetic rate, and membrane stability than non-acclimation pretreated (NA-pt) plants. Combined transcriptome and proteome analysis revealed that a lot of heat-responsive genes still maintained high protein abundance rather than transcript level after the 2-d recovery. Photosynthesis-related genes were highly enriched and most decreased under heat stress (HS: 42°C, 1 h) with a less degree in AR-pt plants compared to NA-pt. Sustainably accumulated chloroplast-localized heat shock proteins (HSPs), Rubisco activase 1 (RCA1), beta-subunit of chaperonin-60 (CPN60β), and plastid transcriptionally active chromosome 5 (pTAC5) in the recovery period probably provided equipped protection of AR-pt plants against the subsequent HS, with less damaged photochemical efficiency and chloroplast structure. In addition, significant higher levels of RCA1 transcripts in AR-pt compared to NA-pt plants in early stage of HS showed a more important role of RCA1 than other chaperonins in heat acclimation memory. The novel heat-induced RCA1, rather than constitutively expressed RCA2 and RCA3, showed excellent thermostability after long-term HS (LHS: 42/35°C, 7 d) and maintained balanced Rubisco activation state in photosynthetic acclimation. This study provides new insights into plant heat acclimation memory and indicates candidate genes for genetic modification and molecular breeding in thermotolerance improvement.

Keywords: heat acclimation, acquired thermotolerance, photosynthesis, Rubisco activase, heat shock protein, proteome, transcriptome, *Rhododendron hainanense*

INTRODUCTION

Sessile plants constantly experience daily and seasonal fluctuations of environmental temperatures in nature. The ability to retain “a memory” or “stress imprint” of prior exposure to certain priming conditions for a certain length of time can make a plant more tolerant to future stress (Bruce et al., 2007; Wu et al., 2013; Martinez-Medina et al., 2016). Defense priming is an adaptive trait for promoting the plant to a persistently primed state of defense readiness for unpredictable environments, resulting in enhanced pest and disease resistance and abiotic stress tolerance (Conrath et al., 2006; Walter et al., 2013; Martinez-Medina et al., 2016). The primed memory can be induced by various natural and synthetic compounds, as well as biotic and abiotic stimuli (Conrath et al., 2006; Conrath et al., 2015). In the primed state, plants have some costs for storage of priming information but will have better performance during the subsequent stress, that is, priming enhanced plant benefit (Martinez-Medina et al., 2016). Moreover, frequent recurring stress memory can extend into future generations (Ramirez-Carrasco et al., 2017), which may be an evolutionary force for plants adapting to rugged environments. Therefore, it is necessary to investigate the mechanisms involved in stress memory and apply it into tolerance improvement or genetic modification for cultivar breeding by regulation of plant natural defense system.

With exposure to moderately elevated temperatures, plants can obtain acquired thermotolerance against subsequent otherwise lethal heat stress (HS), which is termed as heat acclimation (Wu et al., 2013). During this process, plants trigger the genetically reprogrammed heat shock response that activates multiple protection mechanisms. The main defense cascades that have been identified contain heat stress transcription factors (HSFs), which regulate heat shock proteins (HSPs) for protein folding and protection and some antioxidative or metabolic enzymes, such as ascorbate peroxidase 2 (APX2) and galactinol synthase 1 (GOLS1) (Mueller et al., 2015). However, after returning to control temperature after heat acclimation, how plants retain the memory of prior acclimation in the case of recurring HS has not been well understood. HsFA2 has been proven to be a heat-inducible transactivator sustaining the expression of heat-stress-associated 32-kDa protein coding gene (*HSA32*) and class I small HSP genes (*sHSPs*) to extend the duration of acquired thermotolerance after a long recovery period (>24 h) in *Arabidopsis* (Charng et al., 2006; Charng et al., 2007). A subsequent study demonstrated that a positive feedback loop between HSP101 and HSA32 helps to prolong heat acclimation memory (Wu et al., 2013). In addition, the upstream regulation mechanisms, including *miR156* and H3K4 methylation, were also investigated to determine their involvement in heat stress memory (Bäurle, 2016; Liu et al., 2018a). However, these results need more studies to verify, and whether other factors participate in heat memory and how memory is sustained in woody plants warrants further investigation.

Photosystem is the most sensitive component in response to HS. Inhibition of photosynthesis by HS is primarily attributable to the inactivation of ribulose-1,5-bisphosphate carboxylase/oxygenase (Rubisco), the central enzyme of the Calvin cycle for

carbon fixation during photosynthesis (Crafts-Brandner and Salvucci, 2000; Kim and Portis Jr, 2005; Niinemets et al., 2017). The inactivation of Rubisco does not result from its own thermal instability but rather from that of its activator, Rubisco activase (RCA) (Portis, 2003; Salvucci and Crafts-Brandner, 2004). RCA is a nuclear-encoded chloroplast protein that is observed in many photosynthetic organisms. RCA belongs to the AAA+ chaperonin family and repairs Rubisco by removing inhibitory sugar phosphates from the active sites to maintain Rubisco in an active conformation (Bracher et al., 2017). *Arabidopsis* with modified thermostable RCA improves photosynthesis and growth rates under moderate HS compared with the lines expressing wild-type RCA (Kurek et al., 2007). In contrast, silencing of RCA increased the heat sensitivity of photosynthesis, photochemical quantum yield, and Rubisco activation state in *Arabidopsis* and tobacco (Sharkey et al., 2001; Salvucci, 2008). These studies provide evidence that the thermal stability of RCA is a major factor limiting plant photosynthesis under HS, but whether RCA participates in heat acclimation memory has not been determined.

Azaleas, which belong to the genus *Rhododendron*, are well-known woody ornamental plants widely used in landscaping and as houseplants around the world (De Riek et al., 2018). However, wild azalea species are largely distributed in cool environmental conditions, and the majority of azaleas that are now cultivated display poor ornamental effects in hot-summer regions (Geng et al., 2019). High temperature is the primary obstacle affecting the landscape application of azaleas and will become even more relevant with global warming. In view of the rich diversity of azalea species, exploring heat-tolerant germplasm and illuminating the heat response mechanisms for cultivar breeding is an imperative. In our study, a heat-tolerant wild germplasm *Rhododendron hainanense* Merr. (Subgen. *Tsutsusi*) was investigated to elucidate the mechanisms of heat response. *R. hainanense* natively distributes at an altitude of 200 to 900 m in Hainan, the southernmost province of China, and has strong adaptability to high temperature environments (Liu et al., 2018b). We found that heat acclimation with a 2-d recovery to control temperature still can confer acquired thermotolerance to *R. hainanense* against subsequent severe HS, which displays defense memory during the recovery period. The objectives of this study were to characterize the mechanisms and key factors involved in the heat acclimation memory by combined transcriptomic, proteomic, and physiological analyses. Prolonged protection of photosynthetic apparatus by upregulated chaperonins during the recovery period was identified to be critical for the defense memory, and a potential role of the thermostable RCA in photosynthetic acclimation to HS was specifically discussed.

MATERIALS AND METHODS

Plant Growth Conditions and Heat Treatments

Cutting seedlings of *R. hainanense*, collected from Ornamental Germplasm Resource Nursery of Zhejiang University, were

cultivated in a greenhouse with rough temperature control in the range of 15°C to 30°C throughout the year. Uniform two-year-old cutting seedlings were transferred into growth chambers at control temperature (25/18°C, day/night) with 65% relative humidity and a 14-h photoperiod with 90 $\mu\text{mol photons m}^{-2} \text{s}^{-1}$ photosynthetically active radiation (PAR) for one month prior to treatments.

Plants were subjected to three different pretreatments before HS (42/35°C, day/night temperature) (**Figure 1A**): non-acclimation (NA-pt), acclimation (AC-t) (37°C, 1 h), and acclimation (37°C, 1 h) with a 2-d recovery to control temperature (AR-pt). There are three biological replicates for

each treatment. Samples were collected before HS, after 1 h of HS and 7 d of long-term HS (LHS). The two to five fully expanded leaves from the top of one to two branches of each plant were sampled at each time point for a replicate. The samples that are marked with same names (NA in NA-pt, AC-pt, and AR-pt, AC in AC-pt and AR-pt) were mixed. Eighteen samples (including replicates) indicated by green and orange dots were analyzed for transcriptome quantification individually, and 18 samples indicated by green and blue dots were analyzed for proteome quantification. Six samples (replicates mixed) indicated by green and orange dots were used to construct individual SMRTbell libraries, and the libraries were pooled with equimolar ratios

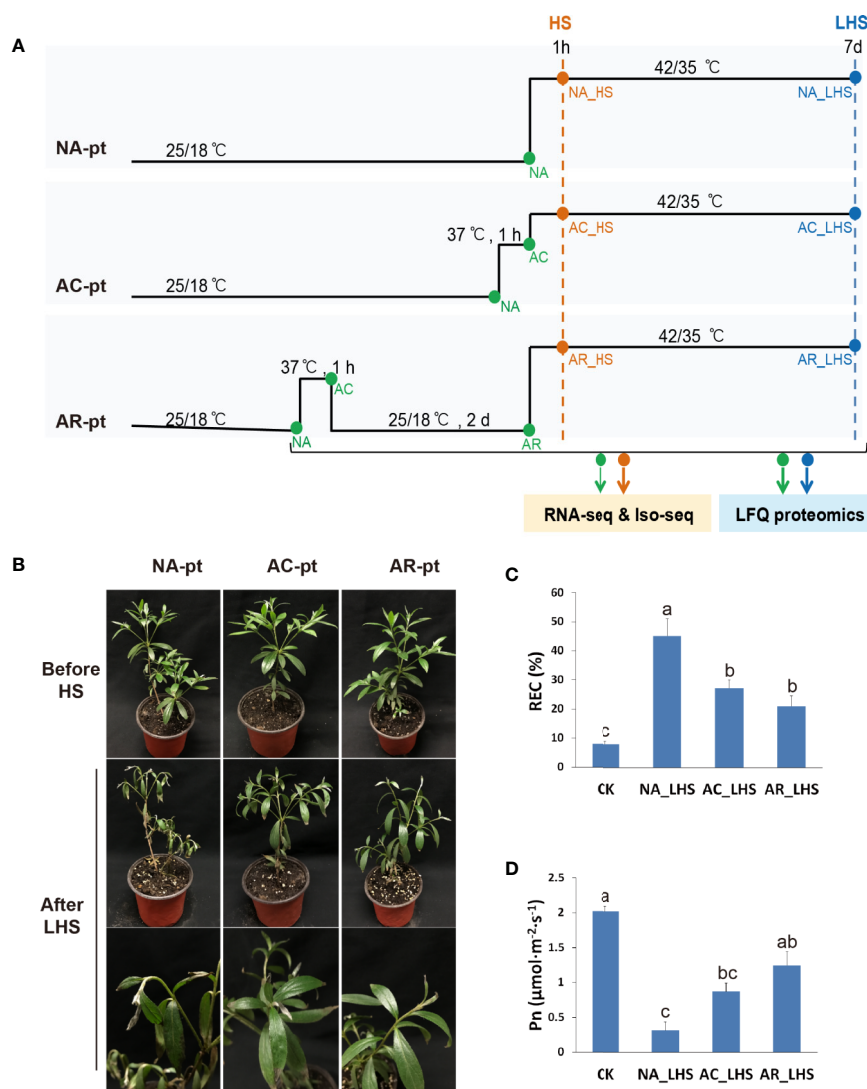


FIGURE 1 | Effects of different pretreatments on *R. hainanense* under heat stress. **(A)** Sketch map of the different pretreatments (pt), heat stress, and sampling time points. NA, non-acclimation; AC, acclimation; AR, acclimation with recovery; HS, heat stress; LHS, long-term heat stress. Green and orange dots indicate samples performed RNA-seq and Iso-seq. Green and blue dots indicate samples performed label-free quantification (LFQ) proteomics. **(B)** Plant phenotypes before HS and after a 7-d LHS. **(C)** Relative electrical conductivity (REC) and **(D)** net photosynthesis rate (Pn) of plants with different treatments. Control (CK), plants without any treatment. Data are expressed as the mean values \pm (standard deviation) SD of three biological replicates. Lowercase letters above the columns indicate multiple comparisons among different samples conducted by Duncan test at a significance level of 0.05.

before isoform-level transcriptome sequencing (Iso-seq) was performed. Collected leaves were flash frozen in liquid nitrogen and stored at -80°C .

Physiological Measurements

The leaf net photosynthetic rate (P_n) was measured using a LI-6400 portable photosynthesis system (LI-COR, Lincoln, NE, USA), with parameters of 500 flow, atmospheric CO_2 concentration, temperature at 25°C and PAR at $90\ \mu\text{mol photons m}^{-2}\text{ s}^{-1}$. Chlorophyll fluorescence, displayed as an F_v/F_m value, was detected by an Imaging-PAM chlorophyll fluorometer (Walz, Effeltrich, Germany). Plants were dark-adapted for 20 min before measurements, and the same position of each leaf was measured. Cellular membrane stability was estimated based on relative electrical conductivity (REC) (Blum and Ebercon, 1981). The initial (C_{ini}) and maximum (C_{max}) levels of REC were measured using a conductance meter (Thermo Scientific, Beverly, MA, USA). REC was calculated as $\text{REC (\%)} = (C_{\text{ini}}/C_{\text{max}}) \times 100$. Rubisco activation state was determined according to a previous method (Xu et al., 2013).

Chloroplast Ultrastructure Observation

For chloroplast ultrastructure observation by transmission electron microscopy, leaf samples measuring 1 mm^2 were fixed with 2.5% glutaraldehyde, embedded with resin, sliced by a Leica EM UC7 ultramicrotome (Leica Microsystems, Nussloch, Germany) and subjected to image acquisition with a HT7700 120KV transmission electron microscope (Hitachi, Tokyo, Japan).

Iso-Seq Analysis

Total RNA from azalea leaves was extracted using the RNeasy Pure Plant Plus Kit (Polysaccharides & Polyphenolics-rich) (TIANGEN, Beijing, China). Poly(A) RNA (mRNA) was enriched by oligo(dT) magnetic beads and quantified using the Agilent 2100 Bioanalyzer. Full-length first-strand cDNA was synthesized using a UMI base PCR cDNA Synthesis Kit (BGI, Shenzhen, China). After large-scale amplification, cDNA was used to construct two SMRT cell libraries (0–5 K and 4.5–10 K) using a DNA Template Prep Kit (Pacific Biosciences of California). SMRT sequencing was carried out on the Pacific Bioscience Sequel platform. Subreads were filtered to obtain high-quality consensus transcripts using the SMRT Analysis Server. Blastx (Altschul et al., 1990) or Diamond (Buchfink et al., 2015) was used for NR, KOG, KEGG, and Swiss-Prot annotation. The Swiss-Prot database version used for protein search is release 2018_08, and taxonomy used for protein search is Viridiplantae. Release 2018_08 of Swiss-Prot contains 558125 sequence entries, comprising 200328830 amino acids. Blast2GO (Conesa et al., 2005) with NR annotation results was used for GO annotation.

Transcriptome Quantification by RNA-Seq

Messenger RNA was obtained according to the method mentioned above, and fragmentation buffer was added to break mRNA into fragments, which were used as templates to

synthesize first-strand cDNA. After second-strand cDNA synthesis, the fragments were purified and subjected to cohesive end repair, “A” addition and adapter ligation. Then, the suitable size of fragments was amplified by PCR. The mRNA libraries were quantified using the Agilent 2100 Bioanalyzer and sequenced on an Illumina HiSeq 4000 platform.

Raw reads were filtered using SOAPnuke software, and clean reads were obtained. Mapping of clean reads to the full-length transcriptome sequences was performed with Bowtie2 (Langmead and Salzberg, 2012), and transcript quantification (FPKM, Fragments Per Kilobase per Million) was calculated using RSEM (Li and Dewey, 2011). Transcript clusters with a time course were obtained with the software package Mfuzz (Kumar and Futschik, 2007). Transcripts with fold changes ≥ 2 and Q values ≤ 0.001 were identified as DETs using the R package DEGseq (Wang et al., 2009). Hierarchical cluster analysis was carried out with the pheatmap function of R software. Enrichment analysis of GO and KEGG terms was performed with the hyper function.

Label-Free Quantification (LFQ) of Proteomics by SWATH-MS

Approximately 0.5 g of leaves were used for protein extraction as described previously (Zeng et al., 2017). Protein concentration was determined using a Bradford assay (Bradford, 1976), and protein quality was detected using SDS-PAGE. Trypsin digestion was performed (enzyme/protein = 1:40 w/w) overnight at 37°C using 100 μg protein for each sample. Peptides were separated on a liquid phase system UltiMate 3000 UHPLC (Thermo Fisher Scientific, San Jose, CA, USA) with a flow rate of 500 nl/min. The SWATH-MS spectral ion library was first generated with mixed samples using data-dependent acquisition (DDA) on a mass spectrometer Q-Exactive HF (Thermo Fisher Scientific). Individual samples were detected with data-independent acquisition (DIA) mode.

MaxQuant (Cox and Mann, 2008) was used for the identification of DDA data, and information satisfying $\text{FDR} \leq 1\%$ will be used to establish the final spectral library. ProteinPilot 4.5 (Sciex) was used to search all of the DDA data thoroughly against the UniProt Swiss-Prot protein database to generate a spectral library. DIA data were quantified with Spectronaut (Bruderer et al., 2015), and differentially abundant proteins (DAPs) at fold change ≥ 2 and P value < 0.05 were identified and enriched using MSstats (Choi et al., 2014). PPI analysis was performed using the STRING database (von Mering et al., 2005), and the first 100 credibility of the interaction relation was selected to draw the network interaction graph. Prediction of subcellular localization of proteins was carried out with WoLF PSORT (Horton et al., 2007).

qRT-PCR Analysis

Total RNA was used to synthesize the first-strand cDNA with the PrimeScript RT Reagent Kit with gDNA Eraser (Perfect Real Time) (Takara, Otsu, Japan). PCR was performed with TB Green[®] Premix Ex Taq (Takara) on a CFX Connect Real-Time System (Bio-Rad, Hercules, CA, USA). Each sample was

performed with three biological replicates. The relative expression level of genes was determined by the $2^{-\Delta\Delta CT}$ method (Livak and Schmittgen, 2001) using 18S rRNA as the respective reference gene. Primers for qRT-PCR are listed in **Supplementary Table S1**.

Immunoblot Assay

Total protein was prepared as mentioned above. The amino acid residues (QAPMDSGTHYAVM, 98–110 aa) representing the antigenic peptide were used to generate an anti-RCA1 rabbit peptide antibody. The commercial antibody anti-HSP21 and anti-GAPDH were ordered from Abcam and Proteintech, respectively. 30 μ g of total soluble protein for each lane were separated on 12% SDS-PAGE and blotted 1 h to PVDF. Blots were blocked with 5% non-fat milk in TBST for 1 h at room temperature with agitation. Blot was incubated in the primary antibody at a dilution of 1:4 000 overnight at 4°C with agitation. The second antibody (HRP-conjugated Affinipure Goat Anti-Rabbit IgG, Proteintech) was diluted to 1:8 000 in blocking solution for use. The blot was developed for 5 min with chemiluminescent detection reagent before image capture using a CCD imager (ChemiDoc MP).

Firefly Luciferase Complementation Imaging Assay

ORFs of *RCA1-X1*, *Lhca2*, and *CCT3* were amplified from cDNA of *R. hainanense* leaves. ORF lacking stop codon of *RCA1-X1* was cloned into pCambia1300-nLUC, and ORFs with stop codons of *Lhca2* and *CCT3* were cloned into pCambia1300-cLUC, respectively. Constructs were sequenced to confirm accurate fusion and then introduced into *Agrobacterium tumefaciens* strain GV3101. Equal bacterial volumes of each construct ($OD_{600} = 1.0$) were mixed before co-infiltration into *Nicotiana benthamiana* leaves. After infiltration, *N. benthamiana* plants were cultivated for 60 h, and the infiltrated leaves then were smeared with one millimolar luciferin. The plants were kept in dark for 5 min before capturing the LUC image by a CCD imaging apparatus. Each assay consisted of at least three replicates.

Statistical Analysis

Physiological data and protein levels of different samples were analyzed using the analysis of variance (ANOVA). Means were compared by the Duncan test at a significance level of 0.05 with SPSS statistical program (IBM Corporation, Armonk, New York, USA).

Data Availability

The transcriptome raw data files were submitted to the Sequence Read Archive (SRA) database with the accession number PRJNA579430. GenBank accession numbers for alternative splicing transcripts of RCA genes are MN729585–MN729594. The mass spectrometry proteomics data have been deposited to the ProteomeXchange Consortium via the PRIDE (Perez-Riverol et al., 2019) partner repository with the dataset identifier PXD017005.

RESULTS

Effects of Different Pretreatments on *R. hainanense* Against Heat Stress

To characterize defense responses to heat acclimation in the thermotolerant azalea *R. hainanense*, three groups of plants were exposed to non-acclimation pretreatment (NA-pt), acclimation pretreatment at 37°C for 1 h (AC-pt), and acclimation with a 2-d recovery pretreatment (AR-pt) (**Figure 1A**), respectively, before HS (42/35°C, day/night). Plants exhibited no changes in phenotype after pretreatments (**Figure 1B**). After 7 d of LHS, NA-pt plants showed severe injury with drooping shoot apex and withered leaves, while AC-pt and AR-pt plants displayed slight damage on the leaf tip. REC, as an indicator of membrane damage, increased after LHS in all treatments, and has a significantly higher level in NA-pt plants than in AC-pt and AR-pt plants (**Figure 1C**). Consistently, net photosynthetic rate (Pn) decreased after LHS and NA-pt plants had a lower level compared to AR-pt plants (**Figure 1D**). The phenotype and physiological measurements of *R. hainanense* after LHS demonstrate acquired thermotolerance through heat acclimation for AC-pt and AR-pt plants. Interestingly, a 2-d recovery to control temperature did not weaken but even enhance the acquired thermotolerance effects, which reveals an extension (or memory) of acquired thermotolerance during the recovery period.

Transcriptome and Proteome Profiles After 1 h of Heat Acclimation

In order to investigate the mechanisms involved in the extension of acquired thermotolerance during the recovery period, we performed the combined omics analysis including RNA-seq and SWATH-MS-based LFQ proteomics for different time points, as shown in **Figure 1A**. A single-molecule long-read sequencing analysis, or termed Iso-seq, was performed as reference. We quantified 76,278 transcripts and 5,512 proteins in the transcriptome and proteome, respectively, and 5,402 members were correlated in both omics. The quantified numbers of molecules in both omics and their high-correlation ratios displayed high-quality of the sequencing data. Differentially expressed transcripts (DETs, **Supplementary Figure S1A, Data S1**) and proteins (DAPs, **Supplementary Figure S1B, Data S2**) of HS and LHS samples are higher than that of AC and AR, and downregulated molecules have more abundance compared to upregulated molecules in all comparisons.

After 1 h of heat acclimation at 37°C, reprogramming of transcriptomic and proteomic level had already occurred. To identify the transcripts and proteins involved in heat acclimation, the KEGG pathway network of DETs and DAPs in AC/NA was employed to investigate primary pathways involved in heat acclimation. In both transcriptome and proteome, the most significantly enriched pathway is “protein processing in endoplasmic reticulum” (**Supplementary Figure S2, Figure 2A**), which is correlated with large amounts of upregulated proteins annotated as HSPs (**Supplementary Data S2**). The molecular weights of these HSPs range from 15 to 70 kDa, and most are in the range of 15 to 23 kDa, that is, the sHSPs. Another significantly

enriched pathway is “photosynthesis-antenna proteins,” and the related DAPs are all downregulated light-harvesting complex chlorophyll a/b binding proteins (Lhca/b), which are key components in light harvesting of photosynthesis. In eukaryotic orthologous group (KOG) analysis (**Supplementary Figure S3A**), the largest number of 40 DAPs, were classified to the group of “posttranscriptional modification, protein turnover, chaperonins.” Moreover, it has the largest ratio of the DAPs localized in chloroplast (**Supplementary Figure S3B**).

Transcriptome and Proteome Profiles After the 2-d Recovery

After the 2-d recovery following heat acclimation, “Protein processing in endoplasmic reticulum” remains the most enriched pathway in transcriptome (**Supplementary Figure S4A**) and proteome (**Supplementary Figure S4B**), and is correlated with numerous upregulated sHSPs (**Supplementary Data S2**). This result indicates that the sHSPs were upregulated in response to 1 h of heat acclimation and continuously

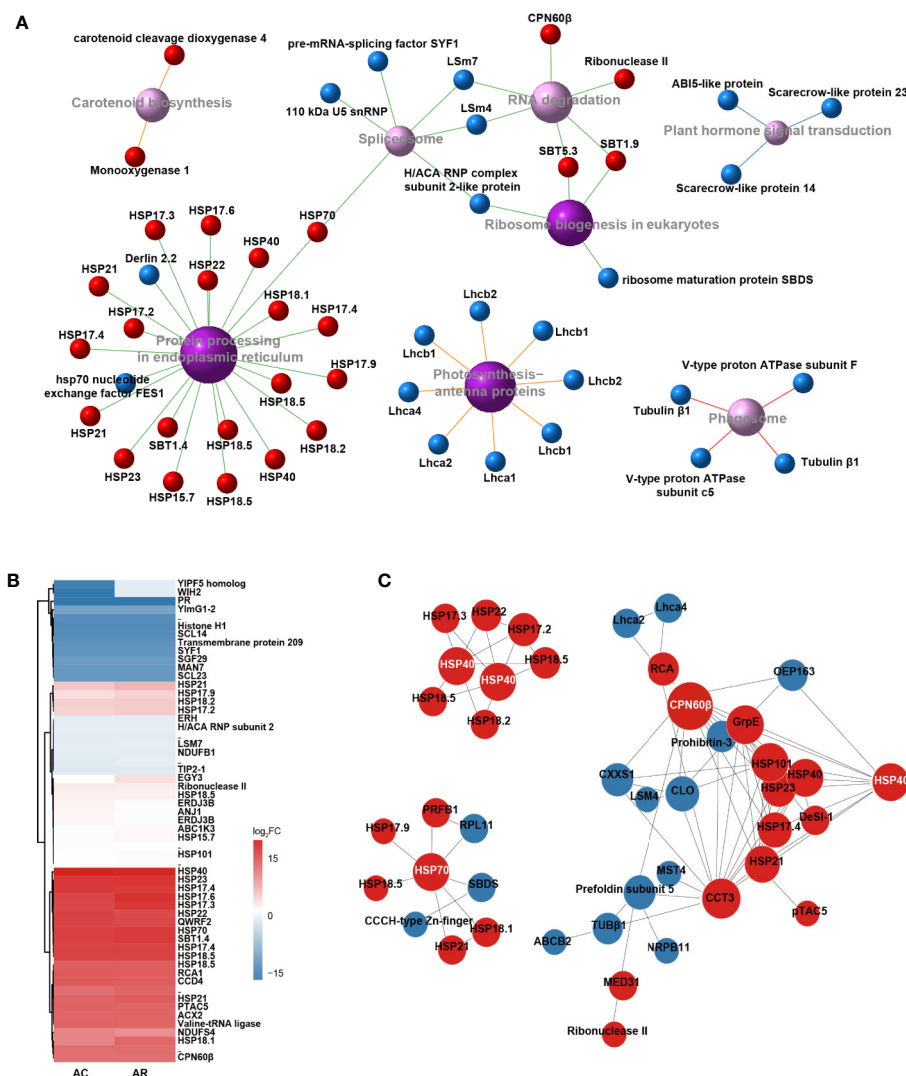


FIGURE 2 | Identification and characteristic of DAPs in AC/NA and AR/NA. **(A)** KEGG pathway enrichment of DAPs in comparison of AC/NA. Red and blue balls represent up- and downregulated proteins, respectively. Purple balls indicate top eight enriched pathways, with dark color meaning significantly enriched and light color meaning enriched but not significantly, and larger areas indicate higher levels of enrichment. Different colors of line represent different classifications of pathway: red line indicates “cellular processes,” blue line indicates “environmental information processing,” green line indicates “genetic information processing” and orange line indicates “metabolism.” The detailed information of the DAPs was listed in **Supplementary Data S2**. **(B)** Heat map of expression patterns of DAPs in the intersection of AC/NA and AR/NA. The protein values are the averages from three biological replicates, normalized to NA, and then log₂ transformed. The detailed information of the DAPs was listed in **Supplementary Data S3**. **(C)** Protein-protein interaction (PPI) analysis of DAPs in the union set of AC/NA and AR/NA. Red and blue circles represent up- and downregulated proteins, respectively. The size of the circle indicates the intensity of relationships, and the protein names that highlighted with white font indicate the high molecular chaperonins that tend to be network nodes. The detailed information of the DAPs was listed in **Supplementary Data S4**.

maintained high levels during recovery to control temperature for 2 d. In addition, the pathway of “carotenoid biosynthesis” with 2/3 upregulated proteins and “cutin, suberine, and wax biosyntheses” with 2 downregulated proteins were significantly enriched in the comparison of AR/NA (**Supplementary Figure S4B**).

The DAP clustered heat map of the intersection between AC/NA and AR/NA shows the proteins that had continuous expression in heat acclimation and the following 2 d of recovery (**Figure 2B**, **Supplementary Data S3**). Accumulation levels of these proteins did not change much between AC and AR, and some proteins even have higher expression levels in AR compared to AC. In addition to the well-known HSPs, other proteins, such as QWRF motif-containing protein 2 (QWRF2), subtilisin-like protease 1.4 (SBT1.4), Rubisco activase (RCA), beta-subunit of chaperonin-60 (CPN60 β), carotenoid cleavage dioxygenase 4 (CCD4) and plastid transcriptionally active chromosome 5 (pTAC5), also have high abundance. According to the protein and protein interaction (PPI) analysis (**Figure 2C**, **Supplementary Data S4**), there are lots of predicted interactions among the HSPs, which indicates their diversified binding patterns. It is worth noting that chaperonins with large molecular weights, such as HSP40, HSP70, and CPN60 β , tend to be network nodes to interact with numerous sHSPs. In addition to the interactions with CPN60 β , RCA was predicted to interact with a chaperonin, t-complex protein 1 subunit gamma (CCT3), and chlorophyll a binding protein Lhca2 and Lhca4. The continuous expressions of these proteins after the 2-d recovery probably play important roles in the extension of heat acclimation, and they would exhibit faster responses to the subsequent HS in AC-pt and AR-pt compared to NA-pt plants.

Essential Factors Involved in Differences Between AR-pt and NA-pt Plants in Early Response to HS

Different early responses to HS can reveal the effects of different pretreatments and lead to divergent plant fates. A comparative transcriptome of AR_HS/NA_HS was investigated to clarify the essential factors involved in determining different fates of AR-pt and NA-pt plants. A total of 13,494 DETs of AR_HS/NA_HS were obtained and subjected to GO term analysis (**Figure 3A**). The terms “ribulose-1,5-bisphosphate carboxylase/oxygenase activity” and “inositol 3-alpha-galactosyltransferase activity,” annotated as 16 RCAs and 13 GOLs, respectively, were significantly enriched. Moreover, these two terms had very high rich ratio, more than 85%, which means that most of the transcripts annotated in the two terms are involved in the different fate of AR-pt and NA-pt plants.

During the pre-treatment of AR plants, FPKM values of the 16 RCA and 13 GOLs transcripts were analyzed to display their expression patterns. Interestingly, transcript levels of RCAs were induced by incubation at 37°C, decreased but not to initial levels after 2 d recovery, and increasing transcript levels were detected after heat shock (**Figure 3B**). This indicated that these RCA transcripts have low expression at control temperature and are heat inducible upon elevated temperatures. However, the

abundance of GOLs transcripts had no significant changes during the pretreatment of AR plants (**Figure 3C**). In addition, RCA transcripts (except Transcript_53437) had higher elevated levels than GOLs in all three groups of plants in early response to HS (**Figure 3D**, **Supplementary Data S5**).

Expression Patterns of Photosynthesis-Related Genes

In the GO analysis of AR_HS/NA_HS (**Figure 3A**), besides “ribulose-1,5-bisphosphate carboxylase/oxygenase activity” and “inositol 3-alpha-galactosyltransferase activity,” other significantly enriched GO terms are most associated with photosynthesis, which indicates potential differences of this process between AR-pt and NA-pt plants. We performed expression analysis of photosynthesis-related genes and the chloroplast-localized chaperonins at both RNA and protein levels (**Figure 4**, **Supplementary Data S6**). From the heat map, we can see that photosynthesis-related genes are most downregulated by AC and the both light-harvesting complex (LHCI and LHCII) genes decrease markedly at protein level. After AR, these genes also recovered close to initial levels in RNA and protein profiles, but proteins of photosystem II (PSII), photosynthetic electron transport (PET) and Calvin cycle had some accumulations. Moreover, these photosynthesis-related genes had a strong downregulation after early HS and LHS in all three groups of plants, but AR-pt plants had less decreases than NA-pt plants.

The chloroplast-localized chaperonins were most upregulated by AC and had significant accumulations at protein level (**Figure 4**, **Supplementary Data S6**). After AR, the chaperonins recovered to initial expressions at RNA level while maintained high accumulations at protein level, especially for sHSPs, RCA1, and CPN60 β . The sustainable accumulation of these chaperonins in AR-pt plants before HS probably provide faster and earlier protection of photosynthesis-related proteins than NA-pt plants in response to the subsequent HS. As described earlier, RCA1 had higher transcript levels in AR-pt plants compared to NA-pt in early HS, but other chaperonins did not show this difference. In addition, all chaperonins, except CPN60 β , had greater protein abundance after 7 d of LHS.

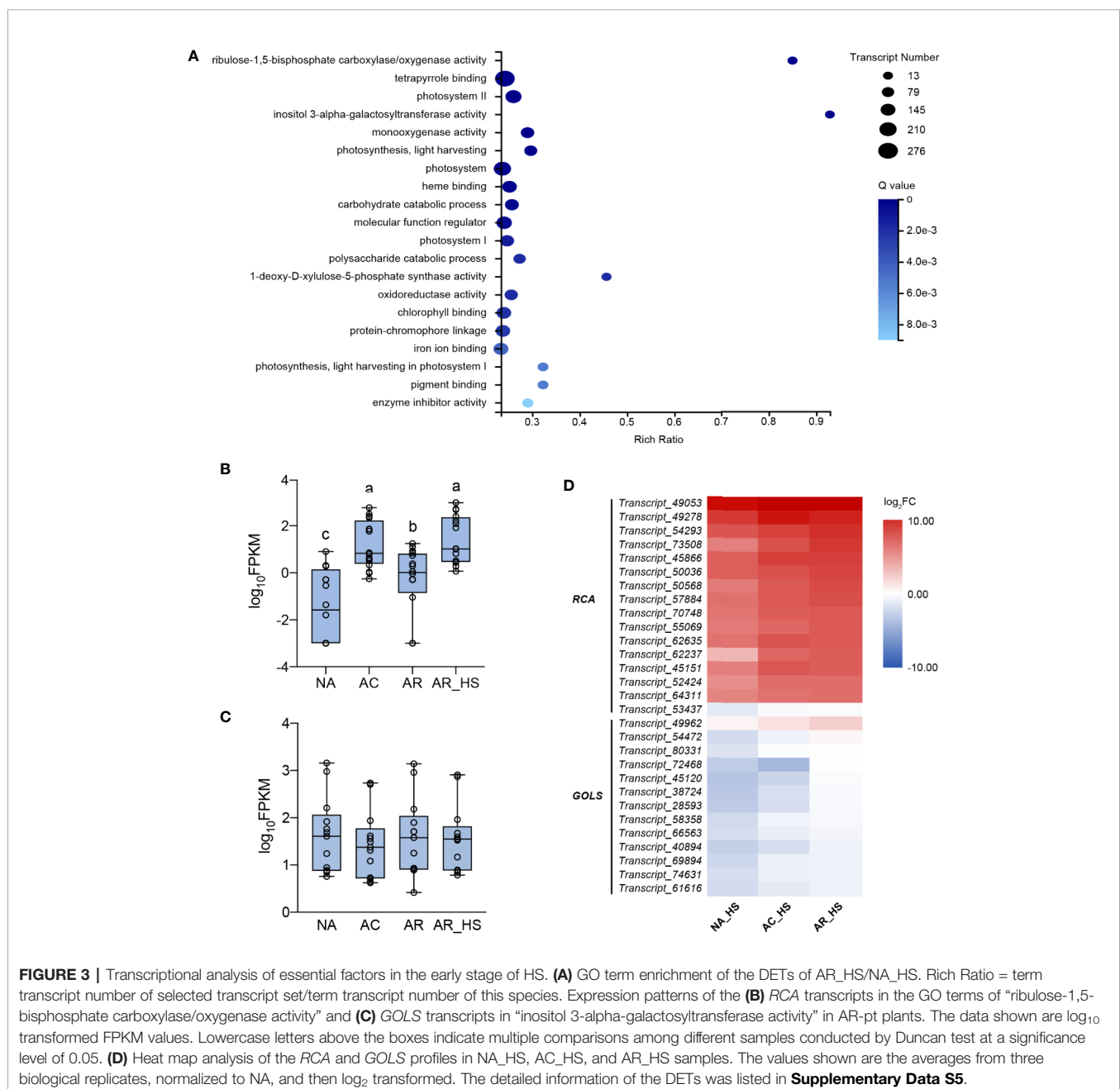
Protein Profiles and Damage Assessment of Photosynthetic Apparatus After 7 d of Heat Stress

After 7 d of LHS, the heat responsive proteins that highly accumulated in AC and AR had no significant difference among AR_LHS, NA_LHS, and AC_LHS (**Supplementary Figure S5A**, **Supplementary Data S7**). In the KEGG enrichment of AR_LHS/NA_LHS, some physiological metabolism pathways were enriched (**Supplementary Figure S5B**). The photosynthesis-antenna proteins, ABC transporters, proteins related to glucuronate metabolism and lipid metabolism had higher levels in AR-pt plants compared to NA-pt plants. Most proteins annotated in the “starch and sucrose metabolism” and “RNA degradation” pathways had lower levels in AR-pt plants. It is likely that the plants enter a relatively balanced state

in the LHS and that AR-pt plants recover some normal physiological activities, such as light harvesting, substrate transport, and lipid metabolism. However, NA-pt plants may still struggle for survival and need more energy from starch and sucrose and need to deal with more RNA degradation caused by HS.

In view of the major participation of photosystems in heat response, we detected maximum photochemical efficiency calculated as Fv/Fm value for monitoring heat effects on photosystem II, which has been considered the primary part of heat impairments on photosynthesis. Three regions (upper, middle, and lower part) including the healthy and necrotic

portion of each leaf were detected (**Figure 5A**). Fv/Fm of all the portions significantly declined after LHS compared to control, with a greater degree in NA-pt than AC-pt and AR-pt plants. The seriously heat-damaged part of leaf tips was necrotic and did not have fluorescence signal, which was most obvious in NA-pt plants. For the chloroplast ultrastructure (**Figure 5B**), plants without HS have regular spindle-shaped and evenly distributed chloroplasts with many starch granules and compact granum lamella and stroma lamella. After LHS, the chloroplast number decreased, and the shape swelled to irregular rotund and oval shapes. The granum lamella and stroma lamella became loose, especially in NA-pt plants.



Structure and Expression Analysis of the Heat-Induced RCA1 and the Constitutively Expressed RCA2 and RCA3

By comprehensive analysis of the transcriptome and proteome, RCA1, which is highly enriched in both omics and, especially in the early stage of HS, was selected for further investigation. To characterize all the RCA genes, all the RCA transcripts were identified from the Iso-seq sequence database and classified into three members (termed RCA1, RCA2, and RCA3) due to sequence identity and BLAST analysis with other species. Moreover, there are alternatively spliced transcripts for each RCA gene member: 5 for RCA1, 3 for RCA2 and 2 for RCA3 (Figure 6A, Supplementary Figure S6), and these transcripts were verified by cloning and sequencing with primers listed in Supplementary Table S1. Most alternatively spliced transcripts are introduced early termination codons, which make shorter coding regions.

To investigate the expression patterns of different RCA gene members, FPKM values (Supplementary Figure S7) and relative

expression levels (Figure 6B) of different alternatively spliced transcripts were investigated. The major alternative splicing isoform of RCA1 is RCA1-X1, which had the highest FPKM values under the stages tested (Supplementary Figure S7A). In NA and AR stage, all the RCA1 isoforms almost had no expression, but under the heat-treated stages (AC, NA_HS, AC_HS, and AR_HS), RCA1-X1 had much higher FPKM values than other RCA1 isoforms. The major alternative splicing isoform of RCA2 is RCA2-X3, whose expression was high before heat (NA) but decreased much after other treatments (Supplementary Figure S7B). Two isoforms of RCA3 also expressed under control temperature and decreased after heat treatments (Supplementary Figure S7B). These results demonstrated that RCA1 gene is heat inducible, and RCA2 and RCA3 are constitutively expressed. Relative levels of the alternatively spliced transcripts for the different time points compared to NA were identified and clustered in the heat map (Figure 6B). The upregulated transcripts all belong to RCA1,

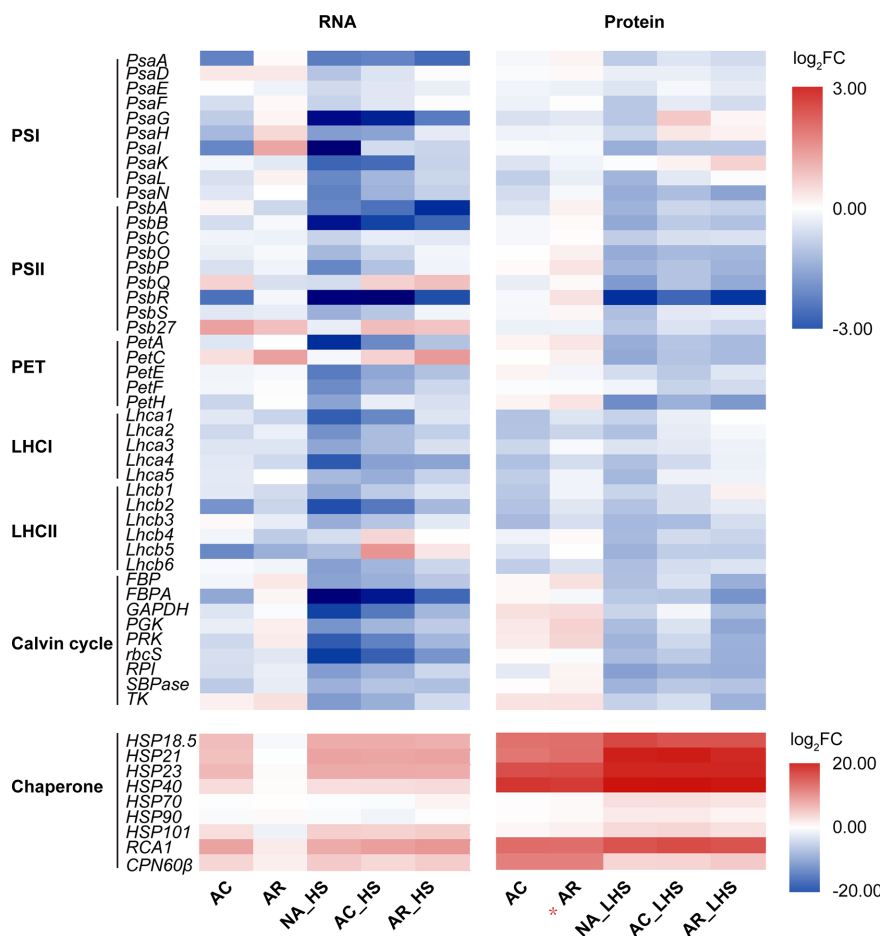


FIGURE 4 | Expression analysis of photosynthesis-related genes at RNA and protein levels. Genes are grouped in the functional categories PSI (photosystem I), PSII, PET (photosynthetic electron transport), LHCI (light-harvesting complex I), LHCII, Calvin cycle, and chloroplast-localized chaperonin. The top panel and bottom panel use different scale legend. The values shown are the averages from three biological replicates, normalized to NA, and then \log_2 transformed. The asterisk (*) indicates the key column that chaperonins sustainably accumulated at high levels. The detailed information on the photosynthesis-related genes was listed in Supplementary Data S6.

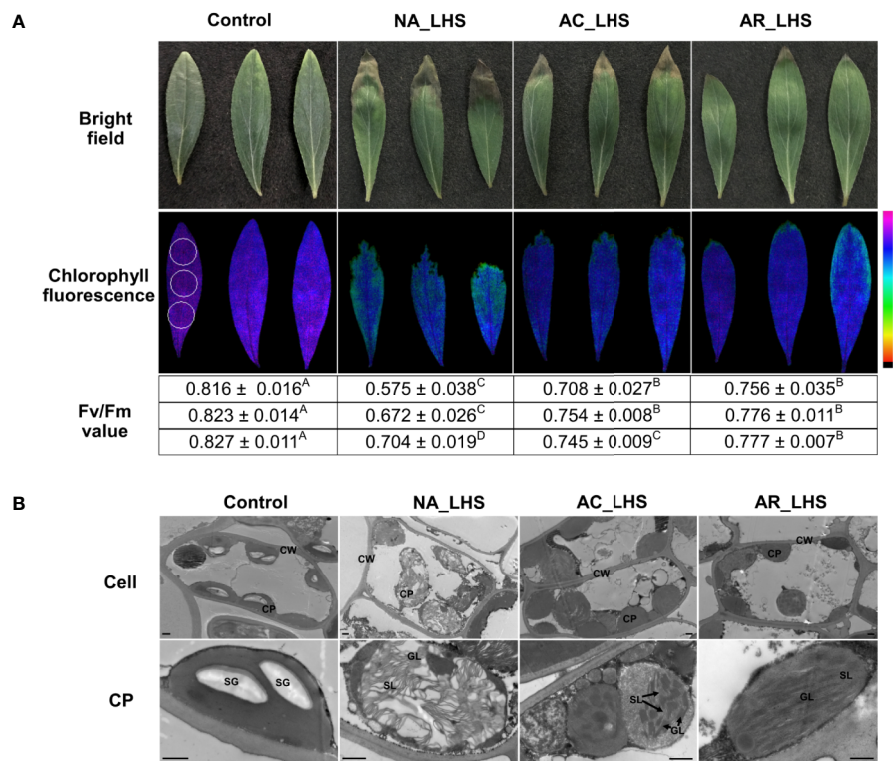


FIGURE 5 | Damage analysis of differentially-pretreated plants after LHS. **(A)** Photochemical efficiency and **(B)** chloroplast ultrastructure observation of the leaves after LHS with non-stressed leaves as control. The fluorescence color indicates Fv/Fm value, and the three circles (1 cm in diameter) that marked in the control image represent detected regions (upper, middle, and lower part) for each leaf. Fv/Fm values of the three detected regions are correspondingly listed below the images, which are shown as mean value ± SD of three biological replicates. Superscript capital letters indicate multiple comparisons among different treatments of the same detected region, which was conducted by Duncan test at a significance level of 0.05. CP, chloroplast; CW, cell wall; SG, starch granule; GL, granum lamella; SL, stroma lamella. Bar indicates 10 μm.

while RCA2 and RCA3 transcripts were generally not changed or slightly downregulated in response to heat. Moreover, all the RCA transcripts had higher levels in AR_HS compared to NA_HS (**Figure 6B**). We also designed specific primers to detect expression levels within 12 h of treatment at different temperatures by qRT-PCR (**Supplementary Figure S8**). The regulation patterns in response to heat are similar with RNA-seq data, and RCA1 showed more intense upregulation and maintained longer expression under 42°C treatment compared to 37°C.

In proteomics, only one protein sequence was identified for each RCA gene member to quantify the protein expression level (**Figure 6C**), which may be due to technical limitations that cannot distinguish the highly similar protein sequences coded by the alternatively spliced transcripts or because some transcripts may be incapable of translating to proteins. RCA1 protein could not be detected at control temperature but was quickly induced by AC, was maintained high levels even after AR, and could be triggered to a greater degree after 7 d of LHS. However, RCA2 and RCA3 are constitutively expressed at control temperature, are not affected by AC and AR, but decreased to a great extent (RCA2) or completely degraded (RCA3) after LHS. Moreover, Rubisco activation state of all the plants decreased after LHS but

has lower level in NA-pt plants compared to AR-pt (**Figure 6D**). Therefore, heat-induced thermostable RCA1 can supplement the depletion of RCA2 and RCA3, which maintains relatively balanced Rubisco activation state and photosynthesis stability under HS (**Figure 6E**). To confirm the thermostability of RCA1, immunoblot assay was performed (**Figure 7A**). After LHS, RCA1 protein had high accumulation in 46 kDa (RCA1-X1) and less in 42 to 43 kDa (probably RCA1-X2–4). The accumulation of RCA1 is similar to that of HSP21, which also had high abundance after LHS in proteomics analysis. Lhca2 and CCT3, which were predicted to have interactions with RCA in PPI analysis, were verified their interactions with RCA1 by firefly luciferase complementation imaging assays (**Figure 7B**).

DISCUSSION

Protein-Level Sustainability of Chaperonins in the Recovery Period Contributes to Heat Acclimation Memory

Acclimation to fluctuating temperatures and possession of acclimation memory for unpredictable environmental challenges

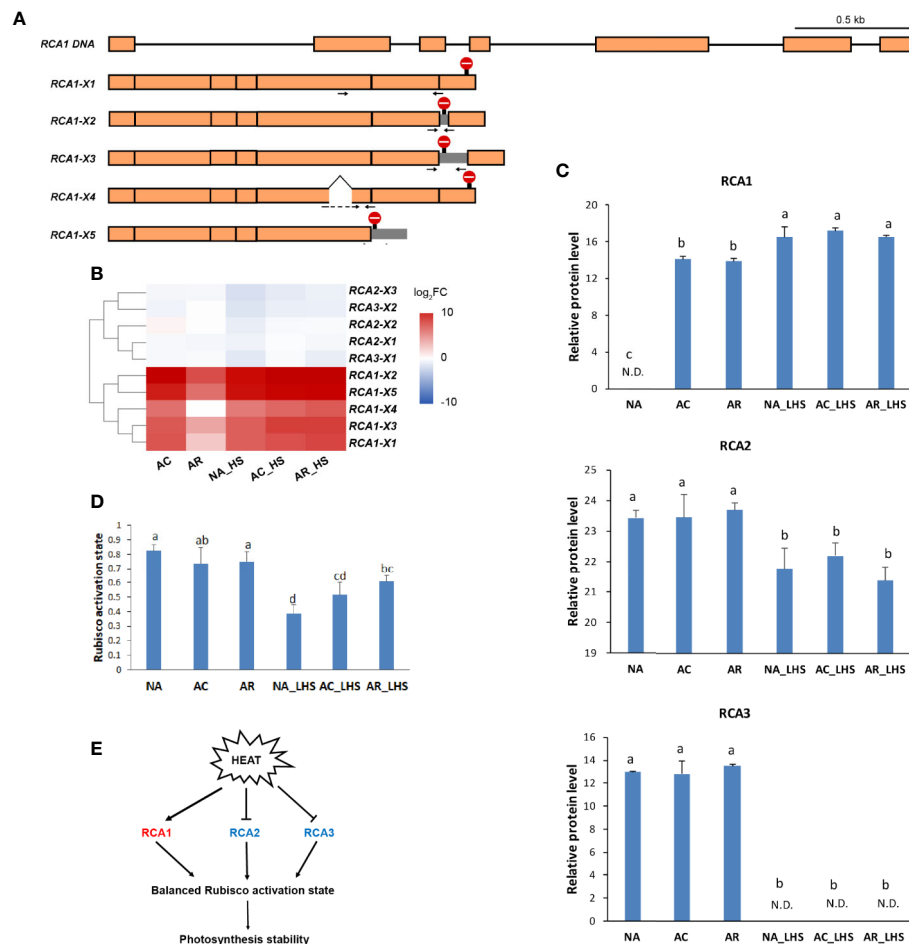


FIGURE 6 | Structural and functional analysis of *RCA* genes in response to heat treatments. **(A)** Schematic diagram of the DNA and alternatively spliced transcripts (X1–5) of *RCA1*. Orange module represents exon and line represents intron. Stop sign indicates the position of termination codon. Gray module represents retained intron. Positions of specific primers for qRT-PCR are marked as arrows and primer sequences are listed in **Supplementary Table S1**. **(B)** Heat map of alternatively spliced transcripts of *RCA*. The values are averages from three biological replicates, normalized to NA, and then \log_2 transformed. **(C)** Protein expression level of *RCA* genes. The values of relative protein level were performed with median normalization and \log_2 transformation. N.D., not detected. **(D)** Rubisco activation state of the plants under different treatments. Lowercase letters above the columns indicate multiple comparisons among different samples conducted by Duncan test at a significance level of 0.05. **(E)** The regulation network that *RCA* involved. Heat induces *RCA1* but inhibits *RCA2* and *RCA3*, which results in a relative balanced Rubisco activation state and photosynthesis stability.

are crucial for plant survival. However, how plants possess the acclimation memory before the reoccurring stress is not well understood. In this study, heat acclimation can confer acquired thermotolerance to *R. hainanense* plants against subsequent severe HS, even when a 2-d recovery to control temperature separates the acclimation and stress periods. From the transcriptome and proteome analyses with physiological measurements, we figure out the response patterns of chaperonins at transcript and protein levels (**Figure 8**). Upon heat acclimation priming, transcript and protein levels of these chaperonins increased rapidly, and the plants were induced into a primed state. When recover to control temperature, transcripts decreased in short time while proteins sustained a prolonged protection at least for 2 d. The higher protein levels in primed than unprimed plants before HS

are the defense readiness, which would provide faster and stronger protection in the early stage of subsequent HS. Although the proteins of unprimed plants had the similar levels as those of primed plants after 7 d of LHS, the different defense power in the early stage of HS determined the different performance of the two groups of plants. The primed plants need some costs for maintaining the reprogrammed primed state but have a better foundation of defense readiness for confronting HS. Therefore, the sustainably accumulated chaperonins in the recovery period are crucial for heat acclimation memory and extension of acquired thermotolerance.

Most of the chaperonins that accumulated in the recovery period are HSPs (**Figure 2B**, **Supplementary Figure S2**). Large amounts of the HSPs were predicted to localize in chloroplast

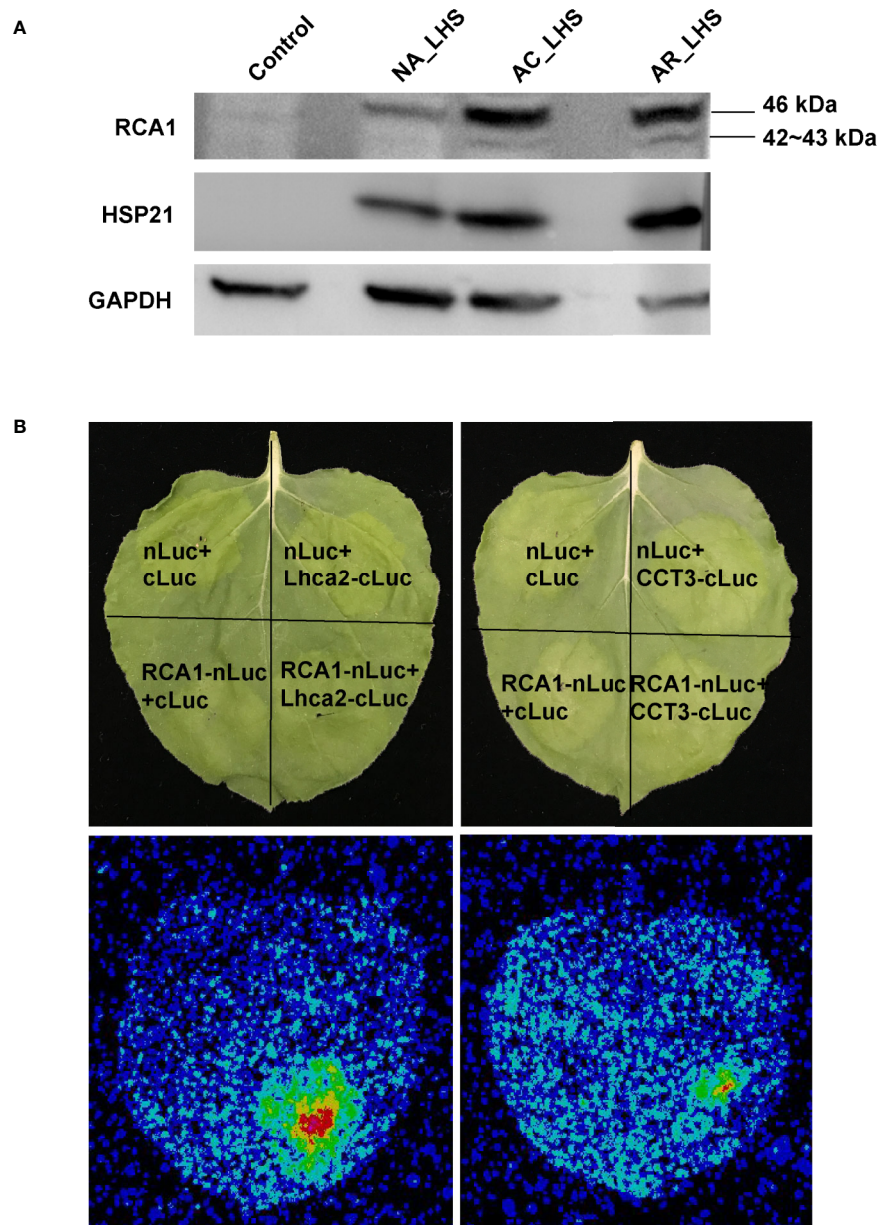


FIGURE 7 | Validation of RCA1 thermostability and interacting proteins. **(A)** Immunoblot assay to confirm thermostability of RCA1. HSP21 was presented as a representative of HSPs and GAPDH as a loading control. **(B)** Firefly luciferase complementation imaging assay to confirm interacting proteins of RCA1. Partial Luc fusion constructs were transiently coexpressed in *N. benthamiana* leaves. Top panel indicate the partition for differentially transformed constructs. Luc signals, observed using a CCD camera, indicate protein interactions.

and other cell components, and sHSPs, ranging from 15 to 23 kDa, have the largest ratio in these proteins. It has been known that unfolded proteins are easy to form large aggregates that severely impede normal cellular functions under HS, and the main function of HSPs is to bind the unfolded proteins to limit misfolding and resolve aggregates (Queitsch et al., 2000; Jacob et al., 2017; Muthusamy et al., 2017). Thus, the HSPs accumulated in the recovery period could play roles in

maintaining proteome homeostasis with refolding or degrading diverse clients when the subsequent HS occurs. High-molecular-weight HSPs tend to be network nodes that connect numerous sHSPs to assemble multimeric complexes as homopolymers or heteropolymers, which is possibly because of the small size and flexibility of sHSPs, and it is conducive to switch on high-efficiency defense system in a short time (Lee and Vierling, 2000; Carra et al., 2017).

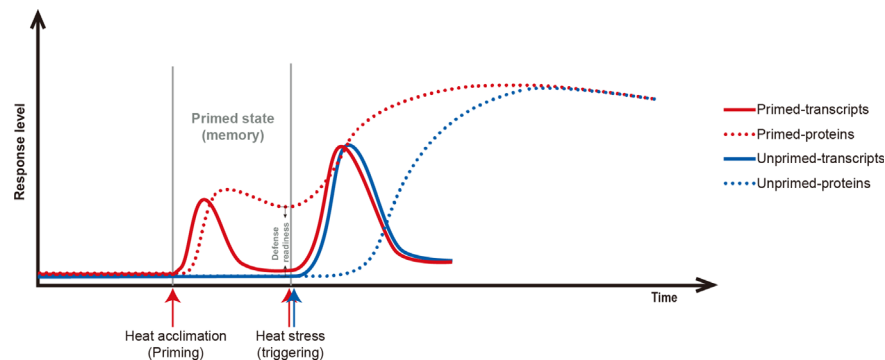


FIGURE 8 | Scheme of the relations of chaperonin genes at transcript (solid line) and protein levels (dotted line) in primed (red line) versus unprimed (blue line) plants. Heat acclimation, as a priming stimulus, induces chaperonin genes at transient transcript level and sustained protein level. After priming, the status is termed primed state or memory for storing reprogrammed information. The difference between primed- and unprimed-proteins are the defense readiness for primed plants. Upon subsequent HS, the chaperonins of primed plants are triggered faster and stronger protection than unprimed plants. After a certain of LHS, the transcript and protein levels of chaperonin genes have no difference between primed and unprimed plants, but the differences in the early stage of HS determine their final different performance.

Equipped Chaperonin Protection of Chloroplast in the Recovery Period Decreases Damage of Photosynthesis Under Subsequent HS

Photosynthesis is considered most susceptible to high temperature stress among plant cell functions, and the primary sites of targets in heat exposure are photosystems (Allakhverdiev et al., 2008; Ahammed et al., 2018). In this study, photosynthesis is also significantly enriched in the heat acclimation memory, and the equipped status of chloroplast in the recovery period is critical for tolerance to the subsequent HS (Figure 9). Both LHCs were sensitive to heat signal and most chlorophyll a/b-binding proteins

(Lhca1/2/4/5 in LHCI and Lhcb1/2/3/6 in LHCII) were reduced probably for cutting down light harvesting to prevent surplus light energy-caused damage. Moreover, some proteins of PET (PSII subunit O and P, PC and FNR), ATP synthase (subunit α , β , γ , a, b) and Calvin cycle (PGK, GAPDH, FBP, TK, SBPase, and PRK) were upregulated, which is possibly for accelerative consume of excess energy. The most important equipped components in the recovery period are the significantly accumulated chloroplast-localized chaperonins that could provide faster and stronger protection for photosystem in the early stage of HS. It has been demonstrated that sHSPs could associate with chloroplast thylakoids and protect oxygen-evolving complex (OEC) proteins

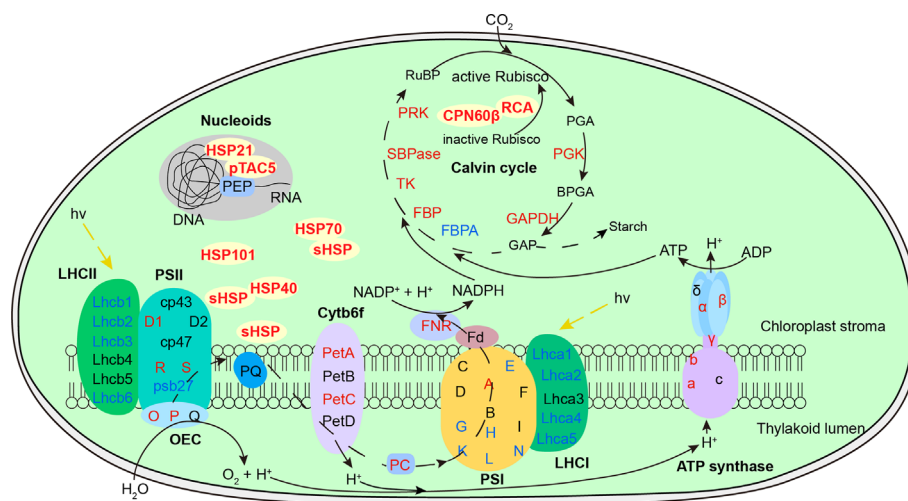


FIGURE 9 | Defense readiness of chloroplast after 2-d recovery following heat acclimation. Different colors of protein names represent different protein level expression with red representing upregulation while blue as downregulation. The level of proteins was determined based on \log_2 fold change of AR compared to NA. After 2-d recovery, most subunits of both light-harvesting complex (LHC) were downregulated. Some subunits of photosynthetic electron transport, ATP synthase and Calvin cycle were upregulated. The significantly accumulated chaperonins provide equipped protection of photosystem, Rubisco activation, and plastid-encoded RNA polymerase (PEP) function against the subsequent HS.

of PSII against HS (Heckathorn et al., 1998). Variation in induced PET thermotolerance of five ecotypes of *Chenopodium album* was as well as highly correlated with chloroplast sHSP protection (Barua et al., 2003). And the interaction of HSP21 and pTAC5 is required for chloroplast development under HS by maintaining plastid-encoded RNA polymerase (PEP) function (Zhong et al., 2013). RCA plays important roles in maintaining the active state of Rubisco to ensure photosynthesis, and CPN60 β was reported to associate with RCA to protect photosynthesis during HS (Salvucci, 2008). In this study, CPN60 β possibly protect RCA2 rather than RCA1 because the protein content of CPN60 β after LHS was decreased similar to changes of RCA2 (**Figure 4**). RCA1 could interact with Lhca2 according to the firefly luciferase complementation imaging assays (**Figure 7B**), which implies that RCA may affect light harvesting of LHCI in addition to carbon fixation in photosynthesis. These diverse functions of the chaperonins demonstrate that it is well equipped for AR-pt plants in the primed state before HS. And the results of Fv/Fm and chloroplast ultrastructure after LHS (**Figure 5**) indicate that the acclimated defense readiness enhanced thermostability of the photosynthetic apparatus.

RCA1 Probably Play Vital Roles in the Photosynthetic Acclimation to High Temperature

It has been proposed that reduced photosynthesis at high temperature is probably due to Rubisco inactivation caused by thermal lability of RCA (Crafts-Brandner and Law, 2000). However, the protein contents of total RCA were increased in the heat acclimation and recovery periods owing to quickly heat-induced RCA1 in *R. hainanense* (**Figure 6C**). Thus, the key factor of Rubisco activation for photosynthesis was not inhibited but improved after heat acclimation. The heat-induced RCA1 has the characteristics of quick and strong response to heat treatment, which is totally different with the constitutively expressed RCA2 and RCA3 but similar to HSPs. Heat-induced RCA is not pervasive in plants but only found in a few of species. It was first identified in maize and verified as a molecular chaperonin rather than a conventional enzyme (Sanchez de Jimenez et al., 1995). In wheat, HS increased the accumulation of the constitutive 42-kDa RCA and induced the synthesis of a putative 41-kDa form, and after 24 h of recovery from HS, the 42-kDa activase returned to control levels while a small amount of the 41-kDa protein was still expressed (Law and Crafts-Brandner, 2001). It was also demonstrated that the induction of a new form of RCA may constitute a mechanism of photosynthetic acclimation to HS in cotton (Law et al., 2001). Thus, heat-induced RCA is very important for confronting HS and needs further study in more plants.

In addition to the heat-inducible characteristic, thermostability is another significant feature of RCA1. After 7 d of LHS, RCA2, and RCA3 decreased or even totally degraded, while RCA1 displayed high thermostability to maintain relatively balanced Rubisco activity and photosynthesis (**Figures 6C, D**). These findings reveal the major role of thermostable RCA1, rather than RCA2 or RCA3, in the activation and protection of Rubisco or possibly other proteins

during LHS in *R. hainanense*. Both RCA1 and HSPs were significantly accumulated in LHS, but RCA1 rather than HSPs has a higher transcript level in AR-pt plants compared to NA-pt plants in the early stage of HS (**Figure 4**), which reflects the effects of accumulation. Moreover, elevated levels of induced and constitutive RCA proteins persist hours after expression of HSPs has decreased to control levels in both maize and wheat leaves (Law and Crafts-Brandner, 2001), which indicates that heat-increased RCA probably play more important roles than HSPs in the maintenance of heat memory. The heat-induced characteristics, sustainable expression in the recovery period and high thermostability of RCA1 indicate that it is a vital factor involved in photosynthetic acclimation to HS. The relationships between RCA1 and the reported heat memory associated factors, such as HSFA2, miRNA, or histone methylation, merit further research.

It is worth noting that RCA1 of *R. hainanense* has five alternatively spliced transcripts (**Figure 6A**), which could be translated to four protein isoforms with discrepant structures. Alternative splicing is a kind of posttranscriptional regulation and has a highly important role in expanding proteomic diversity and functional complexity in higher eukaryotes (Nilsen and Graveley, 2010; Carvalho et al., 2013). We cannot identify all alternative splicing events in response to HS without whole genome sequence of *R. hainanense*. But it has been demonstrated that alternative splicing is involved in most plant processes and is particularly prevalent in plants exposed to environmental stresses (Graveley, 2001). The effects of alternative splicing include the production of protein isoforms with various loss- or gain-of-function and/or posttranslational modification, altered subcellular localization, enzymatic activity or protein stability in various situations (Stamm et al., 2005), which provides additional adaptive advantages to the organisms. It is also reported alternative splicing of RCA genes in other plant species, but most generating two isoforms (Carmo-Silva et al., 2015; Nagarajan and Gill, 2018). The high ratio of alternative splicing of RCA1 transcripts in *R. hainanense* reveals the functional complexity and importance of RCA1 gene in heat tolerance. And the major isoform, RCA1-X1, probably plays more important roles than other RCA1 isoforms. However, alternative splicing sometimes generates nonfunctional mRNAs, which usually contain premature termination codons and can be targeted for degradation by nonsense-mediated decay (NMD) (Wollerton et al., 2004; Carvalho et al., 2013). The transcript diversity of RCA1 likely contributes to thermotolerance, or some transcripts might be degraded by NMD, which will be identified by their gain or loss of function in our future study.

CONCLUSIONS

In summary, we found that a 2-d recovery to control temperature following heat acclimation did not weaken but even enhance the acquired thermotolerance in the heat-tolerant azalea *R. hainanense*. The sustainable accumulations of chaperonins at protein-level rather than transcriptional-level after 2-d recovery

contribute to the extension of heat acclimation memory. And the most affected biological process is photosynthesis, which decreased less in AR-pt plants with the equipped protection of chloroplast-localized chaperonins. Heat-induced RCA1 has high thermostability under LHS and play important roles in balanced Rubisco activation state and photosynthetic acclimation to elevated temperature. Further studies will characterize the functional differences of alternative-spliced transcripts of *RCA1* and find the regulation factors that activate *RCA1*-mediated heat tolerance. In practical application, appropriate priming that can induce defense readiness, which may not be limited to heat acclimation, can be applied to stimulate the plant defense system for enhanced tolerance to upcoming HS. The chaperonins determined in our study can be used as indicators of primed defense readiness and as candidate genes to improve heat tolerance of azalea and other plants through genetic engineering.

DATA AVAILABILITY STATEMENT

The datasets presented in this study can be found in online repositories. The names of the repository/repositories and accession number(s) can be found in the article/**Supplementary Material**.

AUTHOR CONTRIBUTIONS

YX provided support of research expenses. XW, HZ, and YX conceived and designed the study. XW and ZL performed

experiments and wrote the initial manuscript. XW, BL, and ME performed data analysis. All authors contributed to the article and approved the submitted version.

FUNDING

This work was supported by the National Natural Science Foundation of China (grant number, 31901356), Postdoctoral Science Foundation of China (grant number, 2018M632484) and Zhejiang Science and Technology Major Program on Agricultural New Variety Breeding (grant number, 2016C02056-12).

ACKNOWLEDGMENTS

We thank Dr. Danqing Li (Zhejiang University) for instructions of omics data analysis. Thanks to Dr. Liangsheng Zhang, Dr. Kai Shi, and Dr. Zhangjian Hu (Zhejiang University) for critical review of the manuscript. And thanks to Dr. Ze Wu (Nanjing Agricultural University) for the generous gift of pCAMBIA1300-nLUC/cLUC vectors.

SUPPLEMENTARY MATERIAL

The Supplementary Material for this article can be found online at: <https://www.frontiersin.org/articles/10.3389/fpls.2020.01278/full#supplementary-material>

REFERENCES

- Ahammed, G. J., Xu, W., Liu, A., and Chen, S. (2018). COMT1 silencing aggravates heat stress-induced reduction in photosynthesis by decreasing chlorophyll content, photosystem II activity, and electron transport efficiency in tomato. *Front. Plant Sci.* 9, 998. doi: 10.3389/fpls.2018.00998
- Allakhverdiev, S. I., Kreslavski, V. D., Klimov, V. V., Los, D. A., Carpentier, R., and Mohanty, P. (2008). Heat stress: an overview of molecular responses in photosynthesis. *Photosynth. Res.* 98 (1-3), 541-550. doi: 10.1007/s11200-008-9331-0
- Altschul, S. F., Gish, W., Miller, W., Myers, E. W., and Lipman, D. J. (1990). Basic local alignment search tool. *J. Mol. Biol.* 215 (3), 403-410. doi: 10.1016/S0022-2836(05)80360-2
- Barua, D., Downs, C. A., and Heckathorn, S. A. (2003). Variation in chloroplast small heat-shock protein function is a major determinant of variation in thermotolerance of photosynthetic electron transport among ecotypes of *Chenopodium album*. *Funct. Plant Biol.* 30 (10), 1071-1079. doi: 10.1071/FP03106
- Bäurle, I. (2016). Plant heat adaptation: priming in response to heat stress. *Front. Plant Sci.* 7, 1-5. doi: 10.3389/fpls.2016.00001
- Blum, A., and Ebercon, A. (1981). Cell membrane stability as a measure of drought and heat tolerance in wheat. *Crop Sci.* 21 (1), 43-47. doi: 10.2135/cropsci1981.0011183X002100010013x
- Bracher, A., Whitney, S. M., Hartl, F. U., and Hayer-Hartl, M. (2017). Biogenesis and metabolic maintenance of Rubisco. *Annu. Rev. Plant Biol.* 68, 29-60. doi: 10.1146/annurev-arplant-043015-111633
- Bradford, M. M. (1976). A rapid and sensitive method for the quantitation of microgram quantities of protein utilizing the principle of protein-dye binding. *Anal. Biochem.* 72 (1-2), 248-254. doi: 10.1016/0003-2697(76)90527-3
- Bruce, T. J., Matthes, M. C., Napier, J. A., and Pickett, J. A. (2007). Stressful "memories" of plants: evidence and possible mechanisms. *Plant Sci.* 173 (6), 603-608. doi: 10.1016/j.plantsci.2007.09.002
- Bruderer, R., Bernhardt, O. M., Gandhi, T., Miladinović, S. M., Cheng, L., Messner, S., et al. (2015). Extending the limits of quantitative proteome profiling with data-independent acquisition and application to acetaminophen-treated three-dimensional liver microtissues. *Mol. Cell. Proteomics* 14 (5), 1400-1410. doi: 10.1074/mcp.M114.044305
- Buchfink, B., Xie, C., and Huson, D. H. (2015). Fast and sensitive protein alignment using DIAMOND. *Nat. Methods* 12 (1), 59-60. doi: 10.1038/nmeth.3176
- Carmo-Silva, E., Scales, J. C., Madgwick, P. J., and Parry, M. A. J. (2015). Optimizing Rubisco and its regulation for greater resource use efficiency. *Plant Cell Environ.* 38 (9), 1817-1832. doi: 10.1111/pce.12425
- Carra, S., Alberti, S., Arrigo, P. A., Benesch, J. L., Benjamin, I. J., Boelens, W., et al. (2017). The growing world of small heat shock proteins: from structure to functions. *Cell Stress Chaperon.* 22 (4), 1-11. doi: 10.1007/s12192-017-0787-8
- Carvalho, R. F., Feijão, C. V., and Duque, P. (2013). On the physiological significance of alternative splicing events in higher plants. *Protoplasma* 250 (3), 639-650. doi: 10.1007/s00709-012-0448-9
- Chang, Y., Liu, H., Liu, N., Hsu, F., and Ko, S. (2006). Arabidopsis Hsa32, a novel heat shock protein, is essential for acquired thermotolerance during long recovery after acclimation. *Plant Physiol.* 140 (4), 1297-1305. doi: 10.1104/pp.105.074898
- Chang, Y., Liu, H., Liu, N., Chi, W., Wang, C., Chang, S., et al. (2007). A heat-inducible transcription factor, HsfA2, is required for extension of acquired thermotolerance in Arabidopsis. *Plant Physiol.* 143 (1), 251-262. doi: 10.1104/pp.106.091322
- Choi, M., Chang, C., Clough, T., Broudy, D., Killeen, T., MacLean, B., et al. (2014). MSstats: an R package for statistical analysis of quantitative mass spectrometry-based proteomic experiments. *Bioinformatics* 30 (17), 2524-2526. doi: 10.1093/bioinformatics/btu305
- Conesa, A., Götz, S., García-Gómez, J. M., Terol, J., Talón, M., and Robles, M. (2005). Blast2GO: a universal tool for annotation, visualization and analysis in

- functional genomics research. *Bioinformatics* 21 (18), 3674–3676. doi: 10.1093/bioinformatics/bti610
- Conrath, U., Beckers, G. J., Flors, V., García-Agustín, P., Jakab, G., Mauch, F., et al. (2006). Priming: getting ready for battle. *Mol. Plant Microbe* 19 (10), 1062–1071. doi: 10.1094/MPMI-19-1062
- Conrath, U., Beckers, G. J., Langenbach, C. J., and Jaskiewicz, M. R. (2015). Priming for enhanced defense. *Annu. Rev. Phytopathol.* 53, 97–119. doi: 10.1146/annurev-phyto-080614-120132
- Cox, J., and Mann, M. (2008). MaxQuant enables high peptide identification rates, individualized p.p.b.-range mass accuracies and proteome-wide protein quantification. *Nat. Biotechnol.* 26 (12), 1367–1372. doi: 10.1038/nbt.1511
- Crafts-Brandner, S. J., and Law, R. (2000). Effect of heat stress on the inhibition and recovery of the ribulose-1, 5-bisphosphate carboxylase/oxygenase activation state. *Planta* 212 (1), 67–74. doi: 10.1007/s004250000364
- Crafts-Brandner, S. J., and Salvucci, M. E. (2000). Rubisco activase constrains the photosynthetic potential of leaves at high temperature and CO₂. *Proc. Natl. Acad. Sci. U.S.A.* 97 (24), 13430–13435. doi: 10.1073/pnas.230451497
- De Riek, J., De Keyser, E., Calsyn, E., Eeckhaut, T., Van Huylenbroeck, J., and Kobayashi, N. (2018). “Azalea” in *Ornamental Crops*. Springer, 237–271.
- Geng, X. M., Yang, Q. Y., Yue, Y., and Ozaki, Y. (2019). Effects of high temperature on photosynthesis, membrane lipid peroxidation and osmotic adjustment in four *Rhododendron* species. *J. Fac. Agr. Kyushu U.* 64 (1), 33–38.
- Graveley, B. R. (2001). Alternative splicing: increasing diversity in the proteomic world. *Trends Genet.* 17 (2), 100–107. doi: 10.1016/S0168-9525(00)002176-4
- Heckathorn, S. A., Downs, C. A., Sharkey, T. D., and Coleman, J. S. (1998). The small, methionine-rich chloroplast heat-shock protein protects photosystem II electron transport during heat stress. *Plant Physiol.* 116 (1), 439–444. doi: 10.1104/pp.116.1.439
- Heckathorn, S. A., Ryan, S. L., Baylis, J. A., Wang, D., Hamilton III, E. W., Cundiff, L., et al. (2002). In vivo evidence from an *Agrostis stolonifera* selection genotype that chloroplast small heat-shock proteins can protect photosystem II during heat stress. *Funct. Plant Biol.* 29 (8), 935–946. doi: 10.1071/PP01191
- Horton, P., Park, K.-J., Obayashi, T., Fujita, N., Harada, H., Adams-Collier, C. J., et al. (2007). WoLF PSORT: protein localization predictor. *Nucleic Acids Res.* 35 (suppl_2), W585–W587. doi: 10.1093/nar/gkm259
- Jacob, P., Hirt, H., and Bendahmane, A. (2017). The heat-shock protein/chaperone network and multiple stress resistance. *Plant Biotechnol. J.* 15 (4), 405–414. doi: 10.1111/pbi.12659
- Kim, K., and Portis Jr., A. R. (2005). Temperature dependence of photosynthesis in *Arabidopsis* plants with modifications in Rubisco activase and membrane fluidity. *Plant Cell Physiol.* 46 (3), 522–530. doi: 10.1093/pcp/pci052
- Kumar, L., and Futschik, M. E. (2007). Mfuzz: a software package for soft clustering of microarray data. *Bioinformatics* 2 (1), 5–7. doi: 10.6026/97320630002005
- Kurek, I., Chang, T. K., Bertain, S. M., Madrigal, A., Liu, L., Lassner, M. W., et al. (2007). Enhanced thermostability of *Arabidopsis* Rubisco activase improves photosynthesis and growth rates under moderate heat stress. *Plant Cell* 19 (10), 3230–3241. doi: 10.1105/tpc.107.054171
- Langmead, B., and Salzberg, S. L. (2012). Fast gapped-read alignment with Bowtie 2. *Nat. Methods* 9 (4), 357–359. doi: 10.1038/nmeth.1923
- Law, R. D., and Crafts-Brandner, S. J. (2001). High temperature stress increases the expression of wheat leaf ribulose-1, 5-bisphosphate carboxylase/oxygenase activase protein. *Arch. Biochem. Biophys.* 386 (2), 261–267. doi: 10.1006/abbi.2000.2225
- Law, D. R., Crafts-Brandner, S. J., and Salvucci, M. E. (2001). Heat stress induces the synthesis of a new form of ribulose-1, 5-bisphosphate carboxylase/oxygenase activase in cotton leaves. *Planta* 214 (1), 117–125. doi: 10.1007/s004250100592
- Lee, G. J., and Vierling, E. (2000). A small heat shock protein cooperates with heat shock protein 70 systems to reactivate a heat-denatured protein. *Plant Physiol.* 122 (1), 189–198. doi: 10.1104/pp.122.1.189
- Li, B., and Dewey, C. N. (2011). RSEM: accurate transcript quantification from RNA-Seq data with or without a reference genome. *BMC Bioinf.* 12 (1), 323–338. doi: 10.1186/1471-2105-12-323
- Liu, H. C., Lämke, J., Lin, S. Y., Hung, M. J., Liu, K. M., Charng, Y. Y., et al. (2018a). Distinct heat shock factors and chromatin modifications mediate the organ-autonomous transcriptional memory of heat stress. *Plant J.* 95 (3), 401–413. doi: 10.1111/tpj.13958
- Liu, Y., Song, X., Shi, Y., and Zhao, Y. (2018b). Physiological responses comparison of *Rhododendron hainanense* and *Rhododendron mucronatum* (Blume) G. Don under high temperature stress. *Mol. Plant Breed.* 16 (17), 5827–5834.
- Livak, K. J., and Schmittgen, T. D. (2001). Analysis of relative gene expression data using real-time quantitative PCR and the 2^{-ΔΔCT} method. *Methods* 25 (4), 402–408. doi: 10.1006/meth.2001.1262
- Martinez-Medina, A., Flors, V., Heil, M., Mauch-Mani, B., Pieterse, C. M., Pozo, M. J., et al. (2016). Recognizing plant defense priming. *Trends Plant Sci.* 21 (10), 818–822. doi: 10.1016/j.tplants.2016.07.009
- Mueller, S. P., Krause, D. M., Mueller, M. J., and Fekete, A. (2015). Accumulation of extra-chloroplastic triacylglycerols in *Arabidopsis* seedlings during heat acclimation. *J. Exp. Bot.* 66 (15), 4517–4526. doi: 10.1093/jxb/erv226
- Muthusamy, S. K., Dalal, M., Chinnusamy, V., and Bansal, K. C. (2017). Genome-wide identification and analysis of biotic and abiotic stress regulation of small heat shock protein (HSP20) family genes in bread wheat. *J. Plant Physiol.* 211, 100–113. doi: 10.1016/j.jplph.2017.01.004
- Nagarajan, R., and Gill, K. S. (2018). Evolution of Rubisco activase gene in plants. *Plant Mol. Biol.* 96 (1–2), 69–87. doi: 10.1007/s11103-017-0680-y
- Niinemet, Ü., Berry, J. A., von Caemmerer, S., Ort, D. R., Parry, M. A., and Poorter, H. (2017). Photosynthesis: ancient, essential, complex, diverse... and in need of improvement in a changing world. *New Phytol.* 213 (1), 43–47. doi: 10.1111/nph.14307
- Nilsen, T. W., and Graveley, B. R. (2010). Expansion of the eukaryotic proteome by alternative splicing. *Nature* 463 (7280), 457–463. doi: 10.1038/nature08909
- Perez-Riverol, Y., Csordas, A., Bai, J., Bernal-Linares, M., Hewapathirana, S., Kundu, D., et al. (2019). The PRIDE database and related tools and resources in 2019: improving support for quantification data. *Nucleic Acids Res.* 47 (D1), D442–D450. doi: 10.1093/nar/gky1106
- Portis, A. R. (2003). Rubisco activase–Rubisco’s catalytic chaperone. *Photosynth. Res.* 75 (1), 11–27. doi: 10.1023/A:1022458108678
- Queitsch, C., Hong, S.-W., Vierling, E., and Lindquist, S. (2000). Heat shock protein 101 plays a crucial role in thermotolerance in *Arabidopsis*. *Plant Cell* 12 (4), 479–492. doi: 10.1105/tpc.12.4.479
- Ramirez-Carrasco, G., Martinez-Aguilar, K., and Alvarez-Venegas, R. (2017). Transgenerational defense priming for crop protection against plant pathogens: A hypothesis. *Front. Plant Sci.* 8, 696. doi: 10.3389/fpls.2017.00696
- Salvucci, M. E., and Crafts-Brandner, S. J. (2004). Relationship between the heat tolerance of photosynthesis and the thermal stability of Rubisco activase in plants from contrasting thermal environments. *Plant Physiol.* 134 (4), 1460–1470. doi: 10.1104/pp.103.038323
- Salvucci, M. E. (2008). Association of Rubisco activase with chaperonin-60β: a possible mechanism for protecting photosynthesis during heat stress. *J. Exp. Bot.* 59 (7), 1923–1933. doi: 10.1093/jxb/erm343
- Sanchez de Jimenez, E., Medrano, L., and Martinez-Barajas, E. (1995). Rubisco activase, a possible new member of the molecular chaperone family. *Biochemistry* 34 (9), 2826–2831. doi: 10.1021/bi00009a012
- Sharkey, T. D., Badger, M. R., Von Caemmerer, S., and Andrews, T. J. (2001). Increased heat sensitivity of photosynthesis in tobacco plants with reduced Rubisco activase. *Photosynth. Res.* 67 (1–2), 147–156. doi: 10.1023/a:1010633823747
- Stamm, S., Ben-Ari, S., Rafalska, I., Tang, Y., Zhang, Z., Toiber, D., et al. (2005). Function of alternative splicing. *Gene* 344, 1–20. doi: 10.1016/j.jgene.2012.07.083
- von Mering, C., Jensen, L. J., Snel, B., Hooper, S. D., Krupp, M., Foglierini, M., et al. (2005). STRING: known and predicted protein–protein associations, integrated and transferred across organisms. *Nucleic Acids Res.* 33 (suppl_1), D433–D437. doi: 10.1093/nar/gki005
- Walter, J., Jentsch, A., Beierkuhnlein, C., and Kreyling, J. (2013). Ecological stress memory and cross stress tolerance in plants in the face of climate extremes. *Environ. Exp. Bot.* 94, 3–8. doi: 10.1016/j.envexpbot.2012.02.009
- Wang, L., Feng, Z., Wang, X., Wang, X., and Zhang, X. (2009). DEGseq: an R package for identifying differentially expressed genes from RNA-seq data. *Bioinformatics* 26 (1), 136–138. doi: 10.1093/bioinformatics/btp612
- Wollerton, M. C., Gooding, C., Wagner, E. J., Garcia-Blanco, M. A., and Smith, C. W. (2004). Autoregulation of polypyrimidine tract binding protein by alternative splicing leading to nonsense-mediated decay. *Mol. Cell* 13 (1), 91–100. doi: 10.1016/S1097-2765(03)00502-1

- Wu, T., Juan, Y., Hsu, Y., Wu, S., Liao, H., Fung, R. W., et al. (2013). Interplay between heat shock proteins HSP101 and HSA32 prolongs heat acclimation memory posttranscriptionally in Arabidopsis. *Plant Physiol.* 161 (4), 2075–2084. doi: 10.1104/pp.112.212589
- Xu, L., Yu, J., Han, L., and Huang, B. (2013). Photosynthetic enzyme activities and gene expression associated with drought tolerance and post-drought recovery in Kentucky bluegrass. *Environ. Exp. Bot.* 89, 28–35. doi: 10.1016/j.envexpbot.2012.12.001
- Zeng, W., Sun, Z., Cai, Z., Chen, H., Lai, Z., Yang, S., et al. (2017). Proteomic analysis by iTRAQ-MRM of soybean resistance to *Lamprosema Indicate*. *BMC Genomics* 18 (1), 444–465. doi: 10.1186/s12864-017-3825-0
- Zhong, L., Zhou, W., Wang, H., Ding, S., Lu, Q., Wen, X., et al. (2013). Chloroplast small heat shock protein HSP21 interacts with plastid nucleoid protein pTAC5 and is essential for chloroplast development in Arabidopsis under heat stress. *Plant Cell* 25 (8), 2925–2943. doi: 10.1105/tpc.113.111229
- Conflict of Interest:** The authors declare that the research was conducted in the absence of any commercial or financial relationships that could be construed as a potential conflict of interest.

Copyright © 2020 Wang, Li, Liu, Zhou, Elmongy and Xia. This is an open-access article distributed under the terms of the Creative Commons Attribution License (CC BY). The use, distribution or reproduction in other forums is permitted, provided the original author(s) and the copyright owner(s) are credited and that the original publication in this journal is cited, in accordance with accepted academic practice. No use, distribution or reproduction is permitted which does not comply with these terms.



Imaging of Chlorophyll *a* Fluorescence in Natural Compound-Induced Stress Detection

Adela M. Sánchez-Moreiras^{1,2*}, Elisa Graña¹, Manuel J. Reigosa^{1,2} and Fabrizio Araniti³

¹ Department of Plant Biology and Soil Science, Faculty of Biology, University of Vigo, Vigo, Spain, ² CITACA, Agri-Food Research and Transfer Cluster, University of Vigo, Ourense, Spain, ³ Department AGRARIA, University "Mediterranea" of Reggio Calabria, Reggio Calabria, Italy

OPEN ACCESS

Edited by:

Angeles Calatayud,
Instituto Valenciano
de Investigaciones Agrarias, Spain

Reviewed by:

Werner B. Herppich,
Leibniz Institute for Agricultural
Engineering and Bioeconomy (ATB),
Germany
Pei Wang,
Jiangsu University, China

*Correspondence:

Adela M. Sánchez-Moreiras
adela@uvigo.es

Specialty section:

This article was submitted to
Technical Advances in Plant Science,
a section of the journal
Frontiers in Plant Science

Received: 15 July 2020

Accepted: 19 November 2020

Published: 21 December 2020

Citation:

Sánchez-Moreiras AM, Graña E,
Reigosa MJ and Araniti F (2020)
Imaging of Chlorophyll *a* Fluorescence
in Natural Compound-Induced Stress
Detection.
Front. Plant Sci. 11:583590.
doi: 10.3389/fpls.2020.583590

Imaging of chlorophyll *a* fluorescence (CFI) represents an easy, precise, fast and non-invasive technique that can be successfully used for discriminating plant response to phytotoxic stress with reproducible results and without damaging the plants. The spatio-temporal analyses of the fluorescence images can give information about damage evolution, secondary effects and plant defense response. In the last years, some studies about plant natural compounds-induced phytotoxicity have introduced imaging techniques to measure fluorescence, although the analysis of the image as a whole is often missed. In this paper we, therefore, evaluated the advantages of monitoring fluorescence images, presenting the physiological interpretation of different possible combinations of the most relevant parameters linked to fluorescence emission and the images obtained.

Keywords: plant natural compounds, phytotoxicity, imaging fluorescence, photosynthesis, plant stress

INTRODUCTION

Considered as a non-invasive, fast and cheap technique that allows to rapidly detect and localize stressors effects on plants, chlorophyll *a* fluorescence (CF), has been largely used in plant science in the last decades, both clamping- and image-based Chlorophyll *a* fluorescence analysis (CFA) (Dayan and Zaccaro, 2012; de Carvalho et al., 2016). CFA gives the possibility to estimate, almost instantly, the photosynthetic efficiency under stress conditions and is especially useful in the detection of early stress responses (Chaerle and van der Straeten, 2000; Chaerle and Van Der Straeten, 2001; Chaerle et al., 2009). That is the reason why fluorescence measurement has been increasingly used to measure phytotoxicity in the last years.

Considering that herbicides will continue to be the worldwide method of weed control, easily and reproducibly exploring the wide range of molecules that nature offers seems the most appropriate way to search for new eco-herbicides. Secondary plant metabolites with relevant herbicide potential are essential in this context (Duke et al., 2000b), as the use of natural products allows protecting *a priori* the quality of the environment and, at the same time, the health of mammals during the control of weeds (Liebman, 2001). Therefore, in recent years, the study of the mode of action of natural compounds with herbicide potential is occupying a preferential place in integrated agriculture, thanks to the new physiological and molecular techniques that can integrate its multidisciplinary study (Sánchez-Moreiras et al., 2018). Among the several reasons for a long

period without new herbicide target sites is also the difficulty to find new effective modes of actions for killing plants (Duke, 2011).

Looking at natural compounds, which have been undergoing strong evolutionary pressure for hundreds of years, would help to give light on this aspect. In fact, precisely the mode of action of these molecules is one of the potential advantages of secondary metabolites over synthetic herbicides. Natural compounds frequently present a strong structural diversity, which could result in novel molecular sites of action different from those already known for commercial herbicides. This would allow facing the weed resistance problem with a broader arsenal of modes of action (Duke et al., 2000a). The use of natural products as agrochemical compounds must necessarily go through the characterization of their mechanisms of action to know where, when and how they act in plant metabolism. That is the ultimate objective. However, a truly low number of modes of action is known at the current stage of research in plant natural compounds, which complicates their study and classification. Therefore, most studies on phytotoxicity induced by plant secondary metabolites focus on monitoring of their effects from a physiological perspective to detect the early effects of the compounds on roots and shoots. In this sense, CFA analysis is one of the techniques that could easily show the effects of bioherbicides on leaves. As stated by Dayan and Zaccaro (2012), the crucial step in the discovery of natural products that could be acting as photosystem II (PSII) inhibitors is simply evaluating the photosynthetic electron transport activity in leaves. Precise and reproducible CFA provides the demanded detailed analysis of the photosynthesis inhibition.

During the last 20 years, some excellent papers reviewed the use of CFA to measure stress response in plants (Maxwell and Johnson, 2000; Nedbal and Whitmarsh, 2004; Papageorgiou and Govindjee, 2004; Roháček et al., 2008; Kalaji et al., 2014, 2017; Guidi et al., 2019), while others focused on the use of imaging techniques to establish stress-related changes in chlorophyll fluorescence parameters (Chaerle et al., 2009; Martínez-Peñalver et al., 2011; Gorbe and Calatayud, 2012; Guidi et al., 2016). In this paper, we will provide a review of studies that applied chlorophyll fluorescence imaging (CFI) to monitoring the phytotoxic effects induced by plant natural compounds. Furthermore, we will present the physiological interpretation of possible results obtained by CF recording and will highlight the importance of considering both the PSII efficiency and its distribution over the plant.

CHLOROPHYLL FLUORESCENCE ANALYSIS: A SIMPLE METHOD FOR A COMPLEX PICTURE OF PSII

The principles of chlorophyll fluorescence analysis are relatively simple. Basically, absorption of a photon promotes an electron of a chlorophyll *a* molecule to an excited state while a fluorescence photon is immediately emitted again during the return of the molecule to the ground state.

The first observation of fluorescence induced by solar radiation was recorded almost two centuries ago by David Brewster, which observed that illuminating a laurel leaves alcoholic extract with a sunbeam elicited a brilliant red light (Brewster, 1834). Moreover, he also observed that passing through the extract, the emission changed its color varying from red to orange and then to yellow, suggesting for the first time that this transition was probably due to chlorophyll re-absorption (Govindjee, 1995). The term “chlorophyll fluorescence” was coined by Stokes (1852) to describe this emission. Successively, Müller (1874) suggested a link between fluorescence emission and photosynthetic assimilation, which was successively confirmed by Kautsky and Hirsch (1931). These authors described, for the first time, the kinetics of chlorophyll *a* fluorescence emission of leaves previously adapted to dark, and then suddenly irradiated with light, correlating the signature of the initial fluorescence peak and its prompt decay to a lower steady-state to the time course of CO₂ assimilation (for details see Govindjee, 2004).

The covariation between photosynthesis and chlorophyll fluorescence was successively described by McAlister and Myers (1940). They reported and described two different processes: (i) one characterized by an inverse relation between CF intensity and the rate of CO₂ uptake, and the other (ii) considering a direct relationship between these two parameters.

A detailed description of this dual response was successively described by Duysens and Sweers (1963), which used a modulated excitation light for the first time and described, also for the first time, that the fluorescence yield was actively regulated by a process known today as “non-photochemical quenching” (Weis and Berry, 1987; Krause and Weis, 1991). This information was successively used to prove a quantitative relationship between the electron transport rate and the fluorescence yield (Weis and Berry, 1987; Genty et al., 1989).

After that, it became clear that CF is one of the mechanisms for energy dissipation, together with photochemistry and non-photochemical quenching (Schreiber, 1983; Krause and Weis, 1984; Demmig-Adams et al., 1990; Havaux et al., 1991; Björkman and Demmig-Adams, 1995). Therefore, being able to relate CF with changes in the photosynthetic apparatus it allows the quantification of the extent to which CF decreases by photochemistry (namely photochemical quenching) or non-radiative decay (non-photochemical quenching).

From the 1990s on, CFA has been widely used with the attempt to detect modifications occurring in the photosynthetic process, especially in plants under stress conditions (Schreiber and Neubauer, 1987; Endo et al., 1995; Maxwell and Johnson, 2000; Papageorgiou and Govindjee, 2004). CF parameters are very sensitive and detect the emergence of stress, even before visible symptoms appear over the leaf lamina, or a decline of photosynthesis can be determined by gas exchange measurements (Gorbe and Calatayud, 2012). However, in some cases, i.e., in plants subjected to abiotic stressors leading to rapid stomata closure, CF parameters might have a delayed response when compared to gas exchange analyses (Schreiber et al., 1995).

CF can be excited by illuminating green plant tissues with pulsed (Schreiber et al., 1986; Schreiber, 2004) or continuous (Strasser and Govindjee., 1991) visible or ultra violet (UV) light by either single or grouped LEDs (light emitting diode) or halogen lamps. In addition, deuterium lamps were also used in old systems (Schreiber et al., 1993). Using visible light, light-induction kinetics, as well as the measurement in the true steady state, is one of the most widely used approach in CF measurement (Lazár, 2003; Gorbe and Calatayud, 2012). This technique, which uses actinic light illumination, allows monitoring and measuring both the photochemical and non-photochemical processes involved in fluorescence quenching. The pulse amplitude modulated (PAM) fluorometer is the most common and largely used fluorometer in CF monitoring (Bolhar-Nordenkamp et al., 1989; Häder et al., 1998). In addition, also OIJP test is a very informative and routinely used method to evaluate fast kinetics of CF (Hermans et al., 2003; Digrado et al., 2017).

Depending on the state of electron transport chain components and dark/light adaptation of the photosynthetic tissues, five different CF emission signals can be detected: F_0 , F'_0 , F_m , F'_m , and F_s (Maxwell and Johnson, 2000) (Table 1). F_0 and F_m , determined on dark-adapted samples, correspond to both minimum and maximum fluorescence yield before and after a saturating light pulse takes place, respectively. Briefly, a period of dark adaptation (20–30 min) allows all reaction centers to be open and the exposure to modulated weak light ($<1.0 \mu\text{mol photons m}^{-2} \text{s}^{-1}$ which is not sufficient to induce an electron transport chain) induces an increase in the CF yield, namely F_0 (Table 1). Then, a strong saturating light pulse (from 8,000–15,000 $\mu\text{mol photons m}^{-2} \text{s}^{-1}$ which induces the closure of all reaction centers) is applied and induces a rapid increase in the CF yield, namely F_m (Table 1). After that, CF yield decreases and, in the presence of actinic light, it reaches steady-state values (F_s) that correspond to a balance between the reduced and oxidized state of primary electron acceptor Q_A . Conversely, F'_0 and F'_m are determined after sample receives actinic illumination, and represent the minimal and maximal fluorescence yield in light conditions, respectively (Table 1). The determination of F'_0 under light conditions requires the use of far-red light to transiently and selectively excite PSI, and thus to enhance the oxidation of the electron transport chain (Bilger and Schreiber, 1987).

Using these five fluorescence emission signals is possible to calculate other CF parameters. Among them, it is worth to mention the maximal PSII quantum yield (F_v/F_m), the effective PSII quantum yield (Φ_{II}), both photochemical (qp) and non-photochemical quenching (NPQ), as well as the quantum yield of regulated (Φ_{NPQ}) and non-regulated energy dissipation (Φ_{NO}), which compete with Φ_{II} for energy partitioning (i.e., $\Phi_{II} + \Phi_{NO} + \Phi_{NPQ} = 1$; Kramer et al., 2004) (Table 1). Of note, the q_{NP} coefficient consists of three different components: energy-dependent quenching related to the build-up of the trans-thylakoidal pH-gradient, q_E ; quenching due to the state II-I transition of the phosphorylated light harvesting complex of PSII, q_T ; and photo-inhibitory quenching, q_I (Horton and Hague, 1988).

Nowadays, other new parameters have been introduced with the attempt to make CF a very detailed diagnostic tool. In some cases some stress-related parameters, allow to anticipate the occurrence of visible symptoms over the leaf lamina. As an example qPd (photochemical quenching measuring in the dark) enables the detection of earliest signs of photoinhibition (when qPd value is 1 corresponds to 100% of open RCIIIs) (Ruban and Murchie, 2012). In addition, the use of imaging-based instruments provides information on the distribution of CF over a selected area of the sample (Gorbe and Calatayud, 2012).

However, in view of the high number of excellent reviews on CF, both applicative and theoretical, the in-depth description of CF parameters is out of the scope of the present review (for example, for detailed reviews on CF parameters refer to Schreiber and Bilger, 1993; Schreiber et al., 1998; Maxwell and Johnson, 2000; Baker and Rosenqvist, 2004; Gorbe and Calatayud, 2012; Kalaji et al., 2014, 2017; Guidi et al., 2016).

TOOLS FOR IMAGING CHLOROPHYLL FLUORESCENCE

The invention of video imaging systems was an important breakthrough in the field of chlorophyll fluorescence analysis (Omasa et al., 1987; Fenton and Crofts, 1990). In fact, this technique not only allowed to spatially examine the heterogeneity within a sample, but it also made possible to evaluate those changes simultaneously on a wide number of samples, making the CFI more popular as diagnostic (Baker, 2008), screening (Barbagallo et al., 2003) and phenotyping tool (Rühle et al., 2018; Pérez-Bueno et al., 2019).

The use of chlorophyll photometer capable to image CFA is known from decades. At the beginning, the CFI instruments were able to image chlorophyll fluorescence at F_m and F'_m and at F or F_s by using a high incident irradiance, but those instruments were unable to image at F_0 , F'_0 , and F_s under moderate to high incident irradiance (Genty and Meyer, 1995; Siebke and Weis, 1995a,b; Scholes and Rolfe, 1996). Oxborough and Baker (1997) described the first instrument that was able to image those parameters. This instrument, mainly based on an epifluorescence microscopy connected to a CCD camera, was characterized by a large dynamic range, and by the capacity of generating images of CF using low incidence irradiance ($0.1 \mu\text{mol m}^{-2} \text{s}^{-1}$). In addition, it gave the possibility to work on part of the leaf tissue as well as on single cells.

Lichtenthaler et al. (2005) developed a compact flash-lamp fluorescence imaging system, which was based on the Karlsruhe/Strasbourg laser-induced fluorescence imaging system (Lang et al., 1994; Lichtenthaler, 1996; Lichtenthaler and Miehé, 1997). The instrument was produced to replace, as excitation source, the expensive ND:YAG laser by a cheaper xenon flash lamp, which allows measurements with high pulse frequency and short gating times (Buschmann et al., 2000; Lichtenthaler and Babani, 2000; Lichtenthaler et al., 2005).

The technique, as well as the tools to monitor chlorophyll fluorescence emission, was further implemented and

TABLE 1 | List and definition of the most common chlorophyll fluorescence parameters.

Fluorescence parameters	Definition
F_0	Known as dark fluorescence yield it is measured on dark-adapted plants (all PSII reaction centers are open) and represents the minimal chlorophyll fluorescence intensity.
F_m	Also measured on dark-adapted plants during the application of a saturating pulse of light and represent the maximal chlorophyll fluorescence intensity.
F'_0	Parameter measured during the light-adapted state and represents the minimal chlorophyll fluorescence intensity.
F'_m	Parameter measured on light-adapted plants during the saturation pulse and representing the maximal chlorophyll fluorescence intensity.
F_s	Parameter measured during the steady-state, non-saturating actinic illumination, representing the chlorophyll fluorescence intensity
$F_v = (F_m - F_0)$	Parameter measured during the dark-adapted state (non-photochemical processes are at the lowest level) representing the variable chlorophyll fluorescence
F'_v	Parameter F_v measured during the light-adapted state
F_v/F_m	Maximum quantum yield of dark adapted PSII
F'_v/F'_m	Parameter measured during the light-adapted state representing the exciton transfer efficiency from antenna pigments to PSII reaction centers
F_0/F_v	Parameter measured during the dark-adapted state representing the Ratio of minimal chlorophyll fluorescence intensity/variable chlorophyll fluorescence
F_m/F_s	Parameter that indicates the photosynthetic quantum conversion obtained from ratio between the maximal chlorophyll fluorescence intensity (measured in the dark-adapted state) and chlorophyll fluorescence at steady-state.
$RF_d = (F_m - F_s)/F_s$	This parameter (RF_d – chlorophyll fluorescence decreases ratio), correlated with CO_2 fixation rates, is an indicator of the photosynthetic quantum conversion.
$NPQ = (F_m - F'_m)/F'_m$	Stern-Volmer's non-photochemical quenching coefficient
$\Phi_{II} = (F'_m - F_s)/F'_m$	Effective PSII quantum yield
$\Phi_{NO} = 1/[NPQ + 1 + qL (F_m/F_0 - 1)]$	Quantum yield of non-regulated energy dissipation in PSII. High Φ_{NO} values indicate that both protective regulatory mechanisms and photochemical energy conversion are inefficient, suggesting that plant is unable to cope with the incident radiation.
$\Phi_{NPQ} = 1 - \Phi_{II} - \Phi_{NO}$	Quantum yield of regulated energy dissipation in PSII representing the ability of PSII to dissipate the energy in excess in the form of heat
Φ_{NPQ}/Φ_{NO}	Parameter representing the ratio of quantum yield of regulated to non-regulated energy dissipation in PSII. It is connected to the ability of photosynthetic apparatus to activate photoprotection mechanisms
$qN = (F_m - F'_m)/(F_m - F'_0)$	Parameter representing the coefficient of non-photochemical quenching of variable fluorescence
$qP = (F'_m - F_s)/(F'_m - F'_0)$	Parameter based on the puddle model of PSII representing the coefficient of photochemical quenching of variable fluorescence
$qL = qP \times F_0/F_s$	Parameter based on the lake model of PSII representing the coefficient of photochemical quenching of variable fluorescence

The table includes only the most common parameters, for comprehensive reviews on this topic refer to the review of Baker (2008) and Maxwell and Johnson (2000).

hyphenated with phenotyping tools for both diagnostic and breeding purposes.

CFI, associated to phenotyping tools, gives the possibility to early detect plants stress responses to both biotic and abiotic stressors, before the development of visible symptoms. At agricultural level, especially for sustainable/precision agriculture, the use of CFI as research tool could have an extensive field of application. CFI could facilitate the researchers in identifying and evaluating crop stress thresholds allowing, with the help of sensors (e.g., temperature, humidity and conductivity sensors among others), not only to make targeted and/or localized interventions but also to plan them only when necessary. This could permit to anticipate irreversible damages to the photosynthetic apparatus. Anyway, at the moment, CFI technique is too slow and expensive to be used as a commercial diagnostic tool in open field and/or greenhouses.

Depending on the crop and on the pedological and pedoclimatic conditions, it can be used as a research tool to extrapolate the stress-thresholds of a given species, which

can be integrated in more complexes algorithms and used for crop management.

At both laboratory and field levels, Photon Systems Instruments (Brno, Czech Republic), Walz (Effeltrich, Germany), and Technologica Ltd., (Essex, United Kingdom) commercialized several instruments (for more details have a look at the website of the companies) that allow the application of this technology at macroscopic and microscopic levels, and on terrestrial and aquatic organisms (Levin et al., 2017; Ayalon et al., 2019).

Imaging fluorometers have been also integrated with a gas-exchange chamber, which allows to obtain information about CF, the imaging of its parameters, and also about the plant gaseous exchanges, giving wider information concerning the photosynthetic machinery status in response to stress (Daley et al., 1989; Rolfe and Scholes, 1995; Kurepin et al., 2018).

The combination of CFI with the technique of the infra-red gas exchange (IRGA) allows to directly correlating the efficiency of PSII with the CO_2 assimilation rate. This could be achieved avoiding the photorespiration through the increase

of CO₂ concentration or reducing the concentration of O₂. This technique has been used to visualize patterns of CO₂ diffusion in leaves, enabling the determination of gas fluxes within leaves of different species (Morison et al., 2005, 2007; Lawson and Morison, 2006).

Also, the use of CFI tools in combination with other imaging techniques could give important information in plant phenotyping. For example, CFI coupled to hyperspectral imaging was used for early detecting fungal disease in wheat, whereas coupled to thermography it was used to provide information concerning the correlation between photosynthetic rate and stomatal behavior, as well as in imaging intrinsic water use efficiency (Chaerle et al., 2007; Lawson, 2009; Bauriegel et al., 2011).

Moreover, imaging fluorometers integrated with phenotyping platforms, which in the past were exclusively used for research purposes, are now commercially available (e.g., HyperAIXpert from Lemnatech; PlantScreen System from Photon Systems Instruments, etc.). These platforms, in addition to the phenotypic traits, allow imaging of chlorophyll fluorescence in order to get high-throughput analysis of plant phenotype (Awlia et al., 2016). To study plant-pathogen interactions as well as to investigate changes in plant physiology and biochemistry, in response to stress, imaging fluorometers have been integrated with a GFP filter for imaging (not simultaneously) green fluorescent proteins in transformed plants, and/or in plants inoculated with GFP-transformed strains of pathogens, which is extremely useful for molecular and cellular biology studies (Lee et al., 2019; Pérez-Bueno et al., 2019). Other imaging fluorometers have also been adapted to study the photosynthesis in plants growing under water, which allows to evaluate the response of plants to several stressors such as water pollution or CO₂ variations (Papathanasiou et al., 2020).

Other tools, applicable to microscopy, have been also developed in order to allow the monitoring of CFI heterogeneities at the level of single cell (e.g., on algae or stomata guard-cells) and they could allow to taxonomically differentiate algae types, like diatoms, chlorophytes, and cyanobacteria (Oxborough and Baker, 1997; Levin et al., 2017).

For example, through the combination of a microscope CFI system equipped with an IRGA chamber, Lawson et al. (2002) were able to demonstrate that the major sink for guard cell photosynthetic electron transport was the Calvin cycle activity and that the photosynthetic efficiency of the guard cell is not linked to the opening and closing of the stomata.

The majority of CFI tools, to ensure a coverage of actinic illumination and fully saturating pulses on a huge portion of plant area, requires large panels on which light-emitting diode arrays are mounted making these tools extremely large in size and barely usable in open field. Nevertheless, some fluorescence monitoring tools, equipped with a cabinet (for dark-adaptation purposes) and mounted on wheels (to allow movement in the field collecting images over the crops), were built (Murchie and Lawson, 2013; Tan et al., 2018).

Finally, new generations of low-weight dfov (dual field of view) spectrometer systems have been developed to monitor and image solar-induced CF variations in both open fields and

green houses. Those instruments can be managed remotely and located on both fixed and mobile workstations (i.e., drones) (Atherton et al., 2018).

IMAGING OF CHLOROPHYLL FLUORESCENCE IN THE STUDY OF NATURAL COMPOUNDS

The use of CF as a phenotyping and/or diagnostic tool was quickly growing in the last decade. Several reviews were written about it (Humlík et al., 2015; Pérez-Bueno et al., 2019) and new researchers are trying to extend its applications (Weber et al., 2017; McAusland et al., 2019).

Especially in herbicidal studies, CF has been extensively used as a marker for the study of herbicide mode of action or for the identification of weed resistance (Dayan and Zaccaro, 2012). However, although several manuscripts focused on both monitoring CF during several stress, including herbicides, and the pattern of fluorescence changes through imaging, relatively few information is available concerning the use of imaging signatures during the evaluation of the herbicidal potential of natural compounds and extracts.

Because of that, the best way to evaluate natural compounds target and mode of action should be to compare the fluorescence signature induced by natural compounds with that of the most known and used herbicides. Unluckily, the number of studies doing that is little, and the use of CFI tools in this field of the research is extremely low. Moreover, this technique is often used just to get PSII parameters without giving the right importance to the imaging output. As a consequence, the information concerning the pattern of action of natural phytotoxic compounds is fragmented and superficial.

One of the first studies, focusing on the application of CFI analysis on phytotoxic natural compounds, was reported by Beninger et al. (2004). In particular, they evaluated the phytotoxic potential of three phenolic compounds isolated from *Chrysanthemum morifolium* on the model species *Lemna gibba*. They observed that chlorogenic acid and the flavanone eriodictiol strongly affected the photosynthetic activity with deep reductions in F_v/F_m . Both compounds acted as bleaching herbicides causing a loss of photosynthetic pigments and the inhibition of photosynthetic activity. However, interestingly, while overall F_v/F_m values were reduced just in the plants treated with 1000 ppm, the area of the plant experiencing photosynthesis was reduced also in the leaves treated with the lowest concentration (100 ppm), probably due to the loss of photosynthetic pigments.

Kriegs et al. (2010) demonstrated that the quantum yield efficiency (F_v/F_m) of Arabidopsis plants, fumigated with the monoterpene camphor, was directly affected by the treatment. In particular, they reported that during short-time fumigation the parameter F_v/F_m was strongly lowered compared to control, but it promptly recovered at the end of the treatment, and the plant fitness was significantly strengthened. On the other hand, repeated exposure to the monoterpene led to irreversible damages and alteration in plant phenotype. Probably, the negative

effects induced by long-term exposure could be connected to the high cuticular dewaxing ability of camphor as previously demonstrated by Schulz et al. (2007). However, although authors used the imaging apparatus Growscreen-Fluoro, an automated imaging pipeline designed to analyze the chlorophyll fluorescence of rosette plants, no images about the effects of this monoterpene on plants were shown in the manuscript. This is a pity since images could be extremely helpful in understanding the dynamic of the effects of the terpenoid and the overall plant responses to the treatment.

An example of how imaging techniques can broaden our knowledge on natural compound effects was published by Sánchez-Moreiras et al. (2011) with the allelochemical 2-3H-benzoxazolinone (BOA). Previous single-point measurements of photochemical and non-photochemical parameters in BOA-treated plants suggested that increase in fluorescence emission was due to BOA-induced oxidative stress (Sánchez-Moreiras and Reigosa, 2005). However, CFI together with imaging hydrogen peroxide and superoxide anion, revealed that the primary phytotoxic effect of BOA was the induction of premature senescence, and oxidative stress was just a secondary effect of this treatment (Sánchez-Moreiras et al., 2011).

The advantage of obtaining an image of CF and its distribution all over the plant in intact and alive individuals is one of the aspects that can most enrich the study of phytotoxic compounds, as it can give information about the area of the leaf where the effect starts first. Studies carried out on the *trans*-cinnamic derivative *o*-coumaric acid, one of the major constituents of the invasive species *Eupatorium adenophorum*, demonstrated that this molecule significantly affected the photosynthetic machinery of the model species *Arabidopsis thaliana*, pointing out a differential effect on photosynthesis depending on the age of the leaves (Zheng et al., 2012). In particular, they observed that after 7 d of treatment, F_v/F_m dropped dramatically in older leaves, whereas younger central leaves were hardly affected, suggesting that *o*-coumaric acid could promote leaf senescence. In addition, Graña et al. (2013b) demonstrated that adult *Arabidopsis* plants sprayed with the monoterpene citral had a heterogeneous spatial distribution in fluorescence emission, mainly concentrated at the edges of the older leaves, whereas the youngest leaves were not affected. This could suggest the initiation of early senescence processes, where the photosynthetic apparatus is systematically dismantled (Wingler et al., 2004).

Several studies evaluating effects of natural products by CFI indicated that the majority of these products and/or their extracts generally reduced F_v/F_m . This may suggest a direct damage to PSII, whereas the yield of non-photochemical energy dissipation, Φ_{NO} and Φ_{NPQ} , was extremely variable, probably depending on type and/or dose of the extract or compound assayed. In fact, natural compounds that are extremely phytotoxic at high doses can be stimulant at low doses, a phenomenon known as hormesis (Belz and Duke, 2017). For example, the aqueous extract of *Mentha X piperita* may be inhibitory or stimulatory on chlorophyll content and on PSII (analyzed by CFI) of sunflower leaves depending on the concentrations assayed (Skrzypek et al., 2015). The authors observed that low concentrations of peppermint extract significantly increased

F_v/F_m ratio and the Φ_{NPQ} on the entire leaf surface. In contrast, higher concentrations significantly reduced the regulated non-photochemical energy dissipation suggesting a negative effect on the photosynthetic machinery. Skrzypek et al. (2015) observed also that the highest changes in CF were specifically around the petioles and in the distal margins of leaf blade. Those results highlight the importance of imaging parameters, which can give a lot of quick and precise information of the exact stimulatory and inhibitory doses of a given compound, as well as the induced damage.

In adult chalcone-treated *Arabidopsis* plants, Díaz-Tielas et al. (2014) found an early decline in ETR concomitant with a significant increase in Φ_{NO} and a late reduction in maximum PSII efficiency (F_v/F_m). Supported by the imaging of damages localization, they suggested that the chalcone-induced reduction in photosynthetic rate could have resulted in an excessive demand on regulated antenna de-excitation processes inducing damages to the antenna complex and, consequently, F_v/F_m reduction. Based on these previous imaging studies, Díaz-Tielas et al. (2017) observed that chalcone treatment on young *Arabidopsis* seedlings induced progressive pigment degradation and bleaching. They demonstrated that this progressive de-greening, together with F_v/F_m , Φ_{II} reduction and Φ_{NO} increase, was directly linked to early plasma membrane depolarization and dramatic effects on chloroplasts structure and function, as part of chalcone mode of action.

Essential oils (EOs) are among the most studied and commercially used natural extracts with phytotoxic potential. Recent studies demonstrated that pure terpenoids, isolated from EOs, have a wide range of metabolic targets and modes of action (Graña et al., 2013a; Araniti et al., 2017a). It has been proven that several compounds can act synergistically changing completely the effects of these natural mixtures and/or pure molecules on the photosynthetic machinery. For example, Araniti et al. (2018a) demonstrated that EO isolated from *Origanum vulgare* inhibits glutamate and aspartate metabolism in *A. thaliana*. The inhibition of these metabolic pathways induced an accumulation of ammonia in leaf cells and, concomitantly, a cascade of reactions that limited the efficiency of PSII. Through the imaging of F_v/F_m and Φ_{II} parameters authors were able to identify which areas of the leaves were mostly affected by EOs treatment. Moreover, they highlighted through the imaging output an overlap between reactive oxygen species (ROS) accumulation (monitored through *in situ* staining methods) and damages to PSII (reduction in F_v/F_m).

This was not the first work detecting overlap among PSII damage and ROS accumulation in response to terpenoids. Araniti et al. (2017b), studying plant-plant interaction, mimicking natural conditions, demonstrated that volatiles released by the widespread species *Dittrichia viscosa* were able to induce ROS accumulation in lettuce leaves causing F_v/F_m inhibition. Through CFI, they also evidenced an overlap between the leaf area where ROS were accumulating and leaf area characterized by F_v/F_m reduction. Those results suggested that probably the burning activity of the EOs could be mainly due to a side effect (ROS

burst) instead of a direct contact of the chemical mixture with the leaves.

Recently, Synowiec et al. (2019) bioassayed the effects of caraway and peppermint EOs on *Zea mays* and its associated weeds. They demonstrated, through CFI, that the application of caraway EOs at a given concentration strongly affected the PSII of *Echinochloa crus-galli*. However, it was hardly effective on *Z. mays*, highlighting the species-specific effects of EOs, and suggesting that caraway EOs could be a good candidate for weed management in maize crop.

Graña et al. (2013b), bioassaying through sub-irrigation or spraying, the monoterpene citral on adult plants of *A. thaliana* observed that both treatments strongly affected either the photochemical or non-photochemical activity. Citral effects were earlier and more pronounced in sprayed plants than in watered. In fact, while sprayed leaves were severely damaged by the treatment, leaves of sub-irrigated plants were not apparently affected. ETR, Φ_{II} , and F_v/F_m values revealed that photosynthesis was reduced in citral-watered plants as a result of a general slowing down of the metabolism, while citral-sprayed plants were photoinhibited and presented physical damage due to the treatment. These results were also supported by the spatio-temporal CFI. The same experiments carried out by Araniti et al. (2017c), bioassaying the phytotoxicity of *trans*-caryophyllene on Arabidopsis adult plants, didn't show any effects on plants sprayed, whereas PSII of plant sub-irrigated was extremely altered. They concluded that the observed PSII damage would be the consequence of plant water status alterations accompanied by ROS burst and oxidative stress. These results suggest that CFI outputs could be used in screening programs to highlight, depending on the molecule bioassayed, the best method of application of a chemical. In addition, concerning the last two chemicals (citral and *trans*-caryophyllene), the data further highlight the high potential of the imaging techniques as phenotyping tool, which can be helpful in giving hints concerning the target and the potential mode of action of natural phytotoxins.

CFI has been used also to evaluate the phytotoxic effects of natural compounds produced by fungi and bacteria. Guo et al. (2019) demonstrated that gliotoxin, a fungal secondary metabolite, affects both the electron transport through PSII at the acceptor side and the reduction rate of PSI end electron acceptors' pool. Through CFI, authors identified the concentration inducing physical damage to PSII. In addition, Xiao et al. (2020) reported that alamethicin, an antimicrobial peptide isolated from fungus *Trichoderma viride*, acts on PSII with a mechanism similar to the commercial herbicide diuron (Laasch et al., 1983). In particular, this secondary metabolite would interrupt PSII electron transfer beyond the primary plastoquinone at the acceptor side, leading to PSII reaction centers inactivation. In addition, alamethicin destroys the PSII pigment architecture but does not affect the oxygen-evolving complex at the donor side. The damages in the leaves (necrotic areas on leaf surface) were visible only in plants treated with the highest concentrations of alamethicin, whereas the imaging output of the CFI system allowed to understand that even the lower concentrations altered the photosynthetic machinery

(F_v/F_m decrease) although damages were not evident, confirming again the power of this technique.

ADVANTAGES AND LIMITATIONS OF CFI IN NATURAL PRODUCTS STRESS DETECTION

Regarding the study of phytotoxicity induced by plant natural products, the majority of the works reported in literature, based on CF monitoring, were carried out with clamping tools that record single-point measurements on restricted leaf parts. The advantages of monitoring CF through imaging instead of single-point fluorescence have already been discussed (Oxborough, 2004; Lichtenthaler et al., 2005). Martínez-Peñalver et al. (2011) demonstrated that measurements obtained through single-point fluorescence do not always reflect the heterogeneity of the stress-related effects in plants. In their research, authors compared the temporal and spatial distribution of fluorescence emission in plants treated with allelochemicals, abiotic factors, and heavy metals. They observed that some stress factors, as the assayed heavy metals, induced a homogenous inhibition of the maximum PSII efficiency all over the whole plant, while in plants treated with allelochemicals the inhibition was mainly located on the margins of old leaves whereas younger leaves were unaffected. They suggested that these irregularities in CF distribution along plant make difficult any correlation with single-point measurements, typically done through clamping fluorometers.

Gao et al. (2018) bioassayed also the effects of usnic (UA), benzoic (BA), cinnamic (CA), and salicylic acid (SA) on the photosynthetic apparatus of the algae *Chlamydomonas reinhardtii*. They found that UA and SA have probably stronger photosynthetic inhibitory activity than CA and BA acids. The four phytotoxins showed multiple targets in chloroplasts. In particular, UA acid decreased photosynthesis inducing a reduction of PSII O_2 evolution rate, interrupting PSII electron transport (strong ETR reductions), and inactivating the PSII reaction centers (strong F_v/F_m decrease). Based on the JIP-curve, UA-treated cells showed a fast increase of J-step, which is due to the accumulation of Q_A^- when the electron flow beyond Q_A is blocked at the PSII acceptor side. The other site of action of UA would be the oxidizing site of PSII, as indicated by the low PSII O_2 evolution rate. Moreover, UA reduced pigment content, damaging the conformation of antenna pigment assemblies, as suggested by the decreased values of ABS/CS (average antenna size per excited leaf cross-section) and TR_0/CS (trapped energy flux per excited leaf cross-section), resulting in destroyed structure and function of PSII. Gao et al. (2018) suggested also that damages induced by SA on the photosynthetic machinery would be mainly attributed to inhibition of PSII electron transport beyond primary plastoquinone acceptor at the acceptor side, and the inactivation of the PSII reaction centers by decreasing Ψ_{EO} (the probability that an electron moves further than Q_A^-) and ϕ_{EO} (the quantum yield for electron transport). SA induced as well thylakoid membranes destabilization by changes at D1/D2 dimer and the polypeptides of the water-oxidizing complex. Finally, both CA

acid and BA acid would act by reducing PSII electron transport efficiency at the acceptor side and the amount of active PSII reaction centers, but with some differences. In particular, BA disrupted the flow between antenna pigments and PSII reaction center, with decreases of F_t , F_M , F_v/F_m , and TR_0/C , while CA did not affect these parameters, but decreased PSII O_2 evolution rate.

Imaging techniques can be also decisive to study recovering processes. Plants treated with the allelochemical protocatechualdehyde (Martínez-Peñalver et al., 2012) highlighted tolerance to this molecule, as whole-plant images of F_v/F_m showed the greatest number of damage spots among 9 and 24 h after treatment, but images of 96, 144, and 192 h showed the recovering of PSII parameters within a week of treatment.

Recent studies carried on the phenolic acid *trans*-cinnamic acid, assayed at sub-lethal concentration, pointed out that, besides the reduction in growth, *trans*-cinnamic significantly stimulated the photosynthetic machinery of *Zea mays* seedlings (Araniti et al., 2018b). In fact, in plants treated with this known phytotoxic molecule, the dark adapted PSII parameter (F_v/F_m) was not affected, whereas a significant increment in pigment content, and the stimulation of the light adapted PSII efficiency (Φ_{II}), the regulated dissipation of the energy in form of heat (Φ_{NPQ}) and the apparent electron transport rate was observed. At the same time the CFA (Φ_{NO}) was significantly stimulated by the treatment. Those data are supportive for the capability of the plant to cope with *trans*-cinnamic acid effects in different ways. From one hand, *Z. mays* plants increased the level of photochemistry and were able to increase the level of energy channeled toward the electron transport chain (see ETR and Φ_{II} increments). On the other hand, treated plants showed also a higher capacity to dissipate the energy, which exceeds photochemistry through both regulated (see Φ_{NPQ}) as well as unregulated mechanisms (see Φ_{NO}), suggesting that plants were facing phytotoxicity but were able to cope with it (Araniti et al., 2018b).

Similarly, recent studies assayed rutin, a glycoside combining the flavonol quercetin and the disaccharide rutinose, on the model species *A. thaliana*. This metabolite, particularly present in the invasive species *Acacia melanoxylon*, affected the photosynthesis and excitation energy flux responses (Hussain and Reigosa, 2016). Hussain and Reigosa observed that the dark-adapted PSII (F_v/F_m) and the non-photochemical quenching Φ_{NPQ} were significantly inhibited after 7 d of treatment. Moreover, plant response to rutin was characterized by a marked decrease in excitation energy fluxes (Φ_{II} , non-photochemical quenching coefficient (qN) and Φ_{NPQ}), suggesting plant damage.

The aromatic organic compound coumarin has been found to indirectly affect the photosynthetic machinery through induction of ROS burst and inhibition of several enzymes involved in ROS scavenging activity (Araniti et al., 2017d). Authors demonstrated, through an integrated physiological and -omic approach, that coumarin severely inhibited the effective quantum yield of the PSII, the maximum PSII efficiency, the energy dissipation in the form of heat, the estimated electron transport rate and the coefficient of the photochemical quenching. On the other hand,

it significantly stimulated both the fluorescence emission and the coefficient of the non-photochemical quenching.

The identification of the mode of action of a molecule, both synthetic and natural, is a delicate process that needs to exclude from the experimental conditions all the sources of variability (e.g., lack of nutrients, temperature changes, light variation, etc.). CF could be affected by a wide number of both biotic and abiotic factors (e.g., drought, heat, flooding, temperature variation, parasitization, etc.) (Dong et al., 2020; Duarte et al., 2020; Zhou et al., 2020; Zhuang et al., 2020), which makes the evaluation of the mode of action of natural molecules quite impossible because of the overlapping of stressing conditions, which makes impossible to attribute the observed effects to the molecule assayed. Therefore, it is strongly suggested to perform experiments in completely controlled conditions using phytotrons and cropping plants hydroponically or on inert substrates enriched with nutrients and carbon sources (Graña et al., 2013b, 2016; Araniti et al., 2017c). Once identified the target and the potential mode of action of the molecule, the experiments could move to the next step, which consists in bioassays in microcosms trying to mimic natural conditions in greenhouses and/or open fields. This will allow the identification of the effectiveness of the molecules and their impact on the environment (e.g., on soil microorganisms) (Jouini et al., 2020). Barbagallo et al. (2003) used the CFI technique to rapidly screen the leaves metabolic perturbations induced by six different herbicides. However, although the same parameters are used to detect synthetic herbicides effects, those effects are not necessarily similar to natural bioherbicides, especially when secondary metabolites are known to commonly show more than one mode of action.

PHYSIOLOGICAL INTERPRETATION OF MEASURED PARAMETERS BY IMAGING FLUORESCENCE

Multiple combinations of CFI parameters can be found in a leaf when exposed to a stressing factor (Table 2). Therefore, a correct physiological interpretation of the decreases and increases of the different parameters will give information about the ability of the plant to face stress with efficient protection mechanisms or with more toxic and inefficient dissipation mechanisms, which will lead to plant damage and stress. Increases of heat or fluorescence emission can occur in the plant without significantly reduce the PSII photochemical efficiency, (Φ_{II}), as some types of stress do not instantly affect PSII quantum yield (Lopes et al., 2012). Heat increases are sometimes compensated by decreases in fluorescence emission and the other way around (scenarios 1–2, Table 2), because the stress is not strong enough, and effective compensation occurs in the electron transport chain, or because the measurements were recorded in an early phase of the stress response, before damage can be detected.

Decreases of Φ_{II} usually result in increases of non-photochemical quenching (heat) when the plant is able to orchestrate regulated energy dissipation through xanthophylls

TABLE 2 | Relevant parameters to be considered in the physiological interpretation of the measurement of chlorophyll *a* fluorescence.

	Physiological interpretation	Φ_{II}	Φ_{NPQ}	Φ_{NO}	F_v/F_m	ETR
1	Plant copes stressing situation by enhancing regulated energy dissipation. No damages are detected.	=	↑	=/↓	=	=
2	Plant copes stressing situation by enhancing limited fluorescence emission. No damages are detected.	=	=/↓	↑	=	=
3	Plant copes stressing situation by enhancing regulated energy dissipation, but PSII photosystem efficiency is significantly reduced, although ETR remains unchanged. Dynamic photoinhibition starts in the plant.	↓	↑	=	=	=
4	Plant faces stressing situation by enhancing regulated energy dissipation, but this strategy is not enough and fluorescence emission increases. Photosynthetic efficiency is significantly reduced and dynamic photoinhibition occurs.	↓	↑	↑	=	=
5	Plant copes stressing situation by enhancing regulated energy dissipation, but PSII photosystem efficiency and electron transport rate are significantly reduced. Plant is under dynamic photoinhibition.	↓	↑	↑	=	↓
6	Stressing situation reduces photosynthetic efficiency, but the plant cannot enhance regulated energy dissipation and heat emission remains unchanged or even decreases, increasing fluorescence emission. Plant is not damaged yet, but could be in brief.	↓	=/↓	↑	=	=
7	Stressing situation reduces photosynthetic efficiency, increases fluorescence emission and the plant cannot enhance regulated energy dissipation (heat). This situation reduces electron transport rate, but no physical damage is detected in the antennae complex, i.e., photoprotective mechanisms are efficient.	=/↓	=/↓	↑	=	↓
8	Stressing situation reduces photosynthetic efficiency, the plant cannot enhance regulated energy dissipation and fluorescence emission increases. This situation induces physical damage in the antennae complex and chronic photoinhibition occurs. Photoprotective mechanisms are not efficient enough due to an excess of excitation energy.	↓	=/↑/↓	↑	↓	=
9	Stressing situation reduces photosynthetic efficiency, increases fluorescence emission and the plant cannot enhance regulated energy dissipation (heat). This situation induces physical damage in the antennae complex and reduces electron transport rate. Plant undergoes chronic photoinhibition.	↓	=/↓	↑	↓	↓
10	Electron transport rate and photosynthetic efficiency are significantly decreased under stress. This could be induced by an alteration on the biochemical phase of the photosynthesis and results in altered photochemical quenching. Excess energy can be emitted under regulated (heat) or non-regulated (fluorescence) mechanisms.	↓	=/↓	=/↑	=	↓
11	Photosynthetic efficiency increases under stress to respond to the energetic demand required to synthesize molecules involved in the response to stress.	↑	=/↓	=	=	=/↑
		Φ_{II}	Φ_{NPQ}	Φ_{NO}	qN	qP
12	An increase of qN without increase of Φ_{NPQ} suggests that plants are experiencing photoinhibition or about to undergo it	=/↓	=	=/↑	↑	=/↓
13	A reduction in qP suggests physical damage at the PSII reaction centers	↓	=/↑	=/↑	=/↑	↓

cycle, pH regulation, or reversible phosphorylation of light harvesting chlorophyll *a/b* binding proteins (LHCII) (scenarios 3–5, **Table 2**). By contrary, Φ_{II} decreases will result in increases of non-regulated energy emission when photochemical energy conversion fails, and protective regulatory mechanisms are inefficient (scenarios 4–9). However, increases of Φ_{NO} and decreases of Φ_{II} does not necessarily indicate that the plant is already damaged, as might be being protected, albeit weakly, until further radiation occurs or stressing factor remains (scenarios 4–5). The latter was shown by Martínez-Peñalver et al. (2012) with the secondary metabolite protocatechualdehyde, where strong increases in Φ_{NO} didn't result in ETR or F_v/F_m decreases, or by Araniti et al. (2018b) in *Zea mays* seedlings treated with *trans*-cinnamic. Ferredoxin or Mehler reaction can be accepting the electrons diverted from photochemical reactions when no decreases in ETR are observed (scenario 4). The same values of Φ_{NPQ} , Φ_{NO} , Φ_{II} , and F_v/F_m are observed in scenario 5,

although decreases in ETR also occurred related to decreases in the efficiency of PSII.

Scenarios 4–7 of **Table 2** show dynamic photoinhibition, where decreases of photochemical conversion occur and plant has serious problems to cope with the incident radiation, but no physical damage is detected at the photosynthetic apparatus. The latter is suggested by unchanged or very slight decreased F_v/F_m values, which reveal flexible adjustment to environmental conditions (Werner et al., 2002). In contrast, plants showing statistically significant decreases in PSII efficiency (Φ_{II}) and strong increases in fluorescence emission (Φ_{NO}) usually show weak to strong decreases in the maximum PSII efficiency (F_v/F_m), which suggests different degrees of physical damage at the protein-pigment complexes of the light harvesting antennae of PSII (scenarios 8–9, **Table 2**). Consequently, chronic photoinhibition due to acute or long-term environmental stress occurs, as previously found for some natural compounds as

citral or *trans*-caryophyllene (Graña et al., 2013b; Araniti et al., 2017c). Late F_v/F_m decreases can suggest a secondary effect of the stressing factor; i.e., Sánchez-Moreiras et al. (2011) demonstrated that F_v/F_m and Φ_{II} reduced values appeared to be correlated to necrotic processes after secondary oxidative stress, consequence of early senescence processes.

On the other hand (Table 2, scenario 9), plants could be unable to develop strategies of protection (as heat emission) when a stress factor has a direct effect on the photosynthetic machinery, increasing non-regulated emission of energy as fluorescence and inducing photoinhibition. Then, biochemical and photochemical phases of photosynthesis can be affected, altering electron transport and damaging PSII reaction centers, as found by Sánchez-Moreiras et al. (2011) in leaves of *Arabidopsis* plants treated with the secondary metabolite BOA.

Sometimes, similar values of Φ_{II} , Φ_{NPQ} , and Φ_{NO} , and ETR result in totally different impact on the maximum PSII efficiency (F_v/F_m), as previously found by Díaz-Tielas et al. (2014). Authors demonstrated in this study that, although similar values of PSII quantum yield, heat dissipation, fluorescence emission and electron transport rate were found for *Arabidopsis* plants sprayed or watered with the flavonoid *trans*-chalcone, watered plants were able to protect the antennae complex and the reactions centers along the whole experiment, while sprayed plants showed decreased values of F_v/F_m at the end of the experiment, suggesting underprotection and possible physical damage at the antennae complex.

All of these scenarios (1 – 9) are usually found when the natural product affects photochemical phase first, by altering antennae complex, reaction centers, pH gradient through the thylakoid membranes, or competing with other molecules to accept the electrons coming from PSII and PSI. However, in some cases, i.e., senescence processes, stomatal closure or other situations restricting CO₂ assimilation, is the biochemical phase the first part affected of the photosynthetic machinery (Ping et al., 2015), resulting in decreases of electron transport rate (ETR values) without or with slight alterations of the other parameters (scenario 10). When accumulated ROS cannot be detoxified (Paul and Foyer, 2001), and antioxidant systems or other photo-protective mechanisms, as xanthophyll cycle or increased photorespiration, are not enough, physical damages at the PSII

reaction centers or antennae complexes can occur, resulting in a scenario similar to scenario 9 of Table 2. This has been recently found for plants treated with the nitrogen-containing natural compound norharmane (López-González et al., 2020).

On the other hand, the necessity of synthesizing new molecules in response to adverse conditions (i.e., proline, antioxidants, and others; Gonzáles et al., 2008) can lead to increased photosynthetic efficiency in plants (Desotgiu et al., 2012; scenario 11, Table 2). This increase in operating efficiency (Φ_{II}) can be usually obtained by reducing regulated dissipation of light energy (Φ_{NPQ}) as shown by Martínez-Peñalver et al. (2012) in plants treated with 3,4-dihydroxybenzaldehyde, which found a compensatory increase of Φ_{II} at the beginning of the experiment that was correlated with a decrease of Φ_{NPQ} .

Coefficients qN and qP (scenarios 12 and 13, Table 2), can give more information about non-photochemical quenching and status of the PSII reaction centers, making data interpretation easier. The increase of qN without Φ_{NPQ} increase (scenario 12) suggests that plants are experiencing photoinhibition or about to undergo it. The same for the combination shown in scenario 13, where stressing situation reduced the coefficient qP, suggesting a physical damage at the light-harvesting complex II (LHCII), which could firstly occur at the site of PSII reaction center that is associated with PSII electron transport (inhibiting PSII repair), at the water splitting site in the oxygen evolving complex (OEC), or at both sites at the same time (Oguchi et al., 2009, 2011; Zavafer et al., 2015). Similar results were found by Araniti et al. (2017c) in plants treated with an intermediate concentration of *trans*-caryophyllene or by Gao et al. (2018), when testing different secondary metabolites, such as usnic, BA, CA, and SAs.

Finally, Φ_{NPQ}/Φ_{NO} ratio; i.e., the ratio of quantum yield of regulated to non-regulated energy dissipation in PSII, which is connected to the ability of photosynthetic apparatus to activate photoprotective mechanisms (Klughammer and Schreiber, 2008), can tell in a rapid and easy way if the plant is photo-protected (high values) or is undergoing photoinhibition or photodamage processes (low values).

However, all these data cannot provide direct information about where the damage is occurring first, or how the acclimation

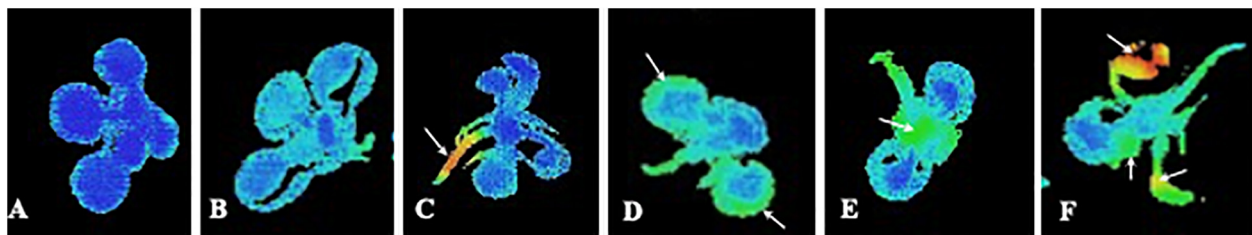


FIGURE 1 | Imaging pictures of maximum PSII efficiency (F_v/F_m) of *Arabidopsis* seedlings at different physiological status. **(A)** Control plant with optimal PSII photosynthetic efficiency; **(B)** Whole decreased of photosynthetic efficiency that is homogenous all over the plant; **(C)** Decreased photosynthetic efficiency in the cells close to the vascular bundles. The rest of the plant remains intact; **(D)** Strong decreased of photosynthetic efficiency in the border of the older leaves; **(E)** Decreased photosynthetic efficiency mainly in the younger leaves; and **(F)** Strong decrease of photosynthetic efficiency in the whole plant, with punctual inhibition spots in the leaves.

responses are being implemented into the leaf. Moreover, the so-called phenomenon of “patchy photosynthesis” due to ununiform stomatal closure or to heterogeneities in the leaves (Meyer and Genty, 1999; Beyschlag and Eckstein, 2001; Lopes et al., 2012) can be a source of errors when recording improperly single-point CF measurements. Imaging techniques avoid misunderstandings due to this phenomenon, as leaf fluorescence is obtained at once (Martínez-Peñalver et al., 2012).

Unfortunately, very few studies have analyzed the whole plant fluorescence emission after natural compound phytotoxicity, even though CFI allows this measurement in an easy and fast way. Therefore, with this paper, we want to encourage researchers in phytotoxicity to record the whole response of the plant and monitoring this response all over the time to obtain a more accurate information about the effect of the compound. Careful spatial analysis of the images of fluorescence emission is appropriate when studying phytotoxic effects in plants, as far as we do not know, before measuring fluorescence, which type of effect will be induced in the plant. This is applicable to sprayed but also to watered application of the compounds, since effects related to some types of stress induced by the compound (i.e., oxidative or water stress) can result in spots of fluorescence emission in the leaves of the treated plants. **Figure 1A** shows an *Arabidopsis* seedling grown under optimal conditions of light, temperature, humidity and CO₂ concentration. As seen, F_v/F_m values are optimal and homogeneous all over the plant. However, some stressing factors, as plant natural compound-induced phytotoxicity, can decrease the overall photosynthetic capacity of the plant decreasing maximum PSII efficiency in young and old leaves, as shown in **Figure 1B**. In this case, the homogeneous distribution of the effect makes single-point measurements of fluorescence precise and accurate, anyway if measurements are done in young or old leaves, or in the center or the border of the leaves. By contrary, some natural compounds induce asymmetric effects on the photosynthetic capacity of the plant (Sánchez-Moreiras et al., 2011; Graña et al., 2013b), as shown in the rest of the images included in **Figures 1C–F**.

An asymmetric effect starting in the cells closed to the vascular bundles is shown in **Figure 1C**, as indicated by orange and red colors related to decreased F_v/F_m values. This effect could be related to early water stress phenomenon, as previously shown in thermal and salt stress by Martínez-Peñalver et al. (2011), which found a characteristic pattern of reduction that affected the central areas of the young leaves close to the vascular bundles. This localized increase of fluorescence could be due to altered water stress status after treatment with a natural product, or to an abscisic acid mimic action of the natural product applied, as suggested by Graña et al. (2013b) when studying the effects of the monoterpenoid citral.

A different asymmetric effect is shown in **Figure 1D**. In this case, greater fluorescence emission is localized at the edges of the older leaves, while the vascular bundles and the youngest leaves in the rosette remain intact. Different studies have indicated that this pattern could be reminiscent of early senescence as suggested by the images of fluorescence distribution in *Arabidopsis* plants

treated with citral (Graña et al., 2013b) or with the secondary metabolite *o*-coumaric acid (Zheng et al., 2012).

Figure 1E shows an unusual distribution of reduced maximum PSII efficiency, with lower values in younger than in older leaves. This scenario could be the case of a natural product inducing a strong effect on target sites directly related to the photosynthetic apparatus. This effect could result in a stronger damage on the fully synthesizing leaves, as that seen by Díaz-Tielas et al. (2017) in chalcone-treated seedlings, which induced early plasma membrane depolarization and dramatic effects on chloroplasts structure and function.

Finally, **Figure 1F** shows an image where heterogeneous damage appears indistinctly for young or old leaves. Arrows point out damaged spots in the different leaves. As indicated by orange and red color, some parts of the leaves remain intact while others are extremely damaged. This effect has been previously related to oxidative stress and necrotic process in *Arabidopsis* plants treated with different natural compounds (Martínez-Peñalver et al., 2011; Sánchez-Moreiras et al., 2011). In this way, Araniti et al. (2017b) demonstrated overlapping of ROS accumulation in the leaf and the area characterized by F_v/F_m reduction when lettuce was treated with volatiles released by *Didymopanax viscosum*. Moreover, this isolated inhibition spots (increased fluorescence emission) could be also found when the studied natural compound is sprayed to the leaves and behaves as a PSII inhibitor directly binding to the D protein and interrupting the electron transfer chain of PSII re-emitting the excitation energy as fluorescence, which will result in an easily discernable decrease of F_v/F_m values, as has been previously found for synthetic herbicides (Muller et al., 2008; Wang et al., 2018). This decrease will happen first in the areas of contact of the sprayed compound with the leaf, resulting in isolated spots of increased fluorescence emission.

CONCLUSION

As reviewed at the beginning of this paper, and analyzed in the physiological interpretations of the images obtained, imaging fluorescence analyses of the whole affected plant provides accurate and fundamental information for the interpretation of plant response to stress not provided by single-point techniques or analyses of photosynthetic parameters independently analyzed of their spatial distribution in the plant. Monitoring imaging fluorescence can help to understand how damage evolves and how response is orchestrated into the plants.

Because of the lack of information and the restricted use of this technique in the field of natural-herbicide discovery, research efforts should be focused on creating a common procedure to study the mode of action of natural compounds, without avoiding protocol innovations. The use of a model sensitive species, such as *A. thaliana*, could allow the standardization of the method, which could be used worldwide allowing the reproducibility of the data. This could allow the creation of a database of the signatures of the CF and the trend of the various parameters in response to the treatments. In addition, this technique could be further used

as a sensitive tool to identify the effective doses (stimulatory and inhibitory) of the natural compounds as alternative or support to the classical dose-responses curve.

AUTHOR CONTRIBUTIONS

AS-M: idea and writing and editing. FA: writing and reviewing. EG: image acquisition and editing. MR: idea and reviewing.

REFERENCES

- Araniti, F., Bruno, L., Sunseri, F., Pacenza, M., Forgiione, I., Bitonti, M. B., et al. (2017a). The allelochemical farnesene affects *Arabidopsis thaliana* root meristem altering auxin distribution. *Plant Physiol. Biochem.* 121, 14–20. doi: 10.1016/j.plaphy.2017.10.005
- Araniti, F., Landi, M., Lupini, A., Sunseri, F., Guidi, L., and Abenavoli, M. R. (2018a). *Origanum vulgare* essential oils inhibit glutamate and aspartate metabolism altering the photorespiratory pathway in *Arabidopsis thaliana* seedlings. *J. Plant Physiol.* 231, 297–309. doi: 10.1016/j.jplph.2018.10.006
- Araniti, F., Lupini, A., Mauceri, A., Zumbo, A., Sunseri, F., and Abenavoli, M. R. (2018b). The allelochemical trans-cinnamic acid stimulates salicylic acid production and galactose pathway in maize leaves: A potential mechanism of stress tolerance. *Plant Physiol. Biochem.* 128, 32–40. doi: 10.1016/j.plaphy.2018.05.006
- Araniti, F., Lupini, A., Sunseri, F., and Abenavoli, M. R. (2017b). Allelopathic potential of *Dittrichia viscosa* (L.) W. Greuter mediated by VOCs: a physiological and metabolomic approach. *PLoS One* 12:e0170161. doi: 10.1371/journal.pone.0170161
- Araniti, F., Sánchez-Moreiras, A. M., Graña, E., Reigosa, M. J., and Abenavoli, M. R. (2017c). Terpenoid trans-caryophyllene inhibits weed germination and induces plant water status alteration and oxidative damage in adult *Arabidopsis*. *Plant Biol.* 19, 79–89. doi: 10.1111/plb.12471
- Araniti, F., Scognamiglio, M., Chambery, A., Russo, R., Esposito, A., D'abrosca, B., et al. (2017d). Highlighting the effects of coumarin on adult plants of *Arabidopsis thaliana* (L.) Heynh. by an integrated-omic approach. *J. Plant Physiol.* 213, 30–41. doi: 10.1016/j.jplph.2017.02.013
- Atherton, J., MacArthur, A., Hakala, T., Maseyk, K., Robinson, I., Liu, W., et al. (2018). "Drone measurements of solar-induced chlorophyll fluorescence acquired with a low-weight DFOV spectrometer system," in *IGARSS 2018-2018 IEEE International Geoscience and Remote Sensing Symposium*, (Piscataway: IEEE), 8834–8836.
- Awlia, M., Nigro, A., Fajkus, J., Schmoeckel, S. M., Negrão, S., Santelia, D., et al. (2016). High-throughput non-destructive phenotyping of traits that contribute to salinity tolerance in *Arabidopsis thaliana*. *Front. Plant Sci.* 7:1414. doi: 10.3389/fpls.2016.01414
- Ayalon, I., de Barros Marangoni, L. F., Benichou, J. I., Avisar, D., and Levy, O. (2019). Red Sea corals under Artificial Light Pollution at Night (ALAN) undergo oxidative stress and photosynthetic impairment. *Global Change Biol.* 25, 4194–4207. doi: 10.1111/gcb.14795
- Baker, N. R. (2008). Chlorophyll fluorescence: a probe of photosynthesis in vivo. *Ann. Rev. Plant Biol.* 59, 89–113. doi: 10.1146/annurev.arplant.59.032607.092759
- Baker, N. R., and Rosenqvist, E. (2004). Applications of chlorophyll fluorescence can improve crop production strategies: an examination of future possibilities. *J. Exp. Bot.* 55, 1607–1621. doi: 10.1093/jxb/erh196
- Barbagallo, R. P., Oxborough, K., Pallett, K. E., and Baker, N. R. (2003). Rapid noninvasive screening for perturbations of metabolism and plant growth using chlorophyll fluorescence imaging. *Plant Physiol.* 132, 485–493. doi: 10.1104/pp.102.018093
- Bauriegel, E., Giebel, A., Geyer, M., Schmidt, U., and Herppich, W. B. (2011). Early detection of *Fusarium* infection in wheat using hyper-spectral imaging. *Comput. Electron. Agr.* 75, 304–312. doi: 10.1016/j.compag.2010.12.006
- Belz, R. G., and Duke, S. O. (2017). "Herbicide-mediated hormesis," in *Pesticide Dose: Effects on the Environment and Target and Non-target Organisms*, eds

All authors contributed to the article and approved the submitted version.

FUNDING

This work was supported by the Spanish Ministry of Science, Innovation and Universities (project number: RTI2018-094716-B-I00).

- S. O. Duke, P. Kudsk, and K. Solomon (Washington, DC: American Chemical Society), 135–148. doi: 10.1021/bk-2017-1249.ch010
- Beninger, C. W., Abou-Zaid, M. M., Kistner, A. L., Hallett, R. H., Iqbal, M. J., Grodzinski, B., et al. (2004). A flavanone and two phenolic acids from *Chrysanthemum morifolium* with phytotoxic and insect growth regulating activity. *J. Chem. Ecol.* 30, 589–606. doi: 10.1023/b:joec.0000018631.67394.e5
- Beyschlag, W., and Eckstein, J. (2001). Towards a causal analysis of stomatal patchiness: the role of stomatal size variability and hydrological heterogeneity. *Acta Oecol.* 22, 161–173. doi: 10.1016/s1146-609x(01)01110-9
- Bilger, W., and Schreiber, U. (1987). "Energy-dependent quenching of dark-level chlorophyll fluorescence in intact leaves," in *Excitation Energy and Electron Transfer in Photosynthesis*, eds J. Govindjee, W. A. Barber, J. H. C. Cramer, J. Goedheer, R. Lavorel, and B. A. Zilinskas (Netherlands: Springer), 157–162. doi: 10.1007/978-94-009-3527-3_19
- Björkman, O., and Demmig-Adams, B. (1995). "Regulation of photosynthetic light energy capture, conversion, and dissipation in leaves of higher plants," in *Ecophysiology of Photosynthesis*, eds E. D. Schulze and M. M. Caldwell (Heidelberg: Springer), 17–47. doi: 10.1007/978-3-642-79354-7_2
- Bolhar-Nordenkamp, H. R., Long, S. P., Baker, N. R., Oquist, G., Schreiber, U., and Lechner, E. G. (1989). Chlorophyll fluorescence as a probe of the photosynthetic competence of leaves in the field: a review of current instrumentation. *Funct. Ecol.* 1989, 497–514. doi: 10.2307/2389624
- Brewster, D. (1834). On the colours of natural bodies. *Roy. Soc. Edinb. Trans.* 12, 538–545. doi: 10.1017/s0080456800031203
- Buschmann, C., Langsdorf, G., and Lichtenthaler, H. K. (2000). Imaging of the blue, green, and red fluorescence emission of plants: an overview. *Photosynthetica* 38, 483–491. doi: 10.1023/a:1012440903014
- Chaerle, L., and van der Straeten, D. (2000). Imaging techniques and the early detection of plant stress. *Trends Plant Sci.* 5, 495–501. doi: 10.1016/s1360-1385(00)01781-7
- Chaerle, L., and Van Der Straeten, D. (2001). Seeing is believing: imaging techniques to monitor plant health. *Biochim. Biophys. Acta* 1519, 153–166. doi: 10.1016/s0167-4781(01)00238-x
- Chaerle, L., Leinonen, I., Jones, H. G., and Van Der Straeten, D. (2007). Monitoring and screening plant populations with combined thermal and chlorophyll fluorescence imaging. *J. Exp. Bot.* 58, 773–784. doi: 10.1093/jxb/erl257
- Chaerle, L., Lenk, S., Leinonen, I., Jones, H. G., Van Der Straeten, D., and Buschmann, C. (2009). Multi-sensor plant imaging: towards the development of a stress catalogue. *Biotechnol. J.* 4, 1152–1167. doi: 10.1002/biot.200800242
- Daley, P. F., Raschke, K., Ball, J. T., and Berry, J. A. (1989). Topography of photosynthetic activity of leaves obtained from video images of chlorophyll fluorescence. *Plant Physiol.* 90, 1233–1238. doi: 10.1104/pp.90.4.1233
- Dayan, F. E., and Zaccaro, M. L. M. (2012). Chlorophyll fluorescence as a marker for herbicide mechanisms of action. *Pest. Biochem. Physiol.* 102, 189–197. doi: 10.1016/j.pestbp.2012.01.005
- de Carvalho, A. C., Salvador, J. P., Pereira, T., de, M., Ferreira, P. H. A., Lira, J. C. S., et al. (2016). Fluorescence of chlorophyll *a* for discovering inhibitors of photosynthesis in plant extracts. *Am. J. Plant Sci.* 7, 1545–1554. doi: 10.4236/ajps.2016.711146
- Demmig-Adams, B., Adams, W. W., Heber, U., Neimanis, S., Winter, K., Krüger, A., et al. (1990). Inhibition of zeaxanthin formation and of rapid changes in radiationless energy dissipation by dithiothreitol in spinach leaves and chloroplasts. *Plant Physiol.* 92, 293–301. doi: 10.1104/pp.92.2.293
- Desotgiu, R., Pollastrini, M., Cascio, C., Gerosa, G., Marzuoli, R., and Bussotti, F. (2012). Chlorophyll *a* fluorescence analysis along a vertical gradient of the

- crown in a poplar (Oxford clone) subjected to ozone and water stress. *Tree Physiol.* 32, 976–986. doi: 10.1093/treephys/tps062
- Díaz-Tielas, C., Graña, E., Maffei, M., Reigosa, M. J., and Sánchez-Moreiras, A. M. (2017). Plasma membrane depolarization precedes photosynthesis damage and long-term leaf bleaching in (E)-chalcone-treated *Arabidopsis* shoots. *J. Plant Physiol.* 218, 56–65. doi: 10.1016/j.jplph.2017.07.014
- Díaz-Tielas, C., Sotelo, T., Graña, E., Reigosa, M. J., and Sánchez-Moreiras, A. M. (2014). Phytotoxic potential of trans-chalcone on crop plants and model species. *J. Plant Growth Regul.* 33, 181–194. doi: 10.1007/s00344-013-9360-6
- Digrado, A., Bachy, A., Mozaffar, A., Schoon, N., Bussotti, F., Amelynck, C., et al. (2017). Long-term measurements of chlorophyll a fluorescence using the JIP-test show that combined abiotic stresses influence the photosynthetic performance of the perennial ryegrass (*Lolium perenne*) in a managed temperate grassland. *Physiol. Plant* 161, 355–371. doi: 10.1111/ppl.12594
- Dong, Z., Men, Y., Liu, Z., Li, J., and Ji, J. (2020). Application of chlorophyll fluorescence imaging technique in analysis and detection of chilling injury of tomato seedlings. *Comput. Electron. Agr.* 168:105109. doi: 10.1016/j.compag.2019.105109
- Duarte, C. I., Martinazzo, E. G., Bacarin, M. A., and Colares, I. G. (2020). Seed germination, growth and chlorophyll a fluorescence in young plants of *Allophylus edulis* in different periods of flooding. *Acta Physiol. Plant* 42, 1–11. doi: 10.9734/ajea/2016/20467
- Duke, S. O. (2011). Why have no new herbicide modes of action appeared in recent years? *Pest. Manag. Sci.* 68, 505–512. doi: 10.1002/ps.2333
- Duke, S. O., Dayan, F. E., and Rimando, A. M. (2000a). “Natural products and herbicide discovery,” in *Herbicides and their Mechanisms of Action*, eds A. H. Cobb and R. C. Kirkwood (Sheffield: Academic Press), 105–133.
- Duke, S. O., Dayan, F. E., Romagni, J. G., and Rimando, A. M. (2000b). Natural products as sources of herbicides: current status and future trends. *Weed Res.* 40, 99–111. doi: 10.1046/j.1365-3180.2000.00161.x
- Duysens, L. N. M., and Sweers, H. E. (1963). “Mechanism of two photochemical reactions in algae as studied by means of fluorescence,” in *Studies on Microalgae and Photosynthetic Bacteria. A Collection of Papers*, ed. Japanese Society of Plant Physiologists (Tokyo: University of Tokyo Press), 353–372.
- Endo, T., Schreiber, U., and Asada, K. (1995). Suppression of quantum yield of photosystem II by hyperosmotic stress in *Chlamydomonas reinhardtii*. *Plant Cell Physiol.* 36, 1253–1258.
- Fenton, J. M., and Crofts, A. R. (1990). Computer aided fluorescence imaging of photosynthetic systems - Application of video imaging to the study of fluorescence induction in green plants and photosynthetic bacteria. *Photosyn. Res.* 26, 59–66. doi: 10.1007/BF00048977
- Gao, Y., Liu, W., Wang, X., Yang, L., Han, S., Chen, S., et al. (2018). Comparative phytotoxicity of usnic acid, salicylic acid, cinnamic acid and benzoic acid on photosynthetic apparatus of *Chlamydomonas reinhardtii*. *Plant Physiol. Biochem.* 128, 1–12. doi: 10.1016/j.plaphy.2018.04.037
- Genty, B., and Meyer, S. (1995). Quantitative mapping of leaf photosynthesis using chlorophyll fluorescence imaging. *Funct. Plant Biol.* 22, 277–284. doi: 10.1071/pp9950277
- Genty, B., Briantais, J. M., and Baker, N. R. (1989). The relationship between quantum yield of photosynthetic electron transport and quenching of chlorophyll fluorescence. *Biochim. Biophys. Acta* 990, 87–92. doi: 10.1016/s0304-4165(89)80016-9
- González, W. L., Suárez, L. H., Molina-Montenegro, M. A., and Gianoli, E. (2008). Water availability limits tolerance of apical damage in the Chilean tarweed *Madia sativa*. *Acta Oecol.* 34, 104–110. doi: 10.1016/j.actao.2008.04.004
- GORBE, E., and Calatayud, A. (2012). Applications of chlorophyll fluorescence imaging technique in horticultural research: a review. *Sci. Hort.* 138, 24–35. doi: 10.1016/j.scienta.2012.02.002
- Govindjee, E. (1995). 63 Years since Kautsky-chlorophyll-a fluorescence. *Aust. J. Plant Physiol.* 22, 131–160. doi: 10.1071/pp9950131
- Govindjee, G. (2004). “Chlorophyll a fluorescence: a bit of basics and history,” in *Chlorophyll a Fluorescence: a Signature of Photosynthesis*, eds G. C. Papageorgiou and Govindjee (Dordrecht, NL: Springer), 1–41. doi: 10.1007/978-1-4020-3218-9_1
- Graña, E., Díaz-Tielas, C., López-González, D., Martínez-Peñalver, A., Reigosa, M. J., and Sánchez-Moreiras, A. M. (2016). The plant secondary metabolite citral alters water status and avoids seed formation in *Arabidopsis thaliana* plants. *Plant Biol.* 18, 423–432. doi: 10.1111/plb.12418
- Graña, E., Sotelo, T., Díaz-Tielas, C., Araniti, F., Krasuska, U., Bogatek, R., et al. (2013a). Citral induces auxin and ethylene-mediated malformations and arrests cell division in *Arabidopsis thaliana* roots. *J. Chem. Ecol.* 39, 271–282. doi: 10.1007/s10886-013-0250-y
- Graña, E., Sotelo, T., Díaz-Tielas, C., Reigosa, M. J., and Sánchez-Moreiras, A. M. (2013b). The phytotoxic potential of the terpenoid citral on seedlings and adult plants. *Weed Sci.* 61, 469–481. doi: 10.1614/ws-d-12-00159.1
- Guidi, L., Landi, M., Penella, C., and Calatayud, A. (2016). Application of modulated chlorophyll fluorescence and modulated chlorophyll fluorescence imaging in studying environmental stresses effect. *Ann. Bot.* 6, 5–22.
- Guidi, L., Lo Piccolo, E., and Landi, M. (2019). Chlorophyll fluorescence, photoinhibition and abiotic stress: does it make any difference the fact to be a C3 or C4 species? *Front. Plant Sci.* 10:174. doi: 10.3389/fpls.2019.00174
- Guo, Y., Cheng, J., Shi, J., Gao, Y., Wang, H., Yin, C., et al. (2019). Novel action targets of natural product gliotoxin in photosynthetic apparatus. *Front. Plant Sci.* 10:1688. doi: 10.3389/fpls.2019.01688
- Häder, D. P., Lebert, M., Figueroa, F. L., Jiménez, C., Viñegla, B., and Perez-Rodriguez, E. (1998). Photoinhibition in Mediterranean macroalgae by solar radiation measured on site by PAM fluorescence. *Aquat. Bot.* 61, 225–236. doi: 10.1016/s0304-3770(98)00068-0
- Havaux, M., Strasser, R. J., and Greppin, H. (1991). A theoretical and experimental analysis of the qP and qN coefficients of chlorophyll fluorescence quenching and their relation to photochemical and nonphotochemical events. *Photosyn. Res.* 27, 41–55. doi: 10.1007/bf00029975
- Hermans, C., Smeyers, M., Rodriguez, R. M., Eyletters, M., Strasser, R. J., and Delhaye, J. P. (2003). Quality assessment of urban trees: a comparative study of physiological characterization, airborne imaging and on site fluorescence monitoring by the OJIP-test. *J. Plant Physiol.* 160, 81–90. doi: 10.1078/0176-1617-00917
- Horton, P., and Hague, A. (1988). Studies on the induction of chlorophyll fluorescence in isolated barley protoplasts. IV. Resolution of non-photochemical quenching. *Biochim. Biophys. Acta Bioenerg.* 932, 107–115. doi: 10.1016/0005-2728(88)90144-2
- Humlík, J. F., Lazár, D., Husícková, A., and Spíchal, L. (2015). Automated phenotyping of plant shoots using imaging methods for analysis of plant stress responses—a review. *Plant Meth.* 11:29.
- Hussain, M. I., and Reigosa, M. J. (2016). Plant secondary metabolite rutin affects the photosynthesis and excitation energy flux responses in *Arabidopsis thaliana*. *Allelopath. J.* 38, 215–228.
- Jouini, A., Verdegue, M., Pinton, S., Araniti, F., Palazzolo, E., Badalucco, L., et al. (2020). Potential effects of essential oils extracted from Mediterranean aromatic plants on target weeds and soil microorganisms. *Plants* 9:1289. doi: 10.3390/plants9101289
- Kalaji, H. M., Schansker, G., Brestic, M., Bussotti, F., Calatayud, A., Ferroni, L., et al. (2017). Frequently asked questions about chlorophyll fluorescence, the sequel. *Photosyn. Res.* 132, 13–66.
- Kalaji, H. M., Schansker, G., Ladle, R. J., Goltsev, V., Bosa, K., Allakhverdiev, S. I., et al. (2014). Frequently asked questions about in vivo chlorophyll fluorescence: practical issues. *Photosyn. Res.* 122, 121–158.
- Kalaji, H. M., Schansker, G., Ladle, R. J., Goltsev, V., Bosa, K., Allakhverdiev, S. I., et al. (2014). Frequently asked questions about in vivo chlorophyll fluorescence: practical issues. *Photosyn. Res.* 122, 121–158.
- Kautsky, H., and Hirsch, A. (1931). Neue versuche zur kohlenassimilation. *Naturwissenschaften* 48:964.
- Klughammer, C., and Schreiber, U. (2008). Complementary PS II quantum yields calculated from simple fluorescence parameters measured by PAM fluorometry and the Saturation Pulse method. *PAM Appl. Notes* 1, 27–35.
- Kramer, D. M., Johnson, G., Kiirats, O., and Edwards, G. E. (2004). New fluorescence parameters for the determination of QA redox state and excitation energy fluxes. *Photosyn. Res.* 79, 209–218. doi: 10.1023/b:pres.0000015391.99477.0d
- Krause, G. H., and Weis, E. (1984). Chlorophyll fluorescence as a tool in plant physiology. *Photosyn. Res.* 5, 139–157. doi: 10.1007/bf00028527
- Krause, G. H., and Weis, E. (1991). Chlorophyll fluorescence and photosynthesis: the basics. *Annu. Rev. Plant Biol.* 42, 313–349.
- Kriegs, B., Jansen, M., Hahn, K., Peisker, H., Šamajová, O., Beck, M., et al. (2010). Cyclic monoterpene mediated modulations of *Arabidopsis thaliana* phenotype:

- effects on the cytoskeleton and on the expression of selected genes. *Plant Signal. Behav.* 5, 832–838. doi: 10.4161/psb.5.7.12032
- Kurepin, L. V., Stangl, Z. R., Ivanov, A. G., Bui, V., Mema, M., Hüner, N. P., et al. (2018). Contrasting acclimation abilities of two dominant boreal conifers to elevated CO₂ and temperature. *Plant Cell Environ.* 41, 1331–1345. doi: 10.1111/pce.13158
- Laasch, H., Urbach, W., and Schreiber, U. (1983). Binary flash-induced oscillations of [¹⁴C]DCMU binding to the Photosystem II acceptor complex. *FEBS Lett.* 159, 275–279. doi: 10.1016/0014-5793(83)80463-3
- Lang, M., Lichtenthaler, H. K., Sowinska, M., Summ, P., and Heisel, F. (1994). Blue, green and red fluorescence signatures and images of tobacco leaves. *Bot. Acta* 107, 230–236. doi: 10.1111/j.1438-8677.1994.tb00790.x
- Lawson, T. (2009). Guard cell photosynthesis and stomatal function. *New Phytol.* 181, 13–34. doi: 10.1111/j.1469-8137.2008.02685.x
- Lawson, T., and Morison, J. (2006). Visualizing patterns of CO₂ diffusion in leaves. *New Phytol.* 169, 641–643. doi: 10.1111/j.1469-8137.2006.01655.x
- Lawson, T., Oxborough, K., Morison, J. I., and Baker, N. R. (2002). Responses of photosynthetic electron transport in stomatal guard cells and mesophyll cells in intact leaves to light, CO₂, and humidity. *Plant Physiol.* 128, 52–62. doi: 10.1104/pp.010317
- Lázár, D. (2003). Chlorophyll *a* fluorescence rise induced by high light illumination of dark-adapted plant tissue studied by means of a model of photosystem II and considering photosystem II heterogeneity. *J. Theor. Biol.* 220, 469–503. doi: 10.1006/jtbi.2003.3140
- Lee, H. Y., Mang, H., Seo, Y. E., Oh, S., Kim, S. B., Park, E., et al. (2019). Genome-wide expression analysis of immune receptors in hot pepper reveals an autonomous NLR cluster in higher plants. *BioRxiv* 2019:878959.
- Levin, R. A., Suggett, D. J., Nitschke, M. R., van Oppen, M. J., and Steinberg, P. D. (2017). Expanding the *Symbiodinium* (Dinophyceae, Süssiales) toolkit through protoplast technology. *J. Eukaryotic Microbiol.* 64, 588–597. doi: 10.1111/jeu.12393
- Lichtenthaler, H. K. (1996). Vegetation stress: an introduction to the stress concept in plants. *J. Plant Physiol.* 148, 4–14. doi: 10.1016/s0176-1617(96)80287-2
- Lichtenthaler, H. K., and Babani, F. (2000). Detection of photosynthetic activity and water stress by imaging the red chlorophyll fluorescence. *Plant Physiol. Biochem.* 38, 889–895. doi: 10.1016/s0981-9428(00)01199-2
- Lichtenthaler, H. K., and Miehe, J. A. (1997). Fluorescence imaging as a diagnostic tool for plant stress. *Trends Plant Sci.* 2, 316–320. doi: 10.1016/s1360-1385(97)89954-2
- Lichtenthaler, H. K., Langsdorf, G., Lenk, S., and Buschmann, C. (2005). Chlorophyll fluorescence imaging of photosynthetic activity with the flash-lamp fluorescence imaging system. *Photosynthetica* 43, 355–369. doi: 10.1007/s11099-005-0060-8
- Liebman, M. (2001). “Weed management: a need for ecological approaches,” in *Ecological Management of Agricultural Weeds*, eds M. Liebman, ChL Mohler, and ChP Staver (Cambridge: Cambridge University Press), 544.
- Lopes, M., Nogués, S., and Molero, G. (2012). “Gas exchange and chlorophyll fluorescence—Principles and applications,” in *Physiological Breeding I: Interdisciplinary Approaches to improve Crop Adaptation*, eds M. P. Reynolds, A. J. D. Pask, and D. M. Mullan (Mexico: CIMMYT), 188.
- López-González, D., Ledo, D., Cabeiras-Freijanes, L., Verdeguez, M., Reigosa, M. J., and Sánchez-Moreiras, A. M. (2020). Phytotoxic activity of the natural compound norharmane on crops, weeds and model plants. *Plants* 9:1328. doi: 10.3390/plants9101328
- Martínez-Peñalver, A., Pedrol, N., Reigosa, M. J., and Sánchez-Moreiras, A. M. (2012). Tolerance of *Arabidopsis thaliana* to the allelochemical protocatechualdehyde. *J. Plant Growth Regul.* 31, 406–415. doi: 10.1007/s00344-011-9250-8
- Martínez-Peñalver, A., Reigosa, M. J., and Sánchez-Moreiras, A. M. (2011). Imaging chlorophyll *a* fluorescence reveals specific spatial distributions under different stress conditions. *Flora* 206, 836–844. doi: 10.1016/j.flora.2011.02.004
- Maxwell, K., and Johnson, G. N. (2000). Chlorophyll fluorescence—a practical guide. *J. Exp. Bot.* 51, 659–668. doi: 10.1093/jxb/51.345.659
- McAlister, E. D., and Myers, J. (1940). Time course of photosynthesis and fluorescence. *Science* 92, 241–243. doi: 10.1126/science.92.2385.241
- McAusland, L., Atkinson, J. A., Lawson, T., and Murchie, E. H. (2019). High throughput procedure utilising chlorophyll fluorescence imaging to phenotype dynamic photosynthesis and photoprotection in leaves under controlled gaseous conditions. *Plant Meth.* 15:109.
- Meyer, S., and Genty, B. (1999). Heterogenous inhibition of photosynthesis over the leaf surface of *Rosa rubiginosa* L. during water stress and abscisic acid treatment: induction of a metabolic component by limitation of CO₂ diffusion. *Planta* 210, 126–131. doi: 10.1007/s004250050661
- Morison, J. I., Gallouët, E., Lawson, T., Cornic, G., Herbin, R., and Baker, N. R. (2005). Lateral diffusion of CO₂ in leaves is not sufficient to support photosynthesis. *Plant Physiol.* 139, 254–266. doi: 10.1104/pp.105.062950
- Morison, J. I., Lawson, T., and Cornic, G. (2007). Lateral CO₂ diffusion inside dicotyledonous leaves can be substantial: quantification in different light intensities. *Plant Physiol.* 145, 680–690. doi: 10.1104/pp.107.107318
- Müller, N. J. C. (1874). Beziehungen zwischen assimilation, absorption und fluoreszenz im chlorophyll des lebenden blattes. *Jahrb. Wiss. Bot.* 9, 42–49.
- Muller, R., Schreiber, U., Escher, B. I., Quayle, P., Nash, S. M. B., and Mueller, J. F. (2008). Rapid exposure assessment of PSII herbicides in surface water using a novel chlorophyll *a* fluorescence imaging assay. *Sci. Total Environ.* 401, 51–59. doi: 10.1016/j.scitotenv.2008.02.062
- Murchie, E. H., and Lawson, T. (2013). Chlorophyll fluorescence analysis: a guide to good practice and understanding some new applications. *J. Exp. Bot.* 64, 3983–3998. doi: 10.1093/jxb/ert208
- Nedbal, L., and Whitmarsh, J. (2004). “Chlorophyll fluorescence imaging of leaves and fruits,” in *Chlorophyll *a* Fluorescence: A Signature of Photosynthesis*, eds G. C. Papageorgiou and Govindjee (Dordrecht, NL: Springer), 389. doi: 10.1007/978-1-4020-3218-9_14
- Oguchi, R., Terashima, I., and Chow, W. S. (2009). The involvement of dual mechanisms of photoinactivation of Photosystem II in *Capsicum annuum* L. plants. *Plant Cell Physiol.* 50, 1815–1825. doi: 10.1093/pcp/pcp123
- Oguchi, R., Terashima, I., Kou, J., and Chow, W. S. (2011). Operation of dual mechanisms that both lead to photoinactivation of Photosystem II in leaves by visible light. *Physiol. Plant.* 142, 47–55. doi: 10.1111/j.1399-3054.2011.01452.x
- Omasa, K., Shimazaki, K., Aiga, I., Larcher, W., and Onoe, M. (1987). Image analysis of chlorophyll fluorescence transients for diagnosing the photosynthetic system of attached leaves. *Plant Physiol.* 84, 748–752. doi: 10.1104/pp.84.3.748
- Oxborough, K. (2004). “Using chlorophyll *a* fluorescence imaging to monitor photosynthetic performance,” in *Chlorophyll *a* Fluorescence: A Signature of Photosynthesis*, eds G. C. Papageorgiou and Govindjee (Dordrecht, NL: Springer), 409. doi: 10.1007/978-1-4020-3218-9_15
- Oxborough, K., and Baker, N. R. (1997). An instrument capable of imaging chlorophyll *a* fluorescence from intact leaves at very low irradiance and at cellular and subcellular levels of organization. *Plant Cell Environ.* 20, 1473–1483. doi: 10.1046/j.1365-3040.1997.d01-42.x
- Papageorgiou, G. C., and Govindjee. (eds) (2004). *Chlorophyll *a* Fluorescence: A Signature of Photosynthesis*. Dordrecht, NL: Springer.
- Papathanasiou, V., Kariofillidou, G., Malea, P., and Orfanidis, S. (2020). Effects of air exposure on desiccation and photosynthetic performance of *Cymodocea nodosa* with and without epiphytes and *Ulva rigida* in comparison, under laboratory conditions. *Mar. Environ. Res* 158:104948. doi: 10.1016/j.marenvres.2020.104948
- Paul, M. J., and Foyer, C. H. (2001). Sink regulation of photosynthesis. *J. Exp. Bot.* 52, 1383–1400. doi: 10.1093/jexbot/52.360.1383
- Pérez-Bueno, M. L., Pineda, M., and Barón Ayala, M. (2019). Phenotyping plant responses to biotic stress by chlorophyll fluorescence imaging. *Front. Plant Sci.* 10:1135. doi: 10.3389/fpls.2019.01135
- Ping, M. A., Tuan-Hui, B. A. I., and Feng-Wang, M. A. (2015). Effects of progressive drought on photosynthesis and partitioning of absorbed light in apple trees. *J. Integr. Agric.* 14, 681–690. doi: 10.1016/s2095-3119(14)60871-6
- Roháček, K., Soukupová, J., and Barták, M. (2008). “Chlorophyll fluorescence: a wonderful tool to study plant physiology and plant stress,” in *Plant Cell Compartments-Selected Topics*, ed. B. Schoefs (Kerala: Research Signpost), 41–104.
- Rolfe, S. A., and Scholes, J. D. (1995). Quantitative imaging of chlorophyll fluorescence. *New Phytol.* 131, 69–79. doi: 10.1111/j.1469-8137.1995.tb03056.x
- Ruban, A. V., and Murchie, E. H. (2012). Assessing the photoprotective effectiveness of non-photochemical chlorophyll fluorescence quenching: a new approach. *Biochim. Biophys. Acta Bioenerg.* 1817, 977–982. doi: 10.1016/j.bbabi.2012.03.026

- Rühle, T., Reiter, B., and Leister, D. (2018). Chlorophyll fluorescence video imaging: A versatile tool for identifying factors related to photosynthesis. *Front. Plant Sci.* 9:55. doi: 10.3389/fpls.2018.00055
- Sánchez-Moreiras, A. M., and Reigosa, M. J. (2005). Whole plant response of lettuce after root exposure to BOA (2(3H)-benzoxazolinone). *J. Chem. Ecol.* 31, 2689–2703. doi: 10.1007/s10886-005-7620-z
- Sánchez-Moreiras, A. M., Graña, E., Díaz-Tielas, C., López-González, D., Araniti, F., Celeiro, M., et al. (2018). “Elucidating the phytotoxic potential of natural compounds,” in *Advances in Plant Ecophysiology Techniques*, eds A. M. Sánchez-Moreiras and M. J. Reigosa (New York, NY: Springer), 419–438.
- Sánchez-Moreiras, A. M., Martínez-Peñalver, A., and Reigosa, M. J. (2011). Early senescence induced by 2-3H-benzoxazolinone (BOA) in *Arabidopsis thaliana*. *J. Plant Physiol.* 168, 863–870. doi: 10.1016/j.jplph.2010.11.011
- Scholes, J. D., and Rolfe, S. A. (1996). Photosynthesis in localised regions of oat leaves infected with crown rust (*Puccinia coronata*): quantitative imaging of chlorophyll fluorescence. *Planta* 199, 573–582.
- Schreiber, U. (1983). Chlorophyll fluorescence yield changes as a tool in plant physiology I. The measuring system. *Photosyn. Res.* 4, 361–373. doi: 10.1007/bf00054144
- Schreiber, U. (2004). “Pulse-amplitude-modulation (PAM) fluorometry and saturation pulse method: an overview,” in *Chlorophyll a Fluorescence. Advances in Photosynthesis and Respiration*, eds G. C. Papageorgiou and Govindjee (Dordrecht, NL: Springer), 279–319. doi: 10.1007/978-1-4020-3218-9_11
- Schreiber, U., and Bilger, W. (1993). “Progress in chlorophyll fluorescence research: major developments during the past years in retrospect,” in *Progress in Botany / Fortschritte der Botanik*, eds H. D. Behnke, U. Lüttge, K. Esser, J. W. Kaderer, and M. Runge (Heidelberg: Springer), 151–173. doi: 10.1007/978-3-642-78020-2_8
- Schreiber, U., and Neubauer, C. (1987). The polyphasic rise of chlorophyll fluorescence upon onset of strong continuous illumination: II. Partial control by the photosystem II donor side and possible ways of interpretation. *Z. Naturforsch. C* 42, 1255–1264. doi: 10.1515/znc-1987-11-1218
- Schreiber, U., Bilger, W., and Neubauer, C. (1995). “Chlorophyll fluorescence as a noninvasive indicator for rapid assessment of *in vivo* photosynthesis,” in *Ecophysiology of Photosynthesis*, eds E. D. Schulze and M. M. Caldwell (Heidelberg: Springer), 49–70. doi: 10.1007/978-3-642-79354-7_3
- Schreiber, U., Bilger, W., Hormann, H., and Neubauer, C. (1998). “Chlorophyll fluorescence as a diagnostic tool: basics and some aspects of practical relevance,” in *Photosynthesis: A Comprehensive Treatise*, ed. A. S. Raghavendra (Cambridge: Cambridge University Press), 320–336.
- Schreiber, U., Neubauer, C., and Schliwa, U. (1993). PAM fluorometer based on medium-frequency pulsed Xe-flash measuring light: a highly sensitive new tool in basic and applied photosynthesis research. *Photosyn. Res.* 36, 65–72. doi: 10.1007/bf00018076
- Schreiber, U., Schliwa, U., and Bilger, W. (1986). Continuous recording of photochemical and non-photochemical chlorophyll fluorescence quenching with a new type of modulation fluorometer. *Photosyn. Res.* 10, 51–62. doi: 10.1007/bf00024185
- Schulz, M., Kussmann, P., Knop, M., Krieger, B., Gresens, F., Eichert, T., et al. (2007). Allelopathic monoterpenes interfere with *Arabidopsis thaliana* cuticular waxes and enhance transpiration. *Plant Signal. Behav.* 2, 231–239. doi: 10.4161/psb.2.4.4469
- Siebek, K., and Weis, E. (1995a). Imaging of chlorophyll-a-fluorescence in leaves: topography of photosynthetic oscillations in leaves of *Glechoma hederacea*. *Photosyn. Res.* 45, 225–237. doi: 10.1007/bf00015563
- Siebek, K., and Weis, E. (1995b). Assimilation images of leaves of *Glechoma hederacea*: analysis of non-synchronous stomata related oscillations. *Planta* 196, 155–165.
- Skrzypek, E., Repka, P., Stachurska-Swakon, A., Barabasz-Krasny, B., and Mozdzen, K. (2015). Allelopathic effect of aqueous extracts from the leaves of peppermint (*Mentha piperita* L.) on selected physiological processes of common sunflower (*Helianthus annuus* L.). *Notul. Bot. Hort. Agr. Cluj-Napoca* 43, 335–342. doi: 10.15835/nbha43210034
- Stokes, G. G. (1852). On the change of refrangibility of light. *Philos. Trans. R. Soc. Lond.* 142, 463–562. doi: 10.1098/rstl.1852.0022
- Strasser, R. J., and Govindjee. (1991). “The Fo and the O-J-I-P Fluorescence Rise in Higher Plants and Algae,” in *Regulation of Chloroplast Biogenesis. Nato ASI Series (Series A: Life Sciences)*, ed. J. H. Argyroudi-Akoyunoglou (Boston, MA: Springer).
- Synowiec, A., Mozdzeń, K., Krajewska, A., Landi, M., and Araniti, F. (2019). *Carum carvi* L. essential oil: A promising candidate for botanical herbicide against *Echinochloa crus-galli* (L.) P. Beauv. in maize cultivation. *Ind. Crops Prod.* 140:111652. doi: 10.1016/j.indcrop.2019.111652
- Tan, S., Smith, N. C., Padilla, K., and Ashley, E. (2018). *Autonomous Ground Photographer*. Washington: Washington University Open Scholarship.
- Wang, P., Li, H., Jia, W., Chen, Y., and Gerhards, R. (2018). A fluorescence sensor capable of real-time herbicide effect monitoring in greenhouses and the field. *Sensors* 18:3771. doi: 10.3390/s18113771
- Weber, J. F., Kunz, C., Peteinatos, G. G., Santel, H. J., and Gerhards, R. (2017). Utilization of chlorophyll fluorescence imaging technology to detect plant injury by herbicides in sugar beet and soybean. *Weed Technol.* 31, 523–535. doi: 10.1017/wet.2017.22
- Weis, E., and Berry, J. A. (1987). Quantum efficiency of photosystem II in relation to ‘energy’-dependent quenching of chlorophyll fluorescence. *Biochim. Biophys. Acta Bioenerg.* 894, 198–208. doi: 10.1016/0005-2728(87)90190-3
- Werner, C., Correia, O., and Beyschlag, W. (2002). Characteristic patterns of chronic and dynamic photoinhibition of different functional groups in a Mediterranean ecosystem. *Funct. Plant Biol.* 29, 999–1011. doi: 10.1071/pp01143
- Wingler, A., Marč, M., and Pourtau, N. (2004). Spatial patterns and metabolic regulation of photosynthetic parameters during leaf senescence. *New Phytol.* 161, 781–789. doi: 10.1111/j.1469-8137.2004.00996.x
- Xiao, W., Wang, H., Liu, W., Wang, X., Guo, Y., Strasser, R., et al. (2020). Action of alamethicin in photosystem II probed by the fast chlorophyll fluorescence rise kinetics and the JIP-test. *Photosynthetica* 58, 358–368. doi: 10.32615/ps.2019.172
- Zavafer, A., Cheah, M., Hillier, W., Chow, W. S., and Takahashi, S. (2015). Photodamage to the oxygen evolving complex of photosystem II by visible light. *Sci. Rep.* 5:16363. doi: 10.1038/srep16363
- Zheng, G., Zhao, X., Zhang, F., Luo, S., Li, S., and Li, W. (2012). o-Coumaric acid from invasive *Eupatorium adenophorum* is a potent phytotoxin. *Chemoecology* 22, 131–138. doi: 10.1007/s00049-012-0105-y
- Zhou, C., Mao, J., Zhao, H., Rao, Z., and Zhang, B. (2020). Monitoring and predicting *Fusarium* wilt disease in cucumbers based on quantitative analysis of kinetic imaging of chlorophyll fluorescence. *Appl. Optics* 59, 9118–9125. doi: 10.1364/ao.399320
- Zhuang, J., Wang, Y., Chi, Y., Zhou, L., Chen, J., Zhou, W., et al. (2020). Drought stress strengthens the link between chlorophyll fluorescence parameters and photosynthetic traits. *PeerJ* 8:e10046. doi: 10.7717/peerj.10046

Conflict of Interest: The authors declare that the research was conducted in the absence of any commercial or financial relationships that could be construed as a potential conflict of interest.

Copyright © 2020 Sánchez-Moreiras, Graña, Reigosa and Araniti. This is an open-access article distributed under the terms of the Creative Commons Attribution License (CC BY). The use, distribution or reproduction in other forums is permitted, provided the original author(s) and the copyright owner(s) are credited and that the original publication in this journal is cited, in accordance with accepted academic practice. No use, distribution or reproduction is permitted which does not comply with these terms.

Advantages of publishing in Frontiers



OPEN ACCESS

Articles are free to read
for greatest visibility
and readership



FAST PUBLICATION

Around 90 days
from submission
to decision



HIGH QUALITY PEER-REVIEW

Rigorous, collaborative,
and constructive
peer-review



TRANSPARENT PEER-REVIEW

Editors and reviewers
acknowledged by name
on published articles

Frontiers

Avenue du Tribunal-Fédéral 34
1005 Lausanne | Switzerland

Visit us: www.frontiersin.org

Contact us: frontiersin.org/about/contact



REPRODUCIBILITY OF RESEARCH

Support open data
and methods to enhance
research reproducibility



DIGITAL PUBLISHING

Articles designed
for optimal readership
across devices



FOLLOW US

@frontiersin



IMPACT METRICS

Advanced article metrics
track visibility across
digital media



EXTENSIVE PROMOTION

Marketing
and promotion
of impactful research



LOOP RESEARCH NETWORK

Our network
increases your
article's readership